

Biochemical basis of activation and inhibition of an NLR immune receptor network

Mauricio P. Contreras

Thesis submitted to the University of East Anglia for the Degree of
Doctor of Philosophy

June 2023

© This copy of the thesis has been supplied on condition that anyone who consults it is understood to recognize that its copyright rests with the author and that use of any information derived from it must be in accordance with current UK Copyright Law. In addition, any quotation or extract must include full attribution.

Abstract

The plant immune system employs intracellular nucleotide-binding domain and leucine-rich repeat (NLR) receptors to identify and respond to pathogen-derived virulence proteins, termed effectors. NLRs function individually or in configurations such as pairs or networks. In solanaceous plants, the NLR required for cell death (NRC) network mediates resistance against various pathogens. The molecular mechanisms by which the NRC network activates are not understood. Moreover, some pathogen effectors can suppress NLRs to promote virulence, and the mechanisms of this suppression are largely unknown.

In this thesis, I characterized a cell death-inducing truncation of the helper NRC4, leading to the identification of a conserved N-terminal motif in CC-NLRs. Using mutated NRC variants, I established a method for monitoring NRC activation and investigated sensor-helper communication in the NRC network. My findings support an activation and release model in which NRC-dependent sensors mediate oligomerization of helper NRCs without joining the helper oligomer. The NB domain can encode the minimal signal for resistosome formation in many NRC-dependent sensors.

I also elucidated the suppression mechanisms of AVRcap1b and SS15, two effectors that inhibit NRC2 and NRC3. AVRcap1b connects activated NRCs to host TOL proteins, suppressing immunity, while SS15 binds inactive NRCs, preventing helper activation and resistosome formation. Understanding the suppression mechanism enabled me to bioengineer NRC variants that evade inhibition. This work presents a model for sensor-helper activation of NLRs, provides insights into pathogen manipulation of NLR signaling, and demonstrates a novel strategy for bioengineering of disease resistance.

Access Condition and Agreement

Each deposit in UEA Digital Repository is protected by copyright and other intellectual property rights, and duplication or sale of all or part of any of the Data Collections is not permitted, except that material may be duplicated by you for your research use or for educational purposes in electronic or print form. You must obtain permission from the copyright holder, usually the author, for any other use. Exceptions only apply where a deposit may be explicitly provided under a stated licence, such as a Creative Commons licence or Open Government licence.

Electronic or print copies may not be offered, whether for sale or otherwise to anyone, unless explicitly stated under a Creative Commons or Open Government license. Unauthorised reproduction, editing or reformatting for resale purposes is explicitly prohibited (except where approved by the copyright holder themselves) and UEA reserves the right to take immediate 'take down' action on behalf of the copyright and/or rights holder if this Access condition of the UEA Digital Repository is breached. Any material in this database has been supplied on the understanding that it is copyright material and that no quotation from the material may be published without proper acknowledgement.

Table of Contents

<i>Abstract</i>	2
<i>List of Figures</i>	9
<i>List of Tables</i>	13
Chapter 1: General Introduction	21
1.1 Overview of the plant immune system	21
1.2 What are NLRs?	23
1.2.1 N-terminal signaling domains.....	24
1.2.2 The NB-ARC domain.....	26
1.2.3 C-terminal LRR domain.....	27
1.2.4 NLR diversity.....	28
1.3 NLRs are intracellular sensors of invading pathogens.	29
1.3.1 NLRs can directly recognise pathogen effectors.....	30
1.3.2 Indirect recognition: the guardee/decoy model.....	30
1.3.3 NLR-IDs: NLRs with unconventional integrated domains.....	32
1.3.4 NLR bioengineering: new recognition specificities.....	33
1.4 NLR signaling configurations: singletons and pairs.	34
1.4.1 Singleton NLRs.....	34
1.4.2 Paired NLRs.....	35
1.5 NLR networks: the next step in NLR evolution.	35
1.5.1 The NRC NLR-PRR network.....	36
1.5.2 The NRG1/ADR1 network.....	38
1.5.3 Evolution of NLR networks.....	38
1.5.4 Phylogenomics of NLR networks.....	39
1.6 Sensor NLRs in the NRC network.	41
1.6.1 Rx and Gpa2.....	41
1.6.2 Bs2.....	44
1.6.3 Rpiamr1 and Rpi-amr3.....	44
1.6.4 Rpi-blb2 and Mi-1.2.....	44
1.6.5 Sw5-b and R8.....	45
1.6.6 Prf.....	46
1.7 NLR activation.	46

1.7.1	Pathogen activation of CC-NLRs	46
1.7.2	Pathogen activation of TIR-NLRs/CC _R -NLRs.....	50
1.7.3	NLR activation in non-plant NLRs.....	51
1.7.4	Cell biology of NLR resistosomes	52
1.7.5	Atypical NLRs: modulators of plant immunity	54
1.8	Pathogen effectors: the basics.	55
1.8.1	Effectors as probes.....	56
1.8.2	The RXLR-WY/LWY family of effectors.	56
1.8.3	The SPRYSEC family of effectors.....	58
1.9	Pathogen suppression of NLRs.....	59
1.9.1	Pathogen suppression of NLRs: indirect inhibition.....	59
1.9.2	Pathogen suppression of NLRs: direct inhibition.	60
1.9.3	Pathogen suppression of the NRC network	62
1.10	TOL proteins and the ESCRT vesicle trafficking pathway.	65
1.10.1	The basics of plant ESCRT trafficking.	65
1.10.2	TOL/ESCRT regulation of programmed cell death.	66
1.11	Aims of the thesis.....	68
Chapter 2: Materials and Methods.		70
2.1	Plant growth conditions.....	70
2.2	General Molecular biology and cloning methods.	70
2.2.1	Polymerase chain reaction (PCR) and PCR product purification	70
2.2.2	Plasmid construction.....	70
2.2.3	Golden Gate cloning.....	71
2.2.4	Bacterial transformation	71
2.3	Agroinfiltration and cell death assays.....	72
2.3.1	Hairpin RNA-mediated gene silencing.....	72
2.4	<i>Phytophthora infestans</i> growth conditions and infection assays.	73
2.5	Phylogenetic analyses of <i>N. benthamiana</i> and <i>Arabidopsis thaliana</i> TOL proteins	73
2.6	Biochemistry methods.	73
2.6.1	Extraction of total proteins for SDS-PAGE assays.	73
2.6.2	Extraction of total proteins for BN-PAGE assays.	74
2.6.3	Extraction of proteins for Co-Immunoprecipitation assays.	74
2.6.4	BN-PAGE assays.	75
2.6.5	SDS-PAGE assays.....	75
2.6.6	Co-Immunoprecipitation assays.....	75
2.6.7	Immunoblotting and detection of BN-PAGE, SDS-PAGE and CoIP assays.....	76

2.6.8	Gel filtration assays with NRC2.....	77
2.6.9	BN and SDS-PAGE assays with PVX infection (agroinfection).....	77
2.6.10	Membrane enrichment assays.....	77
2.7	Confocal microscopy.....	78
2.8	Recombinant protein purification from <i>E. coli</i>.....	78
2.8.1	Purification of AVRcap1b in complex with NbTOL9a domains.....	78
2.8.2	Gel filtration assays with AVRcap1b and NbTOL9a ^{ENTH}	80
2.8.3	Purification of SS15 in complex with SINRC1 ^{NB-ARC}	80
2.9	Crystallography and structural solution.....	82
2.9.1	Crystallization and data collection of AVRcap1b-NbTOL9a ^{ENTH} protein complexes.....	82
2.9.2	Data processing and structural solution for AVRcap1b-NbTOL9a ^{ENTH} protein complex.....	82
2.9.3	Crystallization and data collection of SS15-SINRC1 ^{NB-ARC} protein complex.....	83
2.9.4	Data processing and structural solution for SS15-SINRC1 ^{NB-ARC} protein complex.....	84
Chapter 3: Functional characterization of conserved motifs required for NLR-mediated cell death. 86		
3.1	Introduction.....	86
3.2	Results.....	89
3.2.1	N-terminal 29 amino acids of NRC4 are sufficient to induce HR cell death in <i>Nicotiana benthamiana</i>	89
3.2.2	NRC4 and ZAR1 share an N-terminal MADA motif.....	91
3.2.3	Conserved MADA motif residues are required for NRC4-mediated cell death.....	92
3.2.4	An intact MADA motif is required for NRC4-mediated disease resistance against <i>P. infestans</i>	95
3.2.5	The ZAR1 MADA can functionally complement NRC4 for disease resistance against <i>P. infestans</i>	96
3.3	Conclusions and discussion.....	97
3.4	Research Contributions.....	99
Chapter 4: Biochemical basis of activation in an NLR immune receptor network. 100		
4.1	Introduction.....	100
4.2	Results.....	104
4.2.1	Activation of Rx with <i>Potato virus X</i> coat protein leads to oligomerization of its helper NRC2.....	104
4.2.2	Rx does not oligomerize upon PVX CP perception.....	105
4.2.3	The high molecular weight complex formed by Rx does not contain host protein RanGAP2.....	109
4.2.4	Rx does not enter into a stable complex with NRC2.....	109
4.2.5	The NRC2 oligomer is composed of multiple NRC2 proteins.....	112
4.2.6	Bs2 also mediates NRC2 oligomerization.....	112
4.2.7	Bs2, Rx and Rpi-blb2 activation triggers oligomerization of their helper NRC4.....	115
4.2.8	Activated NRC2 oligomers accumulate in membrane-associated puncta, whereas Rx remains cytoplasmic.....	116

4.2.9	Infection with Potato <i>virus X</i> leads to Rx-dependent oligomerization of NRC2.....	118
4.2.10	<i>Potato virus X</i> infection triggers Rx-dependent formation of membrane-associated NRC2 puncta. .	120
4.3	Conclusions and discussion.	121
4.4	Research Contributions	124
Chapter 5: Understanding sensor helper communication in the NRC network.		125
5.1	Introduction.	125
5.2	Results.....	128
5.2.1	Rx can mediate NRC-dependent cell death when expressed as halves.....	128
5.2.2	Rx halves associate in planta in an NRC-independent manner.....	129
5.2.3	NRC2, but not NRC2 ^{EEE} , mediates Rx halves dissociation upon activation.....	132
5.2.4	Rx halves can mediate NRC2 resistosome formation when expressed in trans.....	134
5.2.5	The LRR domain of Rx is prone to associating non-specifically with multiple proteins.....	136
5.2.6	The NB domain of Rx can activate its downstream helpers NRC2, NRC3 and NRC4 in a p-loop independent manner.	138
5.2.7	The NB domains of other NRC-dependent sensor NLRs can also activate downstream helpers ...	140
5.2.8	Sensor NLR NB domain truncations retain the NRC helper specificities of their full-length counterparts.	140
5.2.9	Single amino acid mutations in Gpa2 ^{NB} -eGFP enhance its capacity to activate NRC4.....	143
5.3	Conclusions and discussion	144
5.4	Research Contributions	148
Chapter 6: Understanding AVRcap1b-mediated suppression of NRC-mediated cell death.		149
6.1	Introduction.	149
6.2	Results.....	153
6.2.1	AVRcap1b does not associate with inactive NRCs.....	153
6.2.2	AVRcap1b associates with host TOL proteins in planta.	154
6.2.3	NbTOL9a does not associate with inactive NRCs.	155
6.2.4	The presence of AVRcap1b does not lead to NbTOL9a associating with inactive NRCs.	156
6.2.5	NbTOL9a negatively modulates the cell death triggered by NRC3 but not NRC4	158
6.2.6	AVRcap1b suppression of NRC3 is compromised in the absence of NbTOL9a.	160
6.2.7	ENTH domain truncations of NbTOL9a associate with AVRcap1b <i>in planta</i>	161
6.2.8	AVRcap1b homologs from other <i>Phytophthora</i> species do not suppress NRCs.....	162
6.2.9	The LWY7 domain of <i>P. infestans</i> AVRcap1b is sufficient to confer NRC3 suppression to <i>P. ipomoeae</i> AVRcap1b.	163
6.2.10	NbTOL9a ENTH AND ENTH-GAT domains can form complexes with AVRcap1b <i>in vitro</i>	164
6.2.11	AVRcap1b binds NbTOL9a ^{ENTH} via its N-terminal WY1 domain.....	167

6.2.12	NbTOL9a binding by AVRcap1b is required for NRC3 suppression.....	170
6.2.13	AVRcap1b associates with Rx/CP-activated NRC2 in planta.	170
6.2.14	AVRcap1b does not prevent NRC2 resistosome formation.	172
6.3	Conclusion and Discussion.	174
6.4	Research contributions.	177
Chapter 7: Resurrection of disease resistance via helper NLR bioengineering.		178
7.1	Introduction.	178
7.2	Results.....	180
7.2.1	SS15 inhibits NRC2 but not NRC4 oligomerization and resistosome formation.....	180
7.2.2	SS15 associates with HD1-1 region in the NB-ARC domain of NRC2.	184
7.2.3	SS15 binds and immobilizes a loop in the HD1-1 to prevent NRC2 oligomerization.	188
7.2.4	Single amino acid variants of NRC2 evade suppression by SS15.	190
7.2.5	A bioengineered NRC2 ^{D317K} variant resurrects the activity of multiple NRC2-dependent sensors in the presence of SS15.....	192
7.3	Conclusions and discussion.	194
7.4	Research contributions.	195
Chapter 8: General discussion.....		196
8.1	The MADA motif: serendipity strikes.	197
8.2	The α1: business end of CC domains.	197
8.2.1	MADA mutants: unlocking new possibilities in CC-NLR research.	199
8.2.2	The MADA motif and CC-NLR N-terminal diversity: the alpha but certainly not the omega.	200
8.3	Activation and release: a new activation mechanism for NLR networks.	201
8.3.1	Sensor-helper activation in the NRC network: immune receptor specialization at its finest.	201
8.3.2	A swift response: re-localization of helpers upon pathogen infection.	203
8.4	Rx as a model NLR: building on solid ground.	204
8.4.1	Rx intramolecular rearrangements: no resistosome but still complex.....	204
8.4.2	Sensor NLR NB domains: A Rosetta stone to decoding the sensor-helper language.....	205
8.4.3	NB domain-mediated helper activation: how did we get here?.....	207
8.4.4	Understanding sensor-helper specificity.	208
8.4.5	Disease resistance without death?.....	209
8.5	Effectors as both activators and suppressors of NLRs.	210
8.5.1	NRC suppression by AVRcap1b and SS15: different approaches with common themes.....	210
8.5.2	NLR suppression: a double-edged sword for pathogens.	211
8.5.3	Gene-for-gene 2.0.....	212
8.5.4	Pathogen suppression of NLRs: the dark matter of R-gene discovery.....	212

8.5.5	ESCRTing the resistosome: a new player in NLR regulation.....	213
8.5.6	More complexity means more regulation?.....	214
8.5.7	NLR networks: making plant immunity more robust.	215
8.6	A bright future for synthetic disease resistance	216
8.7	Concluding remarks and future questions.	217
<i>Appendix I.....</i>		<i>220</i>
<i>Appendix II:.....</i>		<i>241</i>
<i>Appendix III</i>		<i>243</i>
<i>Appendix IV.....</i>		<i>248</i>
<i>Appendix V.....</i>		<i>250</i>
<i>Appendix VI.....</i>		<i>256</i>
<i>References</i>		<i>264</i>

List of Figures

Figure 1.1: The plant immune system.	23
Figure 1.2: The Solanaceous NRC network.	37
Figure 1.3: Evolution of NLR singletons, pairs, and networks.	40
Figure 1.4: Phylogenetics of NLR networks.	43
Figure 1.5: Plant NLR activation mechanisms.	48
Figure 1.6: Potential activation mechanisms in the NRC network.	49
Figure 1.7: AVRcap1b and SS15 are suppressors of NRC2/3-mediated immunity.	64
Figure 1.8: TOL proteins, potential host interactors of AVRcap1b.	67
Figure 3.1: NRC4 ₁₋₂₉ induces cell death in <i>N. benthamiana</i> when fused to YFP independently of endogenous NRC4.	90
Figure 3.2: The MADA motif is conserved at N-termini of NRC4 and ZAR1.	92
Figure 3.3: Triple mutation in conserved residues at positions L9, V10 and L14 impairs cell death mediated by autoimmune NRC4 ^{DV}	93
Figure 3.4: Glutamic acid scan reveals that mutations in conserved amino acids in positions L9, L13 and L17 impair cell death activity of autoactive NRC4 ^{D478V}	94
Figure 3.5: The N-terminal MADA motif of ZAR1 can functionally complement the N-terminus of NRC4 in Rpi-blb2-mediated resistance against <i>Phytophthora infestans</i>	96
Figure 4.1: PVX CP activation of Rx leads to NRC2 oligomerization.	106
Figure 4.2 Size-exclusion gel filtration chromatography can be used to visualize Rx-mediated oligomerization of NRC2.	108
Figure 4.3: Rx, RanGAP2 and PVX CP do not co-migrate in BN-PAGE assays.	110
Figure 4.4: Rx and NRC2 do not form a stable complex upon activation.	111
Figure 4.5: The activated NRC2 ^{EEE} complex is composed of multiple NRC2 monomers.	113
Figure 4.6: Other NRC2-dependent sensors can trigger oligomerization of NRC2 ^{EEE}	114
Figure 4.7: Bs2, Rx and Rpi-blb2 trigger oligomerization of another helper NLR, NRC4.	115
Figure 4.8: <i>Potato virus X</i> coat protein activated NRC2 forms plasma membrane-associated puncta, unlike Rx.	117
Figure 4.9: PVX infection triggers Rx-mediated oligomerization of NRC2.	119
Figure 4.10: <i>Potato virus X</i> infection triggers Rx-dependent NRC2 membrane-associated puncta.	121
Figure 4.11: An activation-and-release working model for sensor-helper pairs in the NRC network.	123

Figure 5.1: Rx halves expressed in trans trigger NRC2/3/4-dependent cell death upon activation with PVX CP.....	130
Figure 5.2: Association between halves of Rx expressed in trans is NRC-independent.....	131
Figure 5.3: Rx halves dissociation is NRC2 and MADA-motif dependent.....	133
Figure 5.4: Activation of the Rx ^{CCNB} /Rx ^{LRR} system mediates NRC2 oligomerization.....	135
Figure 5.5: Unlike Rx ^{LRR} , Rx ^{CCNBARC} interacts specifically with NRC2 but not with SINRC0.	137
Figure 5.6: The NB domain of Rx fused to eGFP triggers cell death in an NRC-dependent and p-loop-independent manner.....	138
Figure 5.7: Rx ^{NB} -eGFP mediates NRC2 ^{EEE} oligomerization.....	139
Figure 5.8: Other sensor NLR NB domain-eGFP fusions trigger NRC-dependent cell death..	141
Figure 5.9: Sensor NLR NB domains retain the NRC helper specificities of their full-length counterparts.....	142
Figure 5.10: Multiple amino acids in Gpa2 NB domain underpin NRC4 signaling efficiency. ..	143
Figure 5.11: Proposed working model for NB-mediated sensor-helper activation in the NRC network.	147
Figure 6.1: Unlike SS15, AVRcap1b does not associate with inactive NRCs <i>in planta</i>	153
Figure 6.2: AVRcap1b associates with NbTOL9a <i>in planta</i>	155
Figure 6.3: NbTOL9a does not associate with inactive NRC proteins.	156
Figure 6.4: NbTOL9a does not associate with inactive NRC proteins in the presence of AVRcap1b.	157
Figure 6.5: Overexpression of NbTOL9a suppresses autoactive NRC3 ^{D480V} but not MEK2 ^{DD} or NRC4 ^{D478V}	158
Figure 6.6: NbTOL9a silencing enhances cell death mediated by NRC3 ^{D480V} but not NRC4 ^{D478V}	159
Figure 6.7: Silencing of NbTOL9a compromises AVRcap1b mediated suppression of NRC3.	160
Figure 6.8: NbTOL9a ENTH domain is sufficient for association with AVRcap1b <i>in planta</i>	162
Figure 6.9: AVRcap1b homologs from other <i>Phytophthora</i> clade 1c species are unable to suppress NRC3-mediated cell death.	163
Figure 6.10: <i>P. ipomoeae</i> AVRcap1b LWY7 chimera gains the capacity to suppress NRC3.....	165
Figure 6.11: AVRcap1b binds the ENTH domain of NbTOL9a <i>in vitro</i>	166
Figure 6.12: Crystal structure of AVRcap1b in complex with NbTOL9a ^{ENTH}	168
Figure 6.13: AVRcap1b P33E and G35E mutants in NbTOL9a binding interface do not associate with NbTOL9a <i>in planta</i>	169

Figure 6.14: Two residues in AVRcap1b-NbTOL9a ^{ENTH} binding interface are required for NRC3 suppression.	171
Figure 6.15: AVRcap1b associates with activated NRC2 <i>in planta</i> via its C-terminal WY7 module.	172
Figure 6.16: AVRcap1b does not inhibit NRC2 oligomerization.	173
Figure 6.17: Working model for AVRcap1b suppression of NRC2/NRC3-mediated cell death.	175
Figure 7.1: SS15 directly inhibits NRC2 but not NRC4 oligomerization.	182
Figure 7.2: SS15 inhibits plasma membrane-association of activated NRC2.	183
Figure 7.3: SS15 inhibits NRC2 by interacting with the HD1-1 region of the NB-ARC domain.	185
Figure 7.4: The HD1-1 region of NRC NB-ARC domain determines sensitivity to SS15.	187
Figure 7.5: Cocystal structure reveals SS15-NRC binding interface and residues contributing to interaction.	189
Figure 7.6: Mutagenesis of NRC2-SS15 reveals mutants that evade SS15 association and inhibition.	191
Figure 7.7: NRC2 ^{D317K} helper restores immune signaling of multiple disease resistance genes in the presence of the effector SS15.	193
Figure 7.8: Resurrection of sensor NLRs via helper NLR bioengineering.	194
Figure AII.1: NRC4 ₁₋₂₉ -YFP cell death is compromised by YFP A206K mutation.	241
Figure AII.2: Mapping loss of function mutations on N-terminal α helices of NRC4.	242
Figure AIII.1: MADA motif mutants of NRC2 are unable to trigger cell death.	243
Figure AIII.2: NRC2 with an intact N-terminal MADA motif also oligomerizes upon Rx-mediated activation.	244
Figure AIII.3: All C-terminally tagged sensors and helpers used retain the capacity to trigger hypersensitive cell death.	245
Figure AIII.4: C-terminally 6xHA tagged sensors retain the capacity to mediate cell death.	246
Figure AIII.5: Fluorescent protein-tagged Rx and NRC2 retain cell death-mediating capacity and can oligomerize upon activation.	246
Figure AIV.1: Gpa2 signals through NRC2 and NRC4.	248
Figure AIV.2: Polymorphic surface-exposed residues in the NB domains of Gpa2 and Rx explain differences in NRC4 activation strength.	249
Figure AV.1: C-terminally tagged versions of AVRcap1b are still able to suppress NRC2 and NRC3 mediated cell-death.	250

Figure AV.2: Maximum-likelihood phylogenetic tree of TOL proteins from <i>N. benthamiana</i> and <i>A. thaliana</i> .	251
Figure AV.3: RNAi: <i>NbTOL9a</i> silencing construct reduces protein accumulation levels of NbTOL9a.	252
Figure AV.4: Expression tests of NbTOL9a and different NbTOL9a domains in <i>E. coli</i> .	253
Figure AV.5: NbTOL9a ^{ENTH-GAT} and NbTOL9a ^{ENTH} domains form a complex with AVRcap1b in vitro.	254
Figure AV.6: Residues predicted to be involved in NbTOL9a binding are conserved between <i>P. infestans</i> and <i>P. ipomoeae</i> AVRcap1b.	254
Figure AVI.1: SS15 suppresses cell death mediated by SINRC1, NRC2 and NRC3 but not NRC4 or NbZAR1.	256
Figure AVI.2: NRC4 ^{HD1-1} chimera is susceptible to inhibition by SS15.	257
Figure AVI.3: SS15 inhibits NRC2 by interacting with the HD1-1 region of the NB-ARC domain.	258
Figure AVI.4: Crystal structure of SS15 in complex with SINRC1 ^{NB-ARC} .	259
Figure AVI.5: NRC2 ^{E316P} and NRC2 ^{D317K} abolish SS15-mediated suppression of Rx.	260
Figure AVI.6: NRC2 ^{D317K} abolishes SS15-mediated suppression of Rx, Gpa2 and Prf.	261
Figure AVI.7: NRC2 ^{D317K} abolishes SS15-mediated suppression of all NRC2-dependent sensors tested and restores NRC2 resistosome formation.	262

List of Tables

Table 1.1: List of published effectors with NLR suppressing activities.....	60
Table AI.1: Constructs used in this thesis.	220
Table AI.2: OD ₆₀₀ used for each experiment.	231
Table AV.1: Summary of X-ray data and model parameters for AVRcap1b – NbTOL9a ^{ENTH} ..	255
Table AVI.1: Summary of X-ray data and model parameters for NRC1 ^{NB-ARC} -SS15.	263

Abbreviations

ADP	Adenosine diphosphate
ADPr-ATP	ADP-ribosylated ATP
diADPR	ADP-ribosylated ADPR
ADR1	Activated disease resistance 1
APAF-1	Apoptotic protease-activating factor 1
ASC	Apoptosis-associated speck-like protein containing a CARD
ATP	Adenosine triphosphate
ATR1	<i>Arabidopsis thaliana</i> -recognised 1
AVR	Avirulence
BIR	Baculoviral inhibitor of apoptosis protein repeat
CARD	Caspase activation and recruitment domain
CC	Coiled-coil
CC _R	RPW8-type coiled-coil
CC _{G10}	G10-subclade coiled-coil
CED-4	Cell death protein 4
C-JID	C-terminal jelly-roll/Ig-like domain
CoIP	Co-Immunoprecipitation
Cryo-EM	Cryogenic electron microscopy
CP	Coat protein
Dpi	Days post infiltration
EDS1	Enhanced disease susceptibility 1
EHM	Extra-haustorial membrane
ENTH	Epsin N-terminal homology
ESCRT	Endosomal sorting complex required for transport
E _{TI}	Effector-triggered immunity
GAT	GGA and Target of Myb 1
Gpa2	<i>Globodera pallida</i> resistance 2
HD1	Helical domain 1

HMA	Heavy metal-associated
HR	Hypersensitive response
HSP90	Heat-shock protein 90
ID	Integrated domain
LRR	Leucine rich repeat
MAMP	Microbe-associated molecular pattern
MAPK	Mitogen-activated protein kinase
MAX	<i>Magnaporthe</i> AvrS and ToxB-like
MHD	Methionine-histidine-aspartate
MLA	Mildew locus A
MVB	Multivesicular bodies
NACHT	NAIP2, C2TA, HET-E and TP1
NAD	Nicotinamide
NAIP	NLR family apoptosis inhibitory protein
NB	Nucleotide-binding
NB-ARC	Nucleotide-binding adaptor shared by APAF1, plant R protein products and CED-4
NEK7	NIMA related kinase 7
NLR	Nucleotide binding and leucine rich repeat
NLRC	NLR family CARD-containing
NLRP	NLR family Pyrin domain-containing
NOD	Nucleotide-binding oligomerisation domain
NRC	NLR required for cell death
NRG1	N required gene 1
PAD4	Phytoalexin deficient 4
PAMP	Pathogen-associated molecular pattern
PBL2	PBS1-like 2
PBS1	AVRPPHB-susceptible 1
PCR	Polymerase chain reaction
Pia	<i>Pyricularia oryzae</i> resistance-a
Pik	<i>Pyricularia oryzae</i> resistance-k
PP2A	Protein phosphatase 2A

pRib-ADP	2'-(5''-phosphoribosyl)-5'-adenosine diphosphate
pRib-AMP	2'-(5''-phosphoribosyl)-5'-adenosine monophosphate
PRR	Pattern recognition receptor
PSR2	<i>Phytophthora sojae</i> suppressor of RNAi 2
PTI	PAMP-triggered immunity
PVX	<i>Potato Virus X</i>
R gene	Resistance gene
RanGAP2	Ran GTPase Activating Protein 2
RAR1	Required for Mla12 resistance 1
RBP1	Ran GTPase-binding protein 1
RGA	Resistance gene analog
RIN4	RPM1-interacting protein 4
RK	Receptor kinase
RLCK	Receptor-like cytoplasmic kinase
RLP	Receptor-like protein
Roq1	Recognition of XopQ 1
ROS	Reactive oxygen species
RP	Receptor protein
Rpi	Resistance to <i>Phytophthora infestans</i>
RPM1	Resistance to <i>Pseudomonas syringae</i> pv. <i>maculicola</i> 1.
RPP1	Recognition of <i>Peronospora parasitica</i> 1
RPP13	Recognition of <i>Peronospora parasitica</i> 13
RPS2	Resistance to <i>Pseudomonas syringae</i> 2
RPS4	Resistance to <i>Pseudomonas syringae</i> 4
RPS5	Resistance to <i>Pseudomonas syringae</i> 5
RPW8	RESISTANCE TO POWDERY MILDEW 8
RRS1	Resistance to <i>Ralstonia solanacearum</i> 1
Rx	Resistance to PVX
SAG101	Senescence-associated gene 101
SD	Solanaceous domain

SGT1	Suppressor of G2 allele of SKP1
SPRY	SP1a and Ryanodine receptor
SPRYSEC	SPRY secreted effector candidate
Sr35	Stem rust resistance 35
SSFR	Superstructure-forming repeats
STAND	Signal transduction ATPases with numerous domains
TALE	Transcription activator-like effector
TIR	Toll/Interleukin-1 receptor
TOL	Target of Myb 1-like
WHD	Winged-helix domain
ZAR1	HopZ-activated Resistance 1
ZED1	HopZ-ETI-deficient 1
ZRK1	ZED1-related kinases

Acknowledgements

Firstly, I would like to thank my PhD supervisor Sophien Kamoun for the past 5 years working under his supervision. My time in his lab has been truly life changing. His guidance and support have helped me grow as a scientist and for that I am forever grateful. Thank you for seeing potential in me that I didn't see in myself. Thank you for believing in people. Thank you for curating the amazing group of humans that is the Kamounity. You're the best, dude.

I would also like to thank my secondary supervisor, Mark Banfield, for being a consistently engaged, insightful and encouraging presence on my committee.

I am grateful to Lida Derevnina, my PostDoc supervisor during the first years of my PhD, for your mentorship, your support, and your friendship. To many more fruitful collaborations.

Thank you to Ola Bialas, Chih-Hang Wu, Aki Adachi, Joe Win, Juan Carlos de la Concepción, Thorsten Langner, Erin Zess, Adeline Harant and Jiorgos “Yolo Swag 420” Kourelis for all your wisdom, support, and patience in the first years of my PhD. Shoutout to the late arrivals, Daniel Lüdke, Cristina Barragan, Clem Marchal, Selva Muniyandi, Madhu Jogi and Yu Sugihara for even more wisdom, support and hopefully less patience in the second half. An extra special shoutout to Jiorgos for being my lab bro. Thank you Hsuan Pai for being a part of Pau, for having infinite patience and for all the teamwork. Thank you Jiorgos, Daniel and Clem for providing insightful comments and suggestions on this thesis. Much love to all the Kamounity members, past and present, for being a stimulating, caring and FUN research environment. You guys are the best. Thanks to all of you I achieved so much more than I could have ever achieved by myself.

To my first scientific mentors, María Eugenia Segretín and Tolga Bozkurt, thank you for believing in me, for building bridges and for providing me and so many others with invaluable opportunities.

I am grateful to Room 200 for the laughs and ridiculous conversations, the memes, the Zoo, the snacks, the fame, the shame, the lame and the CCBL. Sara “Sarantula” Dorhmi, Alexander “Big Al” McClelland, Josh “José Benito” Bennet, AmirAli “AmirAlinho” Toghani, Andrés “Andyman” Posbeyikian, Don Attilio Pascucci, Yufei “Boofei” Li, Jules “Julito” Claeys, Angus “Angoose” Malmgren and Lena “Gorillena” Knorr, you guys are awesome.

To the TSLytherins, thank you for being such a warm, welcoming, supportive and FUN student family. I am grateful for the community that we built together. Special shoutout to Camilla Molinari and Neftaly Cruz-Mireles for your friendship, positive energy, and support.

I am eternally grateful to all TSL members past and present for contributing to the inspiring, fast-paced and vibrant scientific environment that is TSL. What a special place this is. I am glad I got to be a part of it for a few years. Thank you to the Gatsby Charitable foundation for the financial support throughout my PhD.

I am eternally indebted to Big Al McClelland, Franziska “Ziska” Hoerbst, Carlos “El Topo” Gámez and Josh “Hullo” Waites for all the *fig jams*. Making music with you guys has been a blessing.

To the Fine City™, thank you for being my home for the past 5 years. Thank you to Mate and Hello Fresh for fuelling my scientific endeavours.

To my housemate Fede Alfano, thank you for the laughs, the good food and the fantastic, distant amorphisms.

To Lio Messi, Emiliano “Dibu” Martinez and the whole Argentina 2022 men’s football team, for providing an overwhelming dose of joy to 50 million Argentinians.

Thank you to the Carcosians, Fede Tedin and Juano Rodriguez Pereiro, my brothers, for existing and for always finding a way back to one another.

Big thank you to my family, my aunts, uncles, cousins, Ivan Medina and Valeria Rognitz. I love you guys.

To Diana Gómez De La Cruz: thank you for being there from day 1, for being my rock, my partner in crime and my best friend for the past 5 years. Couldn’t have made it without our silliness, our scientific discussions, our long walks here and there, and your company.

Most important of all, **thank you to my parents.**

To my mom Silvia, for her passion for life, her wisdom and for always believing in me. Thank you for teaching me to fight tooth and nail to pursue my dreams, even in the face of fear and uncertainty.

To my dad Mauricio, the most fun, caring, and creative person I ever met. Thank you for sharing your capacity to find beauty in all things with me. Your infinite sense of wonder is what has inspired me to become a scientist. This thesis is for you. I know you'd be proud.

Chapter 1: General Introduction

1.1 Overview of the plant immune system

Plants are constantly exposed to a variety of pathogens and pests. Plant pathogenic viruses, oomycetes, nematodes, bacteria and insects have evolved elaborate strategies to infect susceptible hosts and complete their life cycles. These strategies typically involve the production of virulence proteins, termed effectors, which can exert their function in the extracellular and intracellular space. Effectors allow pathogens to modulate host physiology in their favour and promote disease (Couto & Zipfel, 2016). However, most plants are resistant to most pathogens. This is because they have evolved a sophisticated multi-layered immune system which actively protects them against pathogen invasion. This immune system has historically been conceptualized as consisting of two layers (Jones & Dangl, 2006; Jones *et al.*, 2016; Ngou *et al.*, 2022a). The first layer is composed of cell-surface receptors which perceive the extracellular space. These receptors typically perceive conserved pathogen/microbe associated patterns (PAMP/MAMPs), such as the bacterial flagellin or the chitin that is usually found in fungal cell walls (Ngou *et al.*, 2022a). As such, they are also termed pattern recognition receptors. Cell-surface receptors, also termed pattern-recognition receptors (PRRs) belong to one of two major classes of trans-membrane proteins: receptor proteins (RPs) and receptor kinases (RKs). RPs carry a small cytoplasmic tail, but unlike RKs they lack a C-terminal kinase domain. Following perception of pathogen derived molecules, RPs and RKs initiate immune signaling by forming a complex with co-receptors, leading to a series of auto and trans-phosphorylation events (Macho & Zipfel, 2014). These RP and RK complexes also recruit receptor-like cytoplasmic kinases (RLCKs) which in turn phosphorylate downstream components and initiate a signaling cascade which leads to immune activation, accompanied by production of reactive oxygen species (ROS), cell wall fortification via callose deposition, calcium influx, transcriptional reprogramming, and accumulation of compounds with broad antimicrobial activity. This response is generally known as PAMP-triggered immunity (PTI) and in many cases is sufficient for the host to achieve disease resistance (DeFalco & Zipfel, 2021) (**Figure 1.1**).

To counteract the first layer of the plant immune system, many host-adapted pathogens deploy effectors to the host intracellular space which suppress PTI responses via diverse mechanisms (Couto & Zipfel, 2016). This allows pathogens to successfully colonize the host even following the activation of PTI. However, some intracellular effectors can trip the wire of the

second layer of immunity. This intracellular layer is largely composed of intracellular immune receptors known as nucleotide-binding and leucine-rich repeat (NLR) class (Kourelis & Van Der Hoorn, 2018). Effector recognition by NLRs leads to effector-triggered immunity (ETI) (**Figure 1.1**). ETI is a robust immune response usually accompanied by a form of programmed cell death, known as the hypersensitive response (HR) or hypersensitive cell death, also involving reactive oxygen species (ROS) production, calcium influx, transcriptional reprogramming and phytohormone production (Cui *et al*, 2015).

In the 1950s, Harold Flor first proposed a framework for host-pathogen interactions termed the gene-for-gene model, in which matching pairs of genes from a host and a pathogen determine the outcome of a given interaction (Flor, 1971). In many cases the presence of a single pathogen gene, termed avirulence (AVR) gene, triggers immunity in hosts carrying a single matching NLR gene, following the gene-for-gene model (Jones & Dangl, 2006; Ngou *et al*, 2022a). As such, plant parasites are under constant pressure from their hosts to diversify their effector gene repertoire to evade recognition while maintaining virulence. On the other hand, plants and their NLRs constantly evolve their resistance gene repertoire to keep up with rapidly evolving pathogens. This has resulted in tremendous genetic innovation, with NLR-coding genes being the most diverse genes in plants (Baggs *et al*, 2017; Barragan & Weigel, 2021; Clark *et al*, 2007). Over time, this evolutionary arms race has led to an increase in NLR complexity, with NLRs becoming sub-functionalized and evolving from single individual genetic units, or “singletons” to higher order configurations, such as NLR pairs or networks.

In NLR pairs and networks, multiple immune receptors work together to achieve robust immunity, with one NLR, termed sensor, mediating pathogen perception and cooperating with another NLR, termed helper, to activate downstream immune signaling. Unlike NLR pairs, which function in one-to-one sensor-helper connections, NLR networks simultaneously exhibit many-to-one and one-to-many functional sensor-helper connections, likely contributing to increased robustness and evolvability of the plant immune system (Adachi *et al*, 2019b; Feehan *et al*, 2020; Wu *et al*, 2017; Wu *et al*, 2018). Traditionally, cell-surface receptors and NLRs were thought to induce distinct immune pathways. However, there is an increasing body of work which suggests an intricate crosstalk between the signaling pathways induced by cell surface and intracellular immune receptors. Cell-surface receptors and NLRs have been shown to act in concert and synergize with each other, with NLRs even executing cell death downstream of cell-surface signaling (Kourelis *et al*, 2022; Ngou *et al*, 2021; Ngou *et al*, 2022b; Schulze *et al*, 2022; Yuan *et al*,

2021). The conceptual framework of PTI and ETI therefore needs to be expanded. What used to be considered as two separate branches of plant immunity now appear as two interconnected pathways, providing the plant with robust immunity.

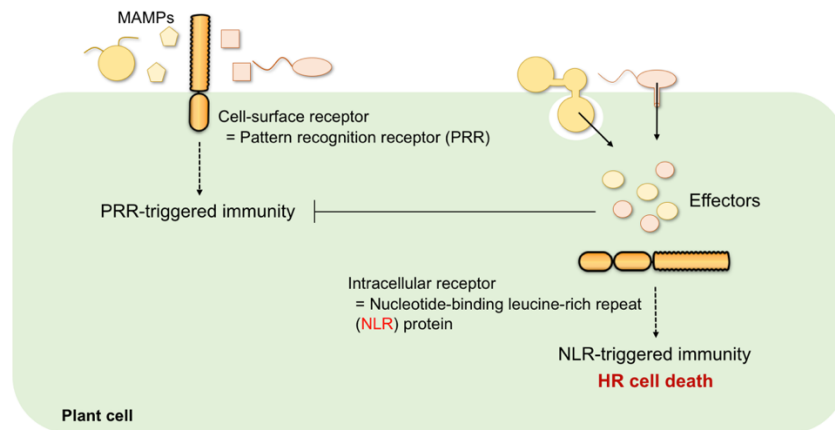


Figure 1.1: The plant immune system.

Plants possess a multi-layered immune system. The first tier involves pattern recognition receptors that perceive pathogen/microbe-associated molecular patterns (PAMP/MAMPs), triggering PRR-triggered immunity (PTI). The second tier involves the perception of intracellular pathogen effectors by NLR proteins, resulting in Effector/NLR-triggered immunity. ETI/NLR-triggered immunity is usually accompanied by a form of programmed cell-death known as the hypersensitive response or hypersensitive cell death. Adapted from Win *et al.* (2012).

1.2 What are NLRs?

NLR proteins are found across all kingdoms of life and exhibit a conserved tripartite modular domain architecture (Duxbury *et al.*, 2021; Gao *et al.*, 2022; Kibby *et al.*, 2023; Uehling *et al.*, 2017). In their broadest definition, they are STAND (signal transduction ATPases with numerous domains) proteins comprised of an N-terminal domain, a central nucleotide-binding and oligomerization domain (NOD) and C-terminal superstructure-forming repeats (SSFRs) (Dyrka *et al.*, 2020; Kourelis *et al.*, 2021). N-terminal domains are usually thought of as signaling domains and often mediate the downstream programmed cell death response following immune receptor activation (Duxbury *et al.*, 2021). Whereas metazoan and prokaryotic NLRs usually typically exhibit a central NACHT (NAIP, C2TA, HET-E and TP1) module, the plant NLR NOD is exclusively an NB-ARC (nucleotide-binding adaptor shared by APAF-1, certain R gene products, and CED-

4) module. C-terminal SSFRs are typically leucine rich repeat (LRR) domains (Kibby *et al.*, 2023; Kourelis *et al.*, 2021).

Plant NLRs, like most STAND proteins, are molecular switches (Takken *et al.*, 2006). They exist in an inactive ADP-bound resting state and conditionally initiate immune signaling upon perception of non-self or modified-self (Gao *et al.*, 2022; Jones *et al.*, 2016; Takken & Goverse, 2012). The central NB-ARC module is critical for mediating conformational changes required for switching between inactive to active states, primarily through the exchange of ADP for ATP at its nucleotide binding pocket (Takken *et al.*, 2006; Wang *et al.*, 2019b). While the C-terminal LRRs is a main determinant in pathogen perception, it also mediates critical autoinhibitory intra-molecular interactions that help keep the receptor in an inactive state prior to activation. Following activation and release of intramolecular auto-inhibition, the N-terminal domains can subsequently mediate downstream immune signaling and likely contribute to stabilization of the activated state (Förderer *et al.*, 2022; Martin *et al.*, 2020; Takken & Goverse, 2012). Following pathogen perception, metazoan and plant NLRs oligomerize into higher order complexes termed inflammasomes or resistosomes, respectively, which lead to induced proximity of the N-terminal signaling domains to activate immunity. More recently, prokaryotic NLR-like proteins have also shown to activate via oligomerization based mechanisms, leading to the assembly of tetrameric resistosome-like complexes (Gao *et al.*, 2022). This indicates that NLRs across all kingdoms of life share similar activation strategies.

1.2.1 N-terminal signaling domains.

N-terminal domains in NLRs have been implicated in signal-transduction, NLR self-association and interactions with co-factors. An emerging concept is that NLR activation and oligomerization leads to induced proximity of these domains, allowing them to execute their signaling functions. Plants NLRs are characterised by distinct N-terminal signaling domains, which can be used to broadly classify NLRs into distinct groups. These groups often follow the phylogeny of the NB-ARC domain (Kourelis *et al.*, 2021). To date, four main N-terminal signaling domains have been characterized in angiosperms: Coiled-coil (CC)-type, RESISTANCE TO POWDERY MILDEW 8 (RPW8)-type (CC_R), G10-type CC (CC_{G10}) and toll/interleukin-1 receptor-type (TIR) (Kourelis *et al.*, 2021). NLRs in non-flowering plants can carry additional types of N-terminal domains, such as α/β hydrolases and kinase domains (Andolfo *et al.*, 2019; Chia *et al.*, 2022). In

general, the class of N-terminal domain is thought to dictate the NLR downstream signaling pathways and activities following effector perception.

In plant NLRs, the N-terminal CC, CC_R and CC_{G10}-domains can mediate intramolecular interactions that prevent misactivation and contribute to immune receptor stabilization (Bentham *et al.*, 2018). Unlike CC_R and CC_{G10} domains, CC domains feature a conserved EDVID motif, which is important for NLR function and mediates critical interactions with the LRR domain (Förderer *et al.*, 2022; Rairdan *et al.*, 2008). Acidic residues in the EDVID motif interact with a conserved patch of arginine residues in the LRR, termed the LRR^{R-cluster}. This CC^{EDVID}-LRR^{R-cluster} interaction, also termed the EDVID clamp, is proposed to be a conserved NLR stabilization mechanism which allows for conformational rearrangements in the NB-ARC domain while maintaining the CC domain and the LRR domain in close proximity (Förderer *et al.*, 2022). Introducing mutations in the EDVID motif can lead to loss of NLR function or autoactivation (Bai *et al.*, 2012). The CC and CC_{G10}-domains of some NLRs have been shown to mediate association with co-factors that are essential for function of the receptor, contributing to pathogen perception and immune signaling (El Kasmi *et al.*, 2017; Mackey *et al.*, 2003; Sacco *et al.*, 2009; Sacco *et al.*, 2007).

N-terminal CC, CC_R and CC_{G10} domains of NLRs have been implicated in cell death induction, with multiple studies reporting that expressing these domains on their own can be sufficient to trigger cell death in the absence of the rest of the NLR (Bentham *et al.*, 2018). Activated CC-NLRs and CC_R-NLR have been shown to act as calcium permeable channels. CC and CC_R domains form a four-helical bundle, which encodes conserved, negatively charged residues which are important for calcium channel activity (Bi *et al.*, 2021; Förderer *et al.*, 2022; Jacob *et al.*, 2021). Recently, the ZAR1 structure revealed that the α 1-helix of this four-helix bundle undergoes a conformational change upon NLR activation, flipping out of the bundle (Wang *et al.*, 2019a; Wang *et al.*, 2019b). Upon resistosome assembly, the five α 1-helices assemble a funnel like structure which inserts itself into the plasma membrane to trigger cell death and calcium influx (Bi *et al.*, 2021; Wang *et al.*, 2019a; Wang *et al.*, 2019b). This has been termed the “death switch” model (Adachi *et al.*, 2019c).

In plants, TIR only, TIR-NB and TIR-NLR proteins act as important mediators of plant immunity (Locci *et al.*, 2023). In the case of TIR-NLRs, the NLR oligomerisation leads to the assembly of a tetrameric NLR resistosome in which the TIRs form a dimer of dimers, as revealed by the Cryo-EM structures of the activated Roq1 and RPP1 complexes (Ma *et al.*, 2020; Martin *et*

al., 2020). This TIR-NLR tetramer acts as a holoenzyme, with the TIR domains exhibiting NADase activity and producing a suite of small molecules which activate the TIR-NLR signaling pathway (Huang *et al.*, 2022; Jia *et al.*, 2022). The small molecules produced by active TIR-NLR holo-enzymes ultimately lead to activation of CC_R-NLRs which act as the final executors of cell death. Unlike CC and CC_R-NLRs, TIR-NLRs resistosomes do not trigger cell death on their own.

1.2.2 The NB-ARC domain.

The central NB-ARC module is the defining feature of the plant NLR protein family. It is the most conserved region among distantly related NLRs and as such is often used to determine evolutionary relationships between plant NLRs (Kourelis *et al.*, 2021). It consists of three domains: the nucleotide binding (NB) domain, the helix domain-1 (HD1) and the winged-helix domain (WHD). The HD1 and WHD have also been referred to as ARC1 and ARC2, respectively. Together, these three subdomains form an ATP binding pocket, which is critical for NLR activities. The NB domain features the Walker A or p-loop motif (GxxxxGK[T/S]) which mediates ADP/ATP binding, and the Walker B motif (hhhDD/E) which coordinates Mg²⁺ and cooperates with the Walker A motif to mediate nucleotide binding and hydrolysis (Bonardi *et al.*, 2012; Takken *et al.*, 2006). The p-loop is glycine rich and features an invariant lysine residue which binds the phosphates of the nucleotide (Saraste *et al.*, 1990). Mutations in this invariant lysine reduce ATP binding and/or hydrolysis of multiple NLRs and usually lead to loss-of-function, highlighting the importance of nucleotide binding in NLR activities (Ahn *et al.*, 2023; Derevnina *et al.*, 2021; Tameling *et al.*, 2002; Williams *et al.*, 2011). The HD1 and WHD also play an important role in regulating NLR signaling and activation. The HD1 contains the conserved GxP (GLPL) motif which was shown to be important for the activity of Rx and RPM1 (Bendahmane *et al.*, 2002; Tornero *et al.*, 2002). The WHD contains a conserved methionine-histidine-aspartate (MHD) motif which also coordinates nucleotide binding and regulates NLR activation states (Van Ooijen *et al.*, 2008). Mutations in the conserved residues of the MHD motif often results in constitutively active NLR variants, also referred to as autoactive NLRs (Bendahmane *et al.*, 2002; Van Ooijen *et al.*, 2008).

Within NLRs, the NB-ARC domain acts as a molecular switch. Recent Cryo-EM structures of the *Arabidopsis* CC-NLR ZAR1 and TIR-NLR RPP1, the wheat CC-NLR Sr35, and the *Nicotiana benthamiana* TIR-NLR Roq have provided invaluable insights into NB-ARC dynamics upon NLR activation. In the inactive state, many intramolecular interactions between the NB, HD1 and WHD

keep the nucleotide binding pocket in a closed, ADP-bound conformation (Burdett *et al.*, 2019; Wang *et al.*, 2019b). Interaction with the ADP molecule also contributes to further stabilizing the NLR in an inactive conformation, preventing misactivation. Pathogen perception mediated by other domains in the NLR allosterically disrupts these intramolecular interactions and triggers a series of conformational changes in the NB-ARC domain. This is reminiscent to what was previously shown in metazoan NLRs, which also undergo large-scale structural rearrangements mediated by their central NACHT domain (Hu *et al.*, 2015; Zhang *et al.*, 2015). Effector recognition in the NLR has been shown to lead to a steric clash with the NB domain, causing it to move relative to the HD1 and WHD, rotating outwards using a loop that connects the NB with the HD1 as a hinge. This in turn leads to ADP release, priming the NLR for oligomerization (Förderer *et al.*, 2022; Wang *et al.*, 2019b). This priming also serves to rotate the nucleotide binding site away from the MHD motif, which is ADP-specific, facilitating ATP binding. Following ATP binding, the primed NLR protomer undergoes subsequent conformational changes in its NB-ARC, with the WHD rotating 180 degrees around the hinge linking the WHD and HD1 units, exposing interfaces critical for oligomerization. The NB-HD1 surface of one protomer intercalates with the NB-WHD surface of another protomer, driving oligomerization. Ultimately, this leads to the assembly of a mature signaling competent resistosome complex (Martin *et al.*, 2020; Wang *et al.*, 2019a; Wang *et al.*, 2019b).

Interestingly, while the NB-ARC is mostly thought of as a molecular switch and not a signaling domain in plant NLRs, the NB domains and NB-ARC domains of some plant NLRs on their own have been shown to trigger cell death when heterologously overexpressed (De Oliveira *et al.*, 2016; Rairdan *et al.*, 2008). Whether this is due to interaction and activation of other, endogenous NLRs or whether this is due to small molecules derived from ATPase activity of these domains is not known.

1.2.3 C-terminal LRR domain.

LRR domain-containing proteins are found in many protein families across all kingdoms, and are typically involved in protein-ligand interactions (Ng & Xavier, 2011). LRR domains are found at the C-terminus of plant NLRs and are defined by the presence of multiple “LxxLxxLxxNxL” motif-containing repeats, which give the domain its name (Wei *et al.*, 2008). A single LRR domain can contain between 2 or 45 repeats, with the number of repeats and overall length of each individual repeat being quite variable. Despite this variability, LRRs exhibit

conserved parallel rigid β -sheets which act as a scaffold, forming a horseshoe shape in the case of NLRs and a more elongated, rod-like shape in the case of cell-surface receptors, with residues in between LRR units being surface exposed. This characteristic structure is shared among a wide variety of receptor families, including plant and metazoan NLRs as well as LRR-containing cell-surface receptors from plants (Förderer *et al.*, 2022; Martin *et al.*, 2020; Sun *et al.*, 2022; Wang *et al.*, 2019a; Wang *et al.*, 2019b; Zhang *et al.*, 2015).

In NLRs, LRR domains have been proposed to mediate pathogen perception and to function as autoinhibitory domains, keeping NLRs inactive via intramolecular interactions. Prior to immune receptor activation, the LRR domain interacts with the NB-ARC and N-terminal domains, contributing to keeping the nucleotide-binding pocket in a closed, ADP bound state (Moffett *et al.*, 2002; Rairdan & Moffett, 2006; Takken *et al.*, 2006). Truncation of the LRR can lead to autoactivity in some NLRs, presumably due to removal of autoinhibition (Bai *et al.*, 2012). This autoinhibition is relieved upon pathogen perception, which LRR domains can play an important role in (Duxbury *et al.*, 2021). Some NLRs have been shown to directly bind pathogen effectors via their LRR domain, as is the case for the CC-NLR Sr35, and the TIR-NLRs Roq1 and RPP1 (Förderer *et al.*, 2022; Ma *et al.*, 2020; Martin *et al.*, 2020). In other examples, the LRR interacts with host proteins required for pathogen perception, as has been shown for ZAR1 (Wang *et al.*, 2019a). Upon ligand binding, steric clashes release the LRR-mediated autoinhibition, leading to NLR activation and oligomerisation (Förderer *et al.*, 2022; Ma *et al.*, 2020; Martin *et al.*, 2020; Wang *et al.*, 2019a). In support of this, LRRs show very low levels of conservation and tend to be highly polymorphic, potentially due to co-evolution with their corresponding ligands (Prigozhin & Krasileva, 2021; Van de Weyer *et al.*, 2019). It should be noted that most of our understanding of LRR domain functions is derived from the study of singleton NLRs. How the LRR domain functions in paired or networked NLRs is not understood.

1.2.4 NLR diversity.

In addition to their role in plant defence, NLRs have also been the subject of extensive investigation in the field of evolutionary biology, as they have undergone rapid evolution and diversification in response to strong selection pressures from rapidly evolving pathogens. Large-scale comparative phylogenomic analyses have revealed that NLR-encoding genes are some of the most diverse and quickly evolving in plant genomes (Barragan & Weigel, 2021; Clark *et al.*, 2007; Prigozhin & Krasileva, 2021). They occur in all major groups of flowering plants (angiosperms)

and non-flowering plants, with some NLR-like genes being found in green algae (Andolfo *et al.*, 2019; Chia *et al.*, 2022; Shao *et al.*, 2019). This phylogenetically informed view of NLRs revealed that they are diverse in many ways. The number of NLRs varies greatly across species, ranging from ~50 in watermelon (*Citrullus lanatus*) and papaya (*Carica papaya*) to >1000 in apple (*Malus domestica*) and hexaploid wheat (*Triticum aestivum*) (Baggs *et al.*, 2017; Jia *et al.*, 2015; Steuernagel *et al.*, 2020). NLRs exhibit lineage-specific expansions and contractions, which usually occur through tandem duplication and/or deletion events in each species, often influenced by transposon content, ecological context and adaptation to their environment (Baggs *et al.*, 2017; Barragan & Weigel, 2021). NLR genes also exhibit tremendous intraspecific diversity, exhibiting presence/absence variation and heterogeneity in allelic variation, largely due to point mutations, intra-allelic recombination and domain fusions or swaps (Lin *et al.*, 2022a; MacQueen *et al.*, 2019; Maekawa *et al.*, 2019; Prigozhin & Krasileva, 2021; Seeholzer *et al.*, 2010; Seong *et al.*, 2020; Shimizu *et al.*, 2022; Van de Weyer *et al.*, 2019).

The recently generated RefPlantNLR collection of over 400 experimentally validated NLRs nicely illustrates our current grasp of NLR diversity in terms of domain architecture and function, showcasing that plants have evolved NLRs to detect effectors from most plant pathogenic organism (Kourelis *et al.*, 2021). Importantly, looking at the plant species represented in the RefPlantNLR dataset highlighted that most NLRs characterized to date come from a relatively small pool of flowering plant species. Our understanding of broader NLR domain structure and molecular function, in particular outside of crop and model plant species or in nonflowering plants is therefore limited. Only recently, a study by Chia *et al.* (2022) functionally characterized NLRs and NLR signaling domains from basal land plants and algae, revealing that there are indeed shared NLR activities spanning the whole spectrum of plant evolution (Chia *et al.*, 2022). Notably, this study leveraged transient heterologous expression in *Nicotiana benthamiana* as a powerful tool to perform functional screens of N-terminal CC, CC_R and TIR-type signaling domains from divergent algal and plant genomes. They found that many of these retained the capacity to trigger HR cell death like their angiosperm counterparts. This indicates that some NLR signaling domains and their functions arose early during plant evolution and have retained these functions over long evolutionary time (Chia *et al.*, 2022). Nonetheless, much NLR functional diversity in underrepresented or understudied plant species remains to be explored.

1.3 NLRs are intracellular sensors of invading pathogens.

1.3.1 NLRs can directly recognise pathogen effectors.

Plant NLRs sense intracellular effectors delivered by pathogens during infection and subsequently trigger an immune response. The strategies by which NLRs recognize effectors can generally be divided into two categories: direct and indirect recognition. Direct recognition of effectors follows a receptor-ligand model, with one NLR protein binding one effector molecule (Baggs *et al.*, 2017). For example, the wheat CC-NLR Sr35 directly binds the effector AvrSr35 via its LRR domain. Effector binding relieves intramolecular autoinhibition in Sr35 and triggers conformational rearrangements which lead to Sr35 activation (Förderer *et al.*, 2022; Zhao *et al.*, 2022). The TIR-NLRs RPP1 from *Arabidopsis* and Roq1 from *N. benthamiana* also recognise their cognate effectors via direct binding. RPP1 recognises the effector ATR1 from the oomycete *Hyaloperonospora arabidopsidis* while Roq1 recognizes the *Xanthomonas perforans* effector XopQ. In both cases, effector binding occurs in the LRR, assisted by a post-LRR region found in some TIR-NLRs, known as the C-terminal jelly roll and Ig-like domain (C-JID). Effector binding by RPP1 and Roq1 also induces conformational rearrangements leading to NLR activation and downstream signaling (Ma *et al.*, 2020; Martin *et al.*, 2020).

Sr35, RPP1 and Roq1 are well studied cases in which Cryo-EM structures of NLRs in complex with their cognate effectors have resolved the ligand binding interfaces with intricate detail, but many additional examples of NLRs that directly recognize effectors exist (Bauer *et al.*, 2021; Catanzariti *et al.*, 2010; Chen *et al.*, 2017; Dodds *et al.*, 2006; Jia *et al.*, 2000; Zhu *et al.*, 2017). In most of these examples, the LRR domain plays a critical role in determining effector recognition specificity. For the tomato CC-NLR Sw-5b, which directly recognizes the NSm viral protein of different tospoviruses (Peiró *et al.*, 2014; Zhu *et al.*, 2017) the LRR also plays a key role in effector binding, although an additional domain located before the N-terminal CC domain, known as the Solanaceous domain (SD) also contributes to direct interaction with the effector (Zhu *et al.*, 2017).

1.3.2 Indirect recognition: the guardee/decoy model.

While direct recognition of effectors by NLRs would seem like the most intuitive and simple strategy to perceive pathogens, there are comparatively more examples in which effectors are indirectly recognized. Some NLRs can monitor or “guard” host components targeted by pathogen effectors, which are therefore termed “guardees” (Jones & Dangl, 2006). The CC-NLR Prf from tomato guards the host kinase Pto by sensing its interaction with the bacterial effectors

AvrPto and AvrPtoB to trigger Prf-dependent immune signaling (Kim *et al.*, 2002). RPS5 CC_{G10}-NLR from *Arabidopsis* guards the host kinase PBS1. Cleavage of PBS1 by the bacterial protease AvrPphB leads to RPS5-mediated immunity (Ade *et al.*, 2007). In their attempts to manipulate host physiology and immunity, different effectors either from the same, or from phylogenetically unrelated pathogens, sometimes converge on the same host proteins to promote disease (Derevnina *et al.*, 2021; Macho & Zipfel, 2015; Mukhtar *et al.*, 2011; Petre *et al.*, 2021; Song *et al.*, 2009). One example is the recognition of the *P. syringae* effectors AvrRpm1, AvrB and AvrRpt2. These three effectors modify the host protein RPM1-interacting 4 (RIN4), phosphorylating it in the case of AvrRpm1 and AvrB or cleaving it in the case of AvrRpt2. In turn, the CC-NLR RPM1 and the CC_{G10}-NLR RPS2 guard RIN4, sensing its phosphorylation or cleavage, respectively, leading to immunity (Axtell & Staskawicz, 2003; Mackey *et al.*, 2003).

A derivation of the guard-guardee model is the decoy model. Whereas some NLR gardees are functional host proteins with discernible physiological roles, decoys are host proteins which evolved to bait pathogen effectors, without other clear functions in host physiology (van der Hoorn & Kamoun, 2008). For example, ZAR1 can recognize a range of bacterial effectors through its partner receptor-like cytoplasmic kinases (RLCKs), also termed ZED1-related kinases (ZRKs) (**Figure 1.3**) (Adachi *et al.*, 2020; Laflamme *et al.*, 2020; Schultink *et al.*, 2019; Seto *et al.*, 2017; Wang *et al.*, 2015a). ZED1 and RKS1 are two such RLCKs, which constitutively form a complex with ZAR1. The *Xanthomonas campestris* *pv. campestris* effector HopZ1a acetylates ZED1, and this modification is sensed by ZAR1, triggering its activation. The effector AvrAC from *P. syringae* uridylylates the RLCK PBL2. This modified PBL2 then conditionally interacts with the pre-formed ZAR1-RKS1 complex, triggering an immune response. Because ZED1 is a pseudokinase and PBL2 uridylylation does not enhance AvrAC-mediated virulence, these host proteins are considered decoys (Lewis *et al.*, 2013; Wang *et al.*, 2015a).

How does indirect recognition aid in keeping up with rapidly evolving pathogen effectors? Indirect effector recognition allows plants to maximize the efficacy of a fixed number of immune receptors. NLRs that indirectly recognize pathogens by guarding common virulence targets are more versatile than direct effector binders, as they hold the potential to recognize multiple effectors simultaneously, even if these effectors are structurally or sequence unrelated. Moreover, outsourcing of effector interactions by NLRs to guardee/decoys is favourable as these are often less evolutionarily constrained than NLRs. Guardee/decoys can potentially accumulate a higher

number of mutations without the risk of losing functionality, allowing them to better keep up with rapidly evolving effectors.

1.3.3 NLR-IDs: NLRs with unconventional integrated domains

Moving beyond the canonical tri-partite domain architecture, around 10% of the NLRome of a given plant species consists of NLRs with additional integrated domains (IDs), which often correspond to effector modified host target proteins (Sarris *et al*, 2016). Within the NLR, IDs are involved in effector sensing, either via direct or indirect recognition (De la Concepcion *et al*, 2018; Fujisaki *et al*, 2015; Maqbool *et al*, 2015). The integrated decoy hypothesis postulates that over evolutionary time, host targets of effectors are genetically integrated within NLRs, baiting pathogen effectors to activate host immunity (Cesari *et al*, 2014). The well characterized rice CC-NLRs Pik-1 and RGA5 feature an additional integrated heavy metal-associated (HMA) domain which directly interacts with various effectors from the rice blast fungus, *Magnaporthe oryzae*, to mediate disease resistance. These NLRs can directly recognize multiple *M. oryzae* effectors: Pik-1 recognizes AVR-Pik and AVR-Mgk1, while RGA5 recognizes AVR1-CO39 and AVR-Pia (Cesari *et al*, 2013; De la Concepcion *et al*, 2018; Guo *et al*, 2018; Maqbool *et al*, 2015; Sugihara *et al*, 2023).

Identification of the host targets of effectors recognized by NLR-IDs supported the hypothesis that IDs are derived from host target integration. For both, Pik-1 and RGA5, the cognate effectors are sequence unrelated but share a conserved structural fold, termed the MAX fold (Magnaporthe AVRs and ToxB-like) (de Guillen *et al*, 2015). MAX fold effectors have been shown to bind endogenous "non-integrated" HMA domain-containing proteins from the host, supporting that over evolutionary time HMAs integrated into NLRs because they were frequently targeted by MAX effectors (Bentham *et al*, 2021; Bialas *et al*, 2021; Maidment *et al*, 2021; Oikawa *et al*, 2020). Another well-studied example is the RRS1 TIR-NLR from *Arabidopsis* which features a C-terminal integrated WRKY transcription factor-like domain. The bacterial effectors AvrRps4 from *P. syringae* and PopP2 from *Ralstonia solanacearum* can modify host WRKY transcription factors to promote disease (Le Roux *et al*, 2015; Pandey & Somssich, 2009; Sarris *et al*, 2015). The C-terminal integrated WRKY domain of RRS1 acts as a bait for these effectors, as RRS1 can sense its modification to activate immunity (Le Roux *et al*, 2015; Mukhi *et al*, 2021). Interestingly, all NLR-IDs functionally characterized to date require a second, genetically linked, NLR to confer disease resistance and are therefore known as a "paired" NLRs (Adachi *et al*, 2019b; Cesari *et al*, 2014)

Many diverse domains have been found in fusion to NLRs, suggesting that there is a degree of flexibility in terms of what domains can potentially be integrated into NLRs (Marchal *et al.*, 2022a; Sarris *et al.*, 2016). A striking case is the *Pias* allelic series from the *Oryza* genus. In this example, alleles of the same NLR exhibit different integrations, including HMA domains, protein-kinase domains or WRKY domains (Shimizu *et al.*, 2022). While recent works have shed light on how IDs evolve following integration, and how intramolecular ID-NLR scaffold interactions shape NLR-ID function (Bialas *et al.*, 2021; De la Concepcion *et al.*, 2021), how NLRs evolve to accommodate novel domains is not fully understood.

1.3.4 NLR bioengineering: new recognition specificities

For some economically important pathogens, few or no *R*-genes have been identified to date. Furthermore, *R*-genes that are deployed in the field can often be quickly defeated as pathogens evolve to evade recognition. This has fuelled attempts to bioengineer made-to-order NLR immune receptors to achieve durable and versatile disease resistance (Cesari *et al.*, 2022; De la Concepcion *et al.*, 2019; Farnham & Baulcombe, 2006; Förderer *et al.*, 2022; Giannakopoulou *et al.*, 2015; Huang *et al.*, 2021a; Kim *et al.*, 2016a; Liu *et al.*, 2021; Maidment *et al.*, 2022; Segretin *et al.*, 2014; Tamborski *et al.*, 2023; Wang *et al.*, 2021). Most attempts at NLR engineering to date have been aimed at obtaining novel disease resistance specificities, a topic that has been reviewed in depth by Marchal and colleagues (Marchal *et al.*, 2022b). In particular, many approaches have focused on NLR-ID engineering, specifically by re-surfacing the structure of IDs by amino acid substitution or by swapping IDs for other closely related proteins to expand the effector recognition specificities of IDs (Bentham *et al.*, 2022; Cesari *et al.*, 2022; De la Concepcion *et al.*, 2019; Liu *et al.*, 2021; Maidment *et al.*, 2022).

More recently, the *Pia* allelic series of NLRs with its diverse IDs suggested that a given NLR scaffold may be able to accommodate the fusion of novel or unrelated domains (Shimizu *et al.*, 2022). In a recent proof-of-concept study, Kourelis and colleagues showed that the integrated HMA domain of the Pik-1 sensor NLR can be replaced with camelid-derived nanobodies, retaining signaling via its downstream helper Pik-2 (Kourelis *et al.*, 2023). These engineered immune receptor pairs, termed Pikobodies, recognize fluorescent proteins (FPs) GFP and mCherry, leading to NLRs with novel, completely synthetic recognition specificities. This implies that NLRs could in theory be developed to recognise any antigen that nanobodies can be raised against, combining

animal adaptive immunity with plant innate immunity. Pikobodies were also shown to confer resistance to FP-expressing strains of *Potato Virus X* (PVX) in transgenic lines to levels comparable to the naturally occurring PVX R-gene, the NLR Rx (Kourelis *et al.*, 2023). This was an important observation, as there are examples of synthetic NLR immune receptors which work in transient assays, but fail to deliver resistance when stably transformed into plant genomes (Cesari *et al.*, 2022; Wang *et al.*, 2021). Importantly, engineering the Pikobody system required the ample breadth of previous knowledge regarding the genetics, biochemical activities and specifically, the evolution of the Pik-1/Pik-2 system and its ID (Białas *et al.*, 2021; De la Concepcion *et al.*, 2021; De la Concepcion *et al.*, 2018; Zdrzałek *et al.*, 2020). This highlights how critical a fundamental understanding of NLR function and evolution is towards developing novel approaches for disease resistance engineering.

1.4 NLR signaling configurations: singletons and pairs.

1.4.1 Singleton NLRs.

Some NLRs function as individual genetic units and are termed singleton NLRs. These can directly or indirectly perceive pathogen effectors and induce a downstream immune response without relying on an additional NLR (**Figure 1.2, Figure 1.3**) (Adachi *et al.*, 2019a). Well studied immune receptors in this category include the CC-NLRs ZAR1 from *Arabidopsis* and Sr35 from wheat. As mentioned previously, ZAR1 indirectly recognizes its cognate effectors via its guardee/decoy RLCKs, while Sr35 recognises AvrSr35 via direct interaction with its LRR (Förderer *et al.*, 2022; Wang *et al.*, 2019a; Zhao *et al.*, 2022). Other NLRs that are considered likely singletons based on their capacity to sense effectors and trigger hypersensitive cell death in heterologous plant systems include Sr50, several NLRs in the MLA allelic series, RPS5, RPP13 and L6 (Chen *et al.*, 2017; Maekawa *et al.*, 2019; Qi *et al.*, 2012; Ravensdale *et al.*, 2012; Saur *et al.*, 2019). To this end, *Agrobacterium tumefaciens*-mediated transient expression of NLR proteins in leaves of *N. benthamiana* has been a useful resource with which to test immune receptor activities heterologously. If an NLR from an unrelated species is capable of triggering cell death in *N. benthamiana*, this suggests it functions as a singleton or a helper. Although this test is not definitive and depends on the degree of conservation of potential downstream signaling partners, decoys or guardees, it is a good first approach to classify NLRs into functional categories and further exemplifies how *N. benthamiana* can be an excellent system with which to quickly functionally characterize and categorize NLRs (Adachi *et al.*, 2019b; Derevnina *et al.*, 2019).

1.4.2 Paired NLRs.

In paired NLR systems, one immune receptor is specialized in pathogen perception, acting as a sensor and requires a downstream executor or helper NLR to induce immune signaling. Some well-studied “model” paired NLR systems include the rice Pik-1/Pik-2 and RGA5/RGA4 CC-NLR pairs and the *Arabidopsis* RRS1/RPS4 TIR-NLR pair. The genes coding for the Pik-1 NLR-ID and its helper NLR Pik-2 are found in head-to-head orientation and are both required for resistance to *M. oryzae*. Pik-1 binding to *M. oryzae* effectors leads to activation of immunity via its helper Pik-2, with both NLRs working cooperatively to mediate disease resistance (De la Concepcion *et al.*, 2021; Zdrzalek *et al.*, 2020). Pik-1 is unable to trigger cell death in the absence of its downstream helper Pik-2. In the case of RGA5 and its helper RGA4, these NLRs work by negative regulation rather than by cooperation (Césari *et al.*, 2014). The RGA4 helper has been shown to be constitutively active, triggering cell death when heterologously expressed in *N. benthamiana* (Césari *et al.*, 2014). Co-expression of its sensor NLR-ID mate RGA5 can suppress this constitutive activity. Upon effector binding by RGA5, this negative regulation is released and RGA4 mediates immune signaling and disease resistance (Césari *et al.*, 2014).

The genetically linked *Arabidopsis* TIR-NLR pair RRS1/RPS4 similarly works via negative regulation. RPS4 is constitutively active in *Arabidopsis*, and its sensor RRS1 acts as a repressor. RRS1 inhibition of RPS4 is conditionally relieved upon effector perception. While RRS1 and RPS4 are genetically linked paired NLRs, they require a downstream genetically unlinked helper CC_R-NLR, N requirement gene 1 (NRG1), to confer disease resistance (**Figure 1.2, Figure 1.3**). In this case, RPS4 is termed an executor NLR rather than helper, as the term helper is associated with a CC or CC_R-type NLR acting downstream of a sensor (Gong *et al.*, 2023). These, as well as additional examples of paired NLR systems have been extensively reviewed (Adachi *et al.*, 2019b; Feehan *et al.*, 2020; Gong *et al.*, 2023; Marchal *et al.*, 2022a; Xi *et al.*, 2022).

1.5 NLR networks: the next step in NLR evolution.

In some cases, NLRs have evolved more complex connections beyond paired sensor-helper configurations. Cases in which more than two NLRs are connected functionally are referred to as NLR networks (Adachi & Kamoun, 2022; Duxbury *et al.*, 2021; Kourelis & Adachi, 2022; Wu *et al.*, 2017). Networked NLRs are usually genetically unlinked yet phylogenetically related and exhibit

a sensor and helper dynamic (**Figure 1.2, Figure 1.3, Figure 1.4**). Unlike paired NLRs which exhibit one-to-one connections, some NLR network components exhibit “one-to-many” and “many-to-one” signaling architectures. Different sensors can converge on one downstream helper and each individual sensor can signal redundantly via more than one helper (Wu *et al.*, 2018). Helpers themselves are not fully redundant, as they exhibit a degree of functional specialization, both in terms of compatibility with upstream sensors and of downstream signaling (Saile *et al.*, 2020; Wu *et al.*, 2017). NLR networks combine the higher degree of receptor evolvability conferred by sensor-helper specialization, as seen in paired NLR systems, with the robustness conferred by genetic redundancy at the helper level (**Figure 1.3**) (Adachi *et al.*, 2019b; Castel *et al.*, 2019; Gong *et al.*, 2023; Wu *et al.*, 2017; Wu *et al.*, 2018).

1.5.1 The NRC NLR-PRR network.

In Solanaceous plants, helper CC-NLRs known as NRCs (NLR Required for Cell death) are genetically required for immune signalling by a multitude of sensor CC-NLRs and cell-surface receptors that mediate perception of diverse pathogens, including oomycetes, fungi, nematodes, viruses, and bacteria (Derevnina *et al.*, 2021; Kourelis *et al.*, 2022; Oh *et al.*, 2023; Wu *et al.*, 2017). Together, NRCs and their sensor NLR mates form the NRC superclade, a well-supported phylogenetic cluster divided into NRC helper clades and 2 large clades that include all known NRC-dependent sensors. These 2 large clades are termed the Rx-type clade and the SD-type clade. The Rx-type clade contains the PVX R protein Rx and other NRC-dependent sensors with N-terminal CC-domains. The SD-type clade contains NRC-dependent sensors with N-terminally fused SDs, such as the oomycete R protein Rpi-blb2.

In *N. benthamiana*, NRC2, NRC3 and NRC4 act as key nodes in this network (Wu *et al.*, 2017). Some sensors in this network, Rx and the bacterial R protein Bs2, can signal redundantly through all three NRC helpers. In contrast, some sensors are more restricted in their downstream helper compatibilities. Rpi-blb2, for example, can only signal through NRC4 (**Figure 1.2**) (Wu *et al.*, 2017). This suggests that there is a degree of sensor-helper co-evolution and specialization, as not all sensors are compatible with all helpers. Nonetheless, the high degree of redundancy exhibited by the downstream helpers contributes towards immune system robustness. Moreover, the acquisition of the SD is likely to be a consequence of the enhanced evolvability granted by the sensor-helper specialization.

NRC helpers are also downstream of several cell-surface receptors. Some cell-surface RPs can trigger a hypersensitive response that is indistinguishable from the NLR-mediated cell death response. In tomato, the RPs Cf-4, Cf-9, Cf-2 and Cf-5 recognize apoplastic secreted effectors of the fungus *Cladosporium fulvum*, while Ve1 recognizes the effector Ave1 from fungi of the *Verticillium* genus (De Jonge *et al.*, 2012; Luderer *et al.*, 2002; Rivas & Thomas, 2005; Seear & Dixon, 2003). Helper NLRs of the NRC family are required for the hypersensitive cell death mediated by these RPs (Fradin *et al.*, 2009; Gabriëls *et al.*, 2006; Gabriëls *et al.*, 2007; Kourelis *et al.*, 2022). Recent work by Kourelis *et al.* involving a combination of *nrc2/3/4* KO plants and genetic complementation revealed that NRC3 is the primary helper NLR required for the hypersensitive response induced by the Cf receptors (Kourelis *et al.*, 2022)

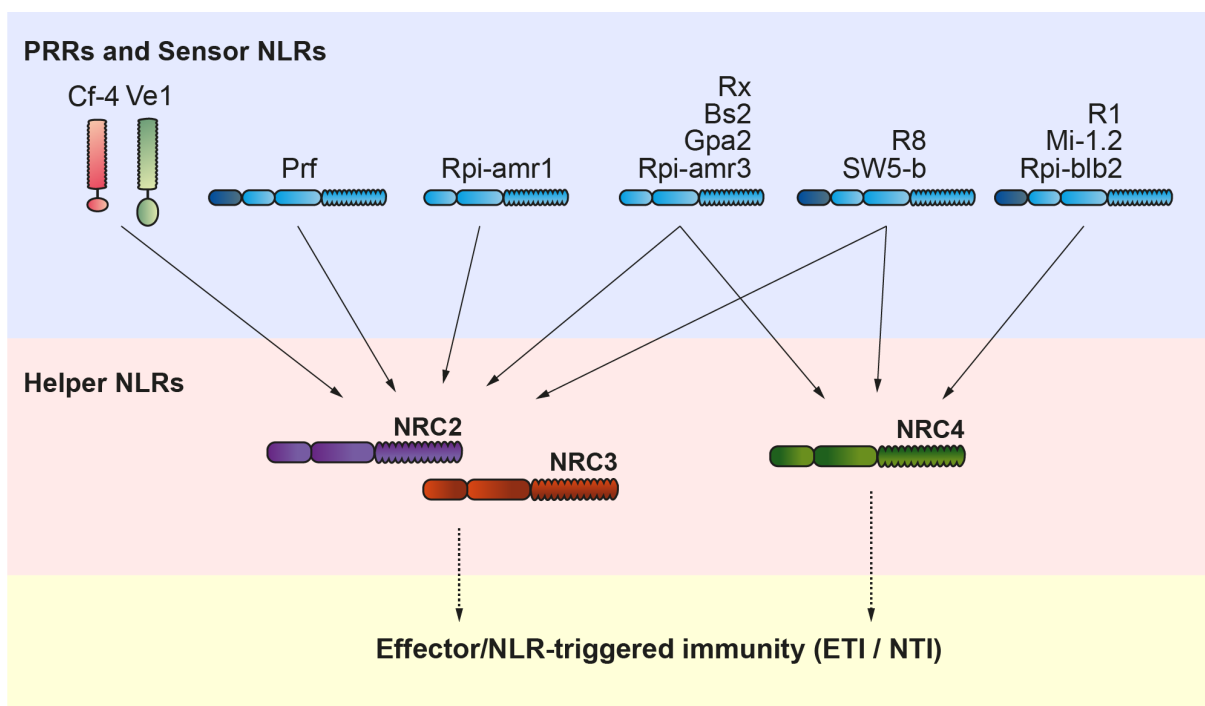


Figure 1.2: The Solanaceous NRC network.

Helper NLRs (NRC2, NRC3, NRC4) function in a partially redundant manner with a series of R genes that confer resistance against multiple pathogens. These R genes encode NLR sensors and PRRs that have specialized in detecting effectors from pathogens as diverse as oomycetes, bacteria, nematodes, viruses and aphids. Many of the NRC-dependent R genes are agronomically important. Adapted from Wu *et al.* (2017) and Kourelis *et al.* (2022).

1.5.2 The NRG1/ADR1 network

Another well characterized example is the NRG1/ADR1 network, in which the CC_R-NLRs NRG1 and Activated Disease Resistance 1 (ADR1) act as helpers. It is composed of TIR-NLR sensors and executors, which require the downstream NRG1 and ADR1 to mediate cell death and disease resistance (Bonardi *et al.*, 2011; Castel *et al.*, 2019; Qi *et al.*, 2018; Wu *et al.*, 2019). Much like in the NRC network, not all sensors can activate NRG1 or ADR1 with the same efficiency. Some sensors can activate both whereas some signal through either NRG1 or ADR1 (Castel *et al.*, 2019; Saile *et al.*, 2020). Following activation, TIR-NLRs communicate with their downstream CC_R-NLR helpers by producing a suite of small molecules which are recognised by Enhanced disease susceptibility 1 (EDS1) and its mates Phytoalexin Deficient 4 (PAD4) and Senescence-associated Gene 101 (SAG101), leading to the assembly of mutually exclusive EDS1-PAD4 and EDS1-SAG101 dimers (Jia *et al.*, 2022). The current working model is that EDS1-PAD4 activates ADR1 whereas EDS1-SAG101 activates NRG1 (Feehan *et al.*, 2023; Locci *et al.*, 2023; Pruitt *et al.*, 2021; Sun *et al.*, 2021). In that sense, sensor-helper specificity in the NRG1/ADR1 network appears to be determined by the small molecule profile generated by the TIR-NLRs and which EDS1 dimer these small molecules assemble. How exactly the EDS1 module decodes the small molecule messages relayed by upstream TIR-NLRs to determine this specificity is not fully understood.

The NRG1/ADR1 networks can also act genetically downstream of cell surface immune receptor activation. In *Arabidopsis*, the EDS1/PAD4/ADR1 and, to a lesser extent, EDS1/SAG101/NRG1 modules are genetically required for a subset of the immune responses triggered by LRR-RPs and LRR-RKs (Pruitt *et al.*, 2021; Tian *et al.*, 2021). EDS1 was also shown to be required for full Ve1 and Cf4-mediated immunity, implying that the NRG1/ADR1 network may also be involved in signaling for these cell-surface receptors (Fradin *et al.*, 2009; Hu *et al.*, 2005). If this is the case, at least two distinct NLR networks have evolved to contribute to cell-surface signaling in Solanaceous plants.

1.5.3 Evolution of NLR networks

The current evolutionary working model for plant CC-NLRs postulates that NLR pairs and networks originate from a common multifunctional “singleton” ancestor (Adachi *et al.*, 2019b) (**Figure 1.3**). This division of labour is critical to be able to keep up with rapidly evolving pathogen

effectors, as it results in reduced evolutionary constraints for both the sensor and helper, thus enhancing evolvability. By specializing, NLR pairs broaden the spectrum of amino acid changes that can be accommodated in each immune receptor, since sensors and helpers no longer need to fulfil both functions (Adachi *et al.*, 2019a). The acquisition of new domains for pathogen sensing in sensor NLRs is likely facilitated by this functional specialization. For example, all characterized NLR-IDs to date are paired NLRs (Marchal *et al.*, 2022a). In the Pik and Pia paired NLR allelic series, most of the variation is found in the sensor NLR, specifically within the effector-sensing ID (Białas *et al.*, 2021; De la Concepcion *et al.*, 2021; Shimizu *et al.*, 2022). In the NRC network, many NRC-dependent sensor NLRs include N-terminal SDs, which can participate in pathogen perception (Li *et al.*, 2019; Lukasik-Shreepaathy *et al.*, 2012; Mucyn *et al.*, 2006).

That NLRs with additional pathogen sensing domains such as IDs, C-JIDs or SDs are found in paired or networked configurations highlights the enhanced evolvability granted by sensor-helper NLR specialization (**Figure 1.3**) (Marchal *et al.*, 2022a; Wu *et al.*, 2017). It is conceivable that the evolutionary steps required for an additional domain to be incorporated without immediately leading to auto-activity would be less likely to occur in a singleton than in a functionally specialized sensor. The prevalence of NLR pairs and networks indicates a need to expand the oversimplified conceptual framework of NLR domains and their functions, which describes the canonical NLR functions in the context of a functional singleton. For example, in the case of helper NLRs which no longer directly co-evolve with effectors, the LRR could have adopted new roles such as in mediating sensor-helper communication.

1.5.4 Phylogenomics of NLR networks

NLRs can be encoded in genetic clusters. In Arabidopsis, around 50% of all NLRs are found in clustered arrangements which are formed by tandem duplication or unequal crossing-over events (Van de Weyer *et al.*, 2019). These duplication events allow NLRs to sub-functionalize and diversify, potentially leading to genetically linked NLR sensor-helper pairs, such as Pik-1/Pik-2 or RGA5/RGA4 (Adachi *et al.*, 2019b). These paired NLRs are often found in tight physical linkage in head-to-head orientation (Białas *et al.*, 2021; Césari *et al.*, 2014) (**Figure 1.4**). In contrast, functional sensors and helpers in NLR networks are often genetically dispersed (Wu *et al.*, 2017). Sensors and helpers in NLR networks usually form structured phylogenetic clusters despite not being physically linked (**Figure 1.4**). For example, NRC-dependent sensors fall in an expanded clade that includes many well characterized R proteins from different plant species, while the

helpers form a tight and well-supported sister clade. A similar phylogenetic arrangement is observed for the NRG1/ADR1 network. In the case of the NRC network, its phylogenetic structure further suggests that they likely share an evolutionary origin and are derived from an ancestral sensor-helper pair, which itself likely evolved from a singleton (**Figure 1.3, Figure 1.4**) (Adachi *et al.*, 2019b; Adachi & Kamoun, 2022; Wu *et al.*, 2017). Their characteristic phylogenetic structure can be useful to identify NLR networks in plant genomes (Adachi *et al.*, 2019a; Adachi *et al.*, 2019b).

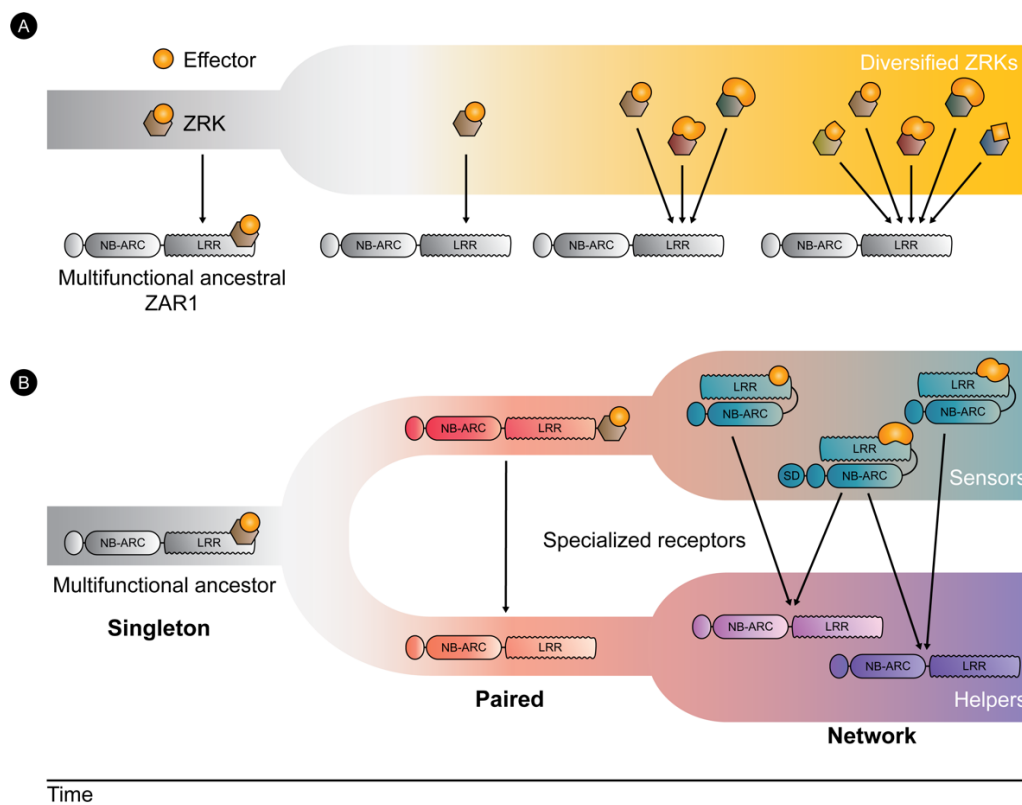


Figure 1.3: Evolution of NLR singletons, pairs, and networks.

(A) The NLR ZAR1 indirectly recognises multiple bacterial effectors by guarding host RLCKs, also termed ZRKs, which bait bacterial effectors. Over evolutionary time, ZRKs have greatly diversified as a result of coevolution with pathogen effectors. In contrast, ZAR1 has remained atypically conserved throughout angiosperm evolution, relying on ZRKs for pathogen recognition and specializing in interacting with ZRKs to mediate immune signaling. (B) NLRs can be categorized into singletons, pairs, and networks. While singletons can mediate both, pathogen sensing and downstream immune signaling, NLRs have duplicated and diversified over evolutionary time leading to the appearance of specialized receptors that can be defined as either ‘sensors’ or ‘helpers’, forming connections that range from pairs to complex networks.

Is there an evolutionary advantage from the lack of genetic linkage in NLR networks? Beyond the functional sensor-helper specialization, it is possible that genetically unlinked NLR networks allow for the generation of more regulatory diversity or for the acquisition of novel domains, such as the SD domain found in many NRC-dependent sensors (**Figure 1.2, Figure 1.3, Figure 1.4**) (Kourelis *et al.*, 2021; Seong *et al.*, 2020). The lack of genetic linkage in the NRC network, which mediates recognition of diverse pathogens, might enable the modular loss of costly sensors when pathogen pressure is no longer present, without affecting resistance to other pathogens. It is possible that the high degree of genetic redundancy exhibited by the helpers combined with the convergence of multiple sensors into one downstream helper facilitates the loss of genetic linkage over evolutionary time, in contrast with paired NLRs where a sensor can exclusively work with one helper. How exactly these NLR networks became unlinked and how the lack of co-regulation provided by physical linkage can be overcome is not understood. Moreover, the existence of networks complicates the evolutionary paradigm initially proposed by the gene-for-gene hypothesis, as sensor NLRs are simultaneously co-evolving with effectors and with their downstream helpers.

1.6 Sensor NLRs in the NRC network.

1.6.1 Rx and Gpa2

Rx is an agronomically important sensor CC-NLR from potato (*Solanum tuberosum*) that confers resistance to PVX, a single-stranded RNA filamentous plant virus, by recognizing its coat protein (CP) (Bendahmane *et al.*, 1999; Bendahmane *et al.*, 1995). Rx is considered a model NLR, as it has been extensively studied at the biochemical level, and was the first plant NLR to be rendered autoactive by MHD mutations (Bendahmane *et al.*, 2002). Prior to activation, Rx is held in an inactive state by intramolecular autoinhibitory interactions between its LRR domain and its CC and NB-ARC domains (Moffett *et al.*, 2002; Rairdan & Moffett, 2006). Inactive Rx constitutively forms a stable complex with the host Ran GTPase activating protein 2 (RanGAP2) via its CC domain as a pre-requisite for effective Rx-mediated PVX resistance (Sacco *et al.*, 2009; Sacco *et al.*, 2007). Interestingly, Rx has been shown to require a balanced nucleocytoplasmic partitioning for proper regulation of disease signaling even though activation of Rx by PVX CP occurs in the cytoplasm (Sacco *et al.*, 2007; Sloomweg *et al.*, 2010; Tameling *et al.*, 2010). Although Rx is nucleocytoplasmically distributed, hyperaccumulation in the nucleus blocks PVX CP-triggered HR. RanGAP2 appears to sequester part of the cellular pool of Rx at the cytoplasm and nuclear envelope, suggesting that

RanGAP2 could be regulating the nucleocytoplasmic partitioning of Rx to ensure correct function (Sacco *et al.*, 2007; Sloomweg *et al.*, 2010; Tameling *et al.*, 2010). Upon CP-triggered activation, Rx undergoes intramolecular rearrangements that include the release of LRR autoinhibition and the exposure of its NB-ARC domain, leading to its activation (Moffett *et al.*, 2002; Rairdan & Moffett, 2006). No direct interaction between CP and Rx has been found, suggesting an indirect recognition mechanism (Tameling & Baulcombe, 2007). Considering this, RanGAP2 could also be a potential guardee targeted by PVX CP and monitored by Rx. The exact mechanism by which Rx and RanGAP2 recognize PVX CP is not fully understood.

We previously showed that Rx-mediated cell death genetically requires at least one of three downstream helpers through which it can signal interchangeably: NRC2, NRC3 or NRC4 (Wu *et al.*, 2017). Rx has previously been shown to function when its different domains are expressed in trans. When co-delivering the CC-NB-ARC domain of Rx together with its LRR domain, the two halves of Rx can complement each other and mediate effector-triggered hypersensitive cell death (Moffett *et al.*, 2002). Beyond highlighting that intramolecular autoinhibitory interactions and their release upon effector perception retain normal function when Rx domains are expressed separately, this indicates that the conformational changes that full-length undergoes and that presumably lead to sensor-helper communication and helper activation are still possible when these domains are expressed in trans. Moreover, NB domain only truncations of Rx have been shown to trigger cell death, suggesting that the NB domain of Rx may be able to communicate with its downstream helper NRCs (Rairdan *et al.*, 2008). However, the mechanisms by which Rx signals through these NRCs are still not understood.

Gpa2 is another NRC2/3/4-dependent sensor NLR, closely related to Rx. It is an R protein that recognizes the RBP1 effector from the potato cyst nematode *Globodera pallida* (Sacco *et al.*, 2009). Much like its allele Rx, Gpa2 has been shown to interact with RanGAP2 via its N-terminal CC-domain and genetically requires this cofactor for cell death mediated upon RBP1 recognition (Sacco *et al.*, 2009; Sacco *et al.*, 2007). The precise mechanism by which Gpa2 recognizes RBP1 is not yet understood, although it is thought to be indirect considering that RBP1 has not been shown to associate with Gpa2. Sacco and colleagues (2009) showed that artificially tethering RBP1 to RanGAP2 could enhance Gpa2-mediated cell death upon effector recognition, in favor of an indirect recognition model in which RanGAP2 acts as a co-factor or guardee.

1.6.2 Bs2.

Bs2 is an NRC2/3/4-dependent sensor NLR from the wild pepper *Capsicum chacoense*. It provides resistance in tomato to bacterial spot disease caused by *Xanthomonas campestris* pv. *vesicatoria* (Tai *et al.*, 1999). Bs2 recognizes the type III secreted effector AvrBs2 from *X. campestris*, which exhibits homology to the *A. tumefaciens* agrocinopine synthase and *E. coli* UgpQ, suggesting a possible enzymatic function as a phosphodiesterase (Andolfo *et al.*, 2019; Swords *et al.*, 1996; Tai *et al.*, 1999). Although Bs2 exhibits only few copies in the tomato and potato genomes, the Bs2 family is massively expanded in pepper (Andolfo *et al.*, 2019; Seo *et al.*, 2016).

1.6.3 Rpi-amr1 and Rpi-amr3.

Rpi-amr1 and Rpi-amr3 are two NRC-dependent R proteins against the oomycete pathogen *P. infestans*. Originally identified in the wild potato relative *Solanum americanum* which is a nonhost to *P. infestans*, both Rpiamr1 and Rpiamr3 have been shown to confer resistance this pathogen in cultivated potato (Witek *et al.*, 2016; Witek *et al.*, 2021). Rpi-amr1 is an NRC2/3 dependent sensor NLR whereas Rpi-amr3 is NRC2/3/4-dependent (Lin *et al.*, 2022b; Lin *et al.*, 2020; Witek *et al.*, 2021). Rpi-amr1 and Rpi-amr3 recognize AVRamr1 and AVRamr3, respectively, and can recognize multiple homologs of their cognate effectors from divergent *Phytophthora* species (Lin *et al.*, 2022b; Lin *et al.*, 2020). This makes them highly versatile, and potentially useful to confer disease resistance against various *Phytophthora*-related diseases in multiple crop species. Recent studies suggest that Rpi-amr1 and Rpi-amr3 are recognizing their corresponding AVRs via direct interaction with the effector, making them the first documented example of direct recognition of a *P. infestans* effector (Ahn *et al.*, 2023; Lin *et al.*, 2022b).

1.6.4 Rpi-blb2 and Mi-1.2.

Rpi-blb2 originates from the wild potato *Solanum bulbocastanum* and encodes a sensor CC-NLR with an N-terminal SD that provides broad-spectrum resistance to *P. infestans* in potato and *N. benthamiana* (Oh *et al.*, 2009; van der Vossen *et al.*, 2005; Wu *et al.*, 2017). Rpi-blb2 recognizes the *P. infestans* RXLR effector AVRblb2, a haustoria-localized RXLR effector that interferes with host vesicle secretion during infection and activates NRC4 (Bozkurt *et al.*, 2011; Oh *et al.*, 2009). The mechanism by which Rpi-blb2 recognizes AVRblb2, however, is not known. Rpi-blb2 activation

by AVRblb2 was shown to trigger changes in localization of its downstream helper NRC4, shifting its localization from periaustorial to PM localized (Duggan *et al.*, 2021).

Mi-1.2 is also an SD-containing NLR that is closely related to Rpi-blb2. It originates from *Solanum peruvianum* and shares 82% amino acid identity with Rpi-blb2 (Milligan *et al.*, 1998; van der Vossen *et al.*, 2005). Mi-1.2 is also NRC4-dependent and is one of only a few documented examples of multiple pathogen recognition by one NLR. Mi-1.2 can confer resistance to the root-knot nematodes *Meloidogyne incognita*, *M. arenaria* and *M. javanica*, the potato aphid *Macrosiphum euphorbiae*, and the sweet potato whitefly *Bemisia tabaci* in tomato (Milligan *et al.*, 1998; Nombela *et al.*, 2003; Rossi *et al.*, 1998). It is tempting to speculate that to recognize such unrelated pathogens, it is likely that Mi-1.2 is recognizing effectors from these pathogens indirectly. However, the effectors recognized by Mi-1.2 are not known. Interestingly, in eggplant, Mi-1.2 confers resistance to root-knot nematodes but not to potato aphid, suggesting that Mi-1.2 could require different host components or guardees for different pathogens.

1.6.5 Sw5-b and R8.

Sw5-b is an SD-containing NRC2/3/4-dependent sensor CC-NLR from the wild tomato *Solanum peruvianum* that confers resistance to Tospoviruses by recognizing their NSm protein (Brommonschenkel *et al.*, 2000). Its N-terminal SD was shown to cooperate with the LRR of Sw5-b to directly interact with NSm (Hallwass *et al.*, 2014; Peiró *et al.*, 2014; Zhu *et al.*, 2017). Interestingly, an NB-ARC domain-only truncation of Sw5-b was shown to be sufficient to trigger cell death, reminiscent of the cell death triggered by the NB domain truncation of Rx, although whether or not this cell death is mediated via canonical NRC-dependent pathways is not known (De Oliveira *et al.*, 2016; Rairdan *et al.*, 2008). Notably, the autoactive variant Sw5-b^{D857V} is NRC2/3-dependent and cannot activate NRC4 like NSm activated Sw5-b, indicating that there may be differences in the mechanisms by which effector activated and autoactive sensors communicate with their downstream helpers (Derevnina *et al.*, 2021). The *Solanum demissum* R protein R8 shares 89% amino acid sequence identity to Sw5-b and is also a SD-containing NRC2/3/4-dependent sensor CC-NLR (Vossen *et al.*, 2016). Despite this sequence similarity, R8 and Sw5-b confer resistance to different pathogens. R8 confers resistance to *P. infestans* isolates carrying the RXLR effector AVR8 (Rietman, 2011; Vossen *et al.*, 2016).

1.6.6 Prf.

Prf is an SD-containing sensor CC-NLR which confers resistance to *P. syringae* in tomato. Prf recognises Type III secreted effector proteins AvrPto and AvrPtoB by constitutively associating and guarding the host kinase Pto (Kim *et al.*, 2002). The N-terminal SD of Prf has been shown to mediate Prf-Pto associations (Gutierrez *et al.*, 2010; Mucyn *et al.*, 2006). AvrPto and AvrPtoB can interact with Pto, and Prf can sense these effector activities and subsequently activate immunity. In *N. benthamiana*, AvrPto can activate the endogenous Prf homolog if the tomato Pto kinase is co-delivered. AvrPto/Pto-triggered cell death mediated by Prf in *N. benthamiana* is NRC2/3 dependent (Wu *et al.*, 2017; Wu *et al.*, 2016).

1.7 NLR activation.

1.7.1 Pathogen activation of CC-NLRs

While the first plant NLR resistance genes were cloned almost 30 years ago (Whitham *et al.*, 1994, Bent *et al.*, 1994), the molecular mechanisms of NLR activation and immune signaling following pathogen perception were only elucidated recently. Using cryo-EM, Wang and colleagues obtained structural insights into the *Arabidopsis* singleton NLR ZAR1 before and after activation (Wang *et al.*, 2019a; Wang *et al.*, 2019b). Following effector perception, ZAR1 undergoes a series of conformational changes largely mediated by the NB-ARC domain and assembles into a pentameric wheel-like homo-oligomer analogous to the mammalian inflammasome (Wang *et al.*, 2019b). This plant NLR oligomer was coined as the resistosome (Hu *et al.*, 2020; Wang *et al.*, 2019a; Wang *et al.*, 2019b). NLR oligomerization leads to induced proximity of the N-terminal signaling domains. In the case of the CC-NLR ZAR1, the α 1-helix of the CC domain flips out upon activation, forming a funnel-like structure that mediates resistosome insertion into the plasma membrane (Bi *et al.*, 2021; Wang *et al.*, 2019a) (**Figure 1.5**).

Following insertion, the ZAR1 resistosome presumably acts as a calcium channel, an activity that is required for the hypersensitive cell death (Bi *et al.*, 2021). More recently, the structure of the activated singleton CC-NLR Sr35 from wheat, and the observed oligomerization of RPP7, revealed that formation of a pentameric resistosome seems to be a conserved activation mechanism for singleton CC-NLRs across distantly related plant species (Förderer *et al.*, 2022; Li *et al.*, 2020; Zhao *et al.*, 2022). Despite these advances, the molecular mechanisms of paired and

networked plant CC-NLR activation are poorly understood. In the case of Pia (RGA4 and RGA5), immune signaling is activated through release of negative regulation (Césari *et al.*, 2014). In contrast, the Pik-1 and Pik-2 pair is activated via receptor cooperation by forming a tri-partite complex with the pathogen effector (De la Concepcion *et al.*, 2021; Zdrzalek *et al.*, 2020).

How does the ZAR1/Sr35 oligomerization and resistosome model translate to CC-NLR pairs and networks (**Figure 1.6**)? Paired NLRs may also activate via oligomerization-based activation mechanisms. Assuming this model, would both sensors and helpers engage in heterocomplexes? Alternatively, sensors and helpers could both oligomerize and form two separate resistosomes. A third option would involve helpers forming resistosomes independently of their upstream sensors (Adachi *et al.*, 2019b). In the case of the CC-NLR pair RGA4/RGA5, the observation that the RGA4 helper triggers cell death in the absence of RGA5 suggests that in this system the helper may be capable of assembling a resistosome in the absence of RGA5 (Césari *et al.*, 2014).

In the NRC network, the NRC-dependent sensors Rx and Sw5-b trigger cell death as NB domain and NB-ARC domain truncations, respectively (De Oliveira *et al.*, 2016; Rairdan *et al.*, 2008). If this cell death is indeed NRC-dependent, this would suggest that NRCs may be able to form activated complexes and trigger cell death in the absence of a full-length sensor. This would be supported by the observation that autoactive NRC variants are capable of triggering cell death in the absence of activated upstream sensor NLRs (Derevnina *et al.*, 2021). Another observation against the heterocomplex hypothesis is that NRC-dependent sensors exhibit diversity in terms of length and presence/absence of N-terminal SD-fusions (Adachi *et al.*, 2019b; Wu *et al.*, 2017). This would structurally complicate the formation of a funnel-like structure like the ZAR1 or Sr35 resistosome, in which the N-termini come together upon CC-NLR oligomerization (Förderer *et al.*, 2022; Wang *et al.*, 2019a; Zhao *et al.*, 2022). Unfortunately, unlike TIR-NLRs which can be studied in their activated state without cell death thanks to genetic backgrounds like the *eds1* KO background, tools with which to study activated CC NLRs are lacking (Gantner *et al.*, 2019; Sun *et al.*, 2021). New resources and further experimental evidence are needed to better understand the precise mechanisms by which paired or networked CC-NLR sensors and helpers communicate and activate (**Figure 1.6**).

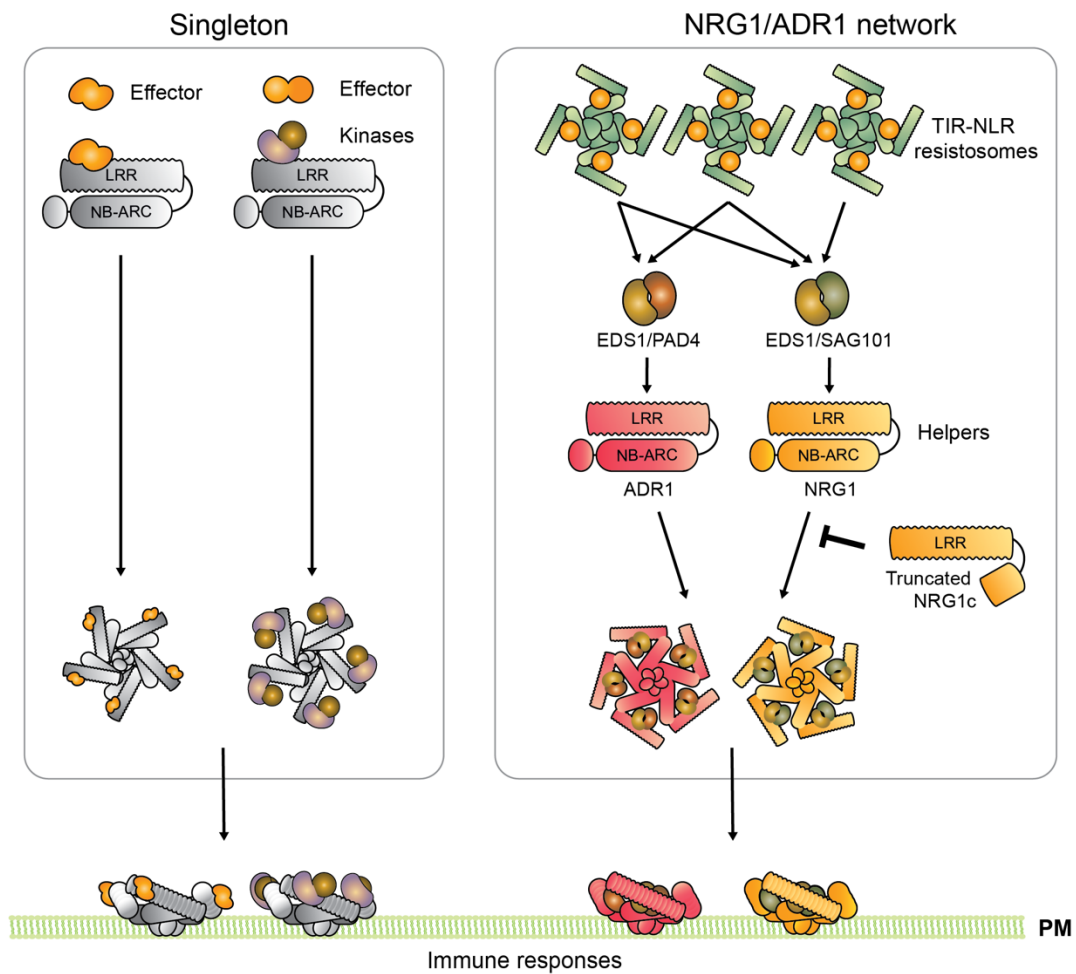


Figure 1.5: Plant NLR activation mechanisms.

Singleton: Upon direct or indirect effector perception, singleton CC-NLRs such as ZAR1 and Sr35 activate via forming homo pentameric complexes termed resistosomes. Resistosomes accumulate at the plasma membrane to initiate immune signaling and mediate programmed hypersensitive cell death, presumably by acting as calcium channels. **NRG1/ADR1 network:** TIR-NLR singletons and pairs form tetrameric resistosomes upon activation. These resistosomes act as holoenzymes, producing a range of small molecules which are perceived by downstream lipase-like protein dimers EDS1-PAD4 and EDS1-SAG101. These activated EDS1-PAD4 and EDS1-SAG101 complexes can interact with the helper CC_R-NLRs ADR1 and NRG1, respectively, leading to their oligomerization into CC_R-NLR resistosomes. Following their activation and oligomerization, the ADR1 and NRG1 resistosomes accumulate on the PM to act as calcium-permeable channels, leading to immune signaling and hypersensitive cell death. This network also features an atypical modulator NLR, NRG1c, which can negatively regulate immune signaling by full length NRG1.

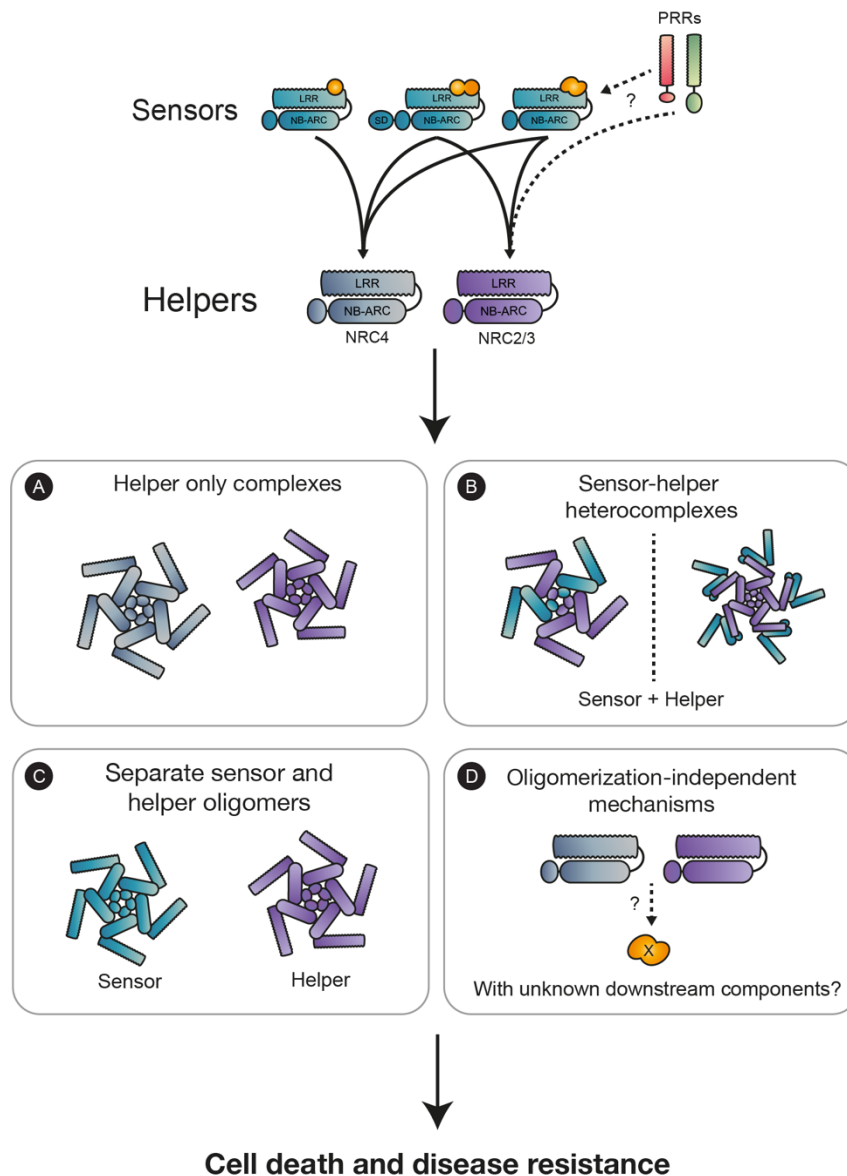


Figure 1.6: Potential activation mechanisms in the NRC network.

NRC-dependent sensor NLRs and PRRs signal through downstream helper NRCs. The exact mechanism by which the NRC network activates to mediate cell death and disease resistance is unknown. (A) Sensors could activate NRC helper oligomers without oligomerizing themselves and without forming part of the activated complex. (B) Sensors and helpers could assemble into oligomeric heterocomplexes reminiscent of the NAIP/NLRC4 inflammasome (left). Alternatively, the sensors could form part of a helper resistosome in the same way than the RLCKs form part of the activated ZAR1 complex (right). (C) Sensors and helpers may trans-activate and oligomerize separately, with each oligomer executing signaling. (D) Alternatively, the NRC network may function via oligomerization independent mechanisms. It is possible that unknown downstream components that are activated by NRCs exist which execute cell death following activation.

1.7.2 Pathogen activation of TIR-NLRs/CC_R-NLRs

The structures of the activated TIR-NLRs Roq1 and RPP1 tetrameric resistosomes, revealed that these phylogenetically distant NLRs also employ oligomerization-based activation mechanisms. Roq1 perceives the bacterial effector XopQ, while RPP1 recognizes ATR1 (Ma *et al.*, 2020; Martin *et al.*, 2020). TIR-NLR resistosomes function as holo-enzymes, with the assembled TIR domains producing a range of small molecules which include 2'-(5''-phosphoribosyl)-5'-ADP (pRib-ADP) or pRib-AMP as well as ADP-ribosylated ATP/ADPR (ADPr-ATP/diADPR) (Huang *et al.*, 2022; Jia *et al.*, 2022) (**Figure 1.5**). These small molecules are, in turn, perceived by a downstream signaling hub, comprised of the lipase-like proteins EDS1, PAD4 and SAG101. Upon activation of upstream TIR-NLRs, EDS1 forms mutually exclusive hetero-dimers with SAG101 or PAD4. The small molecule profile generated by the upstream activated TIR-NLRs determines which EDS1 hetero-dimer is formed (Huang *et al.*, 2022; Jia *et al.*, 2022) (**Figure 1.5**). The EDS1 signaling hub activates downstream helper CC_R-NLRs, NRG1 and ADR1, with these helpers ultimately mediating the induction of cell death. EDS1-SAG101 heterodimers form a complex with NRG1 leading to its oligomerization into an NRG1-EDS1-SAG101 complex (Feehan *et al.*, 2023; Sun *et al.*, 2021) (**Figure 1.5**). Although multiple groups have independently reported oligomerization of activated NRG1 (Feehan *et al.*, 2023; Jacob *et al.*, 2021; Wang *et al.*, 2023b), whether EDS1-SAG101 associates with NRG1 oligomers stably, transiently or in a timepoint-dependent manner, remains to be determined.

In contrast to EDS1-SAG101, EDS1-PAD4 heterodimers, associate with ADR1 and ADR1-like proteins (Huang *et al.*, 2022). Activated NRG1 and ADR1 complexes then associate with the plasma membrane to act as calcium channels (Jacob *et al.*, 2021; Saile *et al.*, 2021; Wang *et al.*, 2023b). Interestingly, NRG1 and ADR1 exhibit functional specialization. Not all TIR-NLRs can signal through both helpers (Castel *et al.*, 2019; Wu *et al.*, 2019) (**Figure 1.5**). Moreover, NRG1 and ADR1 contribute differentially to immunity. While both mediate transcriptional reprogramming downstream of activation, NRG1 appears to be partially specialized in cell death induction, while ADR1 contributes to basal immunity and defence, independent of cell death (Saile *et al.*, 2020). Considering that different TIR-NLRs activate different downstream helper CC_R-NLR, how exactly the enzymatic activity of different TIR-NLRs is decoded by the EDS1 node is not yet clear. Moreover, the functional determinants of diversification and the interplay between NRG1 and ADR1 in immunity is not clear yet.

1.7.3 NLR activation in non-plant NLRs

Before the first resistosome structures had been solved, studies on metazoan NLR proteins had already revealed analogous oligomerization-based activation mechanisms. In mammals, multiple different NAIP sensor NLRs can perceive distinct immune elicitors and switch to an active conformation, contributing to immunity. Following activation, NAIPs require the helper NLR NLRC4 to mediate downstream signaling. NAIPs feature an N-terminal baculoviral inhibitor of apoptosis protein repeat (BIR) domain, which can be involved in ligand perception, and NLRC4 have N-terminal caspase activation and recruitment domains (CARDs) (Kofoed & Vance, 2011; Tenthorey *et al.*, 2017; Vance, 2015; Zhao *et al.*, 2011). These NAIP sensors and their NLRC4 helper are an example of an NLR network in mammals. NAIP2 is one of these sensors. Upon perception of its cognate effector, the bacterial type III secretion inner rod protein PrgJ, NAIP2 initiates sensor-helper signaling via the formation of a heterocomplex with NLRC4 (Hu *et al.*, 2015; Qu *et al.*, 2012; Zhang *et al.*, 2015). This NAIP2/NLRC4 heterocomplex acts as a nucleation point for multiple NLRC4 monomers that leads to the polymerization of a NAIP/NLRC4 inflammasome with a single NAIP and 10 additional NLRC4 units (Hu *et al.*, 2015; Zhang *et al.*, 2015). The assembled inflammasome recruits and activates caspase 1 in an ASC (apoptosis-associated speck-like protein containing a CARD)-dependent or independent manner via its N-terminal CARD of the NLRC4 protomers to trigger inflammation (Poyet *et al.*, 2001; Vance, 2015). Caspase 1 in turn can cleave and activate more than 70 substrate proteins, including pro-inflammatory cytokines and gasdermin D, with caspase 1-mediated gasdermin D cleavage being necessary and sufficient for pyroptotic programmed cell death (Chou *et al.*, 2023; Kayagaki *et al.*, 2015; Shi *et al.*, 2015). Whether plant paired and networked NLRs can form sensor-helper heterocomplexes analogous to the NAIP/NLRC4 inflammasome heterocomplexes is not known.

The recent Cryo-EM structures of the autoinhibited, primed and activated NLRP3 inflammasomes revealed that there may be additional layers of regulation beyond the simplified monomer-to-oligomer NLR activation model. NLRP3 is a mammalian NLR with N-terminal pyrin signaling domains which promote inflammation by recruiting ASC and activating caspase 1. Structural studies of inactive NLRP3 revealed that it can form cage-like oligomers. In this autoinhibited ADP-bound complex, the N-terminal pyrin signaling domains are sequestered in the middle of the cage-like structure, preventing spurious interaction with important downstream signaling components and thus preventing inflammasome activation (Andreeva *et al.*, 2021; Hochheiser *et al.*, 2022). NIMA related kinase 7 (NEK7) is an essential component required for

NLRP3 inflammasome activation. NEK7 forms a complex with NLRP3 which promotes NLRP3 inflammasome assembly. Recent studies showed that, in the absence of activation, NEK7 can dissociate the autoinhibited NLRP3 cages. These NLRP3-NEK7 complexes are still in an autoinhibited ADP-bound conformation prior to activation but are proposed to be more signal competent than the oligomeric cages and are thus primed for activation (Chou *et al.*, 2023; Ohto *et al.*, 2022; Sharif *et al.*, 2019). While the precise trigger of NLRP3 inflammasome assembly is not fully understood, following activation, NLRP3 forms a disc-like inflammasome homocomplex of 10 to 11 units (Xiao *et al.*, 2023). This suggest that inflammasome activation may involve additional regulatory mechanisms beyond the presence or absence of a ligand or trigger.

In prokaryotes, NLR-like proteins were recently found to activate via oligomerization-based mechanisms as well (Gao *et al.*, 2022). Bacteria are under constant threat from phages, and as such have evolved innate immune systems to detect and respond to phage attack via diverse strategies (Boyle & Hatoum-Aslan, 2023). Avs3 from *Salmonella enterica* and Avs4 from *E. coli* are NLR-like STAND proteins with N-terminal nuclease domains (Gao *et al.*, 2022). Upon direct binding of the terminase subunit and the portal protein of tailed phages, respectively, Avs3 and Avs4 form tetrameric resistosome-like complexes, with the N-terminal nuclease domains forming a dimer of dimers reminiscent of the Roq1 and RPP1 tetrameric TIR-NLR resistosomes (Gao *et al.*, 2022; Ma *et al.*, 2020; Martin *et al.*, 2020). The assembled Avs inflammasomes exhibit endonuclease activity, cleaving both linear and circular double-stranded DNA with no specificity for phage DNA. This endonuclease activity leads to a defense strategy termed abortive infection, involving premature death of the phage-infected bacteria (Gao *et al.*, 2022). This indicates that oligomerization-based activation mechanisms are broadly conserved across prokaryotes, metazoans and plants.

1.7.4 Cell biology of NLR resistosomes

While our understanding of the biochemical mechanisms that lead to immunity triggered by NLRs has made tremendous progress over the last decade, we still lack a detailed understanding of the cell biology of these immune receptors. NLRs can exhibit distinct subcellular localizations in their inactive as well as their activated states, reviewed in depth by Lüdke, Shepherd and colleagues (Lüdke *et al.*, 2022; Shepherd *et al.*, 2023). For sensor NLRs these localizations can be rationalized with the need to efficiently detect effector molecules, which in turn can target distinct subcellular compartments in the host (Duggan *et al.*, 2021; Petre *et al.*, 2021; Wang *et al.*, 2018). One

well described example is the previously discussed TIR-NLR pair RRS1/RPS4 which recognizes the activity of effectors that manipulate WRKY transcription factors (Deslandes *et al.*, 2002; Le Roux *et al.*, 2015; Sarris *et al.*, 2015). The inhibited RRS1/RPS4 complex associates with chromatin in the nucleus and is activated upon effector interaction and modification of the RRS1 WRKY domain (Birker *et al.*, 2009; Huh *et al.*, 2017; Le Roux *et al.*, 2015; Narusaka *et al.*, 2009; Sarris *et al.*, 2015; Williams *et al.*, 2014). Moreover, some sensor NLRs are required to associate with guardees or decoys which themselves may exhibit specific subcellular localizations. Examples include the well-known CC-NLRs RPM1 and RPS5, both of which guard kinases at the plasma membrane and therefore require a plasma membrane localization to be functional prior to activation (El Kasmi *et al.*, 2017; Pottinger & Innes, 2020).

In the NRG1/ADR1 network, helper NLRs also exhibit diverse localizations and have been shown to dynamically re-localize upon activation. The ADR1 and NRG1 family of helper CC_R-NLRs, which act downstream of TIR-NLRs, were both shown to reside in the cytoplasm in their inactive state (Saile *et al.*, 2021). In addition, inactive NRG1A and NRG1B were also reported to localize to the endoplasmic reticulum (Wu *et al.*, 2019). Upon TIR-NLR signalling, ADR1 and NRG1 both form higher molecular complexes that shift their localization towards the plasma membrane (Feehan *et al.*, 2023; Saile *et al.*, 2021). Both localization and functionality of NRG1 and ADR1 helpers are phospholipid dependent, as depletion of phosphatidylinositol-4-phosphate results in mis-localization and a loss of cell death activity (Saile *et al.*, 2021; Wang *et al.*, 2023b). However, a re-localization of NRG1 to the nucleus could also be observed upon activation (Feehan *et al.*, 2023). It remains to be determined what the direct function of NRG1 in the nucleus could be. However, the shift from a cytoplasmic to a membrane associated localization has also been observed for the singleton NLR ZAR1, further outlining that subcellular shift towards the plasma membrane could be a general feature of singleton and helper NLRs, presumably for calcium channel formation.

In the NRC network, the localization of sensors and helpers also plays an important role. Recently, Duggan and colleagues (2021) showed that during infection with the *P. infestans* and in the absence of activation, NRC4 focally accumulates at the extra haustorial membrane (EHM), where effectors are delivered into the host cell (Duggan *et al.*, 2021). Following activation of Rpi-blb2, NRC4 loses this focal perihaustral localisation and accumulates as puncta spread throughout the PM, triggering cell death presumably due to the formation oligomeric resistosomes (Contreras *et al.*, 2023a; Contreras *et al.*, 2023b; Duggan *et al.*, 2021). As this localization is specific

to NRC4 and could not be observed for NRC2 or the singleton ZAR1, this outlines that helper NLRs show a degree of specificity in their localization (Duggan *et al.*, 2021).

Sensors co-evolve with their cognate effectors and likely must adapt to their localization. Helpers, in turn, are also co-evolving with their sensors and evolve specialized localization patterns, likely leading to more efficient support of sensor signaling. Interestingly, most *P. infestans* sensors characterised to date are NRC4-dependent, so it is not surprising that NRC4 has evolved a specialized focal role in immunity against this oomycete pathogen (Derevnina *et al.*, 2021; Wu *et al.*, 2018). Indeed, the inactive NRC2 helper can be observed to form fibril-like structures at the EHM during the interaction with *P. infestans* (Duggan *et al.*, 2021). Although it is still not clear how networked CC-NLR sensors communicate and activate their downstream helpers, it can be assumed that a certain degree of subcellular proximity is required for efficient signal transmission.

1.7.5 Atypical NLRs: modulators of plant immunity

An emerging concept in NLR network biology is that NLRs can modulate the activity of other NLRs. The first reports of this phenomenon were the classic examples of some genetically linked sensor-helper pairs where the sensor can suppress a constitutively active helper or executor, as is the case for the RGA5/RGA4 and RRS1/RPS4 pairs discussed above (Césari *et al.*, 2014; Ma *et al.*, 2018). More recently, two studies identified NLR modulators which cannot be classified into the conventional categories of sensor, executor, or helper. Rather, these atypical NLRs act as signaling modulators (Adachi *et al.*, 2023; Wu *et al.*, 2022). The *NRG1* NLR gene cluster in Arabidopsis consists of *NRG1a*, *NRG1b* and *NRG1c*. *NRG1a* and *NRG1b* proteins are known helper NLRs required for immune signaling and induction of cell death downstream of many TIR-NLRs. Both *NRG1a* and *NRG1b* contain all features of canonical NLRs, an N-terminal CC_R domain, central NB-ARC and C-terminal LRR domain. *NRG1c*, on the other hand, is a truncated NLR lacking a CC_R domain and most of the NB-ARC. *NRG1c* can negatively regulate *NRG1a/b* signaling and cell death, presumably by competing with these alleles for interaction with EDS1/SAG101 complexes (**Figure 1.5**) (Wu *et al.*, 2022).

Another example is the full-length CC-NLR NRCX, which phylogenetically clusters with other helper NRCs in the NRC network and is closely related to NRC2 and NRC3. Unlike other NRCs, NRCX carries a non-functional N-terminal MADA motif and is unable to trigger cell death (Adachi *et al.*, 2023). In addition, NRCX silencing leads to autoimmunity in *N. benthamiana*.

Interestingly, this autoimmunity is partially dependent on the NRC family members NRC2 and NRC3, but not NRC4. Concomitantly, NRCX silencing led to enhanced cell death mediated by NRC2 and NRC3, but not NRC4 (Adachi *et al.*, 2023). This points to NRCX as an immunomodulating component in the NRC network, specifically capable of regulating the function of NRC2 and NRC3. Considering its evolutionary relatedness with NRC2 and NRC3, it is tempting to speculate that NRCX arose during NRC evolution to interact with these helpers, interfering with their oligomerization or signaling upon activation. Nonetheless, the precise mechanism by which NRCX negatively regulates these helpers is not understood.

NRG1c and NRCX are atypical because they act as NLR modulators within their respective NLR networks. It is likely that as more complex networked configurations arise, further NLR functional specialization is required to keep up with transitions associated with NLR evolution. Genetic dispersion presumably presents more difficulties in terms of NLR regulation, and these modulators may evolve to regulate these increasingly complex signaling architectures. Understanding the molecular mechanisms by which these modulator NLRs function will shed light on how networked signaling architectures are regulated. Moreover, this knowledge may enable new avenues for bioengineering more efficient signaling in plant immunity by altering the function, intensity, or specificity of these immunomodulators.

1.8 Pathogen effectors: the basics.

Plant pathogen effectors are any proteins or small molecules that are secreted during infection to modulate plant physiology and favour host infection and colonization (Bialas *et al.*, 2018). Apoplastic effectors accumulate in the plant intercellular space, or apoplast, to interact with their target host proteins, sometimes acting as inhibitors of host hydrolases and proteases or scavenging PAMPs such as chitin to avoid detection by cell-surface receptors (Asai & Shirasu, 2015; Buscaill & van der Hoorn, 2021; Ngou *et al.*, 2022a; Rocafort *et al.*, 2020). Cytoplasmic effectors, in contrast, are translocated inside the host cell and are subsequently targeted to different subcellular compartments where they execute their virulence functions (Boevink *et al.*, 2020; Win *et al.*, 2012a). Effectors are highly versatile, with some effectors being able to target multiple host targets. Conversely, because they often target host components that play key roles in host physiology and immunity, sometimes effectors from unrelated pathogens converge on the same target (Derevnina *et al.*, 2021; Kourelis *et al.*, 2022; Petre *et al.*, 2021).

Over the past decade, studies in the field of effector biology have been focused on identifying and characterizing plant pathogen effectors, revealing an astounding diversity in terms of activities, localizations and mechanisms (Hulin *et al.*, 2023; Lovelace *et al.*, 2023; Oh *et al.*, 2009; Petre *et al.*, 2021; Toruño *et al.*, 2016; Wang *et al.*, 2018). Effectors have been shown to possess different enzymatic activities, functioning as phosphatases, kinases, acetyl transferases, NADases and ubiquitin ligases. In some cases, effectors act by binding host proteins to perturb their activity, either by inhibition, altered stability, dysregulation, or perturbed localization (Huang *et al.*, 2021b; Hulin *et al.*, 2023; Toruño *et al.*, 2016; Wang *et al.*, 2023a; Win *et al.*, 2012a). Effectors are also able to modulate entire host pathways, such as vesicle trafficking and autophagy, rerouting nutrients or suppressing immunity to help promote infection (Bozkurt *et al.*, 2015; Dagdas *et al.*, 2018; Pandey *et al.*, 2021; Petre *et al.*, 2021; Yuen *et al.*, 2023).

1.8.1 Effectors as probes

Given that effectors are fine-tuned to target and modulate a variety of plant proteins and pathways, they can be ideal probes with which to study plant physiology and immunity. By characterizing effectors and studying their biology, we have acquired dozens of new molecular probes that have in turn helped identify novel components of different cellular processes, characterize their molecular functions and develop novel biotechnology tools (Deslandes & Rivas, 2012; Lee *et al.*, 2015; Toruño *et al.*, 2016). Pathogen effectors have helped study a wide variety of plant processes, including vesicle trafficking, autophagy, and plant immunity (Bozkurt *et al.*, 2015; Dagdas *et al.*, 2018; Derevnina *et al.*, 2021). A remarkable example of effectors being developed into cutting edge tools with which to study plant physiology are the transcription activator-like effectors (TALEs), mainly occurring in plant-pathogenic species of *Xanthomonas*. These effectors were initially shown to contribute to disease by binding to DNA and modulating specific host genes (Schornack *et al.*, 2013). The targeting of these effectors to specific DNA sequences was found to be encoded in repetitive 33-35 amino acid elements in their DNA-binding domain, knowledge which was subsequently leveraged to engineer TALEs into versatile genome editing and transcription modulation tools (Bogdanove *et al.*, 2010; Schornack *et al.*, 2013).

1.8.2 The RXLR-WY/LWY family of effectors.

Filamentous plant pathogen effectors are typically small, secreted proteins with high sequence diversity. At the sequence level, they usually exhibit little to no similarity to each other or

to other known proteins. Remarkably, despite the absence of overall sequence conservation, they can exhibit similar three-dimensional structures (Bialas *et al.*, 2018). This is the case with the RXLR-WY/LWY family of oomycete effectors. Oomycetes are a notoriously destructive group of pathogens that includes the potato late blight pathogen *P. infestans*, as well as many other plant-pathogenic species of the *Phytophthora* genus (Kamoun *et al.*, 2015).

Oomycetes translocate a large family of effector proteins with a characteristic N-terminal Arg-X-Leu-Arg (RXLR) amino acid motif downstream of a signal peptide. This N-terminal region is followed by a C-terminal effector region encoding the effector's biochemical activities (Win *et al.*, 2012a; Win *et al.*, 2012b). The C-terminal domains of RXLR effectors often include conserved sequence motifs (W, Y and L) resulting in modular folds which confer virulence activity. These folds, called WY-domains, act as a scaffold for the surface-exposed residues to evolve with their host targets, allowing these effectors to keep up with dynamic selection pressures (Bozkurt *et al.*, 2012; Win *et al.*, 2012b). WY-domains can exist as single units or in tandem repeats (Raffaele & Kamoun, 2012). A well-studied example is the *P. infestans* effector PexRD54. PexRD54 is an RXLR-WY effector consisting of 5-tandem WY modules. PexRD54 has been shown to target host autophagy, carrying a canonical C-terminal ATG8-interacting motif (AIM) (Dagdas *et al.*, 2016; Maqbool *et al.*, 2016). PexRD54 preferentially targets the host ATG8CL isoform and outcompetes endogenous autophagy adaptor Joka2 to disarm defense-related autophagy at the pathogen interface (Dagdas *et al.*, 2016; Dagdas *et al.*, 2018; Zess *et al.*, 2022). Intriguingly, PexRD54 does not fully shut down autophagy but instead stimulates the formation of autophagosomes that accumulate around the pathogen interface by bridging ATG8CL to the host vesicle transport regulator Rab8a (Pandey *et al.*, 2021). The pathogen is simultaneously disarming focal immune-related autophagy and reprogramming autophagosome biogenesis and trafficking, potentially to re-route beneficial cargo towards the plant-pathogen interface (Dagdas *et al.*, 2016; Dagdas *et al.*, 2018; Pandey *et al.*, 2021).

More recently, a novel kind of conserved modular fold akin to the WY-domain was identified. This is the LWY-fold, which was first described in *Phytophthora* suppressor of RNA silencing 2 (PSR2), an RXLR-LWY effector secreted by the soybean pathogen *Phytophthora sojae* (He *et al.*, 2019; Li *et al.*, 2023; Xiong *et al.*, 2014). PSR2 consists of seven tandem repeat α -helical units, with one WY fold followed by six LWY folds. Recently, PSR2 was shown to interact with its target, a host Serine/Threonine protein phosphatase 2A (PP2A) to alter phosphorylation of host proteins and promote disease. Structural and biochemical analyses revealed that PSR2 interacts with PP2A

via its LWY2 and LWY3 units. Fusing these PP2A interacting LWY modules to different C-terminal combinations of LWY modules led to diversification in downstream targets of the PP2A-PSR2 holoenzyme, suggesting that protein modularity may promote effector diversity and enhance pathogen virulence (Li *et al.*, 2023). Interestingly these modular RXLR-WY/LWY effectors are prevalent in *Phytophthora* and many other oomycetes (He *et al.*, 2019). However, the mechanisms by which they manipulate host processes to promote infection has not yet been fully elucidated.

1.8.3 The SPRYSEC family of effectors.

Plant-parasitic nematodes also deliver effectors as part of their infection process. These effectors are delivered into the plant via glandular secretions ejected from their oral stylet during feeding (Eves-van den Akker, 2021; Vieira & Gleason, 2019). So far, most of the research on nematodes has focused on the obligate biotrophic cyst nematodes (Genera *Globodera* and *Heterodera*) and root-knot nematodes (genus *Meloidogyne*). Although to date no useful effector-specific motifs such as the oomycete RXLR motif have been identified in phytophagous nematodes, their unique biology allowed for the identification of effector candidates based on tissue-specificity. Featuring dedicated effector-producing glands, genes with a signal peptide and no transmembrane domains that are expressed in these glands can be considered candidate effectors (Eves-van den Akker, 2021). Following this logic, multiple families of nematode effector families have been identified, with the SP1a and Ryanodine receptor (SPRY) secreted effector candidates (SPRYSEC) class being the most well studied.

First characterised in the potato cyst nematodes *G. rostochiensis* and *G. pallida*, SPRYSEC effectors have been associated with immune response modulation, with the genomes of these two nematode species showing remarkable expansions of SPRY-domain containing putative effectors (Ali *et al.*, 2015; Diaz-Granados *et al.*, 2016; Vieira & Gleason, 2019). SPRYSEC effectors have been identified as suppressors of plant immunity (Ali *et al.*, 2015; Postma *et al.*, 2012). Ali and colleagues carried out a screen in *N. tabacum* to find suppressors of the sensor CC-NLR Rx/CP-mediated cell death. They found that three effectors from *G. rostochiensis*, SS4, SS10, SS14, SS19 and SS34 can suppress the hypersensitive cell death mediated by Rx, Gpa2 and other host CC-NLRs, most of them NRC-dependent (Ali *et al.*, 2015; Derevnina *et al.*, 2021; Postma *et al.*, 2012). However, SS effectors can also act as AVRs. The previously discussed *G. pallida* SPRYSEC effector RBP1 can activate the sensor CC-NLR Gpa2, leading to cell death. As a result, RBP1 is highly polymorphic across *G. pallida* populations and appears to be under selection (Carpentier *et al.*, 2012; Sacco *et al.*,

2009). Despite extensive advances in the study of plant-parasitic nematodes and nematode effector biology, SPRYSEC effectors and their activities remain largely uncharacterized.

1.9 Pathogen suppression of NLRs.

1.9.1 Pathogen suppression of NLRs: indirect inhibition.

An emerging concept in NLR biology is that pathogen effectors can act as both triggers and suppressors of NLR-triggered immunity (Derevnina *et al.*, 2021; Wu & Derevnina, 2023). While most effectors studied to date suppress immune pathways induced by PTI, in some cases, adapted pathogens deploy effectors to interfere with host NLR signaling to promote disease. This effector-mediated suppression of NLR signaling can be achieved by various strategies. Some effectors act indirectly, by interfering with host proteins that act downstream of NLR signaling, while others act directly by physically interacting with NLRs to perturb their function (Wu & Derevnina, 2023).

The effector RipAC, from the bacteria *R. solanacearum* interferes with NLR signaling by associating with SGT1, an important host regulator required for NLR homeostasis and function. By forming a complex with SGT1, RipAC prevents mitogen activated protein kinase (MAPK)-mediated phosphorylation of SGT1, which is normally enhanced upon immune activation (Yu *et al.*, 2020). RipAC-SGT1 complex formation also prevents association between SGT1 and RAR1. SGT1, RAR1 and HSP90 normally form a molecular chaperone ternary complex which is required for correct functionality of multiple NLRs (Azevedo *et al.*, 2006). This perturbation of SGT1 phosphorylation and SGT1-RAR1 complex formation by RipAC can suppress immunity mediated by two SGT1-dependent NLRs, R3a and RPS2, as well as immune signaling triggered by the *R. solanacearum* AVR effectors RipAA and RipP1 (Nakano *et al.*, 2020; Yu *et al.*, 2020). A remarkable example is the HopBF1 effector from *P. syringae*. This effector can mimic a host client of the NLR chaperone HSP90, binding HSP90 and phosphorylating it, which results in its complete inactivation. As this chaperone is required to maintain NLRs in a stable, inactive and signal-competent form, this phosphorylation results in compromised NLR signaling (Lopez *et al.*, 2019). Another example is the *Xanthomonas euvesicatoria* effector XopQ, which can suppress NLR signaling by targeting and directly binding TFT4, a protein of the 14-3-3 family with a known role in immunity downstream of NLR activation, presumably by interfering with TFT4-client interactions required for correct immune signalling (Teper *et al.*, 2014). Many additional NLR-inhibiting or

suppressing effectors have been identified to date, although in most cases their precise molecular mechanisms and targets are not yet fully understood (**Table 1.1**).

1.9.2 Pathogen suppression of NLRs: direct inhibition.

Some effectors can suppress NLR signaling by directly targeting NLRs (**Table 1.1**). The effector HopZ3 from *P. syringae* is a YopJ family acetyltransferase that acetylates members of the CC-NLR RPM1 immune complex, thereby inactivating its immune response and promoting pathogen growth (Lee *et al.*, 2015). Another example is the RHA1B effector from the root knot nematode *Globodera pallida*, which functions as a E3 ubiquitin ligase that targets NLRs for degradation, thereby suppressing immunity (Kud *et al.*, 2019). More recently, a study on the bacterial effector AvrPtoB revealed that it can target helper NLRs in the NRG1/ADR1 network for degradation. AvrPtoB has E3 ligase activity and can ubiquitinate and promote degradation of ADR1-L1, with similar but milder effects on ADR1-L2 (Wang *et al.*, 2023a). This suppresses ADR1-L1 and ADR1-L2-mediated cell death, suggesting that targeting helper NLRs in NLR networks is a common virulence strategy (Contreras *et al.*, 2023a; Wang *et al.*, 2023a). Interestingly, AvrPtoB cannot suppress ADR1, and this specificity for helper suppression appears to be encoded in the N-terminal CC_R domain (Wang *et al.*, 2023a).

Table 1.1: List of published effectors with NLR suppressing activities.

Effector	Pathogen	Suppressed NLRs	Host target	Effector activity	References
HopZ3	<i>P. syringae</i>	RPM1	RPM1	Acetylation of host RPM1 results in inactivation of immune complex.	(Lee <i>et al.</i> , 2015)
HopBF1	<i>P. syringae</i>	RPM1	HSP90	Phosphorylation of host HSP90 results in its inactivation.	(Lopez <i>et al.</i> , 2019)
AvrPtoB	<i>P. syringae</i>	ADR1-L1, ADR1-L2	ADR1-L1, ADR1-L2	Ubiquitinates and promotes degradation of helper CC _R -NLRs,	(Wang <i>et al.</i> , 2023a)

				ADR1-L1 and ADR1-L2	
XopQ	<i>X. euvesicatoria</i>	Pto, Gpa2	TFT4	Binding to host TFT4 prevents association with downstream immune-related targets.	(Saunders <i>et al.</i> , 2012)
RipAC	<i>R. solanacearum</i>	R3a, RPS2	SGT1	Association prevents phosphorylation by MAP kinases.	(Yu <i>et al.</i> , 2019)
Lso-HPE1	<i>Candidatus liberibacter</i>	Prf	Unknown	Unknown.	(Levy <i>et al.</i> , 2019)
RHA1b	<i>G. pallida</i>	Prf, Rx, Rpi-blb1, Gpa2, Bs4	Unknown host E2 ubiquitin conjugation enzymes	Ubiquitination of target NLRs prevents their accumulation.	(Kud <i>et al.</i> , 2019)
SS4, SS18, SS19	<i>G. rostochiensis</i>	Rx	Unknown	Unknown.	(Ali <i>et al.</i> , 2015)
SS15	<i>G. rostochiensis</i>	NRC2/NRC3 and all NRC2/3-dependent sensor NLRs	NRC2, NRC3	Binds NB-ARC domain to prevent activation and oligomerization.	(Ali <i>et al.</i> , 2015; Contreras <i>et al.</i> , 2023a; Derevnina <i>et al.</i> , 2021)
SPRYSEC34, SS10	<i>G. rostochiensis</i>	Rpi-blb2	Unknown	Unknown.	(Ali <i>et al.</i> , 2015; Derevnina <i>et al.</i> , 2021)
IPI-O4	<i>P. infestans</i>	RB (also known as Rpi-blb1)	RB	Binding to CC-domain of RB immune signalling.	(Chen <i>et al.</i> , 2012; Karki <i>et al.</i> , 2020)

PITG-15278	<i>P. infestans</i>	Rpi-blb2	Unknown	Unknown.	(Derevnina <i>et al.</i> , 2021; Oh <i>et al.</i> , 2023)
AVRcap1b	<i>P. infestans</i>	NRC2/NRC3 and all NRC2/3- dependent sensor NLRs	TOL proteins	Unknown.	(Derevnina <i>et al.</i> , 2021)
Avr1	<i>Fusarium oxysporum</i> <i>f. sp. lycopersici</i>	I2 and I3	Unknown	Unknown.	(Houterman <i>et al.</i> , 2008)

1.9.3 Pathogen suppression of the NRC network

Considering how critical the NRC network is in mediating immunity in the Solanaceae, it is perhaps unsurprising that pathogens that infect solanaceous plants have evolved effectors to suppress this immune receptor network. As discussed above, multiple SPRYSEC effectors from Solanaceae-infecting nematodes have been shown to suppress host CC-NLRs. Interestingly, most of these can suppress NRC-dependent NLRs such as Rx, Gpa2, Rpi-blb2 and Sw5-b (Ali *et al.*, 2015; Derevnina *et al.*, 2021; Postma *et al.*, 2012). Some of these NRC-network suppressing effectors such as SS10 and SS34 appear to target sensor NLRs or sensor-helper communication, as they cannot suppress autoactive downstream helpers (Derevnina *et al.*, 2021). Previously Lida Derevnina, a postdoc in the Kamoun lab, designed a screen to identify effectors that could suppress NRCs, either at the level of sensors or helpers. This screen revealed that SS15 directly targets the downstream helper NRCs NRC2 and NRC3 and can even suppress autoactive MHD mutants of these two helpers (**Figure 1.7**). In order to do so, SS15 binds the NB-ARC domain of NRCs, potentially to prevent NB-ARC-mediated intramolecular rearrangements or to hinder NLR-NLR interactions (Derevnina *et al.*, 2021). Interestingly, SS15 acts as an NLR suppressor in *N. benthamiana* but is an AVR in *N. tabacum*. This begs the question of whether *N. tabacum* might possess NLRs that guard NRC helpers much like SNC1 guards ADR1 helpers in Arabidopsis (Ali *et al.*, 2015;

Wang *et al.*, 2023a). That effectors can both be activators and suppressors of NLRs raises interesting questions about host-pathogen co-evolution, as these effectors are simultaneously co-evolving with multiple NLRs, both to maintain NLR suppression and avoid NLR recognition. The exact mechanism by which SS15 binding to NRCs leads to immune suppression, however, is not known.

P. infestans also features effectors that suppress the NRC network. The RXLR WY effector PITG-15278 can suppress Rpi-blb2 mediated cell death in *N. benthamiana*. This effector cannot suppress autoactive helpers, indicating that it is likely acting at the sensor level or interfering with sensor-helper communication (Derevnina *et al.*, 2021). The screen carried out by Lida Derevnina and colleagues revealed that the RXLR-LWY effector AVRcap1b can also suppress NRC2 and NRC3-mediated cell death. AVRcap1b features a WY module followed by 6 tandem LWY modules and can suppress cell death of autoactive NRCs, indicating that it is acting at the level of NRC helpers or downstream (**Figure 1.7**). Intriguingly, unlike SS15, AVRcap1b does not associate with inactive NRC helpers. This suggests that it may be acting with an unknown component downstream of helper NLR activation or that it interferes specifically with activated NRCs (Derevnina *et al.*, 2021). Unfortunately, the study of active CC-NLRs remains technically challenging due to the early onset of cell death triggered upon NLR activation. Moreover, genetic resources to study activated NRCs in the absence of cell death, analogous to the *eds1* KO background for TIR-NLRs, are currently lacking (Gantner *et al.*, 2019). Large-scale yeast-two-hybrid assays and discovery proteomics by CoIP and tandem mass spectrometry (IP-MS) carried out by Lida Derevnina revealed Target of Myb 1-like (TOL) proteins as putative host targets of AVRcap1b (Derevnina *et al.*, 2021). TOLs are epsin N-terminal homology (ENTH)-GGA and Target of Myb 1 (GAT) domain-containing protein generally thought to be involved in membrane trafficking (De Craene *et al.*, 2012; Mosesso *et al.*, 2019; Moulinier-Anzola *et al.*, 2020). Whether TOLs are bonafide host targets of AVRcap1b or whether they are involved in NRC or NLR-mediated cell death remains to be tested. Moreover, the mechanism by which AVRcap1b functions as an NRC2/3 suppressor is unknown.

Suppressing helper NLRs is a highly efficient virulence strategy, as taking out the downstream helper nodes can simultaneously compromise multiple sensor NLRs that require these helpers. In the case of SS15 and AVRcap1b, targeting NRC2 and NRC3 allows these effectors to simultaneously act as suppressors of intracellular and cell-surface-mediated immunity. NRC3 was recently shown to mediate cell death downstream of cell surface receptors such as Cf4 and Ve1. By targeting NRC3, SS15 and AVRcap1b compromise Cf4/Avr4 mediated cell death (Kourelis *et*

al., 2022). Nonetheless, these two NRC-suppressing effectors also highlight the enhanced robustness conferred by networked immune signaling configurations. Even in the presence of these two robust immune suppressors, many sensors in the NRC network would retain functionality by signaling through NRC4. A better understanding of NLR suppressing effectors is paramount. Understanding the effector biology that underlies pathogen suppression of NLRs will allow us to develop strategies to bioengineer more resilient immune receptors that cannot be manipulated by effectors.

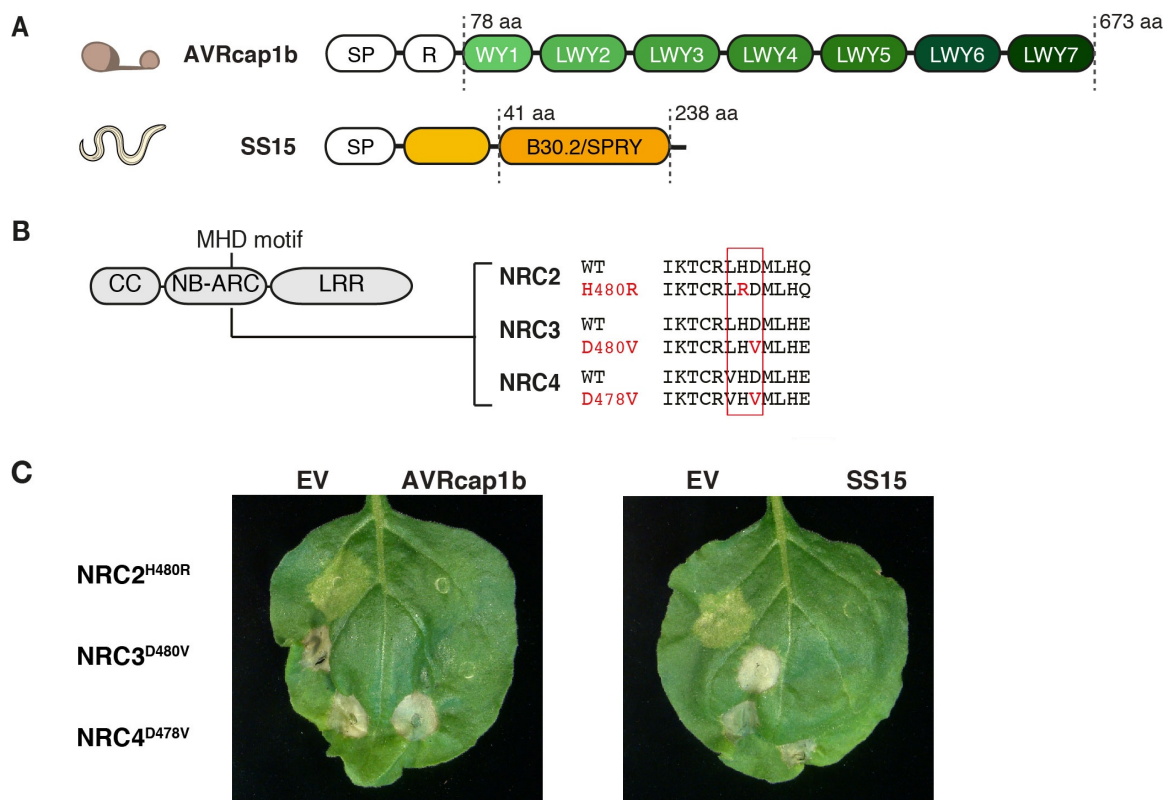


Figure 1.7: AVRcap1b and SS15 are suppressors of NRC2/3-mediated immunity.

(A) Domain organisation of AVRcap1b and SS15. (B) Mutations in the conserved MHD motif in the WHD of the NB-ARC domain (positions highlighted in red) of NRC2, NRC3 and NRC4 lead to autoactive variants that constitutively trigger HR cell death. (C) AVRcap1b and SS15 can suppress the hypersensitive cell death triggered by autoactive mutants of NRC2 and NRC3 but not NRC4 in the absence of an activated sensor NLR. These assays are based on heterologous expression of effector and NLR gene combination by agroinfiltration of leaves of the model plant *Nicotiana benthamiana*. The readout is the hypersensitive cell death visualized by the brownish tissue. EV denotes an empty vector control. Adapted from Derevnina et al., (2021).

1.10 TOL proteins and the ESCRT vesicle trafficking pathway.

1.10.1 The basics of plant ESCRT trafficking.

Correct protein sorting is of paramount importance for correct cellular homeostasis. Multivesicular bodies (MVBs) are known to play a key role in protein sorting across all eukaryotes, displaying a wide variety of functions. MVBs can function as part of the late endosome trafficking pathway, mediating trafficking to different compartments. They can be involved in retrograde endocytic trafficking, targeting membrane-bound proteins to vacuoles or lysosomes for storage or degradation (Jiang *et al.*, 2002). MVBs are also thought to be involved in the anterograde and late Golgi pathway, even contributing to exocytosis (Robinson *et al.*, 2016; Robinson & Neuhaus, 2016). They can also participate in immunity, accumulating at the host-pathogen interface formed during *P. infestans* colonization (Bozkurt *et al.*, 2015). Loading of ubiquitinated plasma membrane cargo into MVBs is mediated by the endosomal sorting complex required for transport (ESCRT) machinery, which in animals and plants consists of three heteromeric sub-complexes that function sequentially, termed ESCRT-I, ESCRT-II and ESCRT-III (Winter & Hauser, 2006).

In plants, ESCRT-0, the ESCRT component required for initial recognition and sorting of ubiquitinated cargo has not been identified. Instead, TOL proteins have emerged as key components of the ESCRT pathway, becoming highly diversified and expanded in plants (Mosesso *et al.*, 2019). TOLs capture ubiquitylated membrane-bound cargo and subsequently initiates recruitment of the first ESCRT subcomplex, ESCRT-1, effectively functioning as a cargo adaptor to load proteins into the ESCRT machinery (Mosesso *et al.*, 2019; Moulinier-Anzola *et al.*, 2020). Tom1 proteins are widely conserved in eukaryotes, with most species featuring one Tom1 protein (Winter & Hauser, 2006). In plants TOLs are particularly expanded in plants, with *Arabidopsis* possessing nine TOL proteins (Korbei *et al.*, 2013; Moulinier-Anzola *et al.*, 2020). This expansion could be indicative of neofunctionalization of these proteins in plants (Mosesso *et al.*, 2019). Interestingly, there seems to be a high degree of redundancy in plant TOLs. In *Arabidopsis*, only higher order quintuple TOL mutants exhibit phenotypic defects (Korbei *et al.*, 2013). As mentioned above Tom1 and TOL family of proteins feature N-terminal ENTH and GAT domains (**Figure 1.8**) (De Craene *et al.*, 2012). While binding of monoubiquitylated cargo is mainly mediated by the GAT domain, the ENTH domain can also participate in ubiquitin binding (Mosesso *et al.*, 2019; Moulinier-Anzola *et al.*, 2020).

1.10.2 TOL/ESCRT regulation of programmed cell death.

The ESCRT machinery has previously been shown to negatively regulate programmed cell death in metazoans. For example components of the ESCRT machinery can negatively regulate pyroptosis and ferroptosis in human cells, presumably by accumulating at the PM and excising damaged sections of membrane in response to gasdermin or MLKL-mediated pore formation and calcium influx (Dai *et al*, 2020; Gong *et al*, 2017; Pedrera *et al*, 2021; Rühl *et al*, 2018). The ESCRT pathway is known to be involved in membrane recycling and repair, being capable of replacing and resealing damaged sections of membrane in response to wounds and different stresses. In this way, the ESCRT machinery in metazoans can function to counteract perturbations of membrane integrity mediated by different agents, including pore-forming toxins (Castro-Gomes *et al*, 2014; Jimenez *et al*, 2014; Raab *et al*, 2016). In plants, the ESCRT machinery has been implicated in trafficking of cell-surface immune receptors, such as FLS2 (Spallek *et al*, 2013). Also, TOL proteins have been identified as proximal to the *P. syringae* effector AvrPto in BioID-based proximity labelling experiments, suggesting potential roles of these proteins in plant immunity (Conlan *et al*, 2018). Nonetheless, the precise roles of TOLs and the ESCRT machinery in regulating immunity programmed cell death and membrane repair in plants are not known.

Recently, our group identified the *P. infestans* AVRcap1b as an NRC network suppressing effector, capable of specifically blocking cell death initiated by NRC2 and NRC3. Lida Derevnina subsequently identified TOL proteins as putative host targets of the *P. infestans* effector AVRcap1b in *N. benthamiana* through yeast-two-hybrid screens and IP-MS experiments (Derevnina *et al*, 2021). Interestingly, all the hits identified in her yeast-two-hybrid screen pointed towards AVRcap1b interacting with TOLs via their N-terminal ENTH-GAT domains, suggesting that the effector could be interfering with TOL membrane tethering or modulating cargo binding (**Figure 1.8**). The fact that AVRcap1b can function as a suppressor of NRC2/3 mediated host immunity coupled with this newfound association with TOLs raises interesting questions.

NLR suppressing effectors can be remarkable tools with which to identify novel components or modulators of NLR signaling and NLR-mediated cell death. Moreover, the link between AVRcap1b and TOL proteins suggests that this effector may be useful as a probe with which to better understand the role of the TOL protein family and the ESCRT pathway in plants. Where traditional mutagenesis screens would fail due to redundancy and potential lethal phenotypes associated with the mutations, using AVRcap1b may yet yield excellent results.

Deciphering the link between AVRcap1b, TOLs and the NRC network could significantly advance our understanding of NLR signaling and the molecular mechanisms that underpin NLR immune networks while simultaneously shedding light on the plant ESCRT trafficking pathway.

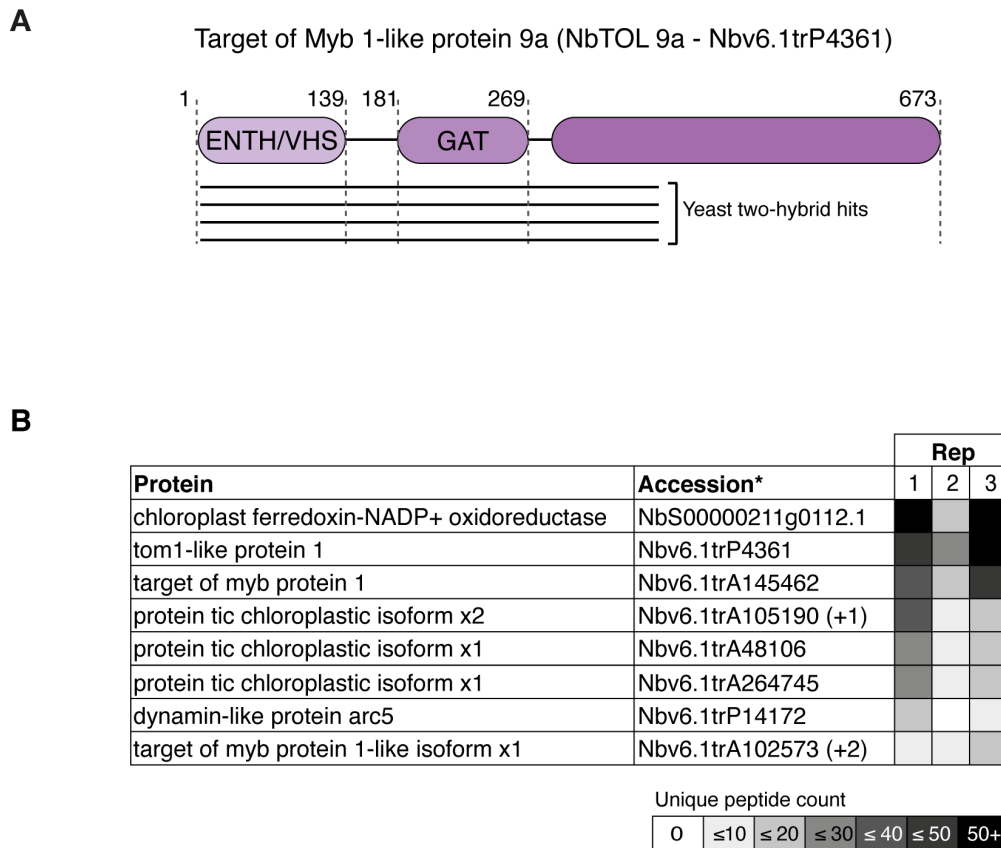


Figure 1.8: TOL proteins, potential host interactors of AVRcap1b.

(A) Domain structure of NbTOL9a consists of an N-terminal ENTH domain followed by a GAT domain. Black lines illustrate the position of the Y2H fragments identified in the screen with AVRcap1b. (B) TOL proteins were found among the top hits recovered in IP-MS experiments performed with AVRcap1b. Nbv6.1trP361 was the top hit in both IP-MS and blind Y2H screens.

1.11 Aims of the thesis

This study is focused on understanding activation and inhibition in the solanaceous NRC immune receptor network. This thesis had two main objectives: to understand the molecular mechanisms by which sensor-helper CC-NLR pairs in the NRC network communicate and activate in response to pathogen perception and to gain mechanistic insights into how AVRcap1b and SS15 suppress immune signaling mediated by NRCs.

In Chapter 3, I collaborated with Hiroaki Adachi to explore a cell death-inducing N-terminal truncation of the CC-NLR helper NRC4. This collaboration led to the discovery of the "MADA" motif, a conserved motif found in approximately one-fifth of angiosperm CC-NLRs. Our study showed that both cell death and disease resistance triggered by NRC4 necessitate an intact MADA motif (Adachi et al., 2019a).

In Chapter 4, I employed NRC MADA mutants to conduct biochemical analyses on sensor-helper activation within the NRC network. The outcome of these investigations led me to propose an activation-and-release model where effector recognition by sensors mediates oligomerization of downstream helpers into resistosome-like complexes. These complexes accumulate at the host plasma membrane, separate from the sensors (Contreras et al., 2023b).

In Chapter 5, I built on previous findings by Peter Moffett and his team related to Rx autoinhibition and signaling to decipher the communication process between NRC-dependent sensors and NRC helpers. This study revealed that the NB domain of several NRC-dependent sensor NLRs acts as the minimal signal required for NRC activation.

In the concluding chapters of this thesis, I utilized the knowledge gained on NRC network activation to explore the mode of action of two previously identified NRC immunosuppressing effectors, AVRcap1b and SS15.

In Chapter 6, I studied the interaction between AVRcap1b, an effector suppressing NRC2/3, and the Target of Myb 1-like (TOL) proteins. I found that AVRcap1b likely suppresses cell death by connecting TOL proteins and activated NRC complexes.

Finally, in Chapter 7, I used the techniques developed in previous chapters to investigate the mechanism by which the potato cyst nematode effector SS15 suppresses NRC2/3-mediated cell death. My data indicated that SS15 binds a critical hinge loop in the NB-ARC domain, likely hindering the conformational changes necessary for NLR activation.

Overall, this thesis enriches our understanding of sensor-helper activation and communication within the NRC network and lays the groundwork for further investigations into how pathogens can manipulate NLR signaling. My findings also serve as a starting point for future bioengineering efforts to enhance disease resistance.

Chapter 2: Materials and Methods.

2.1 Plant growth conditions.

Wild-type, *nrc2/3*, *nrc4a/b* and *nrc2/3/4* CRISPR KO mutant *Nicotiana benthamiana* lines were grown in a controlled environment growth chamber with a temperature range of 22–25°C, humidity of 45–65% and a 16/8-h light/dark cycle.

2.2 General Molecular biology and cloning methods.

2.2.1 Polymerase chain reaction (PCR) and PCR product purification

DNA fragment amplification was performed via polymerase chain reaction (PCR), utilizing Phusion™ High-fidelity DNA polymerase (ThermoFisher Scientific) as per the guidelines provided by the manufacturer. The annealing temperatures were adjusted for each reaction, depending on the primer combination, and these temperatures were determined with the aid of the T_m calculator tool by ThermoFisher Scientific. The duration allocated for elongation during each cycle was set at 30 seconds per kilobase. Following PCR, the products were processed through a 1% (w/v) agarose gel in 1X Tris-borate EDTA (TBE) buffer (containing 0.09 M Tris-borate and 2 mM EDTA), which was dyed with ethidium bromide to facilitate visualization under UV-light. The bands that matched the intended PCR products for cloning were cut out from the agarose gel. These cut-outs were then purified using the NucleoSpin Gel and PCR Clean-up kit (Macherey-Nagel) in strict adherence to the protocol provided by the manufacturer.

2.2.2 Plasmid construction.

The Golden Gate Modular Cloning (MoClo) kit (Weber *et al*, 2011) and the MoClo plant parts kit (Engler *et al*, 2014) were used for cloning, and all vectors are from this kit unless specified otherwise. Cloning design and sequence analysis were done using Geneious Prime (v2021.2.2; <https://www.geneious.com>). Elements used for plasmid construction is described in **Table AI.1**.

2.2.3 Golden Gate cloning

A slightly adjusted Golden Gate assembly protocol from Weber et al., 2011, was employed for Golden Gate cloning. For the level 0 restriction-ligation reaction, the following reagents were mixed: each insert and a level 0 acceptor measured at 100 ng/ μ L; 2 U of BpiI (Thermo Fisher Scientific); 4 U of T4 DNA ligase (Invitrogen); and 1 \times BSA (NEB) in the T4 DNA ligase buffer (Invitrogen), which all amounted to a final volume of 10 μ L. The level 1 restriction-ligation reaction contained: each level 0 module and binary vector with a concentration of 100 ng/ μ L; 2 U of BsaI-HF (NEB); 4 U of T4 DNA ligase (Invitrogen); and 1 \times BSA (NEB) in the T4 DNA ligase buffer (Invitrogen), to a final volume of 10 μ L. Reactions were subjected to a pre-defined Golden Gate program in a thermocycler, which consisted of the following steps: incubate for 30 seconds at 37°C, followed by 26 cycles of: 5 minutes at 37°C, 5 minutes at 20°C, and 10 minutes at 50°C, and finally 10 minutes at 80°C. Subsequent to the completion of these steps, the reaction was introduced into *E. coli* for plasmid amplification and storage as detailed below. Plasmids were isolated using a QIAprep Spin Miniprep Kit (Qiagen) or a NucleoSpin Plasmid kit (Macherey Nagel).

2.2.4 Bacterial transformation

E. coli DH5b subcloning efficiency chemically competent cells were transformed using a heat-shock protocol established in the lab. In summary, the ligation products were combined with the competent cells and chilled on ice for a duration of up to 30 minutes. These cells were then exposed to a heat shock process involving a 45-second incubation at 42°C, followed immediately by a 2-minute cooling period on ice. After this, 250 μ L of lysogeny broth (LB) was added to the cell mixture, which was then incubated under constant shaking at a temperature of 37°C for 60 minutes. The cell mixture was then spread onto agar plates prepared with LB medium and the appropriate antibiotics (either 50 μ g/mL of kanamycin or spectinomycin, or 100 μ g/mL of carbenicillin) and left to incubate overnight at a temperature of 37°C.

The *A. tumefaciens* electrocompetent cells, specifically the GV3101 pMP90 strain, underwent transformation utilizing an electroporation cuvette with a 1 mm gap width and an electroporator, using a Biorad system. The following electroporation parameters were set: voltage at 1.8 kV, resistance at 200 ohms, and capacitance at 25 μ F. Immediately succeeding the electroporation, the cells were combined with 500 μ L of LB medium, then incubated at a

temperature of 28°C for a period of 60 minutes, while being constantly agitated. The resulting cell mixture was then spread on LB agar plates, prepared with the appropriate antibiotics (50 µg/mL of kanamycin and 100 µg/mL of rifampicin; 50 µg/mL of spectinomycin and 100 µg/mL of rifampicin; or 100 µg/mL of carbenicillin and 100 µg/mL of rifampicin), and allowed to incubate at 28°C for roughly 48 hours.

2.3 Agroinfiltration and cell death assays.

Proteins of interest were transiently expressed according to previously described methods (Bos *et al.*, 2006). Briefly, leaves from 4–5-week-old plants were infiltrated with suspensions of *Agrobacterium tumefaciens* GV3101 pMP90 strains transformed with expression vectors coding for different proteins indicated. Final OD₆₀₀ of all *A. tumefaciens* suspensions were adjusted in infiltration buffer (10 mM MES, 10 mM MgCl₂, and 150 µM acetosyringone (pH 5.6)). OD₆₀₀ used for each construct in each experiment can be found in **Table AI.2**. For cell death assays, cell death on the leaves was scored 5 to 7 days using a scale ranging from 1 to 7, adapted from the HR scale developed by Segretin and colleagues (Segretin *et al.*, 2014), and brightfield and UV images were taken. UV imaging was done using UVP Blak-Ray B-100AP lights – 365 nm with a Wratten No.8 Yellow Filter on the camera. The camera setting was ISO 1600, White Balance 6250K, F11 and 10 s exposure for UV images.

2.3.1 Hairpin RNA-mediated gene silencing

The silencing fragments were designed and synthesized using the *N. benthamiana* genome sequence and associated gene silencing target prediction tool (SGN VIGS tool: <https://vigs.solgenomics.net>). Synthetic fragments were cloned into pRNAi-GG vectors according to Yan and colleagues and then transformed into *A. tumefaciens*. Leaves were coinfiltrated with either pRNAi-GG::*NbTOL9a* or pRNAi-GG::*GUS*, at a final OD₆₀₀ of 0.5, together with different proteins indicated in the text with final OD₆₀₀ indicated in **Table AI.2**. The HR cell death on the leaves was scored at 5 to 7 days as described above, and brightfield and UV images were taken. UV imaging was done using UVP Blak-Ray B-100AP lights – 365 nm with a Wratten No.8 Yellow Filter on the camera. The camera setting was ISO 1600, White Balance 6250K, F11 and 10 s exposure for UV images.

2.4 *Phytophthora infestans* growth conditions and infection assays.

P. infestans infection assays were performed by applying droplets of zoospore suspension on detached leaves as described previously (Song *et al.*, 2009). Briefly, leaves of five-weeks old wild-type and *nrc4a/b* *N. benthamiana* plants were infiltrated with *A. tumefaciens* solutions, in which each *Agrobacterium* containing a plasmid expressing Rpi-blb2 (Wu *et al.*, 2017) was mixed in a 1:1 ratio ($OD_{600} = 0.5$ for each strain) with *Agrobacterium* containing either the empty vector, wild type NRC4, or NRC4 variant. At 24 hr after agroinfiltration, the abaxial side of the leaves were inoculated with 10 μ L zoospore suspension (100 zoospores/ μ L) of *P. infestans* strain 88069 prepared according to the methods reported by (Song *et al.*, 2009). The inoculated leaves were kept in a moist chamber at room temperature (21–24°C) for 7 days and imaged under UV light (UVP Blak-Ray B-100AP lights – 365 nm) with Wratten No.8 Yellow Filter for visualization of the lesions. The camera setting was ISO 1600, White Balance 6250K, F11 and 10 s exposure.

2.5 Phylogenetic analyses of *N. benthamiana* and *Arabidopsis thaliana* TOL proteins

Amino acid sequences of the NbTOL paralogs identified in *N. benthamiana* and previously published *A. thaliana* AtTOL proteins (Korbei *et al.*, 2013; Moulinier-Anzola *et al.*, 2020) were aligned using Clustal Omega (Larkin *et al.*, 2007). The alignment was then manually edited in MEGAX (Stecher *et al.*, 2020). The gaps in the alignment were manually removed, and only the ENTH and GAT domains were used to generate the phylogenetic tree. A maximum-likelihood tree of the *N. benthamiana* and *A. thaliana* TOLs was generated in MEGAX using the JTT model and with bootstrap values based on 1,000 iterations. The resulting tree was then visualised using iTOL (Letunic & Bork, 2021). The alignment used to make the tree can be found in the [Supplementary Information of Derevnina et al., \(2021\)](#).

2.6 Biochemistry methods.

2.6.1 Extraction of total proteins for SDS-PAGE assays.

Four to five-week-old *N. benthamiana* plants were agroinfiltrated as described above with constructs of interest and leaf tissue was collected 3 days post agroinfiltration. 6 leaf discs of 5 mm

each were snap frozen in liquid nitrogen and ground using a Geno/Grinder tissue homogenizer. Total protein was subsequently extracted and homogenized in extraction buffer, which was GTEN (10% glycerol, 25 mM Tris-HCl (pH 7.5), 1 mM EDTA, 150 mM NaCl) supplemented with 2% (w/v) polyvinylpolypyrrolidone, 10 mM dithiothreitol, 1× protease inhibitor cocktail (SIGMA) and 0.2% IGEPAL (SIGMA, United Kingdom)). Samples were incubated with extraction on ice for 10 minutes with short vortex mixing every 2 min. After centrifugation at 5,000 ×g for 15 minutes, the supernatant was transferred to a new tube and subjected to a second 15-minute centrifugation at 5,000 ×g. After the second centrifugation, the supernatant was transferred to a new tube and used for SDS-PAGE assays.

2.6.2 Extraction of total proteins for BN-PAGE assays.

Four to five-week-old *N. benthamiana* plants were agroinfiltrated as described above with constructs of interest and leaf tissue was collected 3 days post agroinfiltration or 2 days post agroinfiltration in experiments with NRC4. BN-PAGE was performed using the Bis-Tris Native PAGE system (Invitrogen) according to the manufacturer's instructions. 6 leaf discs of 5 mm diameter each were ground using a Geno/Grinder tissue homogenizer and total protein was subsequently extracted and homogenized in extraction buffer. For NRC2, GTMN extraction buffer was used (10% glycerol, 50 mM Tris-HCl (pH 7.5), 5 mM MgCl₂ and 50 mM NaCl) supplemented with 10 mM DTT, 1x protease inhibitor cocktail (SIGMA) and 0.2% Nonidet P-40 Substitute (SIGMA). For NRC4, GHMN buffer (10% glycerol, 50 mM HEPES (pH 7.4), 5 mM MgCl₂ and 50 mM NaCl) buffer supplemented with 10 mM DTT, 1x protease inhibitor cocktail (SIGMA) and 1% Digitonin (SIGMA) was used for extraction. Samples were incubated in extraction buffer on ice for 10 min with short vortex mixing every 2 min. Following incubation, samples were centrifuged at 5,000 g for 15 min and the supernatant was used for BN-PAGE and SDS-PAGE assays.

2.6.3 Extraction of proteins for Co-Immunoprecipitation assays.

Four to five-week-old plants were agroinfiltrated as described above with constructs of interest and leaf tissue was collected 3 days post agroinfiltration. 2 half *N. benthamiana* leaves were snap frozen in liquid nitrogen and ground using a Geno/Grinder tissue homogenizer. Total protein was extracted with GTEN extraction buffer supplemented with 2% (w/v)

polyvinylpyrrolidone, 10 mM dithiothreitol, 1× protease inhibitor cocktail (SIGMA), 0.2% IGEPAL (SIGMA, United Kingdom). Samples were incubated with extraction on ice for 10 minutes with short vortex mixing every 2 min. After centrifugation at 5,000 ×g for 15 minutes, the supernatant was transferred to a new tube and subjected to a second 15 minute centrifugation at 5,000 ×g. After the second centrifugation at 5,000 ×g for 15 minutes, the supernatant was passed through a Minisart 0.45 μM filter (Sartorius Stedim Biotech) and collected into a new tube. Filtered supernatant was used for Co-Immunoprecipitation assays.

2.6.4 BN-PAGE assays.

For BN-PAGE, samples extracted as detailed above were diluted as per the manufacturer's instructions by adding NativePAGE 5% G-250 sample additive, 4x Sample Buffer and water. After dilution, samples were loaded and run on Native PAGE 3–12% Bis-Tris gels alongside either NativeMark unstained protein standard (Invitrogen) or SERVA Native Marker (SERVA). The proteins were then transferred to polyvinylidene difluoride membranes using NuPAGE Transfer Buffer using a Trans-Blot Turbo Transfer System (Bio-Rad) as per the manufacturer's instructions. Proteins were fixed to the membranes by incubating with 8% acetic acid for 15 min, washed with water and left to dry. Membranes were subsequently re-activated with methanol to correctly visualize the unstained native protein marker. Membranes were immunoblotted as described below, in section 2.7.7.

2.6.5 SDS-PAGE assays.

For SDS-PAGE, samples were diluted in SDS loading dye and denatured at 72 °C for 10 min. Denatured samples were spun down at 5,000 g for 3 min and supernatant was run on 4–20% Bio-Rad 4–20% Mini-PROTEAN TGX gels alongside a PageRuler Plus prestained protein ladder (Thermo Scientific). The proteins were then transferred to polyvinylidene difluoride membranes using Trans-Blot Turbo Transfer Buffer using a Trans-Blot Turbo Transfer System (Bio-Rad) as per the manufacturer's instructions. Membranes were immunoblotted as described below.

2.6.6 Co-Immunoprecipitation assays.

Filtered protein extracts were obtained as described above and divided into “Input” fraction and “Immunoprecipitate (IP)” fraction. SDS loading buffer was added to each Input sample and then samples were boiled at 72 °C for 10 minutes. Boiled input samples were set aside. For the IP fraction, at least 1ml of extract was used for each treatment. Regardless of the volume used, the same volume of IP fraction was set aside for each sample. 30 μ L of the desired antibody-conjugated agarose beads were equilibrated in IP wash buffer (GTEN buffer with 0.2% IGEPAL) and added to each sample. Beads used were GFP-Trap-A agarose beads (Chromotek), anti-c-myc A7470 agarose beads (Sigma), Anti-FLAG M2 Affinity Gel (Sigma), or anti-HA affinity matrix beads (Roche). Samples were incubated for 60 minutes with the beads at 4 °C in a slowly moving rotor to prevent the beads from precipitating and to ensure that the protein extracts are homogeneously exposed to the beads. After the incubation, samples were subjected to 5 consecutive washes. For each wash, samples were subjected to a 1-minute centrifugation at 1000 x g, after which most of the supernatant was removed carefully with a pipette, leaving 100 μ L of liquid to avoid disturbing the pelleted beads. 1 mL of IP wash buffer was added to the tube, and the next centrifugation step took place. After the last wash, instead of adding 1 mL of IP wash buffer, the last 100 μ L of liquid were removed carefully with a syringe and a needle, leaving the beads behind. 60 μ L of SDS loading buffer was added to each sample and proteins were eluted from the beads by boiling at 72 °C for 10 minutes. Each sample was subjected to a 3-minute centrifugation at 5000 x g and the supernatant was used for SDS-PAGE assays. In parallel, boiled Input samples were also used for SDS-PAGE assays, as described above in section 2.6.5.

2.6.7 Immunoblotting and detection of BN-PAGE, SDS-PAGE and CoIP assays.

Blotted membranes were blocked with 5% milk in Tris-buffered saline plus 0.01% Tween 20 (TBS-T) for an hour at room temperature and subsequently incubated with desired antibodies at 4°C overnight. Antibodies used were anti-GFP (B-2) HRP (Santa Cruz Biotechnology), anti-HA (3F10) HRP (Roche), anti-Myc (9E10) HRP (Roche), anti-FLAG (M2) HRP (Sigma) and anti-V5 (V2260) HRP (Roche), all used in a 1:5,000 dilution in 5% milk in TBS-T. To visualize proteins, we used Pierce ECL Western (32106, Thermo Fisher Scientific), supplementing with up to 50% SuperSignal West Femto Maximum Sensitivity Substrate (34095, Thermo Fishes Scientific) when necessary. Membrane imaging was carried out with an ImageQuant LAS 4000 or an ImageQuant 800 luminescent imager (GE Healthcare Life Sciences, Piscataway, NJ). Rubisco loading control was stained using Ponceau S (Sigma) or Ponceau 4R (Irnbru, AG Barr).

2.6.8 Gel filtration assays with NRC2.

Protein was extracted as described above in section 2.6.2. Protein extracts were filtered through a 0.45 μm filter (Sartorius) and 200 μl of filtered extract were analyzed by gel filtration. Extracts were run on a Superdex 200 Increase 10/300 GL column (GE Healthcare) connected to an AKTA Pure system (GE Healthcare), with samples being run at a flow rate of 0.4 ml/min. The buffer used for elution was GTMN extraction buffer (10% glycerol, 50 mM Tris-HCl (pH 7.5), 5 mM MgCl_2 and 50 mM NaCl) supplemented with 1 mM DTT, to match the extraction buffer used for NRC2. The eluted fractions were analyzed by SDS-PAGE as described above and immunoblotted with the corresponding antibodies.

2.6.9 BN and SDS-PAGE assays with PVX infection (agroinfection)

Four to five-week-old plants were agroinfiltrated as described above with constructs of interest. Simultaneously, PVX was delivered by agroinfection using an *A. tumefaciens* strain carrying GFP-labelled PVX (pGR106-PVX-GFP). Final OD_{600} used was 0.3 for each NLR immune receptor used and 0.05 for the *A. tumefaciens* strain carrying PVX or free GFP for a total OD_{600} of 0.65. Leaf tissue was collected 3 days post agroinfiltration. BN-PAGE and SDS-PAGE assays were carried out as described above.

2.6.10 Membrane enrichment assays

Membrane enrichment was carried out by slightly modifying a previously described protocol (Abas & Luschnig, 2010). In brief, leaf material was ground to fine powder using liquid nitrogen and 2x volume of extraction buffer was added. Extraction buffer consisted of 0.81 M sucrose, 5% (v/v) glycerol, 10 mM EDTA, 10 mM EGTA, 5 mM KCl, and 100 mM Tris-HCl (pH 7.5) supplemented with 5 mM DTT, 1% Sigma Plant Protease Inhibitor Cocktail, 1 mM PMSF and 0.5% PVPP. After addition of the buffer, the samples were vortexed for a minute and the cell debris was cleared out by two subsequent centrifugation steps at 1,000 g for 5 min. The supernatant was diluted 1:1 using distilled water and an aliquot of the supernatant was separated as the total fraction (T). The remaining supernatant (200–300 μl) was further centrifuged at 21,000 g for 90 min at 4°C. This centrifugation yielded the supernatant (soluble fraction, S) and membrane

enriched pellet (membrane fraction, M). After separating the soluble fraction, the pellet was resuspended in diluted extraction buffer (without PVPP). All the fractions were diluted with SDS loading dye, and proteins were denatured by incubating at 50°C for 15 min. Western blotting was performed as previously described following SDS–PAGE. Endogenous plasma membrane ATPase was detected using anti-H + ATPase (AS07 260) antibody (Agrisera) as a marker to show the success of membrane enrichment.

2.7 Confocal microscopy

Three to four-week-old plants were agroinfiltrated as described above with constructs of interest. PVX was delivered as before, or the coat protein CP-4xMyc or EV control at OD₆₀₀ 0.1; Rx-RFP at OD₆₀₀ of 0.25 and NRC2^{EEE}-GFP at OD₆₀₀ of 0.25. Leaf tissue was prepared for imaging by sectioning of desired area surrounding an infection spot using a cork borer size 4, and were mounted, live, in wells containing dH₂O made in Carolina Observation Gel to enable diffusion of gasses. The abaxial of the leaf tissue was imaged using a Leica SP8 with 40x water immersion objective. Laser excitations for fluorescent proteins were used as described previously (Duggan *et al.*, 2021), namely 488 nm (Argon) for GFP, 561/594 nm (Diode) for RFP and 405 nm (Diode) for BFP.

2.8 Recombinant protein purification from *E. coli*

2.8.1 Purification of AVRcap1b in complex with NbTOL9a domains

Recombinant AVRcap1b protein (lacking signal peptide and RXLR motif) was expressed by cloning in pOPIN-S3C plasmid, with an N-terminal tandem 6xHis-SUMO followed by a 3C protease cleavage site. pOPIN-S3C:AVRcap1b was transformed into *E. coli* SHuffle cells. Eight litres of these cells were grown at 30°C in autoinduction medium to an OD₆₀₀ of 0.6 to 0.8 followed by overnight incubation at 18°C and harvested by centrifugation. Pelleted cells were resuspended in 50 mM tris-HCl (pH 8), 500 mM NaCl, 50 mM glycine, 5% (v/v) glycerol, and 20 mM imidazole (buffer A) supplemented with cComplete EDTA-free protease inhibitor tablets (Roche) and lysed by sonication. The clarified cell lysate was applied to a Ni²⁺-NTA column connected to an AKTA pure system. 6xHis-SUMO-AVRcap1b was step eluted with elution buffer (buffer A with 500 mM imidazole) and directly injected onto a Superdex 200 26/600 gel filtration column pre-equilibrated

with buffer B [20 mM Hepes (pH 7.5) and 150 mM NaCl]. The fractions containing 6xHis-SUMO-AVRcap1b were pooled, and the N-terminal 6xHis-SUMO tag was cleaved by addition of 3C protease (10 µg/mg of fusion protein), incubating overnight at 4°C. Cleaved AVRcap1b was further purified using a Ni²⁺-NTA column, this time collecting the flow-through to separate the cleaved tag from the AVRcap1b protein. Untagged AVRcap1b was further purified by another round of gel filtration as described above. The concentration of protein was judged by absorbance at 280 nm (using a calculated molar extinction coefficient of 110,810 M⁻¹ cm⁻¹ for AVRcap1b).

Recombinant NbTOL9a subdomains, were also expressed cloning in pOPIN-S3C plasmid as described above. NbTOL9a, NbTOL9a^{ENTH-GAT} and NbTOL9a^{ENTH} and NbTOL9a^{GAT} were cloned into pOPIN-F (Cleavable N-terminal 6xHis tag) and pOPIN-S3C plasmids and transformed into *E. coli* sHuffle cells. First, small scale purification trials were performed, expressing 1 litre of each of the 8 transformed *E. coli* strains. Cells were grown at 37°C in autoinduction medium to an OD₆₀₀ of 0.6 to 0.8 followed by overnight incubation at 18°C and harvested by centrifugation. Pelleted cells were resuspended in 50 mM tris-HCl (pH 8), 500 mM NaCl, 50 mM glycine, 5% (v/v) glycerol, and 20 mM imidazole (buffer A) supplemented with cComplete EDTA-free protease inhibitor tablets (Roche) and lysed by sonication. The clarified cell lysate was applied to a Ni²⁺-NTA column connected to an AKTA pure system. 6xHis and 6xHis-SUMO-tagged proteins were step eluted with elution buffer (buffer A with 500 mM imidazole), and the elution was used for SDS-PAGE assays.

For scaling up purification of 6xHis-SUMO-NbTOL9a^{ENTH-GAT} and 6xHis-SUMO-NbTOL9a^{ENTH}, 8 litres of each *E. coli* sHuffle strain were grown at 37°C in autoinduction medium to an OD₆₀₀ of 0.6 to 0.8 followed by overnight incubation at 18°C and harvested by centrifugation. Pelleted cells were resuspended in 50 mM tris-HCl (pH 8), 500 mM NaCl, 50 mM glycine, 5% (v/v) glycerol, and 20 mM imidazole (buffer A) supplemented with cComplete EDTA-free protease inhibitor tablets (Roche) and lysed by sonication. The clarified cell lysate was applied to a Ni²⁺-NTA column connected to an AKTA pure system. 6xHis-SUMO-tagged proteins were step eluted with elution buffer (buffer A with 500 mM imidazole) and directly injected onto a Superdex 75 26/600 gel filtration column pre-equilibrated with buffer B [20 mM Hepes (pH 7.5) and 150 mM NaCl]. The fractions containing 6xHis-SUMO-NbTOL9a^{ENTH-GAT} or 6xHis-SUMO-NbTOL9a^{ENTH} were pooled, and the N-terminal 6xHis-SUMO tag was cleaved by addition of 3C protease (10 µg/mg of fusion protein), incubating overnight at 4°C. Cleaved NbTOL9a^{ENTH-GAT} or NbTOL9a^{ENTH} was further purified using a Ni²⁺-NTA column, this time collecting the flow-

through to separate the cleaved tag from the protein of interest. Untagged NbTOL9a^{ENTH-GAT} or NbTOL9a^{ENTH} was further purified by another round of gel filtration as described above. The concentration of protein was judged by absorbance at 280 nm (using a calculated molar extinction coefficient of 19,940 M⁻¹ cm⁻¹ for NbTOL9a^{ENTH-GAT} and 15,470 M⁻¹ cm⁻¹ for NbTOL9a^{ENTH}).

To obtain AVRcap1b in complex with NbTOL9a^{ENTH-GAT} or NbTOL9a^{ENTH}, both proteins were incubated in a 1:1 molar ratio overnight at 4°C and subjected to gel filtration on a Superdex 200 26/600 gel filtration column as described above. The fractions containing AVRcap1b in complex with NbTOL9a^{ENTH-GAT} or NbTOL9a^{ENTH} were pooled, concentrated to 10 to 15 mg/ml, and subsequently used for crystallization screens.

2.8.2 Gel filtration assays with AVRcap1b and NbTOL9a^{ENTH}

AVRcap1b and NbTOL9a were purified as described above in section 2.8.1. 200 µl of concentrated protein (5 mg/ml) were run on a Superdex 200 Increase 10/300 GL column (GE Healthcare) connected to an AKTA Pure system (GE Healthcare), with samples being run at a flow rate of 0.4 ml/min. The buffer used for elution was buffer B. Each protein was run individually first. Then, 200 µl of an equimolar mixture of AVRcap1b and NbTOL9a^{ENTH} was run using the same procedure, for comparison. The eluted fractions were analysed by SDS-PAGE as described above and stained with Coomassie.

2.8.3 Purification of SS15 in complex with SINRC1^{NB-ARC}

Heterologous production and purification of SS15 was performed as previously described (Contreras *et al.*, 2023a; Derevnina *et al.*, 2021). Recombinant SS15 protein (lacking signal peptide) was expressed by cloning in pOPIN-S3C plasmid, with an N-terminal tandem 6xHis-SUMO followed by a 3C protease cleavage site. pOPIN-S3C:SS15 was transformed into *E. coli* SHuffle cells. 8 litres of these cells were grown at 30°C in autoinduction medium to an OD₆₀₀ of 0.6 to 0.8 followed by overnight incubation at 18°C and harvested by centrifugation. Pelleted cells were resuspended in 50 mM tris-HCl (pH 8), 500 mM NaCl, 50 mM glycine, 5% (v/v) glycerol, and 20 mM imidazole (buffer A) supplemented with cComplete EDTA-free protease inhibitor tablets (Roche) and lysed by sonication. The clarified cell lysate was applied to a Ni²⁺-NTA column connected to an AKTA pure system. 6xHis-SUMO-SS15 was step eluted with elution buffer (buffer A with 500 mM imidazole) and directly injected onto a Superdex 200 26/600 gel filtration

column pre-equilibrated with buffer B [20 mM Hepes (pH 7.5) and 150 mM NaCl]. The fractions containing 6xHis-SUMO-SS15 were pooled, and the N-terminal 6xHis-SUMO tag was cleaved by addition of 3C protease (10 µg/mg of fusion protein), incubating overnight at 4°C. Cleaved SS15 was further purified using a Ni²⁺-NTA column, this time collecting the flow-through to separate the cleaved tag from the SS15 protein. Untagged SS15 was further purified by another round of gel filtration as described above. The concentration of protein was judged by absorbance at 280 nm (using a calculated molar extinction coefficient of 35,920 M⁻¹ cm⁻¹ for SS15).

Heterologous production and purification of SINRC1^{NB-ARC} was performed as previously described (Steele *et al*, 2019). Recombinant SINRC1^{NB-ARC} protein was also expressed cloning in pOPIN-S3C plasmid as described above. pOPIN-S3C:SINRC1^{NB-ARC} was transformed into *E. coli* Lemo21 (DE3) cells. 8 litres of these cells were grown at 37°C in autoinduction medium to an OD₆₀₀ of 0.6 to 0.8 followed by overnight incubation at 18°C and harvested by centrifugation. Pelleted cells were resuspended in 50 mM tris-HCl (pH 8), 500 mM NaCl, 50 mM glycine, 5% (v/v) glycerol, and 20 mM imidazole (buffer A) supplemented with cComplete EDTA-free protease inhibitor tablets (Roche) and lysed by sonication. The clarified cell lysate was applied to a Ni²⁺-NTA column connected to an AKTA pure system. 6xHis-SUMO-SINRC1^{NB-ARC} was step eluted with elution buffer (buffer A with 500 mM imidazole) and directly injected onto a Superdex 200 26/600 gel filtration column pre-equilibrated with buffer B [20 mM Hepes (pH 7.5) and 150 mM NaCl]. The fractions containing 6xHis-SUMO-SINRC1^{NB-ARC} were pooled, and the N-terminal 6xHis-SUMO tag was cleaved by addition of 3C protease (10 µg/mg of fusion protein), incubating overnight at 4°C. Cleaved SINRC1^{NB-ARC} was further purified using a Ni²⁺-NTA column, this time collecting the flow-through to separate the cleaved tag from the SINRC1^{NB-ARC} protein. Untagged SINRC1^{NB-ARC} was further purified by another round of gel filtration as described above. The concentration of protein was judged by absorbance at 280 nm (using a calculated molar extinction coefficient of 63,370 M⁻¹ cm⁻¹ for SINRC1^{NB-ARC}).

To obtain SINRC1^{NB-ARC} in complex with SS15, both proteins were incubated in a 1:1 molar ratio overnight at 4°C and subjected to gel filtration on a Superdex 200 26/600 gel filtration column as described above. The fractions containing SINRC1^{NB-ARC} in complex with SS15 were pooled, concentrated to 10 to 15 mg/ml, and subsequently used for crystallization screens.

2.9 Crystallography and structural solution.

2.9.1 Crystallization and data collection of AVRcap1b-NbTOL9a^{ENTH} protein complexes

Crystallization screens were performed at 18°C using the sitting-drop vapor diffusion technique. Drops composed of 0.3 µl of protein solution and 0.3 µl of reservoir solution were set up in MRC 96-well crystallization plates (Molecular Dimensions), which were dispensed using an Oryx Nano or an Oryx8 robot (Douglas Instruments). Crystal growth was monitored using a Minstrel Desktop Crystal Imaging System (Rikagu). Crystals of the AVRcap1b-NbTOL9a^{ENTH} complex grew directly from the BCS screen (Molecular Dimensions) in conditions comprised of 0.2 M magnesium chloride hexahydrate, 10% (v/v) ethylene glycol, 0.1 M HEPES pH7.5, 15% (v/v) PEG smear medium, 5% (v/v) 2-propanol. The crystals were cryoprotected using this condition supplemented with 30% (v/v) ethylene glycol, before harvesting by flash-cooling in liquid nitrogen using LithoLoops (Molecular Dimensions). X-ray diffraction data were collected at the Diamond Light Source (Didcot, UK) on beamline I04 using an Eiger2 XE 16M pixel array detector (Dectris) with crystals maintained at 100 K by a Cryojet cryocooler (Oxford Instruments).

2.9.2 Data processing and structural solution for AVRcap1b-NbTOL9a^{ENTH} protein complex

X-ray data were integrated and scaled using DIALS (Winter *et al.*, 2018), as implemented through the XIA2 (Winter, 2010) pipeline, and then merged using AIMLESS (Evans & Murshudov, 2013), via the CCP4i2 graphical user interface (Winn, 2003). The AVRcap1b-NbTOL9a^{ENTH} complex crystallized in space group $P2_12_12_1$ with cell parameters $a = 85.9$, $b = 136.9$ and $c = 195.6$ Å, and yielded diffraction data to 4.1 Å resolution (see **Table AV.1** for a summary of data collection statistics). Structural predictions for the complex were generated using AlphaFold2 (AF2) multimer (Evans *et al.*, 2021), as implemented through ColabFold (Mirdita *et al.*, 2022). There was very good sequence coverage for both proteins, and the five independent models of the individual components were closely similar. The predicted local distance difference test (pLDDT) scores were generally good (e.g., averages of 88 and 83 for AVRcap1b and NbTOL9a^{ENTH} models, respectively, from the rank 1 predictions). However, the relative placement

of the two components varied across the five models, and the corresponding predicted aligned error (PAE) scores indicated very low confidence in these predictions.

Templates for both components were prepared using the “Process Predicted Models” CCP4i2 task, which removed low-confidence regions (based on pLDDT) and converted the pLDDT scores in the *B* factor field of the PDB coordinate files to pseudo *B* factors. Analysis of the likely composition of the asymmetric unit (ASU) suggested that it contained two copies of each component, giving an estimated solvent content of ~63%. Phaser (McCoy *et al*, 2007) was able to place the four chains within the ASU, giving two equivalent complexes without any significant clashes. The structure was then subjected to jelly body refinement in REFMAC5 (Murshudov *et al*, 2011) using ProSMART restraints (Nicholls *et al*, 2014) generated from the AF2 models. After several iterations of rebuilding in using COOT (Emsley *et al*, 2010) and restrained REFMAC5 refinement, the final model was obtained with R_{work} and R_{free} values of 0.225 and 0.306, respectively, to a 4.1-Å resolution (see **Table AV.1** for a summary of refinement statistics). All structural figures were prepared using ChimeraX (Pettersen *et al*, 2021).

2.9.3 Crystallization and data collection of SS15-SINRC1^{NB-ARC} protein complex

Crystallization screens were performed at 18°C using the sitting-drop vapor diffusion technique. Drops composed of 0.3 µl of protein solution and 0.3 µl of reservoir solution were set up in MRC 96-well crystallization plates (Molecular Dimensions), which were dispensed using an Oryx Nano or an Oryx8 robot (Douglas Instruments). Crystal growth was monitored using a Minstrel Desktop Crystal Imaging System (Rikagu). Suitable crystals grew after 72 hours in a Morpheus screen crystallization condition containing 0.1 M MES buffer (pH 6.5), 10% (w/v) PEG-8000 (polyethylene glycol, molecular weight 8000), and 20% (v/v) ethylene glycol (Molecular Dimensions) and were harvested by flash-cooling in liquid nitrogen using LithoLoops (Molecular Dimensions). X-ray diffraction data were collected at the Diamond Light Source (Didcot, UK) on beamline I03 using an Eiger2 XE 16M pixel array detector (Dectris) with crystals maintained at 100 K by a Cryojet cryocooler (Oxford Instruments).

2.9.4 Data processing and structural solution for SS15-SINRC1^{NB-ARC} protein complex

X-ray data were integrated and scaled using X-ray Detection Software (XDS) (Kabsch, 2010), as implemented through the XIA2 (Winter, 2010) pipeline, and then merged using AIMLESS (Evans & Murshudov, 2013), via the CCP4i2 graphical user interface (Winn, 2003). The NRC1^{NB-ARC}-SS15 complex crystallized in space group $P6_1$ with cell parameters $a = b = 128.6$ and $c = 170.7$ Å, and the Most Unexceptional crystal yielded diffraction data to 4.5 Å resolution (see table S3 for a summary of data collection and refinement statistics). Given the small size of the dataset, we assigned 10% of the data (883 unique reflections) for the R_{free} calculation, to give a more statistically meaningful metric. The crystal structure of NRC1^{NB-ARC} alone was already available [Protein Data Bank (PDB) 6S2P], but there was no experimentally determined structure for SS15. Thus, we made use of AlphaFold2 (AF2) multimer (Evans *et al.*, 2021)d, as implemented through ColabFold (Mirdita *et al.*, 2022) to generate structural predictions for the complex. There was very good sequence coverage for both proteins, and the five independent models of the individual components were closely similar. The predicted local distance difference test (pLDDT) scores were generally good (e.g., averages of 82 and 75 for NRC1^{NB-ARC} and SS15 models, respectively, from the rank 1 predictions). However, the relative placement of the two components varied across the five models, and the corresponding predicted aligned error (PAE) scores indicated very low confidence in these predictions.

A comparison of the five NRC1^{NB-ARC} models with the known crystal structure showed a good agreement (e.g., superposition of the rank 1 model gave a root mean square deviation of 1.77 Å). Given that the AF2 model provided starting coordinates for several loops missing from the crystal structure, we decided to use this model in molecular replacement. Templates for both components were prepared using the “Process Predicted Models” CCP4i2 task, which removed low-confidence regions (based on pLDDT) and converted the pLDDT scores in the B factor field of the PDB coordinate files to pseudo B factors. Analysis of the likely composition of the asymmetric unit (ASU) suggested that it contained two copies of each component, giving an estimated solvent content of ~67%. Phaser (McCoy *et al.*, 2007) was able to place the four chains within the ASU, although the second SS15 domain required manual repositioning with respect to its neighbouring NRC1 domain to avoid a number of clashes and improve the fit to the density. This was achieved using COOT (Emsley *et al.*, 2010) and guided by the arrangement of the other NRC1-SS15 complex. The structure was then subjected to jelly body refinement in REFMAC5

(Murshudov *et al.*, 2011) using ProSMART restraints (Nicholls *et al.*, 2014) generated from the AF2 models, giving R_{work} and R_{free} values of 0.357 and 0.401, respectively, to a 4.5-Å resolution.

Now, it was possible to generate more complete models for the components by superposing the original unprocessed AF2 models and trimming these with reference to the improved electron density. Furthermore, a substantial region of positive difference density was present at the cores of both NRC1 domains, which corresponded to the adenosine diphosphate (ADP) in the crystal structure; thus, we incorporated ADP into the model. Because of the low resolution of the dataset, only very limited rebuilding was possible in COOT, where Geman-McClure and Ramachandran restraints were used to maintain good stereochemical parameters. After several cycles of restrained refinement in REFMAC5 and editing in COOT, a reasonable model was obtained with R_{work} and R_{free} values of 0.258 and 0.298, respectively. However, there remained a region of positive difference density near the N termini of both SS15 domains that we could not adequately explain. At this point, we reran the AF2 multimer predictions, but this time with one copy of the complex taken from the crystal structure as a reference template. Although these computational predictions did not produce complexes that were consistent with the x-ray data, and the models for the individual components did not appear to be noticeably improved based on pLDDT scores, we used them as starting points to rebuild the x-ray structure.

Notably, for several models, the N-terminal region of SS15 adopted conformations that partially accounted for the region of positive difference electron density, and this could be improved by careful rebuilding and refinement. This “AlphaFold recycling” procedure was repeated a further two times before finalizing the structure, which included residues 153 to 494 for SlNRC1 (numbered with respect to the full-length protein) and residues 18 to 223 for SS15, where residues 33 to 43 in both copies of the latter formed α helices that occupied the regions of positive difference density observed earlier. For the last refinement in REFMAC5, the following options were used: ProSMART restraints generated from the latest AF2 models, overall B factor refinement with translation/libration/screw (TLS) restraints (where each protein chain was treated as a separate domain), and noncrystallographic symmetry restraints. The final model gave R_{work} and R_{free} values of 0.237 and 0.275, respectively, to a 4.5-Å resolution (see **Table AVI.1**) for a summary of refinement statistics). All structural figures were prepared using ChimeraX (Pettersen *et al.*, 2021).

Chapter 3: Functional characterization of conserved motifs required for NLR-mediated cell death.

Results from this chapter are published as part of a manuscript by H. Adachi, [M. P. Contreras](#) et al. (Adachi *et al.*, 2019a).

Doi: <https://doi.org/10.7554/eLife.49956>

My contributions to this manuscript correspond to the results described in this chapter.

3.1 Introduction

The plant innate immune system heavily relies on intracellular immune receptors of the nucleotide binding and leucine rich repeat (NLR) family (Jones & Dangl, 2006). NLRs recognise pathogen virulence proteins, termed effectors, which are secreted into the host cell to modulate host physiology and suppress immunity. Upon effector recognition, NLRs mediate a robust immune response which is usually accompanied by a form of programmed cell death termed the hypersensitive cell death response (Duxbury *et al.*, 2021). Some NLRs can function individually, executing both pathogen perception and downstream immune signaling. These are termed singletons. An emerging paradigm is that some NLRs can function as functionally specialized receptor pairs and networks in which sensor NLRs, which mediate pathogen perception, cooperate with helper NLRs which activate downstream immune signaling (Adachi *et al.*, 2019b). The working model for the evolution of NLR pairs and networks is that they have evolved from an ancestral singleton receptor (Adachi *et al.*, 2019a; Adachi *et al.*, 2019b). NLR networks are thought to be advantageous to plants, as they increase evolvability of the immune system by removing evolutionary constraints and increase robustness by adding redundancy (Wu *et al.*, 2018). While we possess a robust understanding of their underlying genetics, our knowledge of how NLR networks function biochemically is limited.

NLRs are STAND (Signal transduction ATPases with numerous domains) proteins comprised of an N-terminal domain, a central nucleotide-binding and oligomerization domain (NOD) and C-terminal superstructure-forming repeats (SSFRs) (Dyrka *et al.*, 2020; Kourelis *et al.*, 2021). They are found across all kingdoms of life and exhibit a conserved tripartite modular domain architecture (Duxbury *et al.*, 2021; Gao *et al.*, 2022; Kibby *et al.*, 2023; Uehling *et al.*, 2017).

The plant NLR NOD is exclusively an NB-ARC (nucleotide-binding adaptor shared by APAF-1, certain *R* gene products, and CED-4) domain. C-terminal SSFRs are typically leucine rich repeat (LRR) domains (Kourelis *et al.*, 2021). Their N-terminal domains are usually thought of as signaling domains and often mediate the downstream programmed cell death response following immune receptor activation (Duxbury *et al.*, 2021). N-terminal signaling domains are often used to classify NLRs into distinct groups (Kourelis *et al.*, 2021). To date, four main N-terminal signaling domains have been characterized in angiosperms: Coiled-coil (CC)-type, RESISTANCE TO POWDERY MILDEW 8 (RPW8)-type (CC_R), G10-type CC (CC_{G10}) and toll/interleukin-1 receptor-type (TIR) (Kourelis *et al.*, 2021). In general, the class of N-terminal domain is thought to dictate the NLR downstream signaling pathways and activities following effector perception.

NLRs across all kingdoms of life activate via oligomerization-based mechanisms (Förderer *et al.*, 2022; Gao *et al.*, 2022; Ma *et al.*, 2020; Martin *et al.*, 2020; Vance, 2015; Wang *et al.*, 2019a; Xiao *et al.*, 2023). For example, metazoan NLRs confer immunity to diverse pathogens by assembling a wheel-like inflammasome complex which recruits downstream signaling components and activates caspases. Caspases then act as executors of programmed cell death (Vance, 2015; Xiao *et al.*, 2023). In plants, the recently published Cryo-EM structures of the inactive and activated *Arabidopsis* CC-NLR ZAR1 significantly advanced our understanding of plant NLR activation (Wang *et al.*, 2019a; Wang *et al.*, 2019b). Following indirect effector perception of AvrAC via RKS1 and PBL2, ZAR1 oligomerizes into a pentameric homocomplex termed a resistosome. Resistosome assembly leads to induced proximity of the N-terminal CC signaling domains to activate immunity. Interestingly, upon resistosome formation, the N-terminal α 1-helices of each ZAR1 protomer flip out from within the CC four-helix bundles and assemble a funnel-like structure. This funnel like structure has been proposed to allow the ZAR1 resistosome to insert itself into the plasma membrane and mediate immune signaling and cell death (Wang *et al.*, 2019a). This has been termed the “death switch” model (Adachi *et al.*, 2019c). Plasma membrane-associated CC and CC_R resistosomes have been proposed to act as calcium-permeable channels, with this activity being required for cell death. Mutations in this α 1-helix were shown to abolish ZAR1-mediated cell death and calcium influx, further suggesting that this region plays a critical role in immune signaling (Bi *et al.*, 2021; Wang *et al.*, 2019a).

While the structures of the ZAR1 and Sr35 resistosomes significantly advanced our understanding of how singleton CC-NLRs mediate immune signaling, our understanding of the molecular mechanisms of paired and networked NLRs are more limited. In NLR pairs and

networks, sensors specialize in pathogen perception and then signal through downstream helpers which translate effector recognition into downstream immune signaling and cell death (Adachi *et al.*, 2019b; Wu *et al.*, 2018). In the Solanaceae, the NRC CC-NLR network is composed of multiple agronomically important sensor NLRs which confer disease resistance against diverse pathogens such as viruses, oomycetes, bacteria, nematodes, and insects. These sensors genetically require downstream helper NRCs (NLR required for cell death) to mediate immune signaling (Derevnina *et al.*, 2021; Wu *et al.*, 2017). The NRC network can make up to 50% of the NLRome of a given solanaceous plant species. NRC-dependent sensors and NRCs are phylogenetically related and form two sister clades, one NRC helper clade and a larger clade that includes all known NRC-dependent sensors. The NRC clade and NRC-dependent sensor clade together are termed the NRC superclade (**Figure 1.4**) (Wu *et al.*, 2017). The NRC superclade is proposed to have emerged from an ancestral CC-NLR pair, which in turn evolved from an ancestral multifunctional singleton NLR (Adachi *et al.*, 2019b). How NRC network evolution and NLR functional specialization into sensors and helpers has impacted networked NLR biochemical activities or domains is not fully understood. Moreover, how the singleton CC-NLR pentameric resistosome activation model translates to paired and networked NLRs is not clear.

Previously, the N-terminal CC domains of multiple CC-NLRs have been shown to trigger cell death (Bai *et al.*, 2012; Baudin *et al.*, 2017; Wang *et al.*, 2015b). The exact mechanism by which CC domain truncations function is not understood. It is possible that in the absence of the rest of the NLR chassis, which usually mediates intramolecular autoinhibitory interactions, the CC domains are constitutively assembling into functional calcium channels capable of initiating immune signaling. Previous studies have shown that individual amino acid differences in these domain boundaries can affect the cell death inducing capacity of an NLR CC domain truncation (Casey *et al.*, 2016). All the cell death inducing CC-domains characterized to date belong to singleton NLRs which are known to trigger cell death. Whether the CC domain truncations of CC-NLR helpers in paired and networked signaling configurations, such as NRCs, can activate immune signaling and cell death is not understood. Moreover, whether NRC helpers execute signaling via mechanisms analogous to ZAR1 is not known.

In order to better understand the molecular mechanisms underpinning cell death induction by helper NRCs, Hiroaki Adachi carried out a transposon mutagenesis screen to identify the minimal region required for NRC4-mediated cell death (Adachi *et al.*, 2019a). Using this strategy, Hiroaki Adachi identified a short 29 amino acid N-terminal region in NRC4 (NRC4₁₋₂₉) that was

sufficient to trigger cell death. Interestingly, NRC4₁₋₂₉ approximately corresponds to the N-terminal α 1-helix of NRC4, which suggests that, as in the ZAR1 death switch model, the α 1-helix of NRC4 plays an important role in cell death induction. Following my validation of these NRC4 truncations, Hiroaki carried out a series of computational analyses which revealed that this α 1-helix is defined by a motif which is shared by approximately 20% of angiosperm NLRs. This motif, defined by the consensus “MADAxVSFxVxKLxxLLxxEx” was termed the MADA motif. Hiroaki’s analyses allowed me to identify conserved residues within the MADA motif and identify mutations in the α 1-helix of NRC4 which abolish cell death induction and Rpi-blb2-dependent disease resistance against *Phytophthora infestans*. Motif swapping experiments revealed that the MADA motif is functionally conserved between ZAR1 and NRC4. NRC4 variants carrying the ZAR1 α 1-helix were capable of triggering cell death and mediating Rpi-blb2-dependent disease resistance. I concluded that the MADA motif is critical for the cell death inducing activity of CC domains of various plant NLRs across the plant NLR phylogeny. These data suggest that the ZAR1 death switch mechanism may be widely conserved across cell death inducing singleton and helper CC-NLRs. Importantly, MADA motif mutants could be a useful resource to study activated CC-NLRs in the absence of cell death.

3.2 Results

3.2.1 N-terminal 29 amino acids of NRC4 are sufficient to induce HR cell death in *Nicotiana benthamiana*.

To further validate the cell death-induced by the 29 amino acid truncation of NRC4 (hereafter NRC4₁₋₂₉), I generated C-terminal YFP fusions of NRC4₁₋₂₉ and transiently over expressed them in leaves of *N. benthamiana* (**Figure 3.1A**). In agreement with the results of the transposon mutagenesis screen, these NRC4₁₋₂₉-YFP chimeras triggered a visible cell death response, although cell death intensity was weaker than that of the full-length NRC4^{DV}-YFP (**Figure 3.1B, 3.1E**). I next tested whether the cell death triggered by NRC4₁₋₂₉-YFP required the pool of endogenous NRC4 helper to trigger cell death. To this end, I expressed the NRC4₁₋₂₉-YFP in leaves of two independent *nrc4a/b* KO *N. benthamiana* lines (**Figure 3.1C, 3.1F, 3.1D, 3.1G**). As the cell death was affected in the *nrc4a/b* KO *N. benthamiana* lines, I concluded that NRC4₁₋₂₉-YFP is capable of inducing cell death independently of a full-length NRC4 protein.

The N-terminal CC domains of some CC-NLRs, such as the Arabidopsis ZAR1 and the maize Rp1 are capable of inducing cell death when expressed as fusion proteins with C-terminal fluorescent proteins (Baudin *et al.*, 2017; Wang *et al.*, 2015b). Because fluorescent proteins such as YFP are capable of homo-oligomerizing (Kim *et al.*, 2015), I hypothesized that potentially NRC4₁₋₂₉ was leveraging the C-terminal YFP tag as a scaffold to facilitate its assembly into a homo-complex in order to initiate cell death. To test this hypothesis, I mutated the alanine in position 206 to a lysine (A206K), which was previously shown to greatly reduce homo-oligomer formation in YFP (Zacharias *et al.*, 2002) (**Figure AII.1**). NRC4₁₋₂₉-YFP^{A206K} was compromised in cell death induction compared to NRC4₁₋₂₉-YFP. Full-length NRC4^{DV}-YFP^{A206K} cell death was indistinguishable to the cell death initiated by NRC4^{DV}-YFP (**Figure AII.1**). This suggests that C-terminal YFP tag homo-oligomerization was likely contributing to cell death triggered by NRC4₁₋₂₉-YFP^{A206K}.

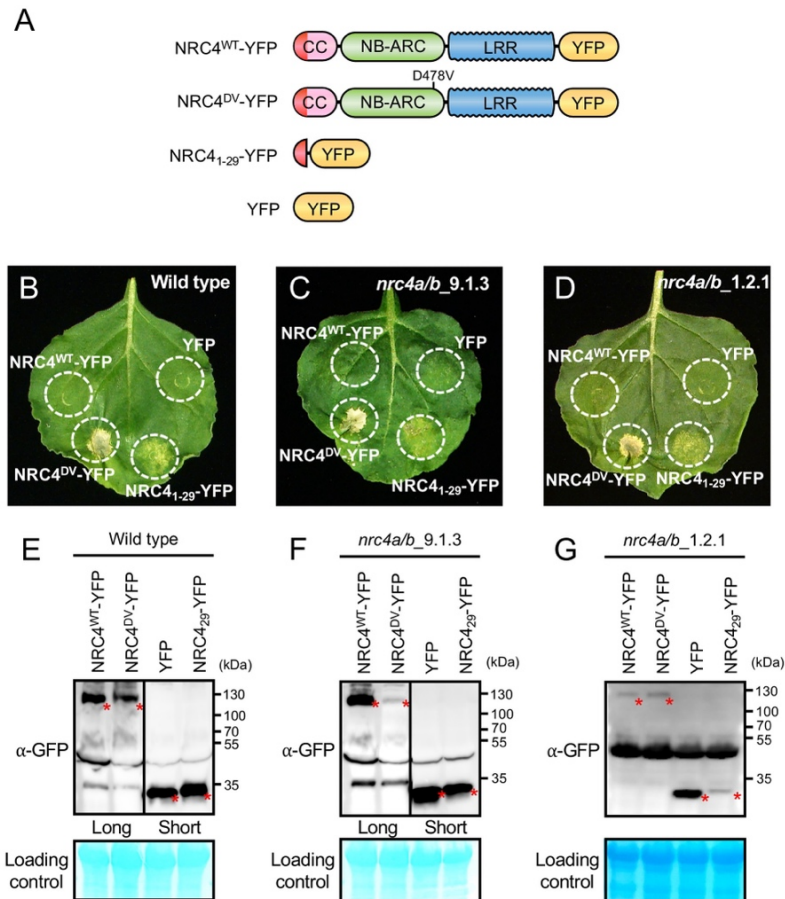


Figure 3.1: NRC4₁₋₂₉ induces cell death in *N. benthamiana* when fused to YFP independently of endogenous NRC4.

(A) Schematic representation of wild-type NRC4-YFP (NRC4^{WT}-YFP) and the variants used for transient expression assays. Red represents the N-terminal 29 amino acids of NRC4. (B) Photo of representative leaves of wild-type *N. benthamiana* showing HR after expression of NRC4₁₋₂₉-YFP. NRC4^{WT}-YFP, NRC4^{DV}-YFP, NRC4₁₋₂₉-YFP and YFP were co-expressed with the gene silencing suppressor p19 and photographed 7 days after agroinfiltration. (C, D) Photo of representative leaves of *nrc4a/b* *N. benthamiana* showing HR after expression of NRC4₁₋₂₉-YFP. Leaves of two independent *N. benthamiana nrc4a/b* lines were used for agroinfiltration assays as described in B. (E, F, G) Anti-GFP Western blots of NRC4^{WT}-YFP, NRC4^{DV}-YFP, NRC4₁₋₂₉-YFP and YFP expressed in *N. benthamiana* wild-type and *nrc4a/b* mutants. Total proteins extracts were immunoblotted with the appropriate antisera labelled on the left. Approximate molecular weights (kDa) of the proteins are shown on the right. Rubisco loading control was carried out using Pierce stain. Given that the full-length NLRs accumulate at much lower levels than the shorter peptide, I show different exposures as indicated by the black line. Red asterisks indicate expected band sizes. All experiments were repeated 3 times with similar results.

3.2.2 NRC4 and ZAR1 share an N-terminal MADA motif.

The validation of the cell death initiated by NRC4₁₋₂₉ prompted Hiroaki Adachi to investigate the degree of occurrence and degree of conservation of this sequence across the plant NLRome (Adachi *et al.*, 2019a). Markov clustering (MCL) analysis carried out with the N-terminal CC and CC_R domains of a CC-NLR database curated for this analysis revealed that NRC4 carries N-terminal sequences that are conserved across distantly related CC-NLRs found across the angiosperm phylogeny. This suggested that there are N-terminal domain sequences that have remained conserved over evolutionary time across distantly related CC-NLRs (Adachi *et al.*, 2019a). Using MEME (Multiple EM for Motif Elicitation) Hiroaki was able to identify conserved sequence patterns in the tribe of N-termini which clustered with NRC4, as well as in other tribes of N-termini identified in his analysis. In the tribe containing NRC4, this MEME analysis revealed a 21 amino acid consensus sequence MADAxVSF_xV_xKL_{xx}LL_{xx}Ex, coined ‘MADA motif’ (Figure 3.2A) (Adachi *et al.*, 2019a). The analysis coincided with the publication of the first structure of an activated plant NLR resistosome (Wang *et al.*, 2019a; Wang *et al.*, 2019b). These papers by Wang and colleagues revealed an oligomerization-based mechanism for activated plant CC-NLRs. In this model, activated ZAR1 form a pentameric resistosome complex, with the N-terminal α 1-helix of the CC-domain flipping out and forming a funnel-like structure (Figure 3.2B). In the analysis mentioned above, the N-terminus of ZAR1 clustered with the N-terminus of NRC4, Hiroaki and I noted that the MADA motif derived from this cluster coincided almost exactly with the N-

terminal α 1-helix of ZAR1 (**Figure 3.2B**). Based on this we concluded that NRC4 and ZAR1 are both MADA-motif containing NLRs.

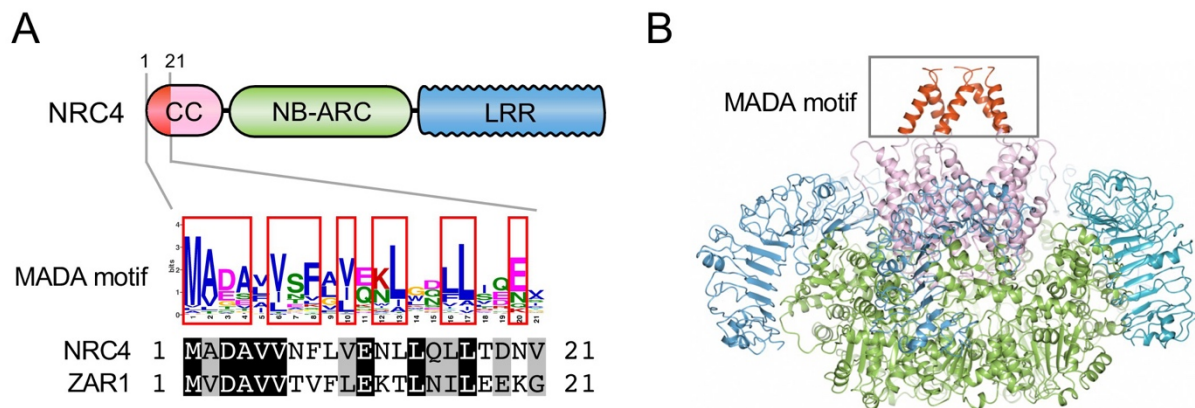


Figure 3.2: The MADA motif is conserved at N-termini of NRC4 and ZAR1.

(A) Schematic representation of a NRC4 highlighting the position of the MADA motif. Consensus sequence pattern of the MADA motif identified by MEME along with an alignment of NRC4 and ZAR1. Red boxes refer to residues conserved over 45% in NLRs found to cluster with NRC4 (Analysis performed by Hiroaki Adachi). (B) A structural homology model of NRC4 based on the activated ZAR1 resistosome illustrating the position of the MADA motif. Each of the modelled five monomers is illustrated in cartoon representation. The MADA motif is in red. The grey box highlights the N-terminal α 1-helices.

3.2.3 Conserved MADA motif residues are required for NRC4-mediated cell death.

Further analyses by Hiroaki Adachi revealed that the MADA motif is primarily found in NLR proteins and that MADA-like sequences occur in the N-termini of about 20% of dicot and monocot CC-NLRs (Adachi *et al.*, 2019a). The high degree of conservation of the MADA motif as well as its overlap with the cell death inducing NRC4₁₋₂₉ truncation as well as with the funnel-forming α 1-helix of ZAR1 led us to hypothesize that it likely is critical for cell death induction by NLRs. This prompted me to functionally characterize this motif using NRC4 as a system. Structure-function analyses of ZAR1 carried out by Wang and colleagues had revealed that three aminoacids (F9, L10 and L14) in the N-terminal α 1-helix of ZAR1 were required for ZAR1-mediated cell death (Wang *et al.*, 2019a). Because both ZAR1 and NRC4 are MADA-motif containing CC-NLRs and these residues are exactly conserved between both their N-termini, I mutated these residues to determine whether they also have an impact in cell death initiated by

NRC4^{DV}. To this end, I mutated F9, L10 and L14 to either alanine (NRC4^{AAA}) or glutamic acid (NRC4^{EEE}) in the NRC4^{DV} background (NRC4^{AAA/DV} and NRC4^{EEE/DV}). (**Figure 3.3A**). I included the glutamic acid mutations because the MADA motif and the mutated L9, V10 and L14 residues are hydrophobic. Glutamic acid is negatively charged and as such, Hiroaki and I hypothesized that it might be more disruptive to the presumed function of the α 1-helix than alanine. Both NRC4^{AAA/DV} and NRC4^{EEE/DV} were impaired in cell death induction in leaves of *N. benthamiana*, as compared to NRC4^{DV}. In agreement with our previous hypothesis, NRC4^{EEE/DV} exhibited a more drastic reduction of cell death intensity relative to NRC4^{AAA/DV} (**Figure 3.3B-C**). Both mutants accumulated to levels similar to NRC4^{DV}, indicating that the reduction in cell death intensity is not due to reduced protein stability (**Figure 3.3D**).

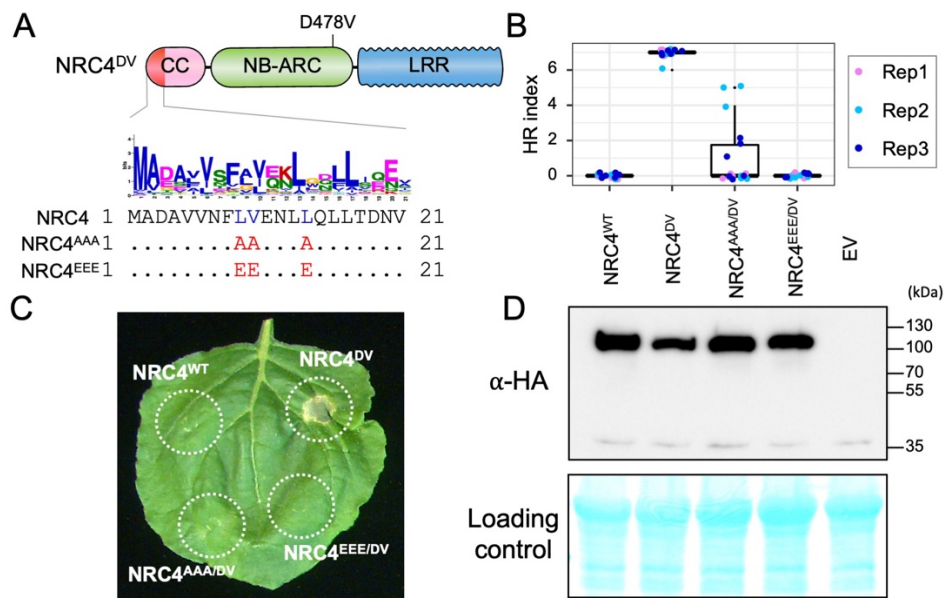


Figure 3.3: Triple mutation in conserved residues at positions L9, V10 and L14 impairs cell death mediated by autoimmune NRC4^{DV}.

(A) Schematic representation of NRC4 and the mutations made in its N-terminal MADA motif (NRC4^{AAA} and NRC4^{EEE}). (B - C) HR cell death assays with C-terminally 6xHA-tagged NRC4 variants, NRC4^{WT}, NRC4^{DV}, NRC4^{AAA/DV} and NRC4^{EEE/DV}. (B) Box plots showing cell death intensity scored as an HR index based on three independent experiments. (C) Photo of representative leaves of wild-type *N. benthamiana* showing HR after expression of different NRC4 variants. Leaves photographed at 5 days after agroinfiltration. (D) Western blots of C-terminally 6xHA-tagged NRC4^{WT}, NRC4^{DV}, NRC4^{AAA/DV} and NRC4^{EEE/DV} expressed in wild-type *N. benthamiana*. Total proteins extracts were immunoblotted with the

appropriate antisera labelled on the left. Approximate molecular weights (kDa) of the proteins are shown on the right. Rubisco loading control was carried out using Pierce stain. All experiments were repeated 3 times with similar results.

Next, I performed a single glutamic acid scan in the N-terminus of NRC4 to reveal additional residues required for NRC4-mediated cell death. I mutated the N-terminal residues 2-21 of NRC4 to glutamic acid, except for residue 11, as glutamic acid is already found in that position. All mutations were made in the NRC4^{DV} background and tested for HR cell death induction by transient expression in *N. benthamiana*. This screen revealed three positions, L9, L13 and L17, which when mutated to glutamic acid, abolished the activity of NRC4^{DV} without affecting protein stability (Figure 3.4). I concluded that residues L9, L13 and L17 in the N-terminal MADA motif are critical for cell death induction.

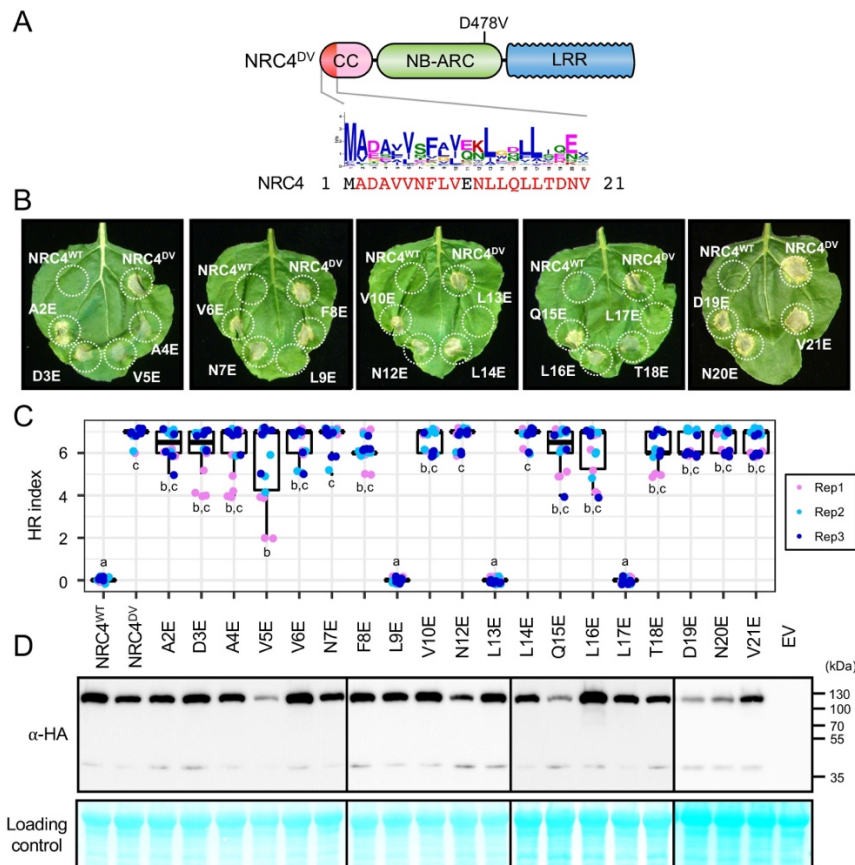


Figure 3.4: Glutamic acid scan reveals that mutations in conserved amino acids in positions L9, L13 and L17 impair cell death activity of autoactive NRC4^{D478V}.

(A) Schematic representation of NRC4 and the mutations made in its N-terminal MADA motif. Residues marked in red were mutated to glutamic acid (E). (B - C) HR cell death assays with C-terminally 6xHA-tagged NRC4 variants, NRC4^{WT}, NRC4^{DV}, and each of the mutants generated in the glutamic acid scan. (B) Photo of representative leaves of wild-type *N. benthamiana* showing HR after expression of different NRC4 variants. Leaves photographed at 5 days after agroinfiltration. (C) Box plots showing cell death intensity scored as an HR index based on three independent experiments. (D) Western blots of C-terminally 6xHA-tagged NRC4 variants expressed in wild-type *N. benthamiana*. Total proteins extracts were immunoblotted with the appropriate antisera labelled on the left. Approximate molecular weights (kDa) of the proteins are shown on the right. Rubisco loading control was carried out using Pierce stain. All experiments were repeated 3 times with similar results.

Finally, mapping of L9, L13 and L17 onto a homology model of the CC domain of NRC4 produced based on the ZAR1 resistosome structure revealed that all three residues were located on the outer surface of the predicted funnel-shaped structure formed by the α 1-helices of NRC4. (Wang *et al.*, 2019a) (**Figure AII.2**). These results suggest that the outer surface of the funnel-shaped structure formed by these N-terminal helices is critical for the function of ZAR1, NRC4 and likely other MADA-type CC-NLRs.

3.2.4 An intact MADA motif is required for NRC4-mediated disease resistance against *P. infestans*.

Next, I investigated whether the MADA motif of NRC4 plays a role in disease resistance. The sensor NLR Rpi-blb2 from *Solanum bulbocastanum* confers resistance to *P. infestans* carrying the matching effector AVRblb2. Rpi-blb2-mediated cell death and resistance upon AVRblb2 recognition is dependent on its downstream helper NRC4 (Oh *et al.*, 2009; Van Der Vossen *et al.*, 2003; Wu *et al.*, 2017). To test the contributions of the MADA motif to *P. infestans* disease resistance, I set up a complementation assay, transiently expressing different NRC4 variants in leaves of *nrc4a/b* KO *N. benthamiana* and subsequently inoculating them with zoospores of the *P. infestans* strain 88069, which carries AVRblb2 (Wu *et al.*, 2017) (**Figure 3.5A**). Unlike wild-type NRC4, NRC4^{AAA} and NRC4^{L9E} did not restore resistance to *P. infestans* in *nrc4a/b* KO *N. benthamiana* (**Figure 3.5B**). These results show that a functional N-terminal MADA motif is required for cell death induction as well as disease resistance.

3.2.5 The ZAR1 MADA can functionally complement NRC4 for disease resistance against *P. infestans*.

In the complementation assays described above, I also included a chimeric ZAR1-NRC4 protein in which the first 17 amino acids of NRC4 were swapped with the equivalent region of ZAR. Notably, this ZAR1₁₋₁₇-NRC4 chimera was capable of restoring disease resistance to *P. infestans* 88069 when co-expressed with Rpi-blb2 in leaves of *nrc4a/b* KO *N. benthamiana* (Figure 3.5B). These experiments suggest that the α 1-helix of ZAR1, containing the MADA motif, is functionally interchangeable with the equivalent α 1-helix of NRC4. This chimera retained the capacity to trigger HR cell death and function with its upstream sensor NLR Rpi-blb2. Based on these results, I speculate that, much like ZAR1, NRC4 is likely operating via a similar oligomerization-based ‘death switch’ mechanism (Wang *et al.*, 2019a).

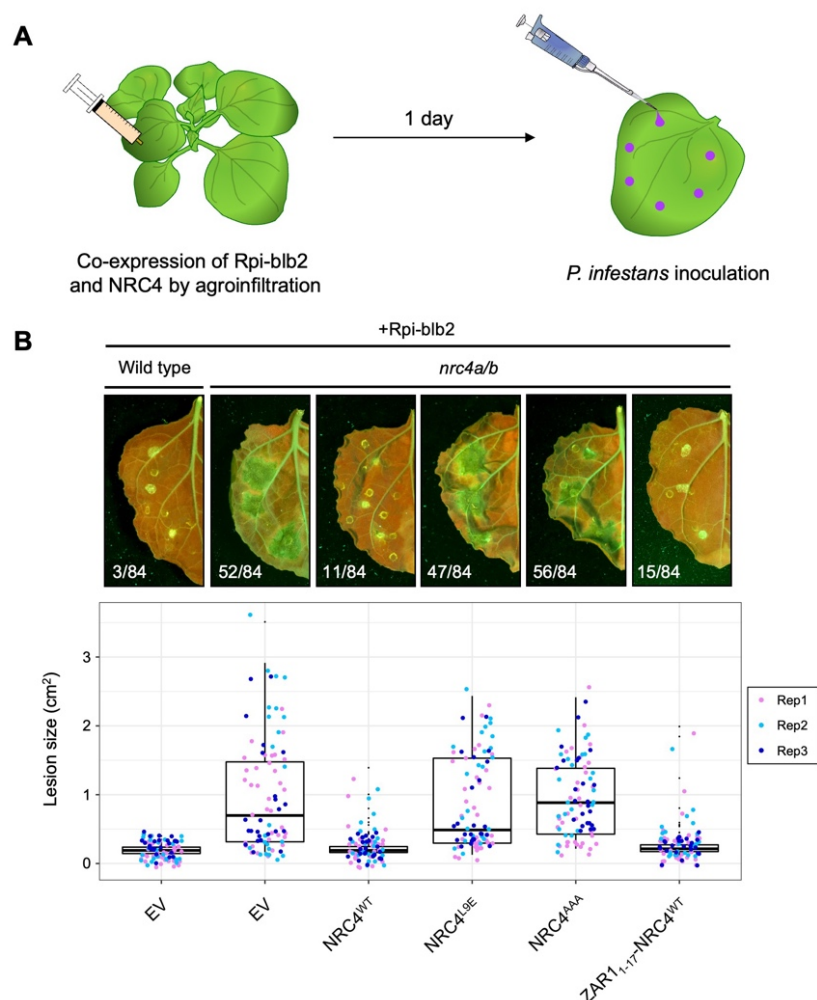


Figure 3.5: The N-terminal MADA motif of ZAR1 can functionally complement the N-terminus of NRC4 in Rpi-blb2-mediated resistance against *Phytophthora infestans*.

(A) Schematic representation of NRC4 complementation assay for Rpi-blb2-mediated resistance against *P. infestans* 88069. Wild-type NRC4 and NRC4 variants were co-expressed with N-terminally RFP-tagged Rpi-blb2 in leaves of *nrc4a/b* KO *N. benthamiana*. 24 hours later, the leaves were drop inoculated with suspensions of *P. infestans* 88069 zoospores. (B) Photo of representative *N. benthamiana* leaves showing resistance and disease phenotypes. Images were taken under UV light at 7 days post inoculation. The experiment was repeated three times, for a total of 84 inoculations. The numbers in each image represent the total number of successful infections out of the total inoculations performed. Lesion size was measured in each image using Fiji and used for comparisons between treatments (bottom panel). Statistical significance of difference in lesion size was determined using a Tukey's HSD test ($p < 0.01$).

3.3 Conclusions and discussion

The work in this chapter stems from a random truncation screen of the helper CC-NLR NRC4 carried out by Hiroaki Adachi. His screen revealed that the very N-terminal 29 amino acids of this protein (NRC4₁₋₂₉) are sufficient to recapitulate the HR cell death triggered by the full-length NRC4. His analyses revealed that this N-terminal 29 amino acid truncation is defined by a consensus sequence termed the MADA motif. This MADA motif is present in about 20% of all angiosperm NLRs including NRC4, and the well characterized CC-NLR ZAR1 (Adachi *et al.*, 2019a). Importantly, this MADA motif spans the length of the α 1-helix of ZAR1 which flips out upon activation to form a funnel-like structure, as part of the so-called 'death switch' mechanism (Wang *et al.*, 2019a). I functionally validated the cell death induction of the NRC4₁₋₂₉ fragment identified in Hiroaki's screen by fusing it to YFP (NRC4₁₋₂₉-YFP), which confirmed that, indeed, this fragment is capable of triggering cell death and accumulates in planta (**Figure 3.1**). Interestingly, we found that cell death was abolished in NRC4₁₋₂₉-YFP^{A206K}, a variant fused to a mutated YFP protein that is impaired in homo-oligomerization (Zacharias *et al.*, 2002) (**Figure AII.1**). This implies that, potentially, NRC4₁₋₂₉-YFP is forming oligomeric complexes via its C-terminal YFP tag. It is possible that this leads to the formation of funnel-like NRC4₁₋₂₉-YFP complexes which trigger cell death via mechanisms analogous to activated ZAR1, which uses its N-terminal α 1-helices to form a funnel-like structure that induces cell death. Whether NRC4₁₋₂₉-YFP is forming oligomers and whether the cell death triggered by these NRC4 truncations is functioning via acting as calcium permeable channels, remains to be determined.

Further characterization of the N-terminal MADA motif identified in NRC4 and ZAR1 revealed that it is critical for cell death induction, as mutating certain amino acids that were previously shown to abolish ZAR1 resistosome-mediated cell death also abolished NRC4-

mediated cell death (**Figure 3.2, Figure 3.3**). This result supports the hypothesis that ZAR1 and NRC4 are functioning via similar ‘death-switch’ mechanisms involving their N-termini. Moreover, the fact that ZAR1₁₋₁₇-NRC4 chimera could mediate Rpi-blb2-dependent *P. infestans* disease resistance in our complementation assays provides strong evidence for functional conservation in the MADA motifs of these distantly related CC-NLRs and suggests that MADA-CC-NLRs may exhibit similar activation mechanisms (**Figure 3.5**). The widespread distribution and functional conservation of this cell-death inducing motif across the angiosperm phylogeny, combined with the fact that it is present in singleton, paired and networked CC-NLRs, implies that NLRs from these distinct functional categories likely originate from a common MADA-motif containing ancestor, which was presumably a singleton NLR (Adachi *et al.*, 2019a). Interestingly, while the MADA motif appears to be conserved in singleton and helper CC-NLRs capable of inducing cell death, this motif appears to be degenerated in singleton NLRs (Adachi *et al.*, 2019a). Because sensor NLRs are reliant on downstream helpers for cell death induction, their N-terminal MADA motifs could become degenerated. All in all, based on these and additional data generated by Hiroaki Adachi, we proposed a working evolutionary model for the transition of CC-NLRs from singletons to pairs and networks (Adachi *et al.*, 2019a; Adachi *et al.*, 2019b). We propose that, over deep evolutionary time, singleton MADA-CC-NLRs duplicated and diversified, giving rise to NLR pairs which themselves gave rise to networks. These NLR pairs and networks feature sensors with degenerated MADA motifs and, in some cases, novel pathogen sensing domains, while helper NLR retain a functional MADA motif for cell death induction (Adachi *et al.*, 2019a).

A glutamic acid scan subsequently allowed us to pinpoint individual amino acids that are of particular importance for cell death induction within the MADA motif. These are highly conserved leucine residues at positions 9, 13 and 17 (**Figure 3.4**). Mutating these residues to glutamic acid resulted in compromised cell death induction and disease resistance (**Figure 3.4, Figure 3.5**). How exactly these mutations perturb NRC4 activation, however, is not known. If NRC4 activates via mechanisms analogous to ZAR1, MADA-motif mutations could be affecting NRC4 oligomerization, plasma membrane insertion or the calcium channel activity that has been recently attributed to activated CC-NLRs. It has not escaped our attention that, if these mutations abolish cell death without preventing other aspects of NLR activation, they could be an incredibly useful tool with which to study CC-NLR biology. For TIR-NLR biology, multiple essential downstream components for immune signaling, such as the EDS1 signaling hub and the CC_R NLRs NRG1 and ADR1 have been identified, which enabled the generation of genetic backgrounds with which to study TIR-NLR activities in the absence of immune signaling (Gantner

et al., 2019; Lapin *et al.*, 2019; Martin *et al.*, 2020; Saile *et al.*, 2020; Sun *et al.*, 2021). Hopefully, MADA motif mutants might provide an analogous resource, enabling the study of the cellular and biochemical mechanisms of activated CC-NLRs.

3.4 Research Contributions

I thank Hiroaki Adachi for extensive collaboration throughout all experiments conducted in this Chapter.

Chapter 4: Biochemical basis of activation in an NLR immune receptor network.

Results from this chapter are published as part of a manuscript by [M. P. Contreras](#) et al. (Contreras *et al.*, 2023b).

Doi: <https://doi.org/10.15252/emj.2022111519>

My contributions to this manuscript correspond to the results described in this chapter.

4.1 Introduction

NLR (nucleotide binding and leucine-rich repeat) receptors are key components of the innate immune systems of plants and metazoan. They play an important role in mediating pathogen recognition and subsequent immune responses (Duxbury *et al.*, 2021; Jones *et al.*, 2016). In plants, NLRs can activate host defence by recognizing pathogen secreted virulence proteins, termed effectors. This recognition leads to immune signaling, often culminating in a form of programmed cell death known as the hypersensitive response (Jones & Dangl, 2006; Kourelis & Van Der Hoorn, 2018; Ngou *et al.*, 2022a). Similarly, metazoan NLRs are capable of sensing pathogen effectors and other classes of pathogen derived molecules, ultimately leading to a form of programmed cell death known as pyroptosis (Maekawa *et al.*, 2023). Some plant and metazoan NLRs can function as single units, with one NLR protein mediating both effector/elicitor perception and subsequent downstream signaling. These are referred to as functional singleton NLRs (Adachi *et al.*, 2019a; Adachi *et al.*, 2019b). However, NLRs can also function as genetically linked receptor pairs or in higher order configurations that can include genetically unlinked receptor networks (Wu *et al.*, 2017; Wu *et al.*, 2018). In these cases, the sensing and signaling functions are uncoupled in two distinct proteins. One NLR acts as the pathogen sensor, requiring a second NLR which acts as a helper (or executor) to mediate immune activation and disease resistance (Adachi *et al.*, 2019b; Feehan *et al.*, 2020; Wu *et al.*, 2018). Although much progress has been made in recent years regarding the biochemical mechanisms of how singleton NLRs activate and signal (Förderer *et al.*, 2022; Martin *et al.*, 2020; Wang *et al.*, 2019a; Wang *et al.*, 2023b; Zhao *et al.*, 2022), our understanding of how paired and networked NLRs operate remains limited.

Plant, metazoan and prokaryotic NLRs belong to the signal transduction ATPases with numerous domains (STAND) superfamily. They usually exhibit a modular, tri-partite structure

with an N-terminal signaling domain, a central nucleotide binding domain and a C-terminal domain with superstructure forming repeats (Chou *et al.*, 2023; Duxbury *et al.*, 2021; Kim *et al.*, 2016b; Kourelis *et al.*, 2021). The N-terminal domains of NLRs can broadly be used to classify these receptors into distinct groups which, in plants, tend to also cluster together in phylogenetic analyses. Plant NLR N-terminal domains can be either coiled-coil-type (CC) NLRs, G10-type CC (CC_{G10}) NLRs, RPW8-type CC (CC_R) NLRs or toll/interleukin-1 receptor-type (TIR) NLRs, whereas metazoan NLRs usually exhibit either N-terminal PYRIN or caspase recruitment domains (CARD) (Chou *et al.*, 2023; Kim *et al.*, 2016b; Kourelis *et al.*, 2021; Lechtenberg *et al.*, 2014). The central nucleotide binding domain is the defining feature of NLRs and is typically a nucleotide-binding adaptor shared by APAF-1, plant R proteins and CED-4 (NB-ARC) domain in plants, while metazoan NLRs can have either an NB-ARC or a NAIP, C2TA, HET-E and TP1 (NACHT) domain. As for their superstructure forming repeats, these can be either leucine-rich repeats (LRR) or tetratricopeptide repeats (TPR) (Chou *et al.*, 2023; Duxbury *et al.*, 2021; Kourelis *et al.*, 2021).

Our knowledge of the molecular mechanisms that underpin NLR activation and signaling are limited compared to our understanding of how NLRs sense their ligands (Kourelis & Van Der Hoorn, 2018; Ngou *et al.*, 2022a). In the case of mammalian NLRs, activation leads to oligomerization and formation of higher order wheel-like complexes, termed inflammasomes. Inflammasomes ultimately recruit caspases which act as the final executors of programmed cell-death (Chou *et al.*, 2023). In contrast, the mechanisms of plant NLR activation were not well understood until the recent elucidation of the structures of inactive and activated ZAR1, a conserved singleton CC-NLR from *Arabidopsis* (Adachi *et al.*, 2020; Wang *et al.*, 2019a; Wang *et al.*, 2019b). The activation of ZAR1 upon recognition of its cognate effectors both *in vitro* and *in vivo* leads to its oligomerization and formation of a higher-order pentameric homo-complex analogous to the inflammasome and coined as the resistosome (Hu *et al.*, 2020; Wang *et al.*, 2019a; Wang *et al.*, 2019b). Oligomerization based activation mechanisms have also been observed *in vivo* for the plant singleton CC-NLR RPP7 and the CC_R-NLR helper NRG1.1 (Jacob *et al.*, 2021; Li *et al.*, 2020). More recently, the structure of the activated wheat CC-NLR Sr35 pentameric resistosome suggests that this activation strategy is likely evolutionarily conserved across plant CC-NLRs (Förderer *et al.*, 2022). The activated complexes of CC-NLRs and CC_R-NLRs act as calcium-permeable membrane-associated pores upon complex formation, an activity that is required for the hypersensitive cell death (Bi *et al.*, 2021; Duggan *et al.*, 2021; Förderer *et al.*, 2022; Jacob *et al.*, 2021). Despite these advances, the molecular mechanisms of paired and networked plant CC-NLR activation are poorly understood. In the case of Pia (RGA4 and RGA5),

immune signaling is activated through release of negative regulation (Césari *et al.*, 2014). In contrast, the Pik-1 and Pik-2 pair is activated via receptor cooperation by forming a tri-partite complex with the pathogen effector (Zdrzalek *et al.*, 2020). However, whether sensor and helper NLRs engage in heteromeric resistosome complexes is unknown.

Networked NLR immune signaling architectures present many advantages to plant and metazoan immune systems. NLR networks likely contribute to immune system robustness and enhance immune receptor evolvability in the face of highly adaptable pathogens (Wu *et al.*, 2018). In mammals, multiple different NAIP sensor NLRs can perceive distinct immune elicitors and initiate immune responses. Following elicitor-triggered activation, NAIPs require the helper NLR NLRC4 to mediate downstream signaling (Chou *et al.*, 2023; Vance, 2015). NAIP2 is one of these sensors. Upon sensing the inner rod of the bacterial type III secretion system of *Salmonella typhimurium*, NAIP2 initiates sensor-helper signaling via the formation of a heterocomplex with NLRC4 (Qu *et al.*, 2012). This NAIP2/NLRC4 heterocomplex acts as a nucleation point for multiple NLRC4 monomers that leads to the formation of a NAIP/NLRC4 inflammasome with multiple additional NLRC4 units (Hu *et al.*, 2015; Zhang *et al.*, 2015). Similar networked signaling architectures have also been described in plants. In asterid flowering plants, a major phylogenetic cluster of CC-NLRs known as the NLR required for cell death (NRC) superclade comprises an immune receptor network with multiple sensor NLRs and downstream helper NLRs which mediated immunity to diverse pathogens (Derevnina *et al.*, 2021; Wu *et al.*, 2017). All sensors in the NRC network signal, often redundantly, through a downstream hub of helper NRCs to mediate cell death and disease resistance. In the previous chapter, I reported that Hiroaki and myself found that NRC helpers contain a key signature in the α -1 helix of their N-termini known as the MADA motif, which is crucial for mediating cell death. This motif is conserved in around 20% of angiosperm CC-NLRs and is functionally conserved between ZAR1, Sr35 and the NRCs, which suggests that the “death switch mechanism” characterized for the ZAR1 resistosome may apply to NRCs as well (Adachi *et al.*, 2019a; Förderer *et al.*, 2022; Kourelis *et al.*, 2022). Considering how widespread and vital this immune network is for several crop species, developing a better mechanistic understanding of how it functions is critical. However, how sensor and helper NLR pairs communicate and initiate immune responses is not understood.

In this study, I selected the NRC-dependent sensor Rx and its helper NRC2 as a model experimental system to study CC-NLR sensor-helper activation. Rx is an agronomically important sensor NLR from potato (*Solanum tuberosum*) that confers resistance to *Potato virus X* (PVX), a

single-stranded RNA filamentous plant virus, by recognizing its coat protein (CP) (Bendahmane *et al.*, 1999; Bendahmane *et al.*, 1995). Prior to activation, Rx is held in an inactive state by intramolecular autoinhibitory interactions between its LRR domain and its CC and NB-ARC domains (Moffett *et al.*, 2002; Rairdan & Moffett, 2006). Upon PVX CP-triggered activation, Rx undergoes intramolecular rearrangements that include the release of LRR autoinhibition and the exposure of its NB-ARC domain, leading to its activation (Moffett *et al.*, 2002; Rairdan *et al.*, 2008; Rairdan & Moffett, 2006). The Kamoun lab previously showed that to mediate hypersensitive cell death and disease resistance, Rx and other sensors in the NRC network genetically require their downstream NRC helpers, with different sensors exhibiting different NRC helper specificities. Rx and the wild pepper (*Capsicum chacoense*) NLR Bs2, for example, can signal interchangeably via NRC2, NRC3 or NRC4. In contrast, the *Solanum bulbocastanum* NLR Rpi-blb2 which confers resistance to *Phytophthora infestans* strains carrying AVRblb2, can only signal through NRC4 (**Figure 4.6A**) (Derevnina *et al.*, 2021; Wu *et al.*, 2017). However, the mechanisms by which sensor NLRs signal through NRCs are still not understood. Like the mammalian NAIP/NLRC4 system, Rx could be forming distinct Rx/NRC higher order hetero-resistosomes with each of its three NRC helpers, reminiscent of the NAIP/NLRC4 inflammasomes. Alternatively, plants may feature distinct activation mechanisms for paired and networked NLRs than those previously shown in mammalian paired systems (**Figure 1.6**). How activation of sensor NLRs translates into helper activation, immune signaling and disease resistance remains an important question in plant immunology.

To dissect the biochemical mechanisms that underpin Rx and NRC activation, I established a resistosome formation assay using Blue Native polyacrylamide gel electrophoresis (BN-PAGE) by taking advantage of the NRC proteins with MADA motif mutations generated in Chapter 3. Studies by Duggan and colleagues previously showed that NRC4 MADA mutants retained dynamic effector-induced re-localization and plasma membrane association, which led us to speculate that these mutants would allow me to study NRC activation without cell death (Duggan *et al.*, 2021). I demonstrate that Rx-mediates oligomerization of its NRC2 helper in *N. benthamiana* following virus perception. My data suggest that the activated NRC2 complex is an NRC2 resistosome that does not include Rx. Confocal live cell imaging and membrane fractionation assays reveal a sub-cellular shift in localization for NRC2 upon resistosome formation, moving from the cell cytoplasm to the plasma membrane to form membrane-associated punctate structures. This points to an activation-and-release model for sensor-helper signaling in the NRC network, whereby Rx can trigger NRC oligomerization without stably forming part of

the activated helper complex. Notably, this model is distinct from the hetero-complexes shown for mammalian NLR paired systems, such as NAIP/NLRC4, implying that plant and metazoan NLR pairs exhibit different activation strategies.

4.2 Results

4.2.1 Activation of Rx with *Potato virus X* coat protein leads to oligomerization of its helper NRC2.

Previously, biochemical *in vivo* studies of activated NLRs have been hindered by the cell death response initiated upon immune receptor activation. I hypothesized that we could circumvent this issue by leveraging mutations in the N-terminal MADA motif identified in Chapter 3 which abolishes cell death induction (Adachi *et al.*, 2019a). Earlier work from our lab revealed that NRC2 is a MADA motif-containing CC-NLR which acts as a downstream helper NLR for multiple sensor NLRs (Adachi *et al.*, 2019a; Kourelis *et al.*, 2022). In Chapter 3, I found that mutating the N-terminal MADA motif of NRC4 prevents NRC4-mediated cell death without impacting protein stability. Consequently, I generated MADA mutations in NRC2, similar to those I previously made in NRC4, resulting in an NRC2^{L9/13/17E} MADA motif mutant (hereafter NRC2^{EEE}) (**Figure 4.1A**). Like the previously studied NRC4 mutants, NRC2^{EEE} does not functionally complement hypersensitive cell death when co-expressed with effector-activated NRC2-dependent sensors in *nrc2/3/4 N. benthamiana* KO lines (**Figure AIII.1**).

I then used Rx and NRC2^{EEE} as a system to study the oligomeric state of both sensor and helper upon effector-induced activation *in vivo*. I transiently co-expressed these proteins via agroinfiltration in the presence or absence of PVX CP in leaves of *nrc2/3/4* KO *N. benthamiana* lines and used total protein extracts for BN-PAGE assays (**Figure 4.1A**). In its inactive state, NRC2^{EEE} is visualized as a fast-migrating band of approximately 200 kDa, independent of the presence or absence of Rx (**Figure 4.1B**). When the system is activated by co-expressing Rx and NRC2^{EEE} along with C-terminally GFP-tagged PVX CP, but not upon co-expression of free GFP as a negative control, NRC2 transitions to a slower-migrating, high-molecular-weight complex with two bands in the 720 to 1,048 kDa range (**Figure 4.1B**). Although this two-band pattern is consistently observed, with a lower molecular weight band of approximately 750 kDa and a higher molecular weight band of roughly 900 kDa, the 900 kDa band is usually more abundant. The shift

of NRC2 to a higher molecular weight upon activation is reminiscent of the *in vivo* resistosome formation previously reported for ZAR1 (Hu *et al.*, 2020), suggesting a similar oligomerization mechanism and resistosome formation for NRC2 upon activation by Rx. In the absence of Rx, co-expression with PVX CP does not lead to NRC2^{EEE} oligomerization (**Figure 4.1B**). I concluded that Rx mediates NRC2 oligomerization upon PVX CP-triggered activation, and that NRC2 does not oligomerize in the absence of an activated upstream sensor.

To rule out that the NRC2 oligomerization we observed above was not an artifact of the MADA motif mutations introduced, I repeated the BN-PAGE assays described above with the wild-type NRC2 carrying an intact N-terminal α 1 helix. Due to the early onset of cell death initiated upon NRC2 activation, I collected tissue at the latest timepoint possible before the appearance of confluent necrosis (38 h post infiltration). Probing for NRC2 in these assays revealed a similar oligomerization pattern to that observed for NRC2^{EEE} (**Figure AIII.2**). However, protein accumulation of NRC2, Rx, and PVX CP was reduced compared to the NRC2^{EEE} treatments, possibly due to the onset of cell death. Consequently, I chose to proceed with NRC2^{EEE} for subsequent experiments to minimize the impact of cell death on protein accumulation.

4.2.2 Rx does not oligomerize upon PVX CP perception.

In the BN-PAGE assays described above, I noted that the Rx sensor consistently migrates as a ~400 kDa band, independent of its activation state (**Figure 4.1, Figure AIII.2**). Interestingly, the presence of this ~400 kDa band is independent of NRC2^{EEE} in *nrc2/3/4* KO *N. benthamiana* lines, indicating that it is likely not a preformed complex between Rx and endogenous NRC2, NRC3, or NRC4 helper NLRs. A single Rx-6xHA monomer is expected to have a size of approximately 115 kDa, which led me to hypothesize that the ~400 kDa band seen for Rx in BN-PAGE assays might correspond to a preformed Rx complex with other host proteins, such as RAN GTPase activating protein 2 (RanGAP2), as previously reported (Tameling & Baulcombe, 2007). Alternatively, Rx could constitutively self-associate, forming a larger complex comprising multiple sensor units. I did not detect any size shifts for Rx upon system activation with PVX CP (**Figure 4.1**). This confirms earlier studies reporting that PVX CP and Rx do not form a stable complex (Tameling & Baulcombe, 2007). Moreover, I could not identify any Rx signal at a size corresponding with the activated higher molecular weight NRC2^{EEE} complex described earlier. This suggests that Rx does not stably integrate into this activated NRC2 complex (**Figure 4.1**). Potentially, Rx and NRC2 activate via a mechanism distinct from the hetero-oligomeric

inflammasome previously documented for mammalian paired NLRs (Hu *et al.*, 2015; Vance, 2015; Zhang *et al.*, 2015).

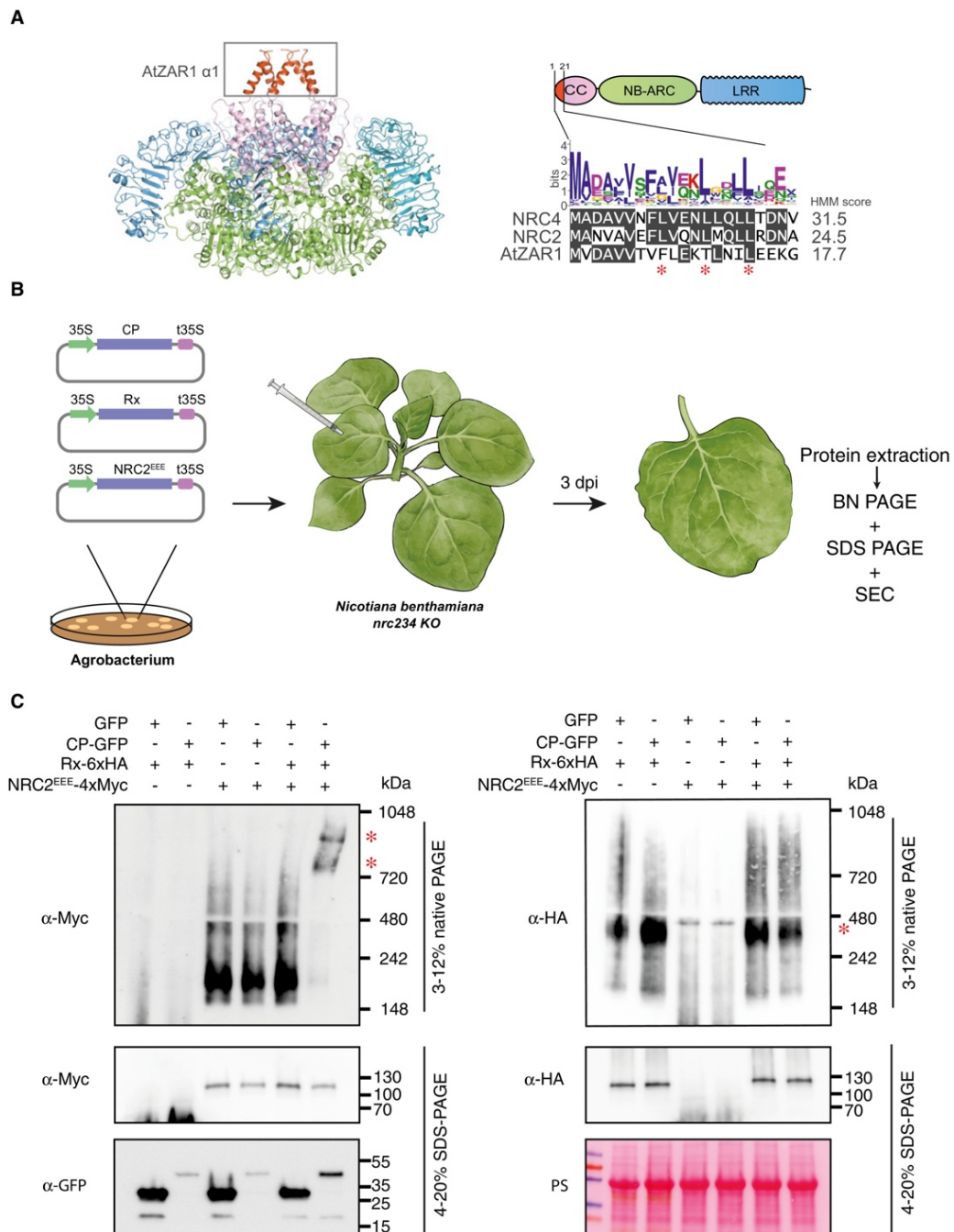


Figure 4.1: PVX CP activation of Rx leads to NRC2 oligomerization.

(A) Structure of the *Arabidopsis thaliana* ZAR1 resistosome. Black box indicates the N-terminal MADA motif-containing $\alpha 1$ helix. Amino acid sequence alignment of the N-termini of NRC4, NRC2 and AtZAR1 along with the consensus sequence pattern for the MADA motif and the HMM score for MADA prediction of each sequence. Red asterisks indicate residues mutated in NRC2^{EEE} mutant (positions 9, 13 and 17). (B)

Schematic representation of the experimental system. *Agrobacterium tumefaciens* was used to transiently express proteins of interest in leaves of *nrc2/3/4* KO *N. benthamiana* mutant lines by agroinfiltration. Leaf tissue was harvested 3 days post-infiltration and total protein extracts were subjected to BN and SDS–PAGE assays. (C) Immunoblots corresponding to BN–PAGE and SDS–PAGE assays with inactive and activated Rx–NRC2. Rx–6xHA and NRC2^{EEE}–4xMyc were co-expressed together with either free GFP or PVX CP–GFP. Free tandem mCherry–4xMyc and mCherry–6xHA fusions were used as controls for NRC2^{EEE}–4xMyc and Rx–6xHA, respectively. Protein extracts were run on native and denaturing PAGE assays in parallel and immunoblotted with the appropriate antisera labelled on the left. Approximate molecular weights (kDa) of the proteins are shown on the right. Red asterisks indicate bands corresponding to the activated NRC2 complex. Rubisco loading control was carried out using Ponceau stain (PS). The experiment was repeated three times with similar results.

To independently corroborate the BN–PAGE experiments with an alternative analytical approach, I expressed Rx and NRC2^{EEE} in leaves of *nrc2/3/4* KO *N. benthamiana* plants in the absence or presence of PVX CP and subjected protein extracts to gel filtration assays. I detected the proteins of interest in the collected fractions via SDS–PAGE analysis, immunoblotting with the corresponding antibodies. Inactive NRC2^{EEE} primarily migrated as a small molecular weight complex, eluting at approximately 15 mL, while Rx migrated at a slightly higher molecular weight, with the majority of the signal eluting at 13 mL (**Figure 4.2**). Upon co-expression of PVX CP–GFP, NRC2^{EEE} shifted its elution volume, migrating mostly as a large complex. This complex eluted at a size between ~440 kDa and ~669 kDa, which assuming an NRC2^{EEE} homo-complex, would correspond to a pentamer (~550 kDa). As all CC–NLR resistosomes characterized to date are pentameric in nature, this would be consistent for the NRC2 resistosome (Förderer *et al.*, 2022; Wang *et al.*, 2019a). In contrast, Rx did not shift its elution volume upon activation. I also did not observe an increase in Rx signal in any of the fractions where the NRC2^{EEE} complex was present. In conclusion, both BN–PAGE and gel filtration assays support a model in which, upon effector perception, Rx mediates NRC2 oligomerization into a higher-order complex of ~550 kDa without stably associating with this complex. Since both methods produced similar outcomes and considering that gel filtration necessitated lengthy sample handling times, I opted to employ BN–PAGE as a readout for the remainder of the investigation.

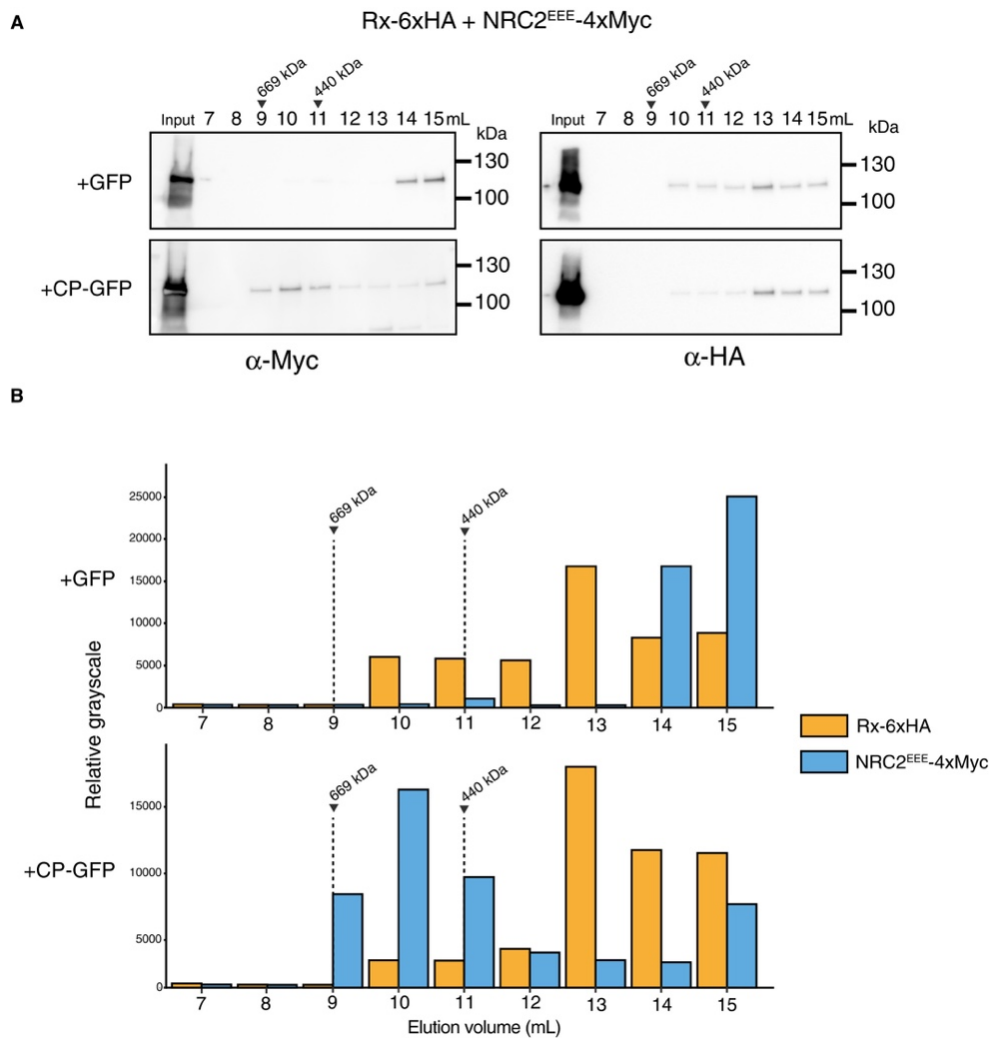


Figure 4.2 Size-exclusion gel filtration chromatography can be used to visualize Rx-mediated oligomerization of NRC2.

(A) Size-exclusion gel filtration assays with inactive and effector-activated Rx-NRC2^{EEE}. Rx-6xHA and NRC2^{EEE}-4xMyc were co-expressed with either free GFP or PVX CP-GFP. Total protein extracts were run on an S200 10/300 analytical column connected to an AKTA Pure system and were fractionated. A range of fractions were subjected to SDS-PAGE and immunoblotted with the appropriate antisera labelled below. Approximate molecular weights (kDa) of the proteins are shown on the right. (B) Relative gray scales indicate the arbitrary densitometry units of different proteins as visualized by immunoblotting. The elution volumes of thyroglobulin and apoferritin (669 kDa and 440 kDa, respectively) are shown above. The experiment was repeated 2 times and representative image are shown.

4.2.3 The high molecular weight complex formed by Rx does not contain the host protein RanGAP2.

Rx has previously been shown to associate with RanGAP2, which is required for PVX resistance (Tameling & Baulcombe, 2007). This led me to hypothesize that the constitutive Rx-specific complex could include RanGAP2. To test this, I generated C-terminally tagged RanGAP2 variants and attempted to visualize an *in vivo* Rx-RanGAP2 complex. I subsequently co-expressed C-terminally 6xHA-tagged Rx and C-terminally 4xMyc-tagged NRC2^{EEE} together with a C-terminally V5-tagged version of RanGAP2 in leaves of *nrc2/3/4* KO *N. benthamiana* mutants and performed BN-PAGE assays. As shown above, Rx migrates at around 400 kDa and does not exhibit any change in size upon activation with PVX CP. RanGAP2 (60 kDa) accumulates to high levels and is visualized primarily as a band of around 160 kDa. I also observed a fainter higher molecular weight band migrating at a size of around 700kDa (**Figure 4.3**). I was, however, unable to detect any obvious signal for RanGAP2 co-migrating with Rx. Interestingly, PVX CP also migrates as a high molecular weight complex of around 500 kDa, which suggests that it may be forming a complex *in vivo*. (**Figure 4.3**). PVX CP also did not co-migrate with Rx, which is in line with previous literature in which it was not shown to form a stable complex with Rx, pointing towards an indirect mechanism of recognition (Tameling & Baulcombe, 2007). Based on these data, we conclude that the ~400 kDa Rx complex does not include RanGAP2.

4.2.4 Rx does not enter into a stable complex with NRC2.

To further challenge the hypothesis that Rx does not constitute part of the activated NRC2 complex, I chose to use an approach based on size shifts induced by different molecular weight tags to study Rx-NRC2 interactions. In my prior experiments, I used C-terminally tagged variants of Rx and NRC2, Rx-6xHA and NRC2^{EEE}-4xMyc respectively (from now on referred to as "light" versions) (**Figure 4.4A**). For this set of experiments, I generated new constructs with C-terminal tandem mCherry-6xHA and mCherry-4xMyc tags, Rx-mCherry-6xHA and NRC2^{EEE}-mCherry-4xMyc respectively (from now on referred to as "heavy" versions) (Fig 2A). I hypothesized that these higher molecular weight versions would allow me to ascertain whether adding a larger molecular weight tag to one of the components of the Rx-NRC2 system could cause a size shift in the other in BN-PAGE assays. I first verified that these new "heavy" versions maintained the capacity to mediate HR cell death (**Figure AIII.3**). I performed complementation assays in leaves of *nrc2/3/4* KO *N. benthamiana* mutant lines with light NRC2^{EEE}-4xMyc alongside heavy Rx-

mCherry-6xHA and subjected protein extracts to BN-PAGE assays. In these experiments, I did not see a size shift for light NRC2^{EEE} in the inactive or activated states, compared to light NRC2^{EEE}-4xMyc co-expressed with light Rx-6xHA (Fig 2B). Heavy Rx-mCherry-6xHA, on the other hand, exhibited a size shift on both BN-PAGE and SDS-PAGE relative to light Rx-6xHA (**Figure 4.4B**). In accordance with this result, co-expression of heavy NRC2^{EEE}-mCherry-4xMyc with light Rx-6xHA does not result in a size shift for Rx in BN-PAGE compared to light NRC2^{EEE}-4xMyc co-expressed with light Rx-6xHA. Again, a size shift was observed for heavy NRC2^{EEE}-mCherry-4xMyc relative to light NRC2^{EEE}-4xMyc in both inactive and activated states in BN-PAGE and SDS-PAGE assays (**Figure 4.4B**). Based on these data, I postulated that Rx and NRC2 are unlikely to form stable complexes with each other at resting state and that NRC2, once activated by its upstream sensor, oligomerizes and forms a higher-order complex that does not stably incorporate Rx.

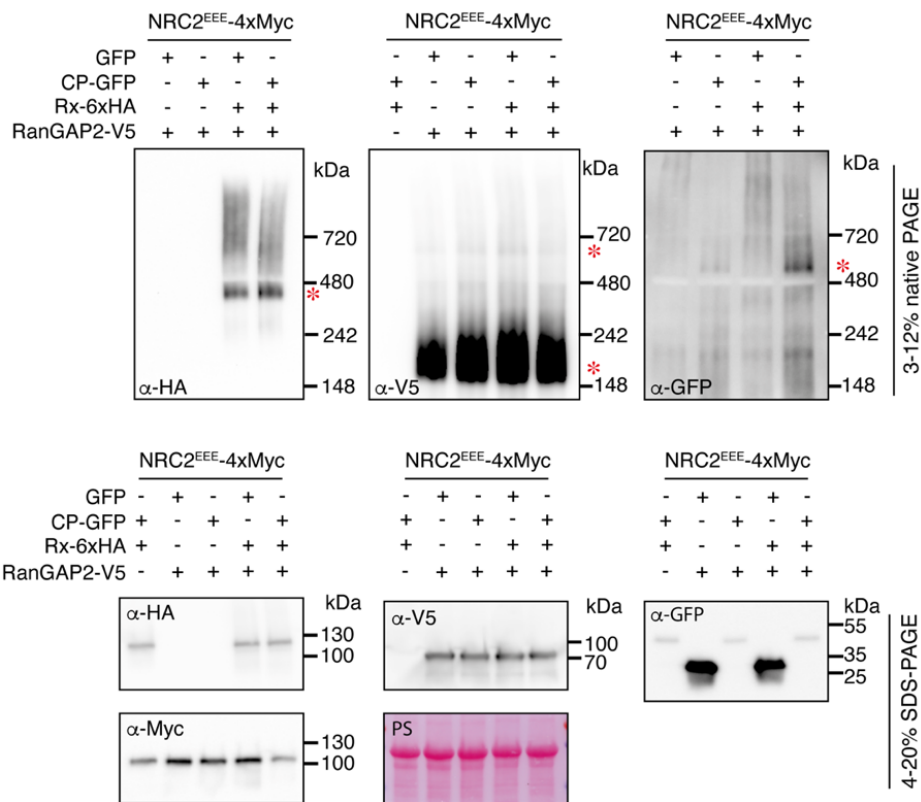


Figure 4.3: Rx, RanGAP2 and PVX CP do not co-migrate in BN-PAGE assays.

BN-PAGE and SDS-PAGE assays with inactive and activated Rx-NRC2. C-terminally 6xHA tagged Rx, C-terminally 4xMyc-tagged NRC2^{EEE} and C-terminally V5-tagged RanGAP2 were co-expressed with either free GFP or C-terminally GFP-tagged PVX CP. Total protein extracts were run on native and denaturing

PAGE assays in parallel and immunoblotted with the appropriate antisera labelled on the left. Approximate molecular weights (kDa) of the proteins are shown on the right. Rubisco loading control was carried out using Ponceau stain (PS).

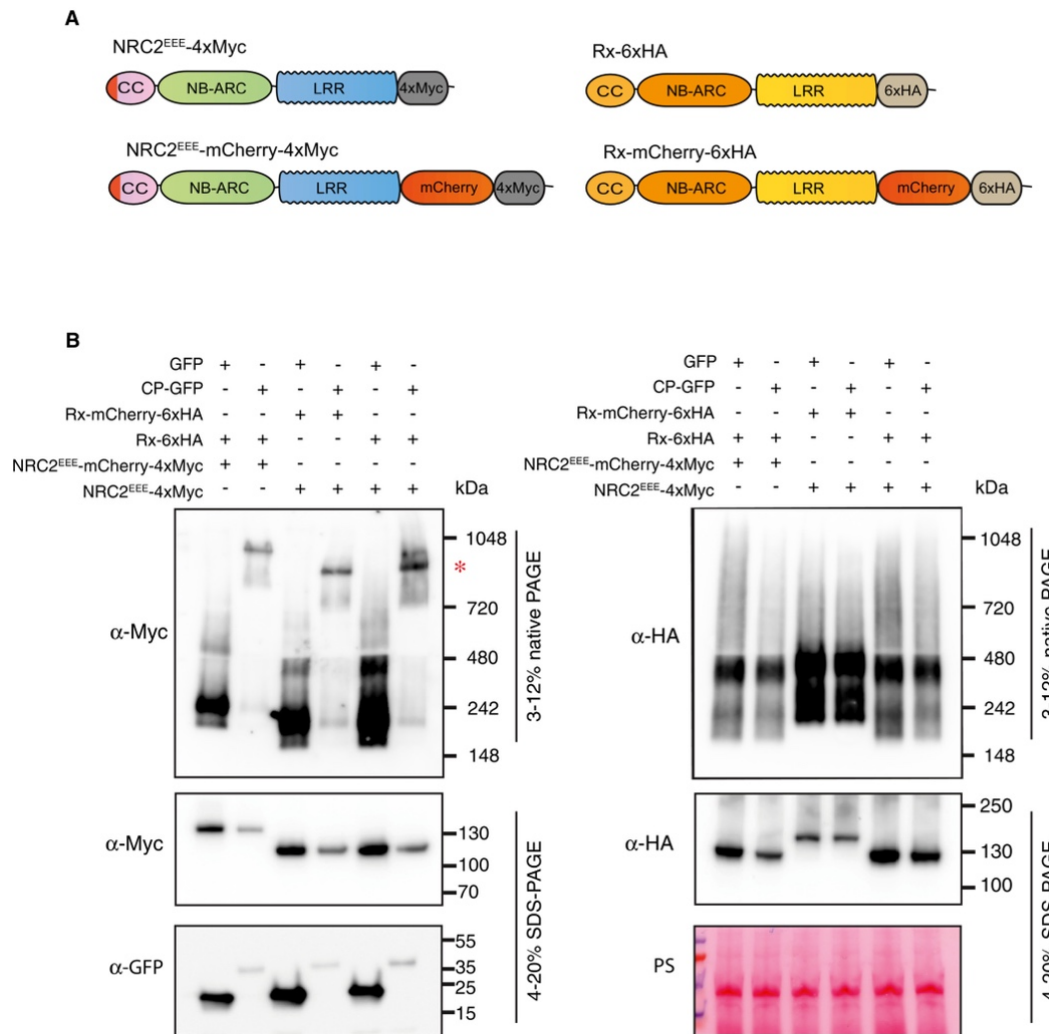


Figure 4.4: Rx and NRC2 do not form a stable complex upon activation.

(A) Schematic representation of NRC2^{EEE} and Rx with C-terminal tags of different sizes. NRC2^{EEE}-4xMyc and Rx-6xHA used in previous experiments (shown above) were termed “light” versions NRC2^{EEE}-mCherry-4xMyc and Rx-mCherry-6xHA (shown below) were termed “heavy” versions. (B) BN-PAGE and SDS-PAGE assays with “heavy” and “light” Rx-NRC2 sensor-helper combinations. Total protein extracts were run on native and denaturing PAGE assays in parallel and immunoblotted with the appropriate antisera labelled on the left. Approximate molecular weights (kDa) of the proteins are shown on the right. Red asterisks indicate bands corresponding to the activated NRC2 complex. Rubisco loading control was carried out using Ponceau stain (PS). The experiment was repeated 3 times.

4.2.5 The NRC2 oligomer is composed of multiple NRC2 proteins.

As my findings support a model in which Rx does not form part of the active NRC2 complex, I shifted my focus towards characterizing the nature of this NRC2 oligomer. I leveraged the heavy and light tag approach described above to determine if NRC2 monomers were indeed forming a complex upon activation. I hypothesized that if the NRC2 complex was composed of multiple NRC2 monomers, a heterogeneous pool of differently sized NRC2 molecules would result in a size shift of the activated complex, compared to a homogeneous pool of heavy or light NRC2 complexes. To test this, I co-expressed Rx-6xHA with either light NRC2^{EEE}-3xFLAG (104 kDa), heavy NRC2^{EEE}-mCherry-4xMyc (133 kDa), or a combination of heavy and light NRC2 variants in leaves of *nrc2/3/4* KO *N. benthamiana* mutant lines (**Figure 4.5A**). As anticipated, both inactive and activated heavy NRC2^{EEE}-mCherry-4xMyc displayed a higher molecular weight than the respective inactive and activated light NRC2^{EEE}-3xFLAG complexes (**Figure 4.5B**). Upon expressing a mixture of both heavy NRC2^{EEE}-mCherry-4xMyc and light NRC2^{EEE}-3xFLAG, the activated NRC2 complex exhibited an intermediate molecular weight, compared to either light NRC2^{EEE}-3xFLAG or heavy NRC2-mCherry-4xMyc complexes (**Figure 4.5B**). That combining differently sized NRC2 variants results in a complex with intermediate molecular weight suggests that, upon activation by Rx, both heavy and light NRC2 variants are forming part of the same complex. Intriguingly, I could not detect any change in size for inactive NRC2^{EEE} when mixing the two molecular weight variants (**Figure 4.5B**). I conclude that the lower molecular weight band observed for inactive NRC2 is likely not a complex of multiple NRC2 monomers. Based on this data, I propose a model for Rx-NRC2 activation in which Rx activates its downstream helper NRC2 following effector-triggered activation, leading to NRC2 oligomerization into a resistosome complex consisting of multiple NRC2 units, likely pentameric in nature.

4.2.6 Bs2 also mediates NRC2 oligomerization.

Having determined that Rx can initiate oligomerization of NRC2, I investigated whether other NRC-dependent sensors can also mediate NRC2 oligomerization. I conducted complementation assays by co-expressing NRC2^{EEE} in leaves of *nrc2/3/4* KO *N. benthamiana* mutants alongside the inactive or effector-activated NRC2/3/4-dependent sensor Bs2, or Rpi-blb2, an NRC4-dependent sensor incapable of signaling through NRC2 as a negative control (**Figure 4.6A**) (Wu et al, 2017, Duggan et al, 2021). Protein extracts were subjected to BN-PAGE assays. Prior to conducting BN-PAGE assays, I performed HR cell death assays with C-terminally

6xHA-tagged variants of these sensors to confirm that tagging does not impair their function (**Figure AIII.4**). My BN-PAGE assays showed that, like Rx, Bs2 activation with AvrBs2 could initiate NRC2^{EEE} resistosome formation. In contrast, no NRC2^{EEE} oligomerization was observed upon Rpi-blb2 activation with AVRblb2 (**Figure 4.6B**). These data show that sensor-mediated NRC2 oligomerization is part of the activation strategy of at least one other NRC2-dependent sensor. Additionally, the observation that only sensors which genetically require NRC2 can mediate its oligomerization indicates that the previously characterized sensor-helper dependencies within the NRC network can be recapitulated biochemically in BN-PAGE-based helper oligomerization assays.

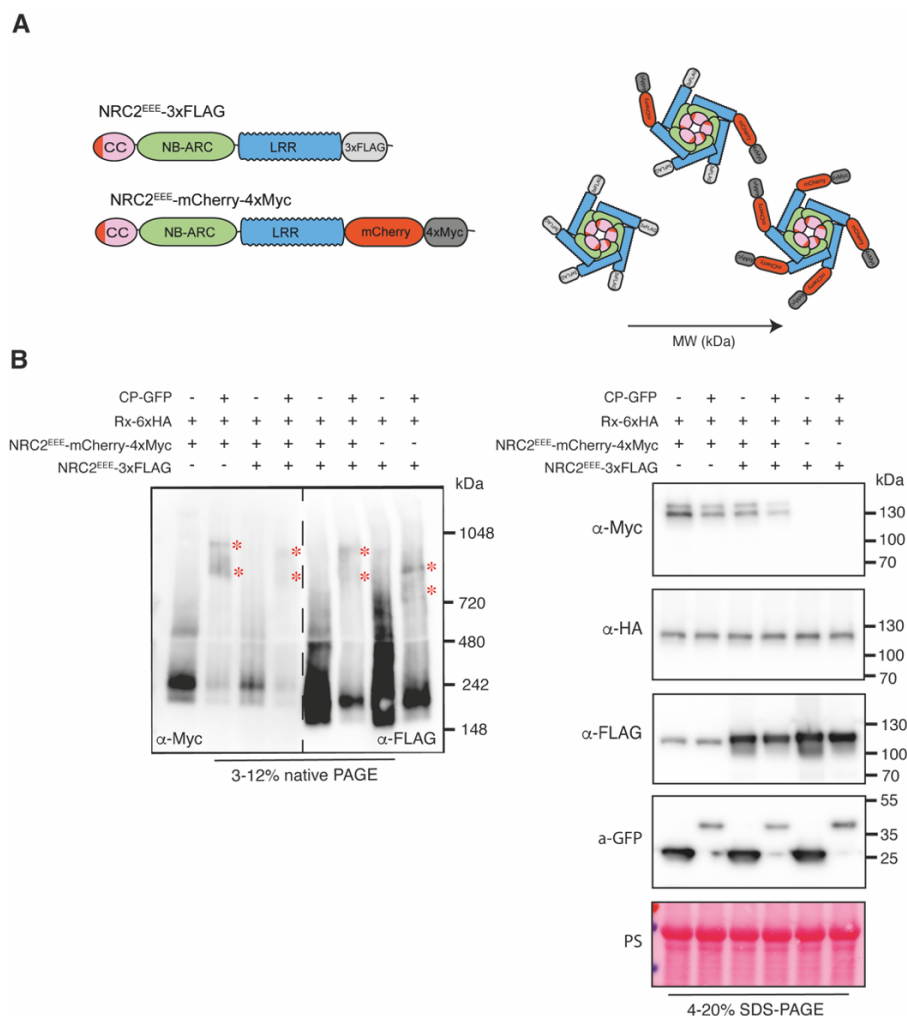


Figure 4.5: The activated NRC2^{EEE} complex is composed of multiple NRC2 monomers.

(A) Schematic representation of NRC2^{EEE} variants used, “light” NRC2^{EEE}-3xFLAG and “heavy” NRC2^{EEE}-mCherry-4xMyc. Schematic representation of our hypothesis. If NRC2 forms homo-oligomers, a heterogeneous mixture of “heavy” and “light” NRC2 monomers should, upon activation, exhibit a

molecular weight that is intermediate relative to homogeneous “light” or homogeneous “heavy” NRC2 monomers. **(B)** BN-PAGE and SDS-PAGE assays with “heavy” and “light” NRC2 helper combinations. In all instances, NRC2 was activated with Rx-6xHA and PVX CP-GFP. Free GFP was used as a control for PVX CP-GFP. Total protein extracts were run on native and denaturing PAGE assays in parallel and immunoblotted with the appropriate antisera labelled on the left. Approximate molecular weights (kDa) of the proteins are shown on the right. Red asterisks indicate bands corresponding to the activated NRC2 complexes. Rubisco loading control was carried out using Ponceau stain (PS). The experiment was repeated 3 times.

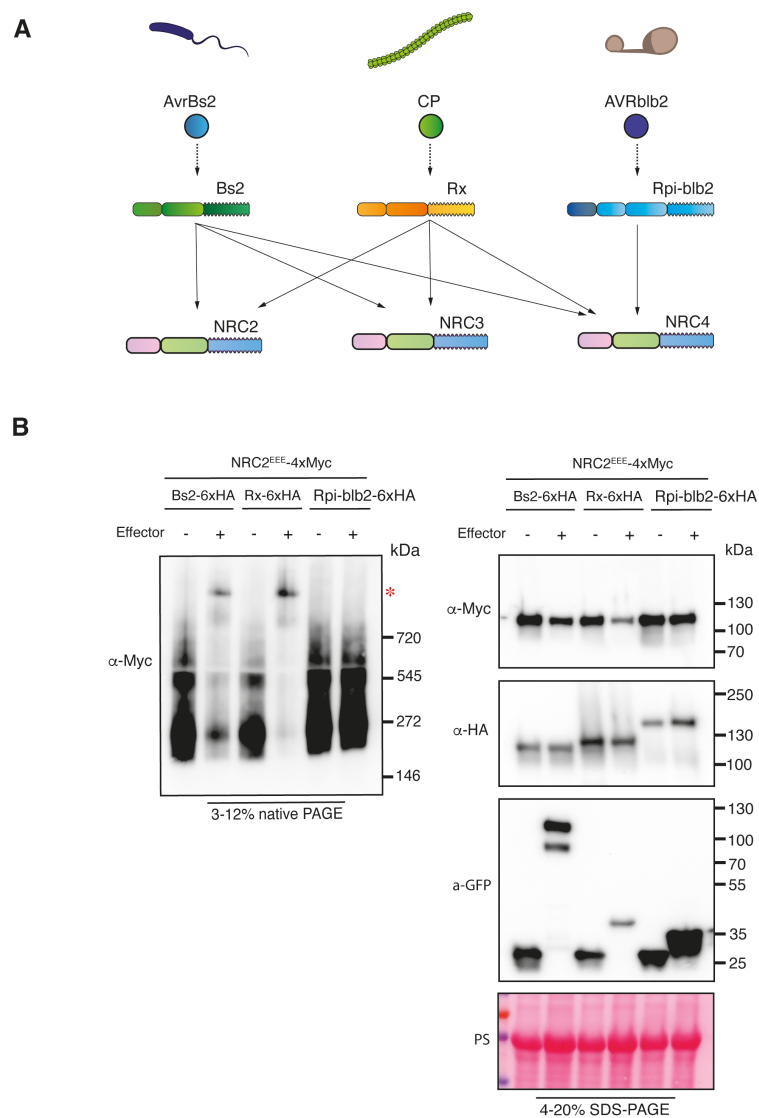


Figure 4.6: Other NRC2-dependent sensors can trigger oligomerization of NRC2^{EEE}.

(A) Schematic representation of the NRC genetic dependencies of sensors used in this experiment. **(B)** BN-PAGE and SDS-PAGE assays with inactive and activated NRC-dependent sensors and NRC2 using

different sensors. Total protein extracts were run on native and denaturing PAGE assays in parallel and immunoblotted with the appropriate antisera labelled on the left. Approximate molecular weights (kDa) of the proteins are shown on the right. Red asterisks indicate bands corresponding to the activated NRC2 complexes. Rubisco loading control was carried out using Ponceau stain (PS). The experiment was repeated 3 times.

4.2.7 Bs2, Rx and Rpi-blb2 activation triggers oligomerization of their helper NRC4

Next, I determined whether the NRC2 activation mechanism is also relevant to another NRC helper, NRC4, which can support signaling by Bs2, Rx, and Rpi-blb2 (**Figure 4.6A**) (Wu *et al.*, 2017). I used the NRC4^{AAA} generated in Chapter 3, with L9A/V10A/L14A mutations in its N-terminal MADA motif (NRC4^{AAA}), which is impaired in hypersensitive cell death induction and allows for *in planta* biochemical analyses. I conducted complementation assays by co-expressing NRC4^{AAA} in leaves of *nrc2/3/4* KO *N. benthamiana* mutants alongside the inactive or effector-activated sensors mentioned earlier. Effector-triggered activation of Bs2, Rx, and Rpi-blb2 mediated oligomerization of NRC4^{AAA} (**Figure 4.7**). This finding indicates that sensor-mediated oligomerization of NRC helpers upon effector perception appears to be a common activation mechanism for multiple sensor-helper pairs within the NRC network.

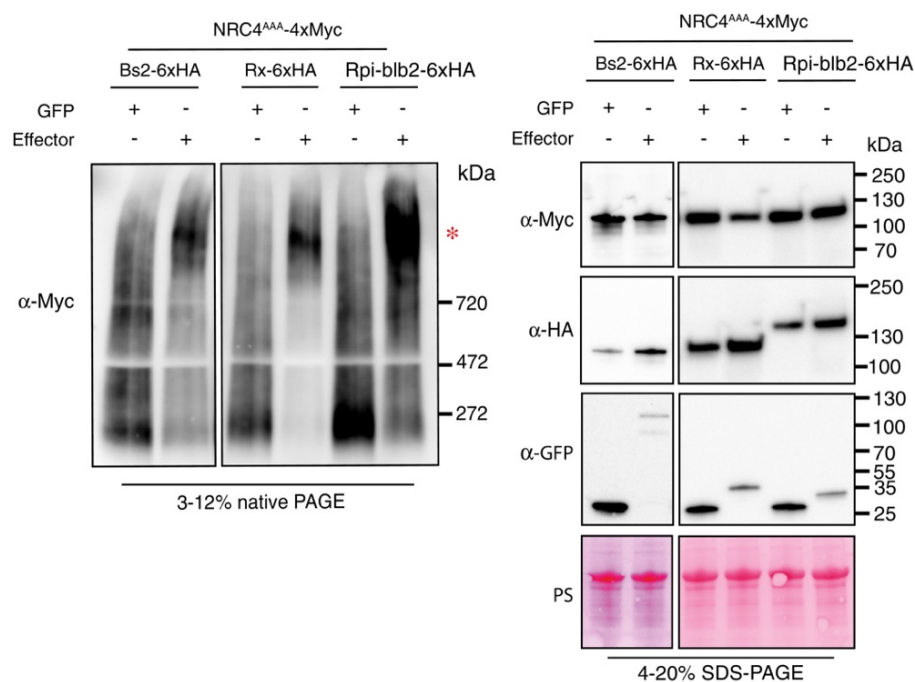


Figure 4.7: Bs2, Rx and Rpi-blb2 trigger oligomerization of another helper NLR, NRC4.

BN-PAGE and SDS-PAGE assays with inactive and activated NRC4-dependent sensors and NRC4^{AAA}. Total protein extracts were run on native and denaturing PAGE assays in parallel and immunoblotted with the appropriate antisera labelled on the left. Approximate molecular weights (kDa) of the proteins are shown on the right. Red asterisk indicates bands corresponding to the activated NRC4 complexes. Rubisco loading control was carried out using Ponceau stain (PS). The experiment was repeated three times.

4.2.8 Activated NRC2 oligomers accumulate in membrane-associated puncta, whereas Rx remains cytoplasmic.

The cellular biology of activated NLRs remains poorly understood. Collaborators in the Bozkurt lab previously showed that the NRC helper NLR NRC4 exhibits dynamic spatiotemporal changes in subcellular localization following effector-triggered activation of its upstream sensor NLR Rpi-blb2 (Duggan *et al.*, 2021). I collaborated with the Bozkurt lab on this project and attempted to apply similar methods to study the sub-cellular dynamics of the Rx-NRC2 system by transiently co-expressing fluorescently tagged versions of Rx-RFP and NRC2^{EEE}-GFP in leaves of *nrc2/3/4* KO *N. benthamiana* mutants. These experiments were done in collaboration with Cian Duggan and Yasin Tumtas from the Bozkurt lab. I activated the Rx-NRC2 system by expressing 4xMyc-tagged PVX CP or a 4xMyc-tag empty vector (EV) control and monitored sensor and helper localization using confocal live-cell imaging (**Figure 4.8**). As a plasma membrane (PM) marker, I co-expressed RPW8.2-BFP (Duggan *et al.*, 2021). In parallel, protein was extracted from the same leaf tissue used for microscopy to confirm that the tags do not interfere with Rx-mediated NRC2 cell death and oligomerization by BN-PAGE assays (**Figure AIII.5**). In their inactive state, both Rx-RFP and NRC2^{EEE}-GFP co-localize to the cytoplasm in 100% of observations (N = 16 images) (**Figure 4.8A**). Strikingly, when co-expressing PVX CP, activated NRC2^{EEE}-GFP predominantly localizes to puncta which frequently co-localize with the PM, marked by RPW8.2-BFP. In contrast, Rx-RFP does not exhibit major changes in subcellular localization. The sensor remains in the cytoplasm and does not concentrate in the NRC2 puncta (15/16 images taken). These puncta are uniformly distributed throughout the PM (**Figure 4.8B**).

To investigate the membrane association of the activated oligomeric NRC2 complex, I obtained protein extracts from the same tissues used for microscopy and carried out membrane fractionation assays in nondenaturing conditions using the same experimental setup described above and performed SDS-PAGE assays using the different fractions (**Figure 4.8C**). In line with live-cell imaging experiments, I found that in the inactive state, both Rx and NRC2^{EEE} are mainly

present in the soluble fraction. Following activation, NRC2^{EEE} is equally distributed between the soluble and membrane fractions, indicating a shift in subcellular localization and increased membrane-association. Rx, however, exhibits no such shift upon activation and remains predominantly in the soluble fraction. I conclude that upon effector-triggered activation of Rx, the sensor subsequently mediates activation of its helper NRC2^{EEE} in the cytoplasm. The activated NRC2 units form oligomeric resistosomes that dynamically re-localize and form membrane-associated puncta that are separate from the sensor.

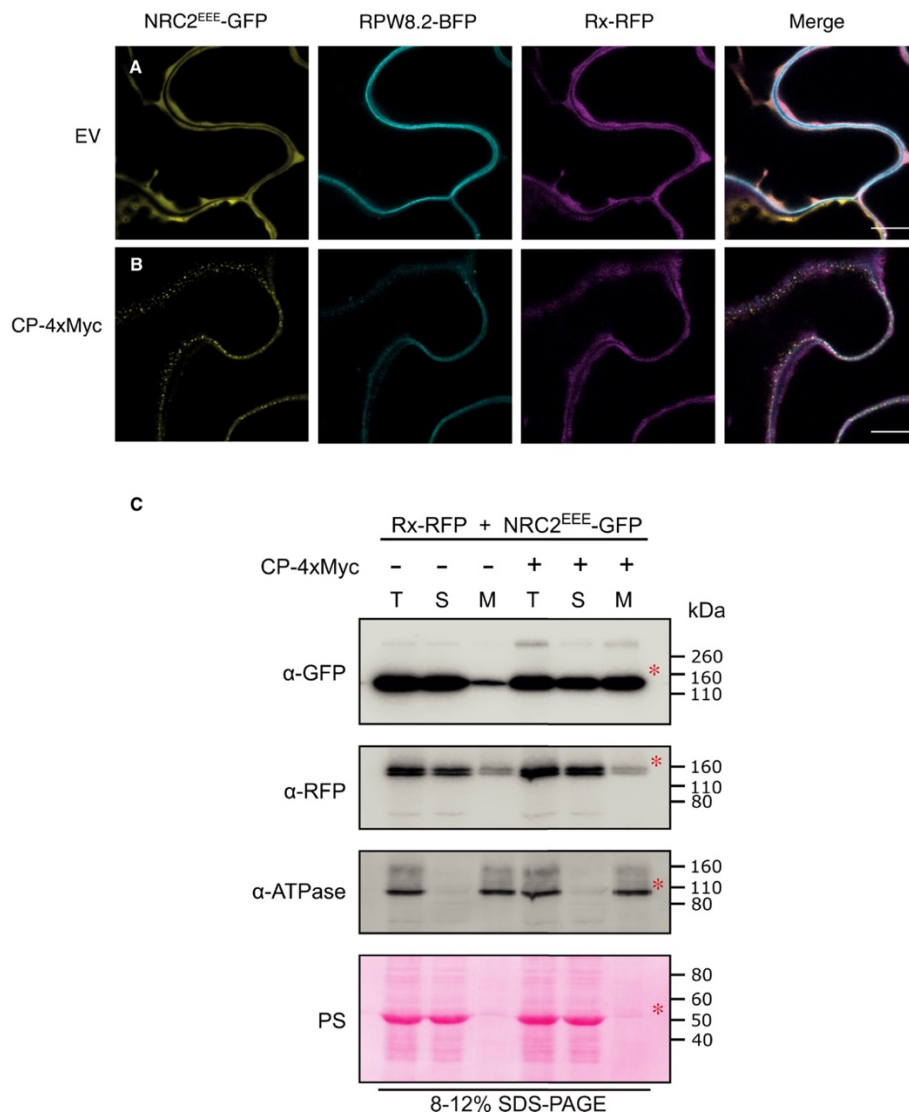


Figure 4.8: *Potato virus X* coat protein activated NRC2 forms plasma membrane-associated puncta, unlike Rx.

C-terminally GFP-tagged NRC2^{EEE} and C-terminally RFP-tagged Rx were co-expressed either with an EV-4xMyc construct or a PVX CP-4xMyc construct in leaves of *nrc2/3/4* KO *N. benthamiana* mutant lines. (**A-**

B) Single-plane confocal micrographs show the localization of both components of the inactive and active Rx-NRC2 system, together with PM marker RPW8.2-BFP. Scale bars represent 10 μm . **(A)** NRC2^{EEE}-GFP and Rx-RFP co-localize in the cytoplasm prior to activation. **(B)** Upon co-expression of PVX CP and activation of the system, NRC2^{EEE} forms puncta associated with the PM while Rx remains in the cytoplasm. **(C)** Membrane enrichment assays are consistent with microscopy, showing that inactive NRC2^{EEE}-GFP is mostly present in the soluble (cytoplasmic) fraction, whereas activated NRC2^{EEE}-GFP exhibits equal distribution across soluble and membrane fractions. Rx is mostly present in the soluble fraction and exhibits no change upon activation of the system with PVX CP. T = total, S = soluble, M = membrane. ATPase was used as a membrane marker. Rubisco was used as a marker for total and soluble fractions and visualized by Ponceau staining (PS). Red asterisks indicate bands matching the expected MW for each protein. The experiment was repeated two times.

4.2.9 Infection with Potato *virus X* leads to Rx-dependent oligomerization of NRC2.

To verify my earlier findings in the context of pathogen infection rather than activation using heterologously expressed effectors, I leveraged our BN-PAGE-based oligomerization readout to study NRC2 activation during viral infection. I transiently expressed Rx and NRC2^{EEE} in leaves of *nrc2/3/4* KO *N. benthamiana* mutant lines and activated the system by infecting leaf tissues with PVX. We used a GFP-tagged PVX variant (pGR106::PVX::GFP), carrying out infections as previously described (Derevnina *et al.*, 2021). Our negative control for infection consisted of free GFP. Three days after infection with the virus, protein extracts from infected or uninfected leaf tissues were used for BN-PAGE assays (**Figure 4.9A**). In line with earlier results in our assays with heterologously expressed PVX CP, PVX infection led to oligomerization of NRC2^{EEE} in an Rx-dependent manner (**Figure 4.9B**). Notably, a very strong GFP signal was observed in SDS-PAGE assays for all PVX treatments, suggesting that the virus can replicate in *nrc2/3/4* *N. benthamiana* in the presence of Rx and NRC2^{EEE}. It appears that while the leucine to glutamic acid mutations introduced in the N-terminal MADA motif of NRC2 do not hinder resistosome formation mediated by Rx, the NRC2^{EEE} mutant is unable to mediate Rx-dependent PVX resistance (**Figure 4.9B**). I conclude that for sensor-helper pairs in the NRC network, pathogen recognition by sensor NLRs leads to immune receptor activation. Following activation, sensors can signal to their downstream NRC helpers, leading to their oligomerization and resistosome formation. Additionally, I conclude that a functional MADA-motif is necessary for Rx-NRC2-mediated resistance to PVX.

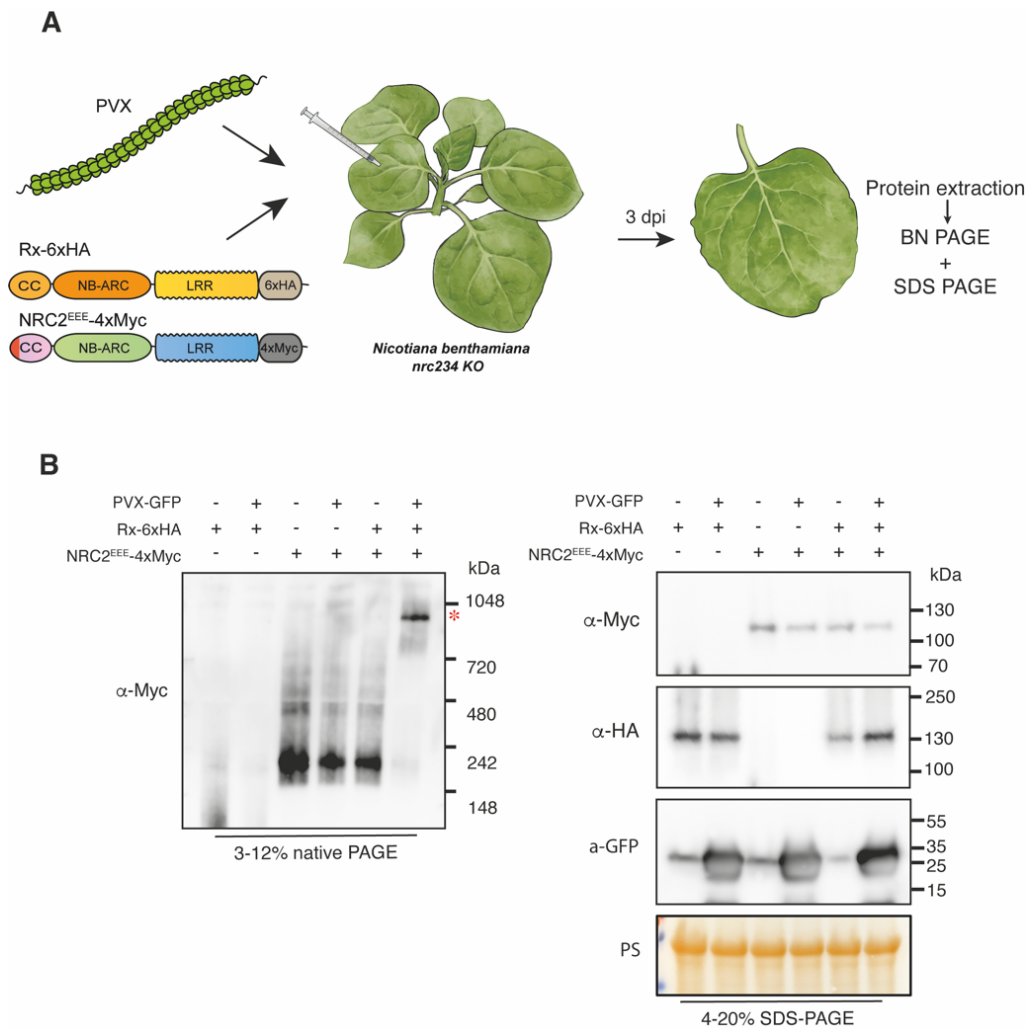


Figure 4.9: PVX infection triggers Rx-mediated oligomerization of NRC2.

(A) Schematic representation of the experimental pipeline used. *A. tumefaciens* strains were used to transiently express proteins of interest in leaves of *nrc2/3/4* KO *N. benthamiana* mutant lines by agroinfiltration. Simultaneously, the same leaves were infected with PVX by expressing a GFP tagged PVX by agroinfection. Leaf tissue was harvested 3 days post-infiltration and total protein extracts were used for BN and SDS-PAGE assays. (B) BN-PAGE and SDS-PAGE assays with infected and uninfected leaves expressing Rx and NRC2. Total protein extracts were run on native and denaturing PAGE assays in parallel and immunoblotted with the appropriate antisera labelled on the left. Approximate molecular weights (kDa) of the proteins are shown on the right. Red asterisks indicate bands corresponding to the activated NRC2 complexes. Rubisco loading control was carried out using Ponceau stain (PS). The experiment was repeated 3 times.

4.2.10 *Potato virus X* infection triggers Rx-dependent formation of membrane-associated NRC2 puncta.

I next sought out to study the sensor-dependent subcellular reorganization of NRC2 described above in the context of pathogen infection. To this end, I transiently co-expressed NRC2^{EEE} either with Rx-RFP or free RFP in leaves of *nrc2/3/4* KO *N. benthamiana* mutant lines and activated the system by infecting leaf tissues with PVX (pGR106::PVX), as described previously (Derevnina *et al.*, 2021). These experiments were also done in collaboration with Cian Duggan from Tolga Bozkurt's lab. After 3 days, I monitored sensor and helper localization using confocal live-cell imaging (**Figure 4.10**). Under these infection conditions, the helper NRC2^{EEE}-GFP remains in the cytoplasm in the absence of its upstream sensor Rx (18/18 images taken) (**Figure 4.10A**). Consistent with previous results, when co-expressing NRC2^{EEE}-GFP together with Rx-RFP and infecting with PVX, the helper predominantly localizes to PM-associated puncta. In contrast, Rx remains in the cytoplasm during PVX infection and does not exhibit co-localization with NRC2 (18/18 images taken) (**Figure 4.10B**). My data indicate that the dynamic re-localization and PM-association of NRC2 I observed following treatment with PVX CP (**Figure 4.8**) also occurs during pathogen infection.

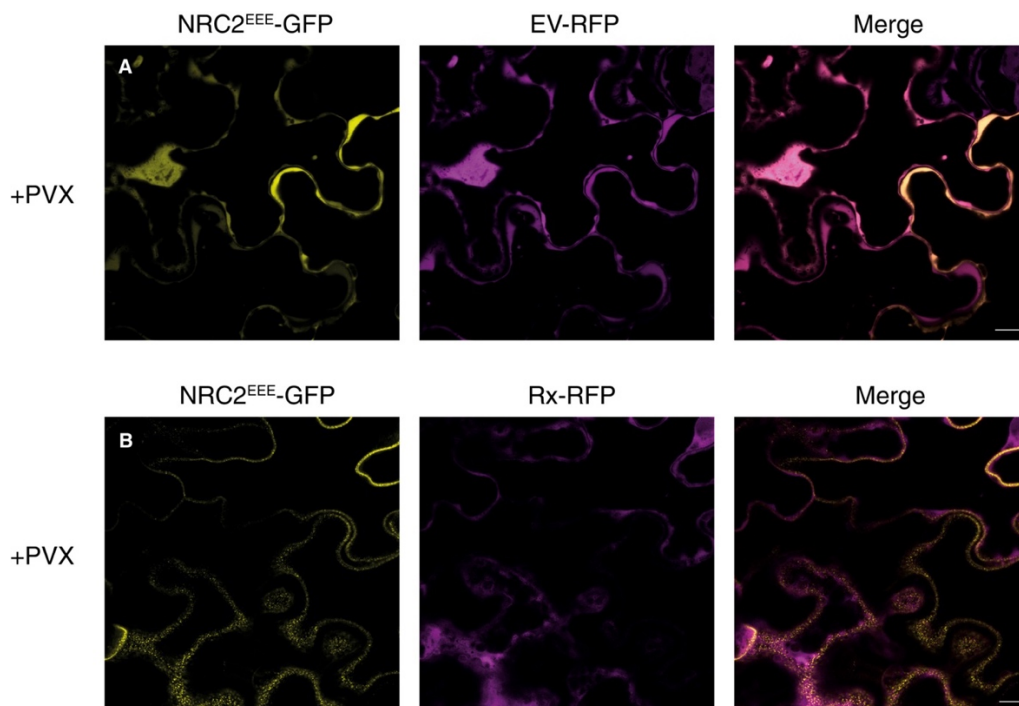


Figure 4.10: *Potato virus X* infection triggers Rx-dependent NRC2 membrane-associated puncta.

(A-B) Single-plane confocal micrographs show the localization of NRC2 together with Rx or free RFP during PVX infection. C-terminally GFP-tagged NRC2^{EEE} was co-infiltrated with either EV-RFP or Rx-RFP in leaves of *nrc2/3/4* KO *N. benthamiana* mutant lines and infected with PVX by agroinfection. Scale bars represent 10 μ m. (A) In the absence of Rx, NRC2^{EEE}-GFP is localized to the cytoplasm during PVX infection. (B) When Rx is present, NRC2^{EEE} forms puncta associated with the PM during PVX infection.

4.3 Conclusions and discussion.

The objective of the work in this chapter was to gain deeper insights into the molecular mechanisms driving the activation of paired and networked plant NLR immune receptors. Previously, in planta studies were hindered by the cell death response initiated by activated NLRs. The mutations in the N-terminal MADA motif identified in **Chapter 3**, which eliminate the cell death response without affecting activation, allowed me to develop readouts for resistosome-like oligomer formation and address various questions related to helper NLR activation. By leveraging biochemical and cellular biology techniques, I developed a working model for the activation of the NRC network sensor NLRs Rx, Bs2, Rpi-blb2, and their helpers NRC2 and NRC4 (Derevnina *et al.*, 2021; Wu *et al.*, 2017). My findings indicate that these sensor NLRs can mediate NRC oligomerization (**Figures 4.1-4.5**) upon activation with their corresponding effectors and, in the case of Rx, during pathogen infection (**Figure 4.9**). For NRC2, I show that sensor activation also mediates helper re-localization to the PM during pathogen infection with PVX (**Figure 4.8, Figure 4.10**). This activated NRC2 complex seems to be an oligomer containing multiple NRC2 units, excluding the sensor NLR (**Figure 4.2, Figure 4.4, Figure 4.5**), which suggests a sensor-helper activation model that differs from mammalian paired NLR systems, such as NAIP/NLRC4 (Vance, 2015; Zhang *et al.*, 2015). For Rx, we observed that it was constitutively forming an oligomer which did not shift in size upon PVX CP perception (**Figure 4.1, Figure 4.2, Figure 4.4**) This oligomer did not appear to include the previously reported Rx co-factor, RanGAP2 (**Figure 4.3**) (Tameling & Baulcombe, 2007). These findings (Contreras *et al.*, 2023b), along with those from a co-published study on NRC2 oligomerization after activation of the oomycete resistance proteins Rpi-amr1 and Rpi-amr3 (Ahn *et al.*, 2023), have led me to develop an activation-and-release working model for NLRs in the NRC network (**Figure 4.11**).

Previous work has shown that following PVX CP-triggered activation, Rx undergoes a series of conformational changes that lead to cell death and immune activation (Moffett *et al.*, 2002; Rairdan *et al.*, 2008; Rairdan & Moffett, 2006). Nonetheless, how a signal is relayed from sensor to helper remains unknown. While Rx does not oligomerize upon activation, the conformational switch may allow Rx to interact transiently with NRC2 to mediate its activation. To date, conclusive evidence that NRC-dependent sensors and their NRC helpers form stable complexes has not been obtained, possibly because the complexes are transient. Regardless of whether a direct or indirect interaction between sensor and helper mediates NRC activation, my findings indicate that the mature NRC2 resistosome is released from the activated sensor. In this scenario, one Rx or Bs2 could potentially activate multiple NRC2 molecules, possibly triggering an NRC2 oligomerization cascade independent of the sensor. Alternatively, NRCs may form transient sensor-helper heterocomplexes with their sensor, which could act as an intermediate polymerization scaffold for the putative NRC resistosome, reminiscent of the first stages of NAIP/NLRC4 inflammasome maturation.

A mechanism in which one sensor molecule can activate multiple NRC resistosomes would be much more efficient in amplifying immune signals as opposed to an activated sensor stably engaging in a sensor-helper heterocomplex. Such an amplification would be analogous to the working model for TIR-NLR/CC_R-NLR sensor-helper pairs, where small molecules produced by activated TIR-NLR sensors lead to downstream helper activation via the enhanced disease susceptibility (EDS1) signaling hub, triggering CC_R-NLR resistosome formation (Huang *et al.*, 2022; Jacob *et al.*, 2021; Sun *et al.*, 2021). What is the precise nature of the activation signal relayed from sensor to helper? What are the precise dynamics of NRC resistosome assembly? How do the molecular determinants for sensor-helper specificity translate into resistosome formation? Addressing these questions in the future holds the potential to advance our understanding of the diversity of plant NLR immune activation beyond functional singleton NLRs.

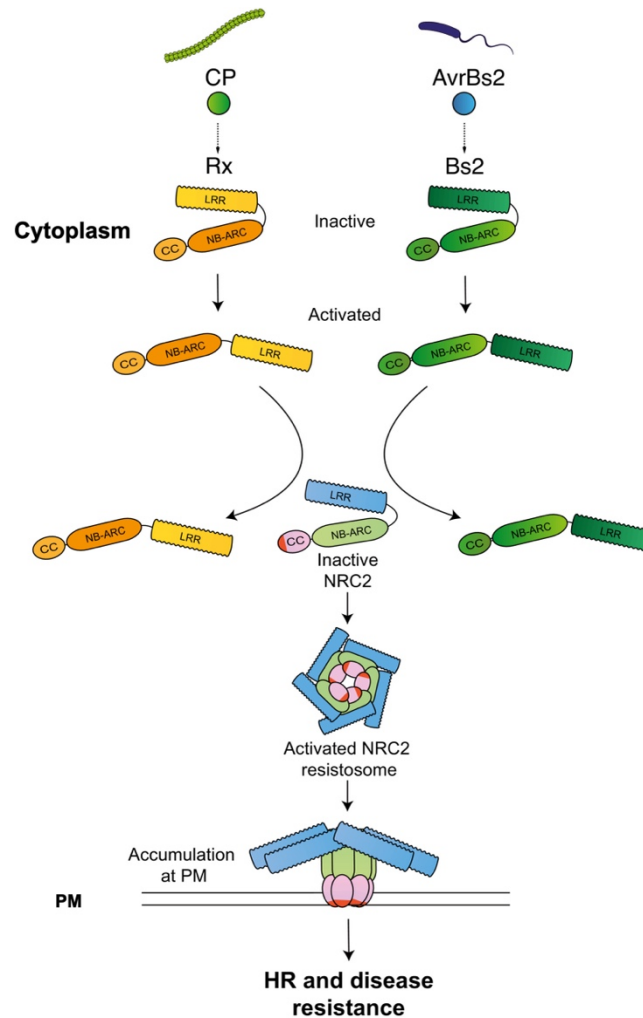


Figure 4.11: An activation-and-release working model for sensor-helper pairs in the NRC network.

Prior to effector-triggered activation, NRC-dependent sensors such as Rx and Bs2 are held in an inactive conformation by intramolecular interactions. Upon perceiving their cognate effectors, the sensors undergo a series of conformational changes that allow them to signal to NRC2 and mediate its homo-oligomerization and resistosome formation. The activated NRC2 resistosome separates from the sensors and accumulates at the PM. The sensors remain in the cytoplasm, separate from the activated helper.

4.4 Research Contributions

I thank Cian Duggan, Enoch L. H. Yuen and Yasin Tumtas (Imperial College, London, UK) for assistance with cell biology experiments and membrane fractionation assays. I thank Jiorgos Kourelis (The Sainsbury Laboratory, Norwich, UK) for providing constructs used in various experiments. I thank Angel Vergara-Cruces for assistance with BN-PAGE assays with agroinfection. I thank Hsuan Pai (The Sainsbury Laboratory, Norwich, UK) for general assistance with various *in planta* biochemistry assays.

Chapter 5: Understanding sensor helper communication in the NRC network.

5.1 Introduction.

NLRs (nucleotide binding and leucine-rich repeat) are intracellular innate immune receptors of eukaryotes and prokaryotes. In plants, they directly or indirectly sense pathogen effectors and translate effector recognition into robust immune signaling and disease resistance (Jones & Dangl, 2006). NLRs exhibit a conserved domain architecture which is broadly conserved, consisting of an N-terminal signaling domain, a central NB-ARC (nucleotide-binding domain shared by APAF1, R gene product and CED-4) a C-terminal leucine-rich repeat (LRR) region. Based on their N-terminal domain features, angiosperm NLRs can be broadly categorized into Toll/Interleukin-1 receptor (TIR)-type, coiled coil (CC)-type, CC_{G10}-type and RPW8 coiled coil (CC_R)-type, which follow the NB-ARC-based NLR phylogeny (Kourelis *et al.*, 2021). NLRs can exhibit different signaling configurations. Some NLRs, like the well characterized CC-NLRs ZAR1 and Sr35 from *Arabidopsis* and wheat, respectively, function as multifunctional “singleton” receptors, mediating both pathogen perception and immune signaling (Förderer *et al.*, 2022; Wang *et al.*, 2019a; Wang *et al.*, 2019b). In some cases, pathogen perception and immune signaling can become uncoupled into two functionally specialized NLRs. One NLR acts as a sensor and relies on a downstream helper to mediate immune signaling and disease resistance. An emerging paradigm is that these one-to-one functional pairings can become increasingly complex, leading to the NLR networks with multiple interconnected sensors and helpers that cooperate to mediate pathogen perception and disease resistance (Adachi *et al.*, 2019b; Wu *et al.*, 2018).

In the Solanaceae, the NLRs required for cell death (NRC) network is composed of multiple sensor CC-NLRs and pattern recognition receptors (PRRs) which genetically require an array of downstream helper CC-NLRs known as the NRCs. This immune receptor network is of great agronomical importance, mediating immunity to diverse plant pathogenic oomycetes, nematodes, viruses, bacteria, and insects (Derevnina *et al.*, 2021; Wu *et al.*, 2017). Unlike the one-to-one sensor-helper connections of paired NLRs, NLR networks exhibit one-to-many and many-to-one sensor-helper pairings (Wu *et al.*, 2018). Interestingly, not all NRC-dependent sensors are capable of activating all helpers, indicating that there is a degree of specificity likely established over time by sensor-helper co-evolution (Adachi *et al.*, 2019b). In *Nicotiana benthamiana*, for

example, Rx, Sw5-b, Gpa2, Bs2 and Rpi-amr3 sensors can signal through NRC2, NRC3 or NRC4. Prf and Rpi-amr1 can signal through NRC2 and NRC3 but not NRC4. In contrast, Rpi-blb2 can signal through NRC4 but not NRC2 or NRC3 (**Figure 5.9**) (Ahn *et al.*, 2023; Contreras *et al.*, 2023b; Derevnina *et al.*, 2021; Wu *et al.*, 2017). How this specificity evolved, however, is not understood. Moreover, the molecular determinants of sensor-helper specificity remain unknown.

In Chapter 4, I used Blue Native polyacrylamide gel electrophoresis (BN-PAGE)-based approaches to establish an activation-and-release model for sensor-helper pairs in the NRC network, using the NRC-dependent sensors Rx, Bs2 and Rpi-blb2 and the helpers NRC2 and NRC4 as a system (Contreras *et al.*, 2023b). Based on my model, I propose that upon effector perception, sensor NLRs mediate oligomerization of their downstream helper NRCs into resistosome complexes. These NRC resistosomes accumulate at the plasma membrane, separate from the sensors that activated them (Contreras *et al.*, 2023b). Recent work by our collaborators in the Jones group also confirmed that this activation mechanism applies to the NRC-dependent oomycete resistance proteins Rpi-amr1 and Rpi-amr3 (Ahn *et al.*, 2023). Interestingly, the activation-and-release mechanism differs from the activation mechanism of metazoan networked NLRs such as NAIP/NLRC4, where sensors and helpers assemble into inflammasome hetero-complexes that include both sensor and helper (Chou *et al.*, 2023). The precise dynamics of NRC resistosome formation, however, are not yet clear. What is the nature of the signal by which NRC-dependent sensors activate NRCs? Whether transient sensor-helper intermediate complexes exist at any point in the NRC activation process is unknown.

Major advances have been made in recent years towards understanding how sensor-helper communication occurs in the context of the N required gene 1 (NRG1)/Activated disease resistance 1 (ADR1) network. For TIR-NLRs, the current model is that effector-dependent assembly of tetrameric TIR-NLR holoenzymes leads to the production of small molecules which lead to the assembly of mutually exclusive dimers of the lipase-like proteins enhanced disease susceptibility 1 (EDS1) – senescence activated gene 101 (SAG101) and EDS1- phytoalexin deficient 4 (PAD4). The assembly of these EDS1-SAG101 and EDS1-PAD4 dimers is sensed by the NRG1 and ADR1 helpers, respectively, leading to the assembly of CC_R helper resistosomes (Feehan *et al.*, 2023; Huang *et al.*, 2022; Jia *et al.*, 2022; Lapin *et al.*, 2019; Saile *et al.*, 2020; Sun *et al.*, 2021). In this case, communication between sensors and helper is indirect, mediated by the immunogenic small molecules and by the EDS1 signaling hub which acts as a mediator in between the TIR-NLRs and CC_R-NLR helpers. Sensor-helper specificity in the NRG1/ADR1 network

appears to be determined by the small molecule profile produced by upstream TIR-NLRs (Huang *et al.*, 2022; Jia *et al.*, 2022). How exactly the EDS1 hub decodes the small molecule signals is not fully understood.

In contrast, the mechanisms by which CC-NLR pairs and networks communicate or regulate each other are poorly understood. In the case of the RGA4/RGA5 CC-NLR pair from rice, immune activation is based on release of negative regulation (Césari *et al.*, 2014). The RGA4 helper is constitutively active and the RGA5 sensor suppresses RGA4-mediated immune signaling. Upon effector perception, RGA5 inhibition of RGA4 is released, presumably triggered by a series of conformational changes in the sensor (Césari *et al.*, 2014). However, many paired and networked CC-NLRs are thought to work by co-operation rather than negative regulation, as the helpers are not constitutively active (Zdrzalek *et al.*, 2020). No enzymatic activity has been attributed to N-terminal CC-domains to date, making small molecule-based signaling unlikely (Gong *et al.*, 2023). Moreover, before the identification of the MADA motif discussed in Chapter 3, studies of activated CC-NLRs were hindered by the strong hypersensitive cell death triggered by immune receptor activation. Understanding how CC-NLR sensors activate their helper mates remains an area of ongoing research.

Rx is an agronomically important NRC-dependent sensor NLR which mediates resistance to *Potato virus X* (PVX) by recognizing the coat protein (CP) of this virus by an unknown, likely indirect, mechanism (Bendahmane *et al.*, 1999; Bendahmane *et al.*, 1995; Tameling & Baulcombe, 2007). In Chapter 4 I showed that, unlike the NRCs, Rx does not appear to assemble into resistosome-like complexes upon activation. Previous works using Rx domains expressed in trans (or Rx “halves”) have shown that Rx exhibits strong intramolecular interactions that are thought to maintain it in an autoinhibited state in the absence of PVX CP (Moffett *et al.*, 2002). While it does not conditionally assemble oligomers, PVX CP perception has previously been shown to induce conformational changes in Rx which disrupt some of these intramolecular interactions (Moffett *et al.*, 2002). These effector-induced conformational changes in the sensor are presumably required to activate its downstream helpers NRC2, NRC3 and NRC4 (Wu *et al.*, 2017). Interestingly, work by Rairdan and colleagues (2008) showed that truncated variants of Rx encoding only its nucleotide-binding (NB) domain fused to GFP (Rx^{NB}-eGFP) can constitutively trigger cell death when transiently expressed in leaves of *N. benthamiana* and *N. tabacum* (Rairdan *et al.*, 2008). Whether this cell death is NRC-dependent is not known. My hypothesis was that if

Rx^{NB}-eGFP were triggering NRC-dependent cell death, this would suggest that the NB domain can encode the minimal signal for NRC helper activation.

In this chapter I leveraged the previously published Rx halves and Rx^{NB}-eGFP systems to study sensor-helper communication in the NRC network. I hypothesized that studying these two systems might provide insights into how sensors activate their downstream helpers. By using complementation assays in *nrc2/3/4* KO *N. benthamiana* lines, I show that the Rx halves trigger cell death in an NRC-dependent manner, by mediating oligomerization of NRC2. As previously shown, Rx halves associate and dissociate upon activation. My data reveals that while their association is not NRC-dependent, their dissociation requires NRCs with an intact MADA motif. I also report that the cell death mediated by Rx^{NB}-eGFP is NRC-dependent, involves NRC resistosome formation and that NB domain truncations of other sensors in the network can trigger NRC-dependent cell death. NB domain truncations of Rx, Gpa2 and Rpi-amr1e recapitulate the helper specificity profile of their full-length counterparts. Furthermore, I identified mutations in the Gpa2 NB domain which contribute to efficiency in Gpa2/Rx and NRC4 sensor-helper communication. All in all, I determined that the NB domain of some sensor NLRs in the NRC network can encode a minimal signal for helper activation.

5.2 Results

5.2.1 Rx can mediate NRC-dependent cell death when expressed as halves.

Previous work by Moffett and colleagues showed that the sensor NLR Rx retains the capacity to induce cell death upon PVX CP perception when its domains are delivered in trans (Moffett *et al.*, 2002). Moreover, the Rx^{CC-NBARC} domains and the Rx^{LRR} domains of Rx delivered in trans were shown to associate prior to activation and dissociate upon activation with PVX CP, suggesting that the different domains of Rx undergo conformational changes following PVX CP perception (Moffett *et al.*, 2002). As Rx is now known to be an NRC-dependent sensor NLR (Wu *et al.*, 2017), I decided to build on this work and further explore the functionality of Rx domains expressed in trans as a system with which to study sensor-helper activation in the NRC network. I started by re-creating the constructs used in the study by Moffett *et al.*, cloning different C-terminally tagged variants of the Rx CC domain (Rx^{CC}), CC-NB-ARC domain (Rx^{CCNBARC}), NB-ARC-LRR (Rx^{NBARCLRR}) and the Rx LRR (Rx^{LRR}) domain (**Figure 5.1A**).

I tested whether the cell death mediated by these domains functioning in trans requires downstream helpers much like the full-length Rx sensor by expressing Rx^{CCNBARC} and Rx^{LRR} or Rx^{CC} and Rx^{NBARCLRR} or full-length Rx with or without PVX CP in leaves of *nrc2/3*, *nrc4a/b* or *nrc2/3/4* KO *N. benthamiana* mutant lines. The constitutively active NbZAR1^{D481V} mutant was used as a control for NRC-independent cell death. Like wild-type Rx, cell death mediated by Rx^{CCNBARC} and Rx^{LRR} or Rx^{CC} and Rx^{NBARCLRR} complementation in trans was only abolished in the *nrc2/3/4* background but not in the *nrc2/3* and *nrc4* backgrounds, suggesting that it is also NRC2/3/4-dependent (**Figure 5.1B**). I also carried out complementation assays in *nrc2/3/4* KO *N. benthamiana* mutant lines to confirm the NRC-dependency of the cell death mediated by Rx^{CCNBARC} and Rx^{LRR} acting in trans. I expressed the two Rx halves with PVX CP in the *nrc2/3/4* background and complemented with NRC2, NRC3 and NRC4 or SINRC0, a tomato NRC that full length Rx is unable to signal through. The cell death mediated by the Rx^{CCNBARC}/Rx^{LRR} system was restored upon complementation with NRC2, NRC3 and NRC4, but not SINRC0 (**Figure 5.1C**).

5.2.2 Rx halves associate in planta in an NRC-independent manner.

I next sought to determine whether the previously reported in planta association of Rx domains when expressed in trans was NRC-dependent (Moffett *et al.*, 2002). To that end, I co-expressed Rx^{CCNBARC} and Rx^{LRR} or Rx^{CC} and Rx^{NBARCLRR} in leaves of WT and *nrc2/3/4* KO *N. benthamiana*. and performed CoIP assays. By immunoprecipitating the Rx^{LRR}, Rx^{CCNBARC} was recovered in both WT and *nrc2/3/4* KO mutant *N. benthamiana* lines, suggesting that the previously reported association between the two separate Rx halves is not NRC-dependent (**Figure 5.2**). This fits with my previous findings in Chapter 4, where I show that Rx forms a complex even in *nrc2/3/4* KO *N. benthamiana* mutant lines. However, this conclusion requires further experimentation. In all treatments both co-expressed proteins associate in the pulldown, meaning that this experiment lacks a true negative control. Further CoIP assays with more robust controls will allow us to draw further conclusions.

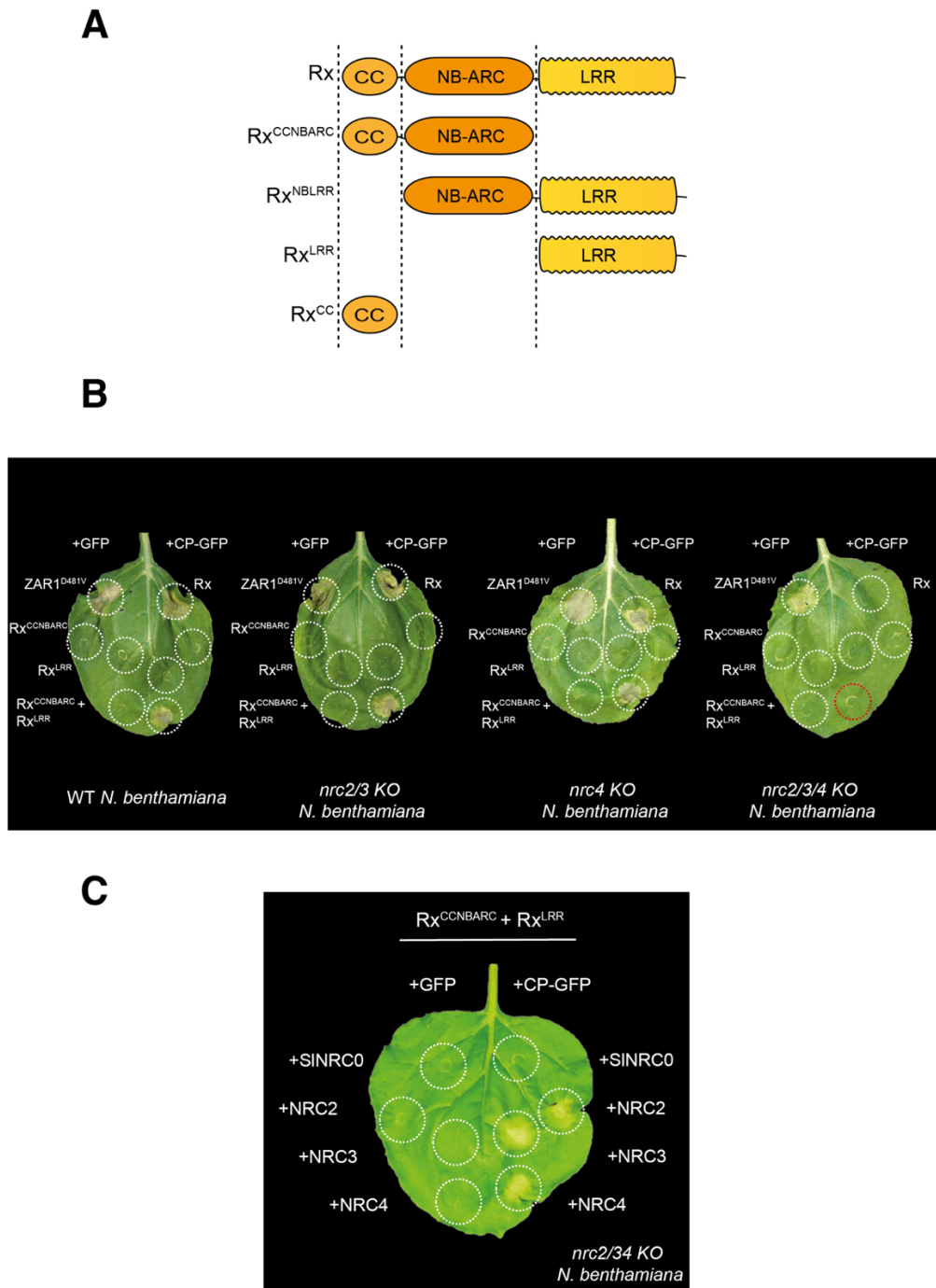


Figure 5.1: Rx halves expressed in trans trigger NRC2/3/4-dependent cell death upon activation with PVX CP

(A) Schematic representation of all Rx domain constructs generated. All constructs were cloned with C-terminal 4xMyc, 6xHA or V5 tags. (B-C) Representative leaves of different *N. benthamiana* lines agroinfiltrated to express constructs shown and photographed 5-7 days after infiltration. (B) Cell death mediated by Rx^{CCNBARC} and Rx^{LRR} complemented in trans is only abolished in *nrc2/3/4* KO *N. benthamiana* plants. Red dotted circle highlights absence of hypersensitive cell death in *nrc2/3/4* KO background. Wild-

type Rx was included for comparison. NbZAR1^{D481V} was included as a control for NRC-independent cell death. (C) Cell death mediated by PVX CP-activated Rx^{CCNBARC} and Rx^{LRR} is complemented by NRC2, NRC3 and NRC4 in leaves of *nrc2/3/4* KO *N. benthamiana* mutant lines when activated by co-expression of PVX CP. Free GFP was used as a negative control (EV) for C-terminally GFP-tagged PVX CP. SINRC0 was used as a negative control as it is a helper NRC that does not get activated by Rx.

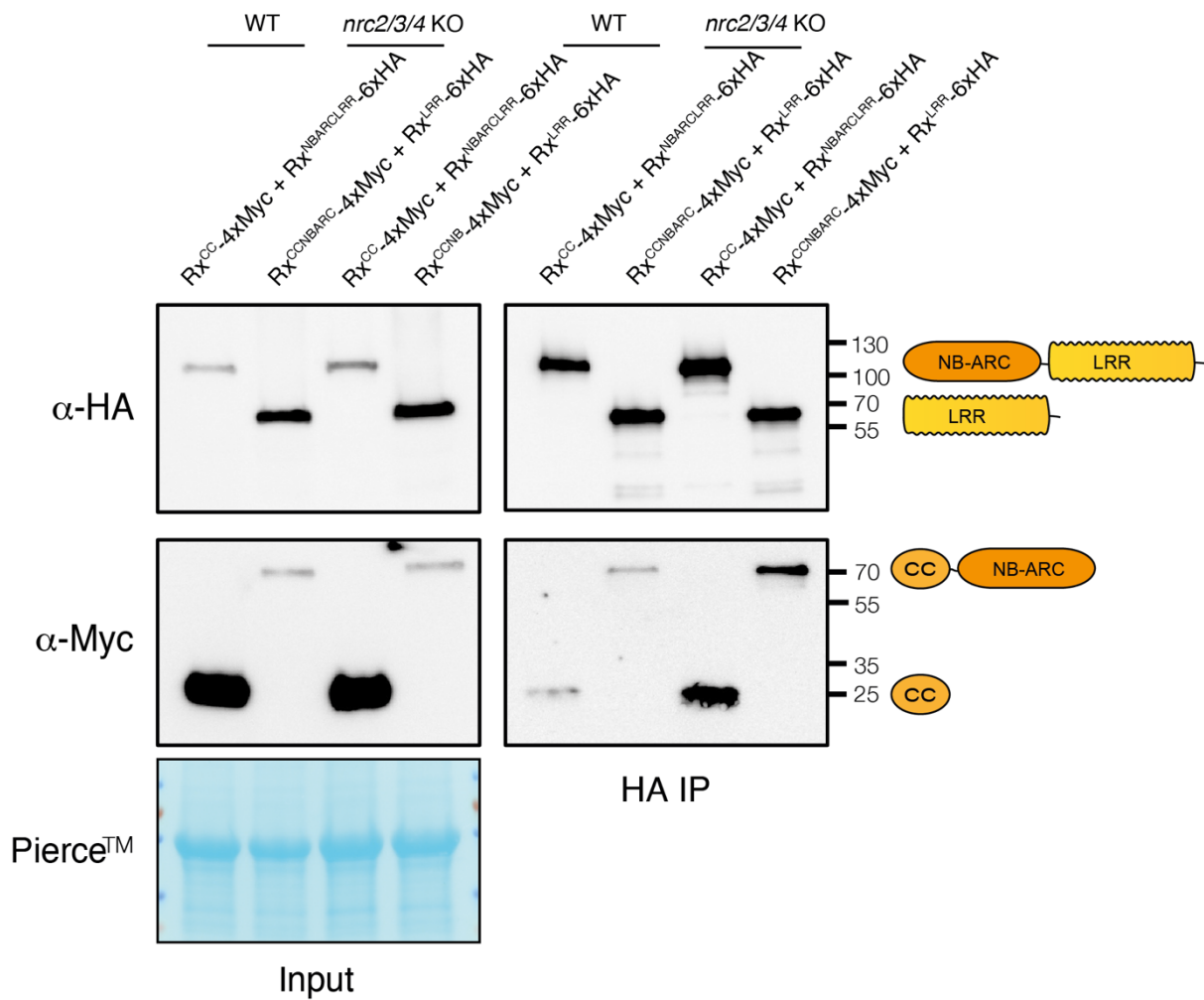


Figure 5.2: Association between halves of Rx expressed in trans is NRC-independent.

Co-immunoprecipitation experiment between Rx^{CC} and Rx^{NBARCLRR} or Rx^{CCNBARC} and Rx^{LRR} expressed in leaves of WT and *nrc2/3/4* KO mutant *N. benthamiana*. Immunoprecipitants (IPs) were obtained using HA antiserum-conjugated beads. Total protein extracts and IPs were immunoblotted using appropriate antisera (indicated to the left of each panel). Approximate molecular weights as well as a schematic of the constructs expressed is shown on the right. Experiment was repeated 3 times with similar results.

5.2.3 NRC2, but not NRC2^{EEE}, mediates Rx halves dissociation upon activation.

Having concluded that the Rx^{CCNBARC} and Rx^{LRR} association is not NRC-dependent, I tested whether the Rx^{CCNBARC} and Rx^{LRR} dissociation reported by Moffett and colleagues was NRC-dependent (Moffett *et al.*, 2002). I co-expressed the inactive and PVX CP-activated Rx^{CCNBARC} and Rx^{LRR} system in leaves of *nrc2/3/4* KO *N. benthamiana* plants and complemented the system with either NRC2 NRC2^{EEE} or SINRC0 as a negative control. All samples were harvested at 48 hours to avoid the onset of cell death triggered by PVX CP activation of the Rx halves in the treatment with NRC2 complementation. We included NRC2^{EEE} to have a treatment where helper activation took place without cell death. Protein extracts were subjected to CoIP assays by pulling down on Rx^{CCNBARC} and Rx^{LRR}. In the treatment with PVX CP activation and NRC2 complementation, I could no longer observe any association between Rx^{CCNBARC} and Rx^{LRR}. I did not observe any dissociation of the Rx halves in the treatments with PVX CP and SINRC0 or NRC2^{EEE} complementation. This suggests that the dissociation between the Rx halves may be dependent on NRC-dependent signaling (**Figure 5.3**). However, this experiment was inconclusive as the overall expression levels of all proteins in the treatments with ongoing cell death were comparatively lower to the other treatments. While no macroscopic cell death was observable on the leaves infiltrated at the 48-hour timepoints, there is likely ongoing immune signalling and cell death that is affecting protein stability in general.

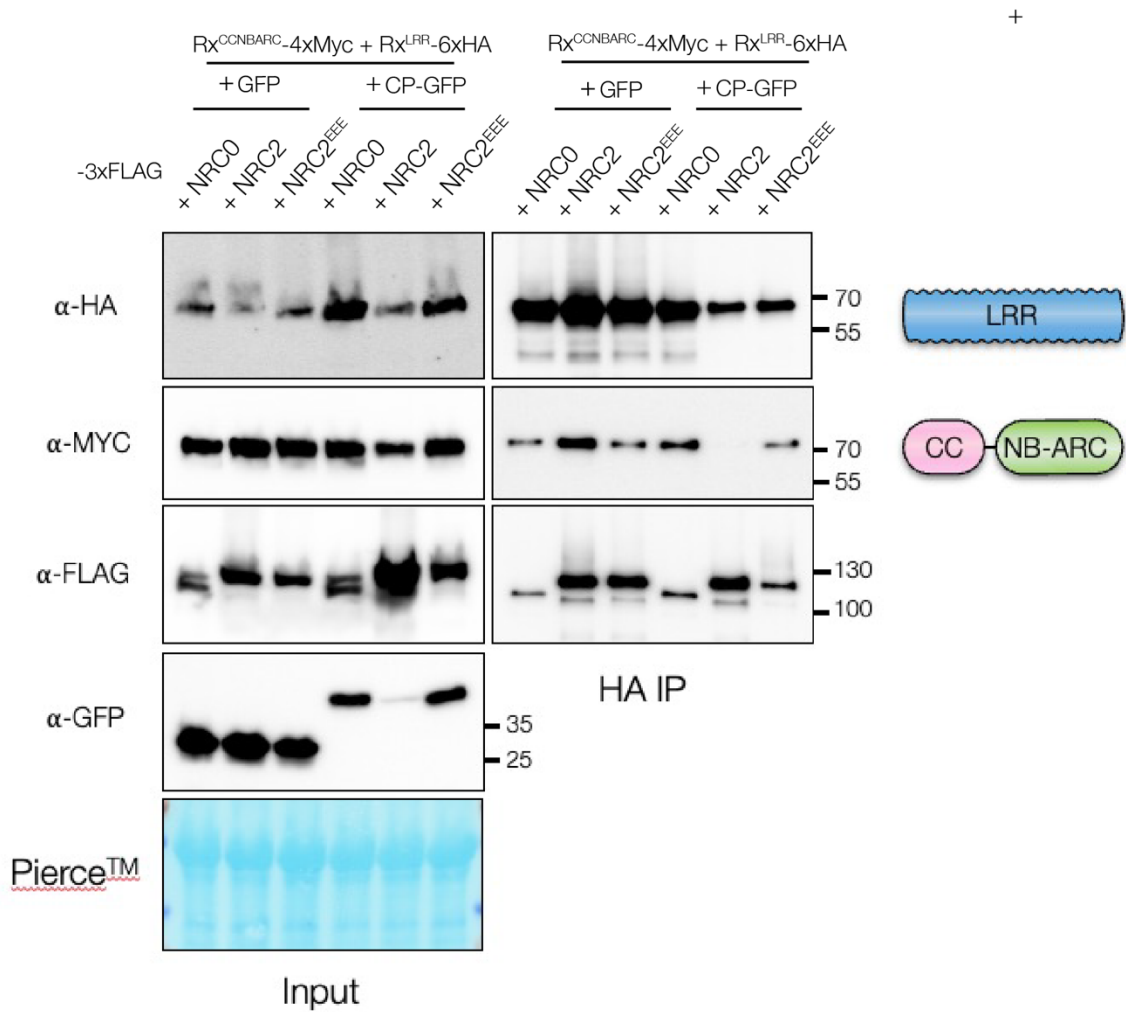


Figure 5.3: Rx halves dissociation is NRC2 and MADA-motif dependent.

Co-immunoprecipitation experiment between the inactive and PVX CP-activated Rx^{CCNBARC}-Rx^{LRR} system complemented with SINRC0, NRC2 and NRC2^{EEE}. Inactive or activated Rx^{CCNBARC}-4xMyc and Rx^{LRR}-6xHA were transiently co-expressed with SINRC0-3xFLAG, NRC2-3xFLAG or NRC2^{EEE}-3xFLAG. Each of these combinations was co-expressed with either free GFP or PVX CP-GFP. Immunoprecipitants (IPs) were obtained using HA antiserum-conjugated beads. Total protein extracts and IPs were immunoblotted using appropriate antisera (indicated to the left of each panel). Approximate molecular weights are indicated on the right (in kDa). While Rx^{LRR} interacts with all NRCs tested, Rx^{CCNBARC} exhibits association with NRC2 and NRC2^{EEE} but not with SINRC0. The previously reported dissociation of Rx^{CCNBARC} and Rx^{LRR} could be observed when complementing the system with NRC2, although the decreased protein accumulation in this treatment complicates interpretation of the results. Experiment was repeated 3 times with similar results.

5.2.4 Rx halves can mediate NRC2 resistosome formation when expressed in trans.

In Chapter 4, I showed that Rx activation can mediate NRC2 oligomerization and resistosome formation. To test whether the activation of the Rx^{CCNBARC}/Rx^{LRR} system also leads to oligomerization of NRC2 as has been observed with the CP activated full-length Rx, I expressed the inactive or activated Rx^{CCNBARC}/Rx^{LRR} domains in leaves of *nrc2/3/4* KO *N. benthamiana* plants, complementing with NRC2^{EEE}, and subjected protein extracts to BN-PAGE assays. Much like wild-type Rx, when delivered together, Rx^{CCNBARC} and Rx^{LRR} mediate NRC2 oligomerization (**Figure 5.5**). I previously showed that both Rx halves are required to trigger cell death in response to PVX CP (**Figure 5.1**). In agreement with this, both Rx halves are required to mediate NRC2 resistosome formation upon PVX CP perception. Expressing either Rx half alone in the presence of PVX CP does not lead to NRC2 oligomerization. Notably, the band visualized for the NRC2 oligomer formed upon Rx^{CCNBARC}/Rx^{LRR} activation exhibits the same size as the oligomer formed upon activation by wild-type Rx (**Figure 5.5**).

In BN-PAGE assays, Rx^{CCNBARC} is visualized as a complex of around 400 kDa, migrating slightly faster than full length Rx. Rx^{LRR}, however, is visualized at a range of molecular weights, from around 400 to 1000 kDa. In both cases, the migration patterns reported for each Rx half are independent of the presence of the other Rx half and are also independent of activation with PVX CP. It appears that Rx^{CCNBARC} forms a stable complex of a molecular weight similar, although relatively slightly smaller, to the full-length Rx complex. On the other hand, the Rx^{LRR} domains appear to form what could be aggregates or protein complexes of a range of different sizes (**Figure 5.5**). These could be multiple Rx^{LRR} domains forming homo-oligomers or Rx^{LRR} associating non-specifically with various proteins. Notably, we did not observe co-migration in BN-PAGE for Rx^{CCNBARC} and Rx^{LRR}. I did not detect signal for Rx^{CCNBARC} at a molecular weight matching the signal obtained for Rx^{LRR} and vice-versa (**Figure 5.5**). Interestingly, both domains are required to trigger NRC2-dependent cell death and reproducibly associate in CoIP assays. The lack of co-migration in our BN-PAGE assays suggest that these two domains are not forming stable complexes and only associate transiently, or that the Rx^{CCNBARC}-Rx^{LRR} complex dissociates in the BN-PAGE conditions used. Understanding the precise biochemical mechanisms that underpin activation of the Rx^{CCNBARC}-Rx^{LRR} system and how these two halves can trigger activation of NRC2^{EEE} remains to be tested.

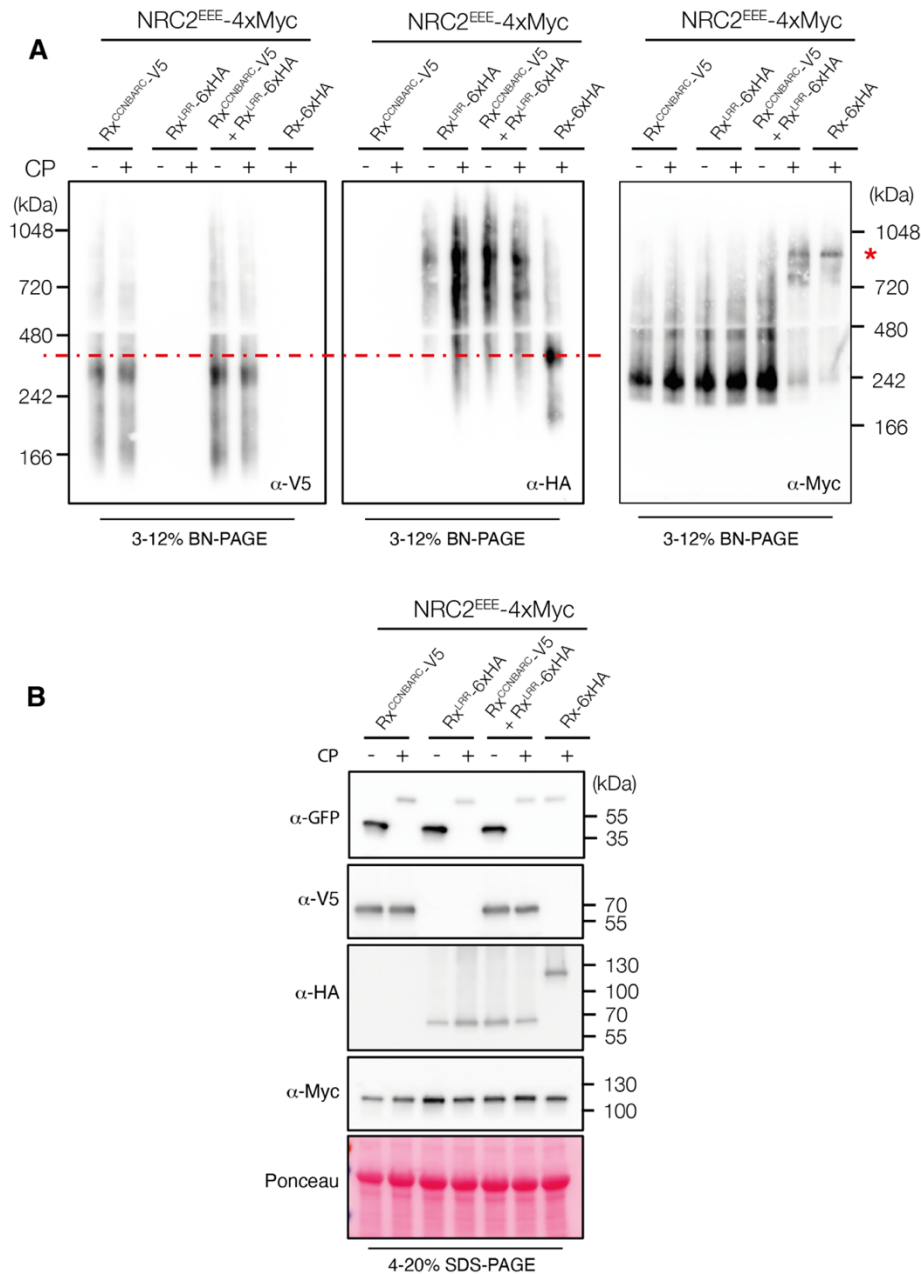


Figure 5.4: Activation of the Rx^{CCNB}/Rx^{LRR} system mediates NRC2 oligomerization.

(A) BN-PAGE assays with the inactive and PVX CP-activated Rx^{CCNB}/Rx^{LRR} system co-expressed with NRC2. C-terminally V5-tagged Rx^{CCNB}, 6xHA-tagged Rx^{LRR} and 4xMyc-tagged NRC2^{EEE} were co-expressed with either free GFP or C-terminally GFP-tagged PVX CP. Wild-type Rx was included for comparison and as a positive control for NRC2 oligomerization. Protein extracts were run on BN-PAGE assays and immunoblotted with the appropriate antisera labelled on the bottom right corner of each blot. Approximate molecular weights (kDa) of the proteins are shown on the right. Red asterisks on the right indicates size of bands corresponding to the activated NRC2 complex. Red dotted lines indicate the molecular weight at which the wild-type Rx complex migrates. Red asterisk on V5 and HA blots indicate these were run on the same gel to allow for precise

comparison of molecular weights. **(B)** SDS-PAGE accompanying BN-PAGE. Protein extracts were run on SDS-PAGE assays and immunoblotted with the appropriate antisera labelled on the left. Approximate molecular weights (kDa) of the proteins are shown on the right. Rubisco loading control was carried out using Ponceau stain (PS). Experiments were repeated 3 times.

5.2.5 The LRR domain of Rx is prone to associating non-specifically with multiple proteins.

In the experiments shown in **Figure 5.4**, the LRR forms high molecular-weight complexes independently of activation status. This was in line with several CoIP assays I performed previously which indicated that the LRR non-specifically associates with other proteins, prompting me to explore further. To determine whether the Rx^{CCNBARC} and Rx^{LRR} halves associated with downstream helper NRC2 used for complementation, I performed further CoIP experiments with the same experimental setup as above, this time immunoprecipitating both Rx^{CCNBARC} and Rx^{LRR}. SINRC0 was included as a negative control. When pulling down Rx^{LRR} we detected associations between Rx^{LRR} and all helpers tested, including SINRC0, both in the inactive and activated states. (**Figure 5.4**). In contrast, the inactive and PVX CP activated Rx^{CCNBARC} domain associates with NRC2 and NRC2^{EEE} but not SINRC0 (**Figure 5.4**). Considering that the cell death mediated by both wild-type full-length Rx and the Rx^{CCNBARC}-Rx^{LRR} system is not SINRC0-dependent, association of Rx^{LRR} with SINRC0 may be non-specific. In contrast, the Rx^{CCNBARC} domain appears to associate more specifically with its downstream helper NRC2 and not with SINRC0.

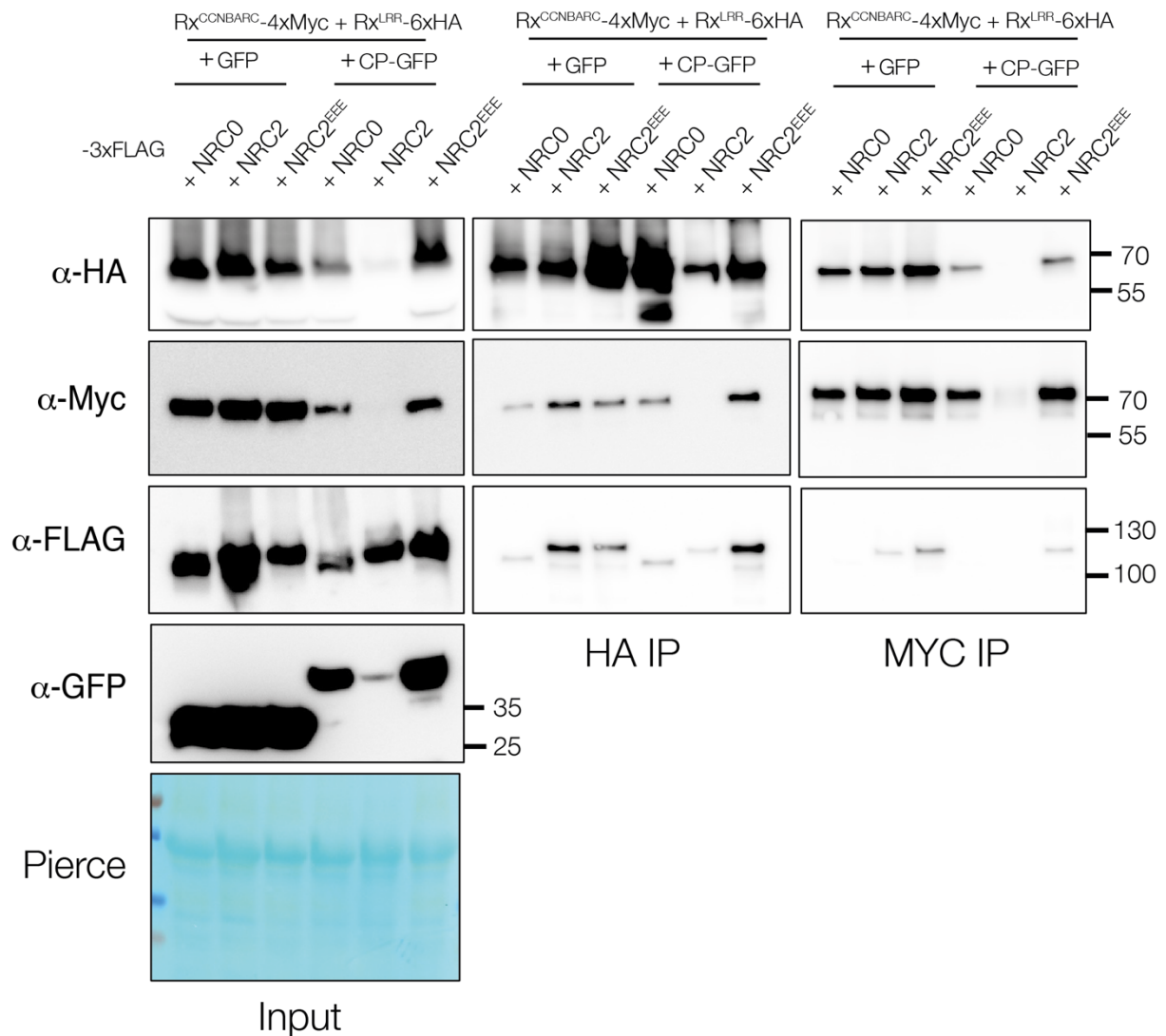


Figure 5.5: Unlike Rx^{LRR} , $Rx^{CCNBARC}$ interacts specifically with NRC2 but not with SINRC0.

Co-immunoprecipitation experiment between the inactive and PVX CP-activated Rx^{CCNB}/Rx^{LRR} system and SINRC0, NRC2 and NRC2^{EEE}. Inactive or activated $Rx^{CCNBARC}$ -4xMyc and Rx^{LRR} -6xHA were transiently co-expressed with SINRC0-3xFLAG, NRC2-3xFLAG or NRC2^{EEE}-3xFLAG. Each of these combinations was co-expressed with either free GFP or PVX CP-GFP. Immunoprecipitants (IPs) were obtained using Myc or HA antiserum-conjugated beads. Total protein extracts and IPs were immunoblotted using appropriate antisera (indicated to the left of each panel). Approximate molecular weights are indicated on the right (in kDa). While Rx^{LRR} interacts all NRCs tested, $Rx^{CCNBARC}$ exhibits association with NRC2 and NRC2^{EEE} but not with SINRC0. The previously reported dissociation of $Rx^{CCNBARC}$ and Rx^{LRR} could be observed when complementing the system with NRC2, although the decreased protein accumulation in this treatment complicates interpretation of the results. Experiment was repeated 3 times with similar results.

5.2.6 The NB domain of Rx can activate its downstream helpers NRC2, NRC3 and NRC4 in a p-loop independent manner.

While the experiments discussed in Chapter 4 point to an activation-and-release model for sensor-helper activation in the NRC network, the exact mechanism by which sensors and helpers communicate remains unknown. Rairdan and colleagues showed that a truncated version of the NRC-dependent sensor Rx encoding only its NB domain fused to eGFP (Rx^{NB} -eGFP) was capable of constitutively triggering cell death in *N. benthamiana* and *N. tabacum* (Rairdan *et al.*, 2008). I hypothesized that potentially the NB domain of Rx alone was somehow capable of activating its downstream helpers leading to their oligomerization and resistosome formation. This would imply that, within the sensor, the signal for helper activation might be encoded exclusively within the NB domain of the sensor. To test this, I performed cell death assays with Rx^{NB} -eGFP in WT and *nrc2/3/4* KO *N. benthamiana* plants (Figure 5.6). I also included Rx^{NB} p-loop mutants to test whether the cell death triggered requires ATP binding. The cell death mediated by both Rx^{NB} -eGFP and $Rx^{NB-p-loop}$ -eGFP was abolished in *nrc2/3/4* KO *N. benthamiana* leaves, indicating that Rx^{NB} -eGFP triggers cell death via canonical NRC-dependent and p-loop independent pathways (Figure 5.6).

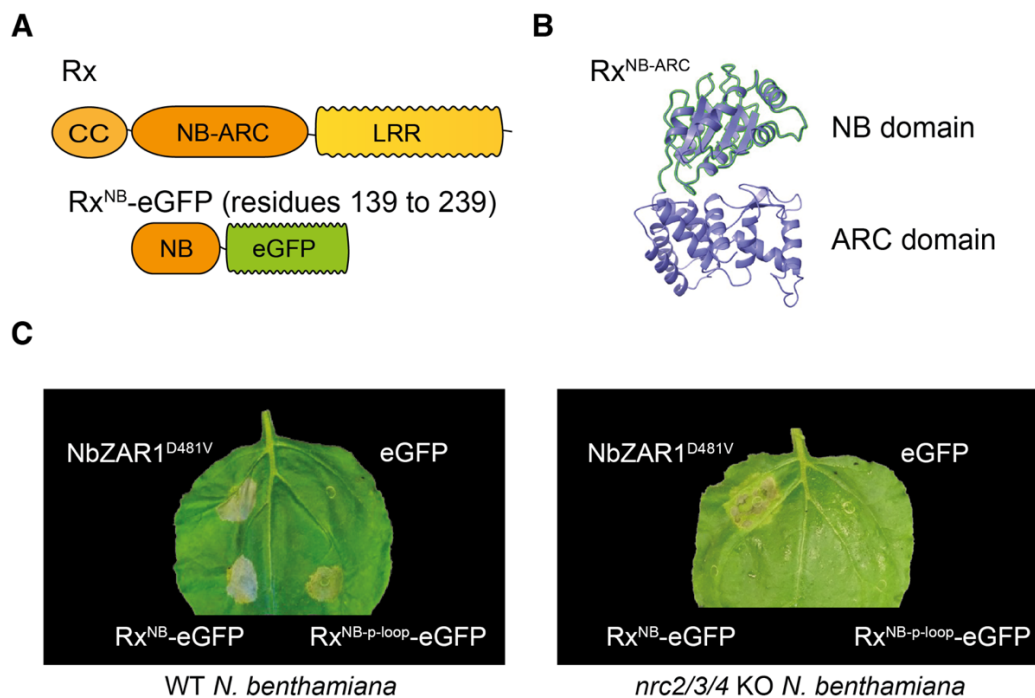


Figure 5.6: The NB domain of Rx fused to eGFP triggers cell death in an NRC-dependent and p-loop-independent manner.

(A) Schematic representation of Rx^{NB}-eGFP constructs. (B) AlphaFold2 prediction of the of Rx NB-ARC domain. The region corresponding to Rx^{NB} is outlined in green. (C) Representative leaves of HR assays with Rx^{NB}-eGFP and Rx^{NB}-p-loop-eGFP. NbZAR1^{D481V} and eGFP were included as positive and negative controls for cell death, respectively. Leaves were agroinfiltrated to express the constructs indicated and photographed 5-7 days after infiltration. One representative leaf is shown.

To determine if NRC dependent cell death triggered by the Rx^{NB}-eGFP construct is accompanied by NRC2 oligomerization and resistosome formation, I performed BN-PAGE assays with the split Rx system and NRC2^{EEE}. I co-expressed NRC2^{EEE}-4xMyc together with Rx^{NB}-eGFP. I included Rx-6xHA/PVX CP-eGFP as a positive control for NRC2 oligomerization. Rx^{NB}-eGFP was capable of triggering NRC2 oligomerization like its wild-type counterpart, Rx (Figure 5.7). Rx^{NB}-eGFP activation of NRC2^{EEE} resulted in helper NLR oligomer of the same size as the NRC2^{EEE} oligomer triggered by wild-type Rx upon PVX CP perception, providing further evidence for Rx not being a part of the activated NRC2 complex (Figure 5.7).

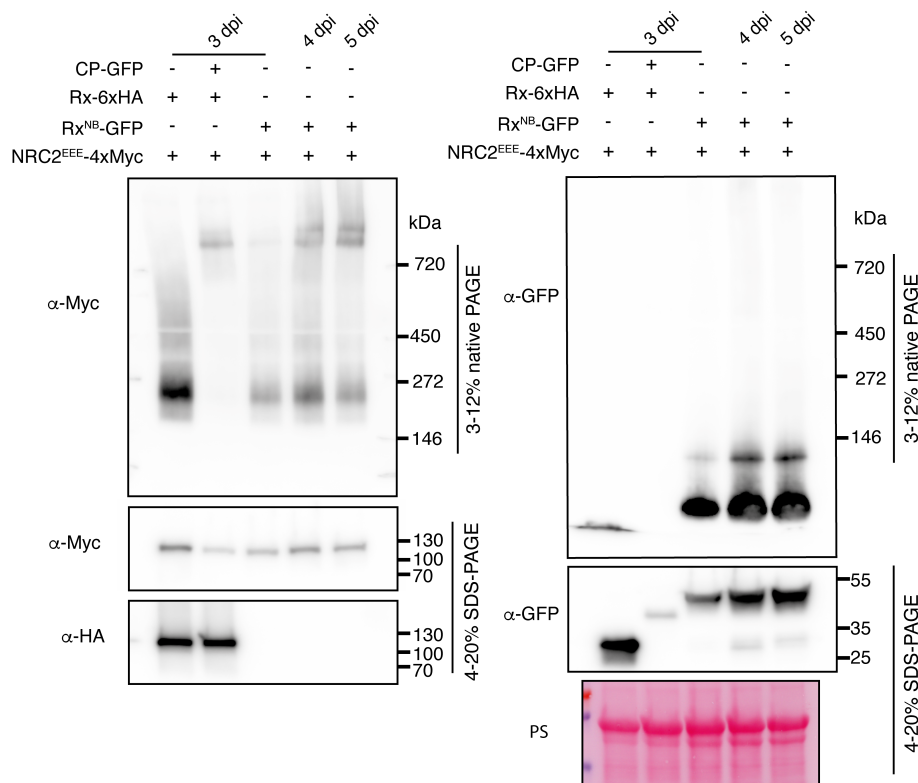


Figure 5.7: Rx^{NB}-eGFP mediates NRC2^{EEE} oligomerization.

BN-PAGE and SDS-PAGE assays with inactive and activated C-terminally 4xMyc-tagged NRC2^{EEE}. NRC2^{EEE} was activated either with C-terminally 6xHA-tagged Rx and PVX CP-GFP or C-terminally eGFP

tagged Rx^{NB}. Total protein extracts were run on native and denaturing PAGE assays in parallel and immunoblotted with the appropriate antisera labelled on the left. Approximate molecular weights (kDa) of the proteins are shown on the right. Rubisco loading control was carried out using Ponceau stain (PS). The experiment was repeated 3 times with similar results.

5.2.7 The NB domains of other NRC-dependent sensor NLRs can also activate downstream helpers.

I next sought to determine whether this NB domain-mediated activation of helper NLRs is a feature shared with other NRC-dependent sensors other than Rx. To this end, I generated NB domain-eGFP fusions for a panel of NRC dependent sensor NLRs, including the Rx-type sensors Gpa2, Rpiamr1e, Rpiamr3 and Bs2, and the Solanaceous domain (SD)-type sensors Mi, and Rpi-blb2. Like Rx^{NB}-eGFP, other Rx-type sensors Gpa2, Rpi-amr1e and Rpi-amr3 also triggered NRC-dependent cell death. Bs2 did not, although Western blot analysis of protein accumulation revealed that Bs2 did not accumulate to high levels. NB domain-eGFP fusions of both SD-type sensors tested, Mi and Rpi-blb2 did not trigger cell death despite protein accumulation levels comparable to Rpi-amr1e^{NB}-eGFP (**Figure 5.8A-B**). These results suggest that NB domain-mediated activation of downstream NRC helpers is not exclusive to Rx and can also be triggered by other Rx-type sensors in the NRC network.

5.2.8 Sensor NLR NB domain truncations retain the NRC helper specificities of their full-length counterparts.

Given that the cell death triggered by the NB domain-eGFP fusions of Rx, Gpa2 and Rpi-amr1e were NRC-dependent, we wanted to further understand if these NB domains retained the same NRC-specificity profile exhibited by their full-length counterparts. PVX CP-activated Rx and RBP1 activated Gpa2 can signal interchangeably via NRC2, NRC3 and NRC4. AvrAmr1 activated Rpiamr1e can signal via NRC2, NRC3 but cannot activate NRC4 (**Figure 5.9A, Figure AIV.1**) (Contreras *et al.*, 2023a; Derevnina *et al.*, 2021; Wu *et al.*, 2017). To test the NRC helper specificity profiles of Rx^{NB}-eGFP, Gpa2^{NB}-eGFP and Rpiamr1e^{NB}-eGFP we performed complementation assays expressing these NB domains and NRC2, NRC3 or NRC4 in leaves of *nrc2/3/4* KO *N. benthamiana*. We included complementation with SINRC0 as a negative control as none of these sensors can activate this helper. Rx^{NB}-eGFP and Gpa2^{NB}-eGFP could activate NRC2, NRC3 and NRC4. Gpa2^{NB}-eGFP could activate NRC2 and NRC3 and triggered weak cell death when

complemented with NRC4. Rpiamr1e activated NRC2 and NRC3 but not NRC4. (**Figure 5.9B**). This indicates that, NB domain-eGFP fusions largely retain the same helper NRC preferences of their full-length counterparts.

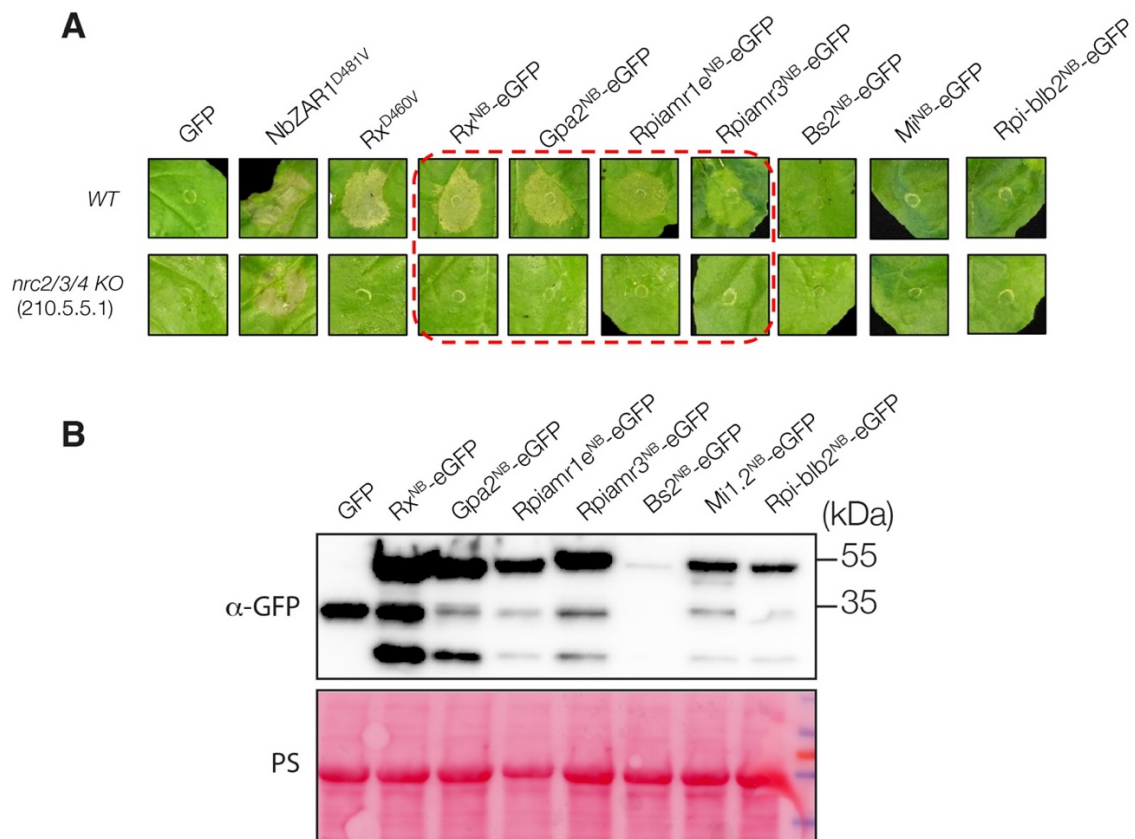


Figure 5.8: Other sensor NLR NB domain-eGFP fusions trigger NRC-dependent cell death.

(A) Representative photos of HR assays with the constructs indicated in leaves of either WT or *nrc2/3/4* KO *N. benthamiana*. NbZAR1^{D481V} and eGFP were included as positive and negative controls for cell death, respectively. Rx^{D460V} was included as a control for NRC-dependent cell death. Leaves were agroinfiltrated to express the constructs indicated and photographed 5-7 days after infiltration. One representative leaf is shown. (B) SDS-PAGE assays with sensor NLR NB domain-eGFP fusions. Total protein extracts were run on denaturing PAGE assays and immunoblotted with the appropriate antisera labelled on the left. Approximate molecular weights (kDa) of the proteins are shown on the right. Rubisco loading control was carried out using Ponceau stain (PS). The experiment was repeated 2 times with similar results.

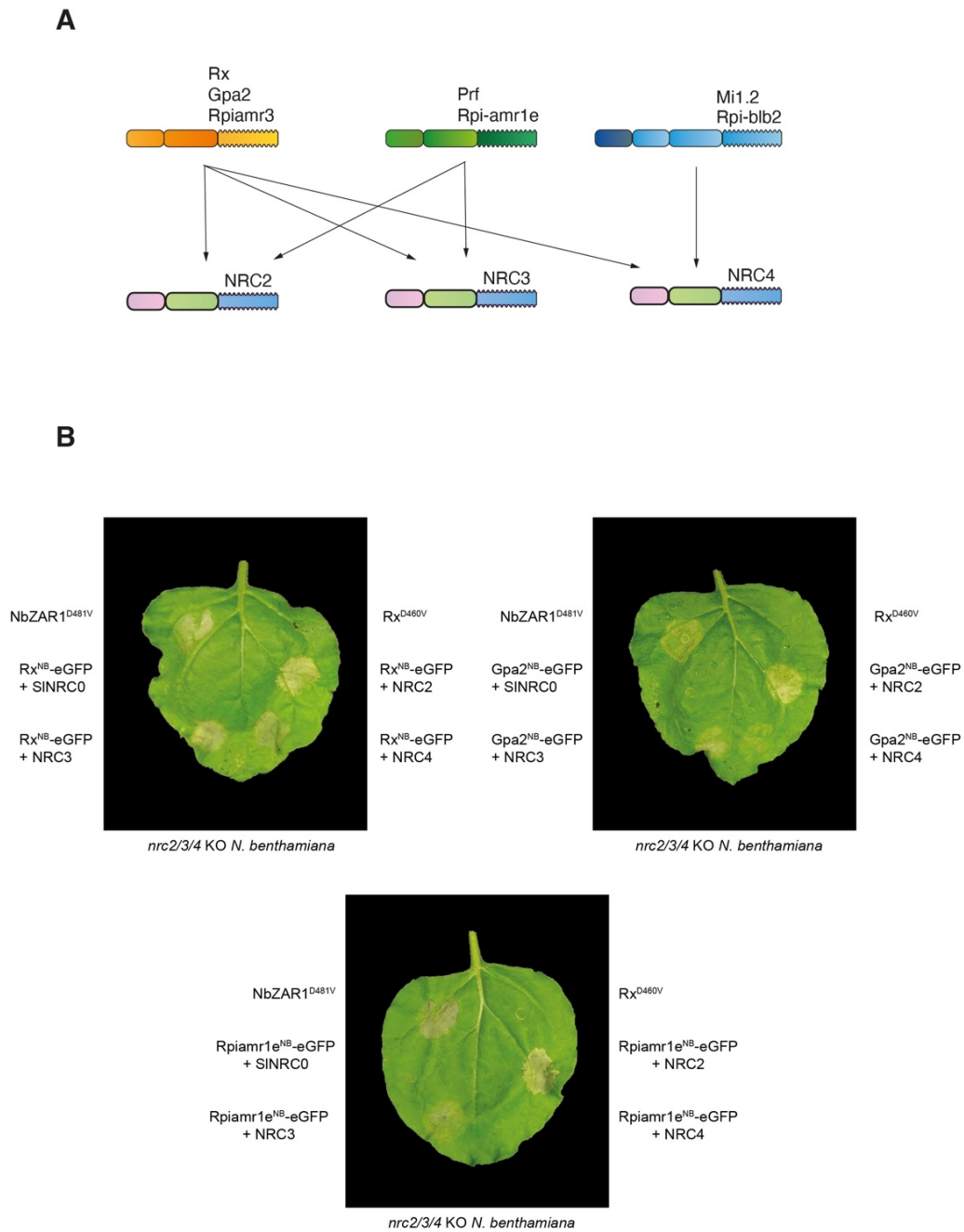


Figure 5.9: Sensor NLR NB domains retain the NRC helper specificities of their full-length counterparts.

(A) Schematic representation of sensor helper signaling specificities in the NRC network. (B) Representative photos of HR assays with Rx^{NB}-eGFP, Gpa2^{NB}-eGFP and Rpiamr1e^{NB}-eGFP complemented with either SINRC0, NRC2, NRC3 or NRC4 in leaves of *nrc2/3/4* KO *N. benthamiana*. NbZAR1^{D481V} and Rx^{D460V} were included as positive and negative controls for cell death, respectively. Leaves were infiltrated with the constructs indicated and photographed 5-7 days after infiltration. One representative leaf is shown.

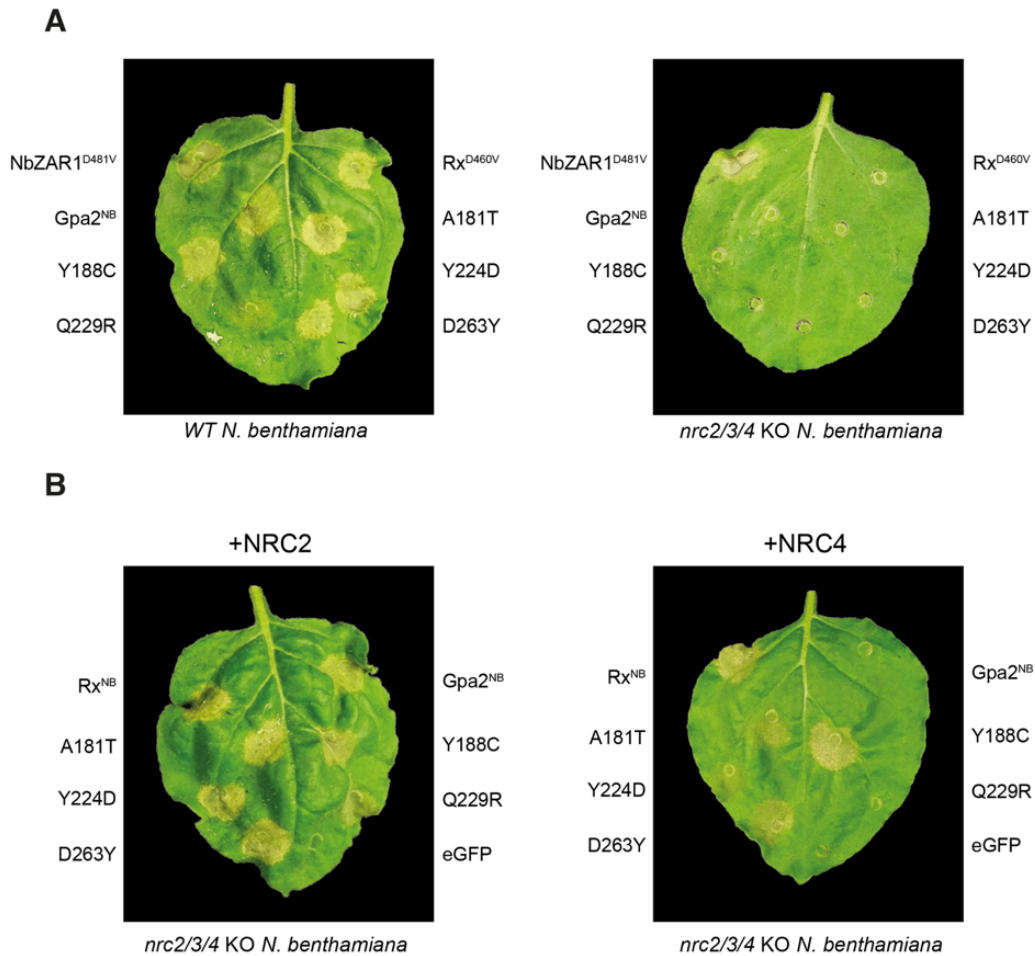


Figure 5.10: Multiple amino acids in Gpa2 NB domain underpin NRC4 signaling efficiency.

(A) Representative photos of HR assays with Gpa2^{NB}-eGFP and multiple Gpa2^{NB}-eGFP mutant variants in leaves of WT or *nrc2/3/4* KO *N. benthamiana*. NbZAR1^{D481V} and Rx^{D460V} were included as positive controls for NRC-independent and NRC-dependent cell death, respectively. Leaves were agroinfiltrated to express the constructs indicated and photographed 5-7 days after infiltration. One representative leaf is shown. (B) Representative photos of HR assays with Rx^{NB}-eGFP, Gpa2^{NB}-eGFP and multiple Gpa2^{NB}-eGFP mutant variants complemented with NRC2 or NRC4. eGFP was included as a negative control for cell death. Leaves were agroinfiltrated to express the constructs indicated and photographed 5-7 days after infiltration. One representative leaf is shown.

5.2.9 Single amino acid mutations in Gpa2^{NB}-eGFP enhance its capacity to activate NRC4.

As Rx and Gpa2 are very closely related sensor NLRs, I leveraged the small number of polymorphisms present between them, particularly within the NB domain, to identify residues

responsible for determining the difference in NRC4 activation (**Figure AIV.2**). Amino acid sequence alignment of the NB domains of Rx and Gpa2 revealed that there are only 5 amino acid differences between Rx^{NB} and Gpa2^{NB}. I mutated each of these residues in Gpa2^{NB} to the corresponding amino acid in Rx and tested single amino acid swaps for gain of NRC4 activation. Out of the five NB domain-eGFP fusion mutants tested, four mutants, Gpa2^{NB-A181T}, Gpa2^{NB-Y188C}, Gpa2^{NB-Y224D} and Gpa2^{NB-D263Y} gained the capacity to signal efficiently through NRC4, to levels comparable to Rx (**Figure 5.10**). These mutants also retained the capacity to activate NRC2. In particular, the Gpa2^{NB-Y188C} mutant triggered stronger cell death than all other mutants tested, suggesting that this residue may play a critical role in determining helper specificity. Gpa2^{NB-Q229R} could activate NRC2 but did not gain the capacity to signal through NRC4 (**Figure 5.10**). These results indicate that the NB domain at least partially contributes to determining sensor helper specificity. Whether individual residues in the NB domain contribute to efficiency in sensor-helper communications should be tested in the full-length context to draw stronger conclusions.

5.3 Conclusions and discussion

Prior to the identification and characterization of the NRC network, Rx was shown to function when its domains were expressed in trans (Moffett *et al.*, 2002). Moreover, the NB domain of Rx was shown to be sufficient to trigger cell death when fused to eGFP (Rairdan *et al.*, 2008). In this chapter I revisited these findings and re-interpreted them in the context of the NRC network and the activation-and-release biochemical model, as Rx is now known to be an NRC-dependent sensor NLR (Wu *et al.*, 2017). I attempted to leverage these previous findings to study sensor-helper communication in this NLR immune receptor network. In the first half of this chapter, I showed that the PVX CP-triggered cell death mediated by the CC-NBARC (Rx^{CCNBARC}) and LRR (Rx^{LRR}) domains of Rx expressed in trans is NRC-dependent (**Figure 5.1**). I also observed that, upon effector perception, Rx^{CCNBARC} and Rx^{LRR} can mediate the formation of an NRC2 oligomer that is indistinguishable from the oligomer mediated upon full-length Rx activation (**Figure 5.5**). I was also able to reproduce the previously reported association of Rx^{CCNBARC} and Rx^{LRR} and showed that it is independent of endogenous helper NRCs (**Figure 5.2**). Interestingly, the previously reported dissociation of Rx^{CCNBARC} and Rx^{LRR} upon activation of the system with PVX CP appears to be NRC-dependent (**Figure 5.3**). The dissociation of Rx^{CCNBARC} and Rx^{LRR} could be rescued by complementing with NRC2 but not with NRC2^{EEE}, suggesting that it requires a compatible NRC with an intact MADA motif or MADA-dependent downstream immune signaling (**Figure 5.3**). Nonetheless, this result needs to be further validated, as the ongoing cell

death and resulting reduction in protein accumulation when complementing with *WT* NRC2 complicates interpretation of these results.

I also found that the previously reported constitutive cell death triggered by Rx NB domain truncations fused to eGFP (Rx^{NB}-eGFP) is NRC-dependent (**Figure 5.6**). Rx^{NB}-eGFP appears to be functioning via the same activation-and-release mechanism exhibited by its full-length counterpart, mediating oligomerization of NRC2 into a putative resistosome (**Figure 5.7**). Importantly, I showed that the constitutive downstream NRC helper activation triggered by these NB domain-eGFP fusions is not unique to Rx^{NB} but is a feature shared by NB domain truncations of other sensor NLRs such as Gpa2, Rpi-amr1e and Rpi-amr3 (**Figure 5.8**). These sensor NLR NB domain truncations retained their downstream helper specificity profiles (**Figure 5.9**). Interestingly, Gpa2^{NB}-eGFP exhibited a drastically reduced NRC4 signaling efficiency compared to Rx^{NB}-eGFP. By substituting individual amino acids in Gpa2^{NB}-eGFP for their equivalent residue in Rx^{NB}-eGFP I was able to enhance its capacity to efficiently activate NRC4. Notably, all of these residues are surface exposed (**Figure AIV.2**). It is important to note that the contribution of eGFP to Rx^{NB}-mediated activation of NRCs is not fully understood. Rairdan and colleagues proposed that eGFP acts by contributing to Rx^{NB} stability (Rairdan *et al.*, 2008). As mentioned in Chapter 3, GFP and other fluorescent proteins can form higher order complexes (Kim *et al.*, 2015). Whether this is required for Rx^{NB}-eGFP could be tested by fusing Rx^{NB} to monomeric variants of eGFP incapable of oligomerizing. Considering that eGFP is a tag of a relatively large size (28 kDa), it is also possible that it is contributing to Rx^{NB}-NRC interactions via potential steric clashes that may be important for helper activation, assuming a model in which Rx^{NB} and NRCs physically interact.

Based on these results, I propose that the NB domain encodes the minimal unit for NRC helper activation (**Figure 5.11**). In the full-length sensor NLR context, the NB domain is hidden prior to effector perception. Following sensor activation, various p-loop dependent intramolecular rearrangements in the sensor lead to a conditional exposure of this NB domain, which is subsequently perceived by the NRCs leading to their activation and oligomerization. In NB domain truncations, the constitutive exposure of this domain activates NRCs in a p-loop independent manner. In this sense, helper NLRs such as the NRCs “sense” the exposure of sensor NLR NB domains. Notably, all the NB domains that successfully activated downstream NRCs corresponded to sensors with Rx-like N-termini i.e., without SD-type N-terminal extensions. The NB domains of SD-containing sensors tested, Mi-1.2 and Rpi-blb2, did not activate NRCs. It is possible that this NB domain-based mechanism of activation is specific to Rx-like sensors and that

SD-containing sensors function via a different mechanism. Previously the NB-ARC domain of Sw-5b, an SD-containing sensor, was shown to trigger cell death (De Oliveira *et al.*, 2016). It is possible that the incorporation of the SD has led to changes in sensor-helper communication which require exposure of the entire NB-ARC is required to trigger helper activation compared to the presumably ancestral Rx-like sensors.

Interestingly, while Rx CC-NB domain truncations (without the HD1 and WHD that compose the rest of the ARC region) are also constitutively active, Rx^{CC} and Rx^{CC-NBARC} are not, suggesting that the HD1 and WHD are engaged in intramolecular interactions that are sufficient to prevent the NB domain from communicating with downstream helpers (**Figure 5.1**) (Moffett *et al.*, 2002; Rairdan *et al.*, 2008). In Rx transcomplementation experiments, Rx^{CCNB} cannot perceive PVX CP on its own and requires the Rx^{LRR} half to be able to convert effector perception into activation (**Figure 5.1**) (Moffett *et al.*, 2002). This implies that the LRR can perceive PVX CP in trans and mediate conformational changes in Rx^{CCNB} that relieve autoinhibition imposed by the HD1 and WHD on the NB domain, potentially with CC domain involvement as well. Based on my data, I propose that, for many Rx-type sensors, the activation signal from sensor to helper is encoded in the NB domain, and that its conditional exposure upon effector perception can lead to helper activation (**Figure 5.11**). Nonetheless, how exactly the sensor NB domain activates helpers is not understood. Whether direct interactions between NB domain and NRCs lead to NRC activation or whether other intermediate proteins are involved is not clear.

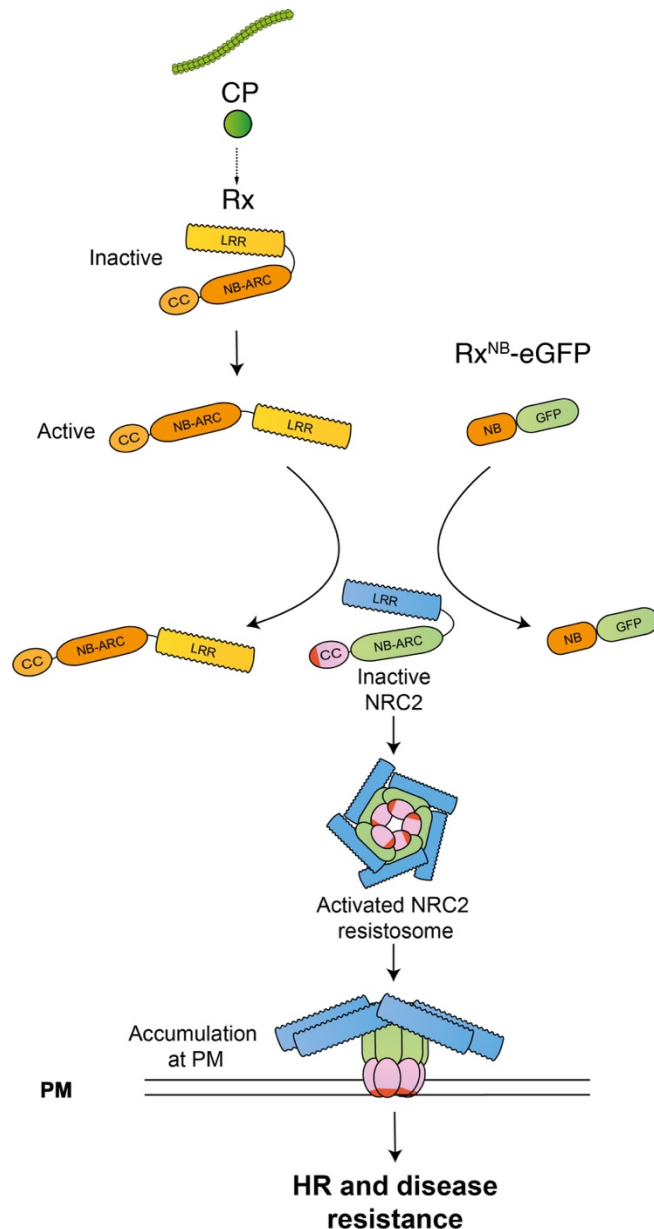


Figure 5.11: Proposed working model for NB-mediated sensor-helper activation in the NRC network.

Prior to effector-triggered activation, NRC-dependent sensors such as Rx are held in an inactive conformation by intramolecular interactions. These intramolecular interactions hide the sensor NLR NB domain. Upon perceiving their cognate effectors, the sensors undergo a series of p-loop dependent conformational changes that expose the NB domain. This conditional NB domain exposure is perceived by downstream helpers such as NRC2 leading to its homo-oligomerization and resistosome formation. In the case of the NB domain-eGFP fusions, the NB domain is exposed and therefore constitutively activates downstream helpers. Because no intramolecular rearrangements are required, the p-loop mutation does not affect this cell death.

5.4 Research Contributions

I thank Hsuan Pai (The Sainsbury Laboratory, Norwich, UK) for assistance with cloning. I thank Jules Claeys (The Sainsbury Laboratory, Norwich, UK) for assistance with Western blot experiments of all sensor NB domains.

Chapter 6: Understanding AVRcap1b-mediated suppression of NRC-mediated cell death.

Part of the results from this chapter are published as part of a manuscript by L. Derevnina, M.P. Contreras et al. (Derevnina *et al.*, 2021).

Doi: <https://doi.org/10.1371/journal.pbio.3001136>

My contributions to this manuscript correspond to some of the results described in this chapter.

6.1 Introduction.

Our understanding of the pathogenicity mechanisms of plant pathogens has been significantly broadened over the years. It is now well established that diverse plant parasites secrete virulence proteins, termed effectors, to manipulate a variety of host processes to promote disease. Host processes targeted by effectors include cell-surface and intracellular immunity, vesicle trafficking, autophagy and proteostasis, and plant development (Ali *et al.*, 2015; Bozkurt *et al.*, 2015; Dagdas *et al.*, 2016; Derevnina *et al.*, 2021; Huang *et al.*, 2021b; Kourelis *et al.*, 2022; Pandey *et al.*, 2021; Wang *et al.*, 2023a; Wu & Derevnina, 2023). As such, effectors have emerged as molecular probes that can be leveraged to study plant physiology and identify novel components of plant processes, including plant immunity (Toruño *et al.*, 2016). For example, the *Phytophthora infestans* effector PexRD54 has been shown to target host autophagy via a canonical C-terminal ATG8 interacting motif (Dagdas *et al.*, 2016; Maqbool *et al.*, 2016). Studying PexRD54 and its virulence function has advanced our understanding of immune-related autophagy and how this process is subverted by pathogens. Moreover, PexRD54 derived peptides can be used as proteinaceous autophagy inhibitors, serving as useful tools for autophagy research (Dagdas *et al.*, 2016; Dagdas *et al.*, 2018; Maqbool *et al.*, 2016; Pandey *et al.*, 2021).

Although secretion of effectors into the host extracellular or intracellular space enhances pathogen colonization, effectors can lead to pathogen recognition and immune activation in the host. These are termed avirulence effectors (AVRs). The plant immune system can directly or indirectly perceive apoplastic or intracellular effectors via cell-surface receptors and nucleotide binding and leucine-rich repeat (NLR) receptors respectively leading to a robust immune response (Jones & Dangl, 2006). In the case of NLR-mediated immune responses, this often leads to disease resistance which is usually accompanied by a form of programmed cell death termed the

hypersensitive response or hypersensitive cell death (Takken *et al.*, 2006). Some NLRs are multifunctional receptors, mediating both effector recognition and downstream signaling. In contrast, some NLRs function as pairs or in higher order configurations such as NLR networks of functionally specialized receptors (Adachi *et al.*, 2019b). In these cases, sensor NLRs specialize in effector recognition and cooperate with downstream helpers to mediate immunity. The sensors on their own are incapable of mediating downstream immune signaling and instead rely on their downstream helper NLRs to do so (Adachi *et al.*, 2019b; Adachi & Kamoun, 2022). Unlike pairs which involve two functionally connected NLRs with a one-to-one sensor-helper connection, NLR networks involve multiple functionally connected sensors and helpers, usually exhibiting one-to-many and many-to-one sensor-helper pairings. This high degree of genetic redundancy is thought to contribute to the robustness of the immune system (Wu *et al.*, 2018).

In Chapter 4, I proposed an activation-and-release model for sensor-helper pairs in the NRC (NLR required for cell death) network, in which effector perception by sensors leads to oligomerization of NRC helpers into a resistosome-like complex (Contreras *et al.*, 2023b). The NRC immune receptor network is found in solanaceous plants and is composed of cell-surface and sensor CC-NLRs which signal through an array of downstream helper NLRs, the NRCs (NLR required for cell death) (Kourelis *et al.*, 2022; Wu *et al.*, 2017). The NRC network includes many agronomically important R genes against diverse plant pathogenic viruses, bacteria, oomycetes, nematodes, and insects. In some species this network can encompass up to 50% of the NLRome, highlighting its importance to immunity in solanaceous crops (Wu *et al.*, 2017). The NRCs act as the executors of immune signaling and disease resistance and as such are a critical node in the network (Derevnina *et al.*, 2021; Wu *et al.*, 2017; Wu *et al.*, 2018).

Considering the robust immunity provided by NLRs, it is perhaps unsurprising that adapted pathogens can deploy effectors to interfere with NLR signaling (Wu & Derevnina, 2023). Some effectors directly bind to NLRs to suppress immunity (Derevnina *et al.*, 2021; Karki *et al.*, 2021; Wang *et al.*, 2023a; Yen *et al.*, 2015). In other cases, effectors target downstream components required for NLR signaling (Chai *et al.*, 2022; Derevnina *et al.*, 2021; Lopez *et al.*, 2019). In NLR networks, helper NLRs are critical nodes required downstream of multiple PRRs and sensor NLRs and, as such, they represent an ideal target for pathogen effectors. Indeed, an emerging paradigm is that some pathogens compromise immunity mediated by NLR networks by secreting effectors that target helper NLRs (Derevnina *et al.*, 2021; Wang *et al.*, 2023a).

Previously, Derevnina and colleagues identified two effectors capable of suppressing immune signaling in the NRC network. SS15 from the potato cyst nematode *Globodera rostochiensis* and AVRcap1b from the potato late blight pathogen *Phytophthora infestans* can suppress immune signaling and cell death mediated by the helpers NRC2 and NRC3 (Derevnina *et al.*, 2021). SS15 and AVRcap1b are capable of suppressing cell death mediated by autoactive variants of NRC2 and NRC3, indicating that they are acting at the level of helper NLR activation (Derevnina *et al.*, 2021). That two distantly related pathogens, a nematode and an oomycete, have convergently evolved effectors to counteract NRCs highlights how critical this network is in mediating immunity against solanaceous pathogens. Moreover, whereas SS15 was shown to interact directly with the NB-ARC domain of NRCs, AVRcap1b did not show association with inactive NRCs in coimmunoprecipitations studies, indicating that they suppress NRCs via distinct mechanisms (Derevnina *et al.*, 2021).

Like many characterized oomycete effectors, AVRcap1b belongs to the RXLR-WY/LWY family (He *et al.*, 2019; Li *et al.*, 2023). Effectors in this family feature an N-terminal Arg-X-Leu-Arg (RXLR) motif downstream of a signal peptide, followed by a C-terminal effector domain composed of 1 or more tandem WY/ LWY domains (Lovelace *et al.*, 2023; Win *et al.*, 2012a; Win *et al.*, 2012b). Well studied examples in this family include the RXLR-WY effector PexRD54 from *P. infestans* and the RXLR-WY/LWY effector Phytophthora suppressor of RNAi 2 (PSR2) from *Phytophthora sojae* (He *et al.*, 2019; Li *et al.*, 2023; Maqbool *et al.*, 2016). AVRcap1b features a C-terminal effector domain composed of one WY domain and 6 tandem LWY domains (**Figure 1.7**). It was first identified as an AVR in the wild potato *Solanum capsicibaccatum*, and has homologs in all Phytophthora clade 1c species, which include *Phytophthora andina*, *Phytophthora ipomoeae* and *Phytophthora mirabilis* (Kroon *et al.*, 2004; Rietman, 2011; Zess *et al.*, 2022). Previously, AVRcap1b was shown to suppress NRC2 and NRC3-mediated cell death via indirect mechanisms (Derevnina *et al.*, 2021). IP-MS and Yeast-2-Hybrid screens performed previously revealed Target of Myb 1-like (TOLs) proteins as putative AVRcap1b virulence targets. The precise mechanism by which AVRcap1b suppresses NRC-mediated cell death is not known (Derevnina *et al.*, 2021).

TOLs have previously been shown to act as ubiquitinated cargo adaptors in the endosomal sorting complex required for transport (ESCRT) vesicle trafficking pathway (Moulinier-Anzola *et al.*, 2020). TOL proteins feature an N-terminal epsin N-terminal homology (ENTH) domain followed by a GGAs and Target of Myb 1 (GAT) domain with which they bind ubiquitinated plasma membrane (PM)-associated cargo, and subsequently recruit the ESCRT-1 complex as well

as other downstream components of the ESCRT pathway (Moulinier-Anzola *et al.*, 2020; Winter & Hauser, 2006). This usually results in loading of the target cargo into multi-vesicular bodies and subsequent trafficking to various sub-cellular compartments for storage or degradation. The ESCRT trafficking pathway has previously been involved in modulation of signaling by plasma membrane-localized receptors such as FLS2 (Spallek *et al.*, 2013). Interestingly, in non-plant model systems the ESCRT trafficking pathway has also been shown to negatively regulate various forms of programmed cell death including pyroptosis and ferroptosis (Castro-Gomes *et al.*, 2014; Dai *et al.*, 2020; Gong *et al.*, 2017; Jimenez *et al.*, 2014; Pedrera *et al.*, 2021; Raab *et al.*, 2016; Rühl *et al.*, 2018). Whether TOLs and the ESCRT pathway can modulate programmed cell death in plants is unknown. Considering that AVRcap1b, a suppressor of NRC-mediated cell death, potentially targets TOL proteins, it is tempting to speculate that TOLs and the ESCRT pathway may be regulating NRC-mediated programmed cell death. Understanding the interplay between AVRcap1b, TOLs and NRCs holds the potential to shed light on the regulatory mechanisms that govern plant immunity and programmed cell death.

In this chapter, I attempted to determine the mechanism by which AVRcap1b suppresses NRC-mediated cell death. I started by following up on Lida's IP-MS and Y2H data, which pointed to TOL proteins as putative AVRcap1b targets. I was able to show that in *N. benthamiana*, AVRcap1b preferentially interacts with NbTOL9a. This interaction is direct and largely mediated between WY1 domain of AVRcap1b and the N-terminal ENTH domain of NbTOL9a. Knock-down and overexpression studies of NbTOL9a revealed that this protein is capable of negatively regulating cell death mediated by NRC2 and NRC3. Interestingly, this negative regulation is specific to NRC2/3, as NbTOL9a does not negatively regulate cell mediated by NRC4 or by other NLRs and non-NLR proteins. Importantly, knock-down of NbTOL9a partially compromises AVRcap1b immune suppression of NRC2/3, suggesting that the effector requires NbTOL9a to fully execute its virulence activities. In support of this hypothesis, structure-guided mutations in AVRcap1b that abolish NbTOL9a binding fully compromise immune suppression. Finally, I was able to show that although AVRcap1b does not interact with inactive NRCs, it interacts with the Rx/CP-activated form of NRC2, likely via its C-terminal LWY7 domain. Interestingly, this interaction does not inhibit NRC2 resistosome formation. My results suggest that NbTOL9a can negatively regulate NRC-mediated cell death and that *P. infestans* likely deploys AVRcap1b to co-opt this regulatory pathway by bridging NbTOL9a and activated NRC oligomers.

6.2 Results.

6.2.1 AVRcap1b does not associate with inactive NRCs.

In this chapter, I set out to understand the mechanism by which the *P. infestans* effector AVRcap1b suppresses NRC-mediated cell death. SS15 and AVRcap1b were identified as suppressors of NRC2 and NRC3, and SS15 was shown to associate with these helper NLRs in planta (Derevnina *et al.*, 2021). I repeated these experiments including AVRcap1b to determine if this effector is also directly targeting NRCs to suppress them. To this end, I co-expressed AVRcap1b-6xHA with C-terminally 4xMyc-tagged NRC2, NRC3 and NRC4 in leaves of WT *N. benthamiana* and performed a MYC pulldown. In parallel, I tested AVRcap1b-6xHA for suppression of NRCs in cell death assays to make sure that C-terminal tagging is not interfering with effector activities (**Figure AV.1**). In these experiments I could not detect any association between AVRcap1b and NRCs. This suggested that AVRcap1b suppression of NRC2 or NRC3 might be indirect, potentially via targeting other host protein involved in NRC signaling (**Figure 6.1**). The SS15 control associated with NRC2 and NRC3, as expected.

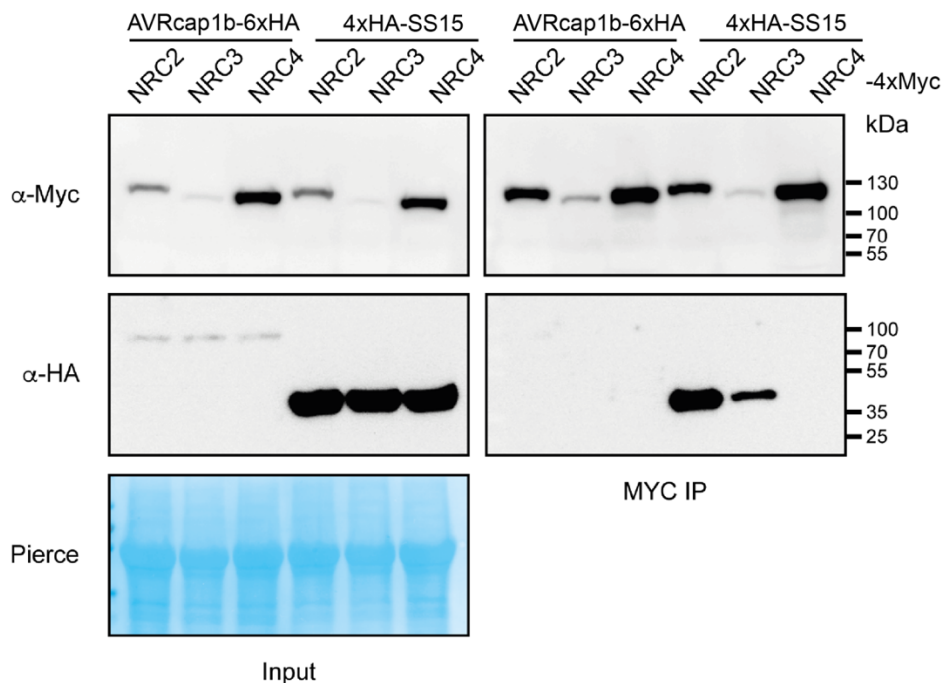


Figure 6.1: Unlike SS15, AVRcap1b does not associate with inactive NRCs *in planta*.

CoIP experiment of C-terminally 4xmyc-tagged NRC2, NRC3, and NRC4 with C-terminally HA-tagged AVRcap1b::6xHA and N-terminally tagged 4xHA:SS15 (labelled above). Proteins obtained by coIP with

MYC beads (MYC IP) and total protein extracts (input) were immunoblotted with the appropriate antisera labelled on the left. Approximate molecular weights (kDa) of the proteins are shown on the right. Rubisco loading control was carried out using Pierce staining. The experiment was performed more than 3 times under different pulldown conditions with similar results.

6.2.2 AVRcap1b associates with host TOL proteins in planta.

Previous yeast-two-hybrid and IP-MS data suggested that *N. benthamiana* TOLs could be AVRcap1b's putative host targets. I leveraged previously generated C-terminal 6xHA fusion proteins of all five TOLs present in *N. benthamiana* with different epitopes. C-terminal fusions were deemed more apt considering that both previously characterized domains found in TOLs are present at the N-terminus, making N-terminal fusions more likely to perturb the protein's functions. I termed the five TOLs NbTOL3, NbTOL6, NbTOL9a, NbTOL9b and NbTOL9c, based on previously published Arabidopsis nomenclature (**Figure AV.2**) (Moulinier-Anzola *et al.*, 2020). To validate the association between AVRcap1b and NbTOL proteins, I co-expressed GFP-AVRcap1b with C-terminally 6xHA tagged fusions of the five TOL paralogs, in *N. benthamiana* leaves, and performed anti GFP and anti HA immunoprecipitations. AVRcap1b associated with NbTOL9a, and to a lesser extent with NbTOL9b and NbTOL9c in the GFP pulldown (GFP IP). However, AVRcap1b only associated with NbTOL9a in the reciprocal HA pulldown (HA IP) (**Figure 6.2**). In both experiments, NbTOL9a protein did not associate with the negative control GFP-PexRD54. These results indicate that AVRcap1b associates with members of the NbTOL family, exhibiting a stronger affinity for NbTOL9a. The results suggest that AVRcap1b could be preferentially targeting certain TOL homologs to execute its suppressor functions. Moreover, it suggests that different TOL homologs may execute different functions or exhibit specialization towards different targets or pathways. This is supported by previous findings with Arabidopsis TOL proteins, which exhibit different localizations and different KO phenotypes depending on the mutated TOL protein (Korbei *et al.*, 2013; Moulinier-Anzola *et al.*, 2020). Based on this conclusion, I focused subsequent experiments on NbTOL9a.

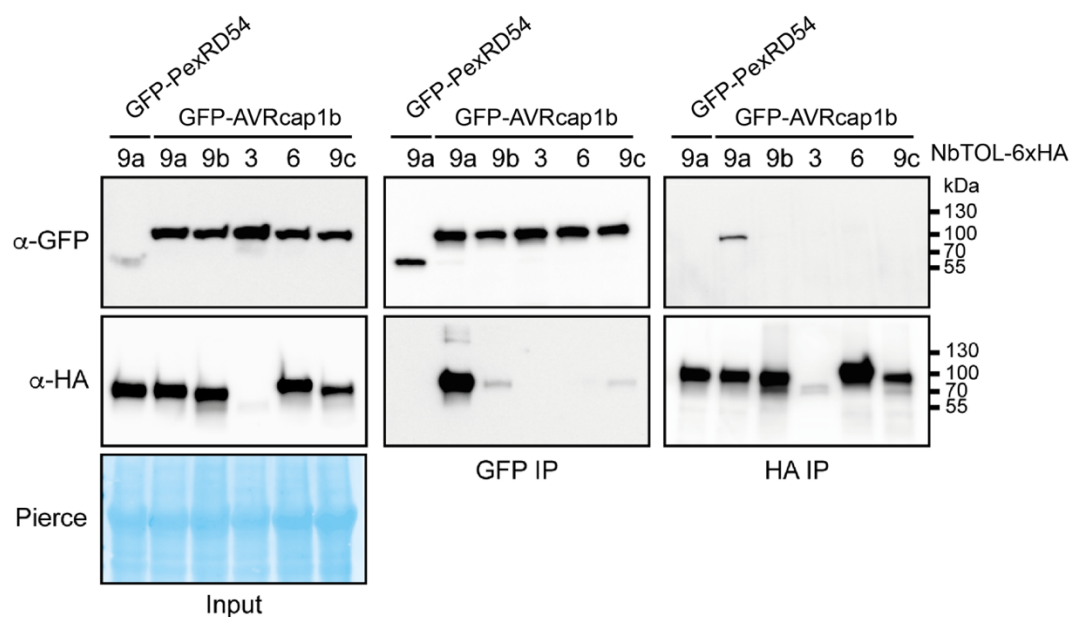


Figure 6.2: AVRcap1b associates with NbTOL9a *in planta*.

Co-immunoprecipitation experiment between AVRcap1b and five NbTOL family proteins (NbTOL9a, NbTOL9b, NbTOL3, NbTOL6, NbTOL9c). N-terminally GFP-tagged AVRcap1b was transiently co-expressed with all five NbTOL proteins fused to a C-terminal 6xHA tag. N-terminally GFP-tagged PexRD54 was used as a negative control. IPs were performed with agarose beads conjugated to either GFP (GFP-IP) or HA (HA-IP) antibodies. Total protein extracts were immunoblotted with appropriate antisera labelled on the left. Approximate molecular weights (kDa) of the proteins are shown on the right. Rubisco loading controls were conducted using Pierce™ staining. This experiment is representative of three independent replicates.

6.2.3 NbTOL9a does not associate with inactive NRCs.

As AVRcap1b does not associate with inactive NRCs but associates with host TOL proteins, I wanted to determine whether NbTOL9a associates with NRC proteins. I tested this using *in planta* CoIP, focusing on NbTOL9a as it exhibits more robust association with AVRcap1b. I decided to start by testing association between NbTOL9a and inactive NRCs. I also included AVRcap1b as a positive control for NbTOL9a association and NRCX as a non-cell death inducing NRC as a negative control (Adachi *et al.*, 2023). My CoIP experiments revealed that NbTOL9a does not associate with NRC2, NRC3, NRC4 or NRCX *in planta* (**Figure 6.3**). This suggests that if NbTOL9a has a role in NRC-mediated immunity, this function may not involve direct

association with inactive NRCs. Potentially NbTOL9a-NRC interactions may only occur following NRC activation. It is also possible that NbTOL9a-NRC interactions are too transient to be detected in *in planta* CoIP.

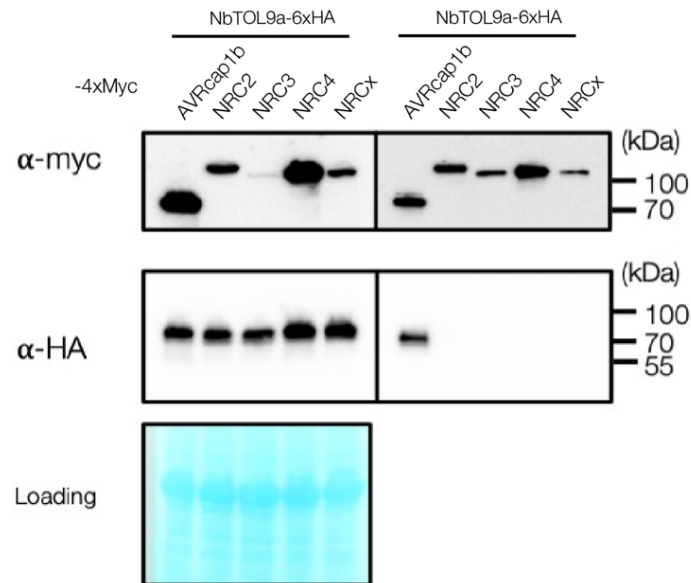


Figure 6.3: NbTOL9a does not associate with inactive NRC proteins.

Co-immunoprecipitation experiment between NbTOL9a and NRC2, NRC3 and NRC4. NbTOL9a-6xHA was transiently co-expressed with NRC2-4xMyc, NRC3-4xMyc or NRC4-4xMyc. AVRcap1b-4xMyc was included as a positive control for NbTOL9a association. Immunoprecipitants (IPs) were obtained using Myc antiserum-conjugated beads. Total protein extracts and IPs were immunoblotted using appropriate antisera (indicated to the left of each panel). NbTOL9a-6xHA did not associate with NRC2, NRC3 or NRC4. The association with AVRcap1b was still observed. The experiment was repeated 3 times with similar results.

6.2.4 The presence of AVRcap1b does not lead to NbTOL9a associating with inactive NRCs.

I next sought out to test whether AVRcap1b can mediate NbTOL9a association with the NRCs. Considering that AVRcap1b and NbTOL9a associate *in planta*, it is possible that the effector is acting as a bridge between NbTOL9a and inactive NRC2 or NRC3. We tested association between NbTOL9a and inactive NRCs again, in the presence or absence of AVRcap1b. We included AVRcap1b again as a positive control for association with NbTOL9a. My CoIP

experiments revealed that NbTOL9a does not associate with NRC2, NRC3 or NRC4 *in planta* in the presence of AVRcap1b (**Figure 6.4**). This suggests that not only NbTOL9a does not stably associate with the NRCs, but that AVRcap1b does not execute its suppressor functions by acting as a bridge between NbTOL9a and inactive NRCs.

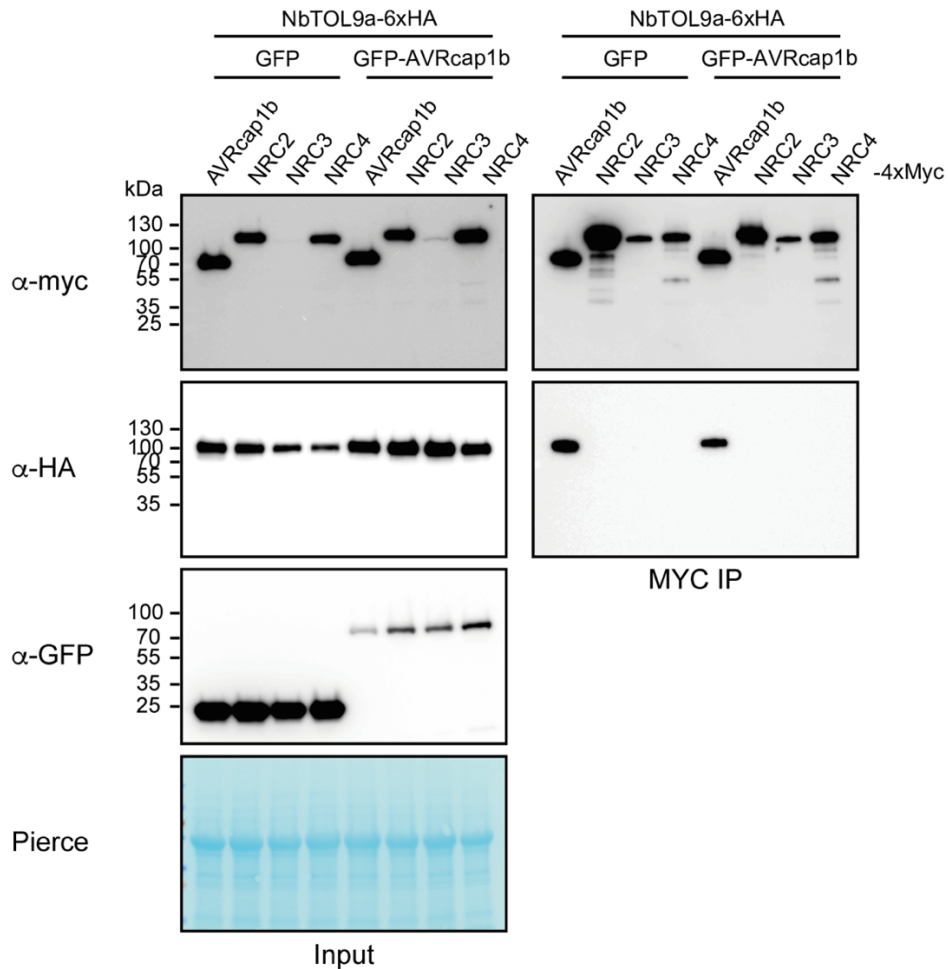


Figure 6.4: NbTOL9a does not associate with inactive NRC proteins in the presence of AVRcap1b.

Co-immunoprecipitation experiment between NbTOL9a and NRC2, NRC3 and NRC4 in the presence or absence of AVRcap1b. NbTOL9a-6xHA was transiently co-expressed with NRC2-4xMyc, NRC3-4xMyc or NRC4-4xMyc. AVRcap1b-4xmyc was included as a positive control for NbTOL9a association. Each of these combinations was co-expressed with either free GFP or GFP-AVRcap1b. Immunoprecipitants (IPs) were obtained using Myc antiserum-conjugated beads. Total protein extracts and IPs were immunoblotted using appropriate antisera (indicated to the left of each panel). NbTOL9a-6xHA did not associate with NRC2, NRC3 or NRC4 in the presence or absence of AVRcap1b. The association with AVRcap1b was still observed. The experiment was repeated two times with similar results.

6.2.5 NbTOL9a negatively modulates the cell death triggered by NRC3 but not NRC4.

As AVRcap1b suppresses NRC2 and NRC3-mediated cell death and associates with NbTOL9a, I decided to determine whether NbTOL9a plays any role in regulating NRC mediated hypersensitive cell death. To do so, I first attempted to study the effects of NbTOL9a overexpression in *N. benthamiana*. I transiently co-expressed NbTOL9a-6xHA with the autoactive NRC3^{D480V} variant in leaves of *WT N. benthamiana*. I included the constitutively active mitogen-activated protein kinase-kinase (MAPKK) MEK2^{DD} as a control for NRC-independent cell death and the autoactive NRC4^{D478V} mutant as it is an NRC that does not get suppressed by AVRcap1b. NbTOL9a overexpression quantitatively reduced the cell death response triggered by NRC3^{D480V} but did not affect NRC4^{D478V} or the constitutively active MEK2^{DD} controls (**Figure 6.5**).

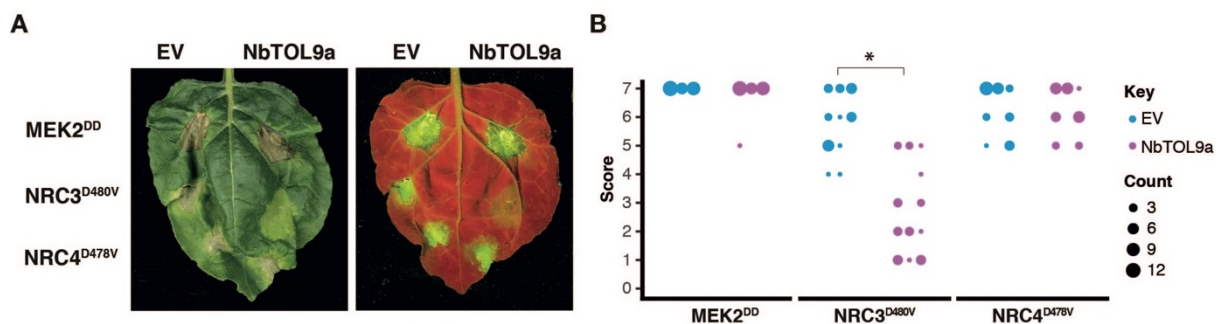


Figure 6.5: Overexpression of NbTOL9a suppresses autoactive NRC3^{D480V} but not MEK2^{DD} or NRC4^{D478V}.

(A) Photo of representative *N. benthamiana* leaves showing HR after co-expression of EV and NbTOL9a (labelled above leaf panels) with MEK2^{DD}, NRC3^{D480V} and NRC4^{D478V}. HR response was scored and photographed 5 days after agroinfiltration (left panel under white light, right panel autofluorescence under UV light). MEK2^{DD} was included as a positive control for cell death. (B) HR results are presented as dot plots, where the size of each dot is proportional to the number of samples with the same score (count). Three biological replicates were completed, indicated by columns for EV, NbTOL9a in each treatment (MEK2^{DD}, NRC3^{D480V}, NRC4^{D478V}). Significant differences between the conditions are indicated with an asterisk (*).

Next, I investigated the effect of silencing *NbTOL9a* on NRC autoimmunity. We generated a hairpin-silencing construct (RNAi::*NbTOL9a*) that mediates silencing of *NbTOL9a* in transient expression assays in *N. benthamiana* leaves (**Figure AV.3**). I then co-expressed RNAi::*NbTOL9a* with NRC3^{D480V} using agroinfiltration of *N. benthamiana* leaves. As NRC3^{D480V} gives strong cell

death, I used three different concentrations of *A. tumefaciens* expressing NRC3^{D480V} (OD₆₀₀ = 0.1, 0.25 or 0.5) to test the degree to which silencing of *NbTOL9a* affects NRC3-mediated cell death. Silencing of *NbTOL9a* at all tested OD₆₀₀ concentrations enhanced the cell death response triggered by NRC3^{D480V}, but did not affect NRC4^{D478V}, compared to the RNAi::GUS silencing control (**Figure 6.6**). Altogether, these two sets of experiments indicate that NbTOL9a modulates NRC3 activity in a manner consistent with a negative regulatory role in NRC3 mediated immunity. Thus, I conclude that AVRcap1b is potentially co-opting the immune modulator NbTOL9a to suppress NRC mediated immunity.

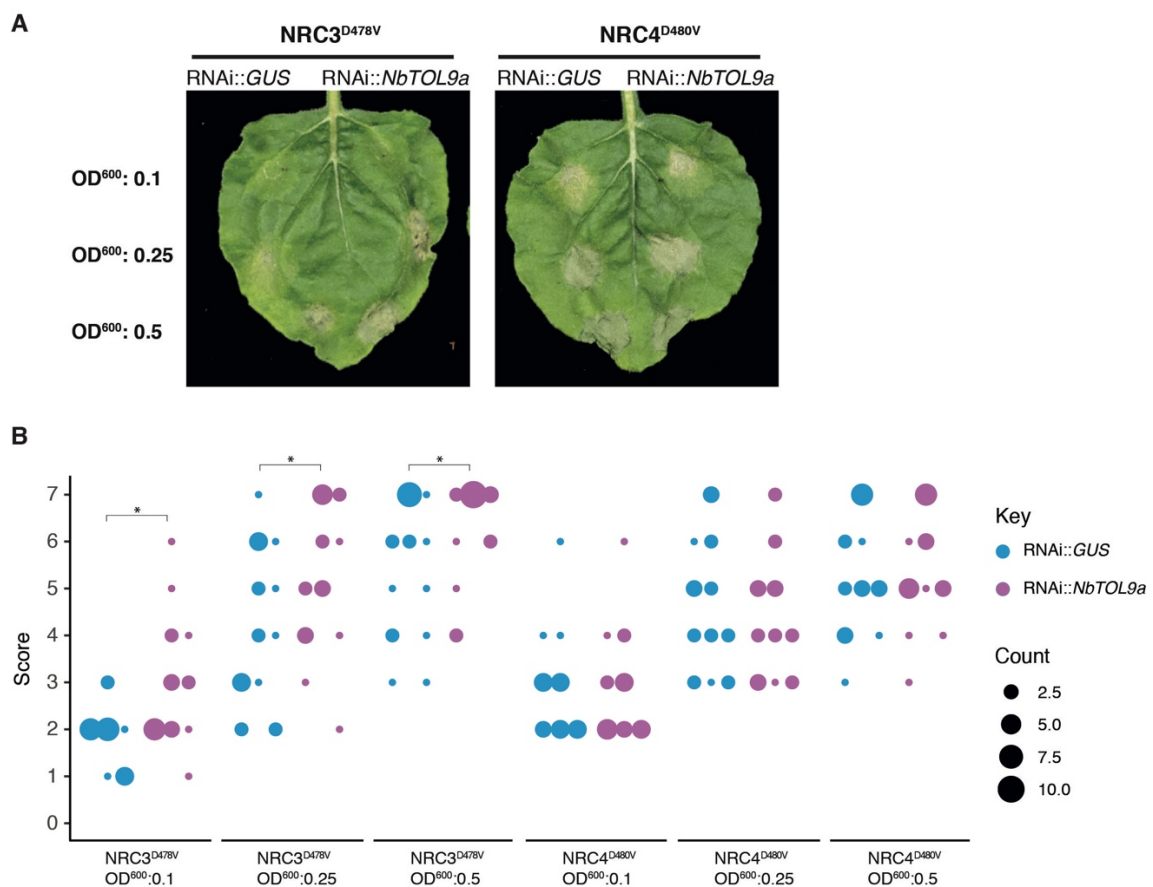


Figure 6.6: NbTOL9a silencing enhances cell death mediated by NRC3^{D480V} but not NRC4^{D478V}.

(A) Photo of representative *N. benthamiana* leaves showing HR after co-expression of NRC3^{D480V} and NRC4^{D478V}, with RNAi::GUS (control) and RNAi::NbTOL9a (labelled above leaf panels). To improve the robustness of the assay we used increasing concentrations of *A. tumefaciens* expressing NRC3^{D480V} and NRC4^{D478V} (OD₆₀₀ = 0.1, 0.25 or 0.5). HR response was scored and photographed 5 days after agroinfiltration. (B) HR results are presented as dot plots, where the size of each dot is proportional to the

number of samples with the same score (count). Three biological replicates were completed, indicated by columns for RNAi::GUS and RNAi::NbTOL9a, for each treatment combination. Significant differences between the conditions are indicated with an asterisk (*).

6.2.6 AVRcap1b suppression of NRC3 is compromised in the absence of NbTOL9a.

To test the hypothesis that NbTOL9a is co-opted by AVRcap1b to execute its suppression activity, I co-expressed AVRcap1b with the autoimmune mutants NRC3^{D480V} or NRC4^{D478V} in *N. benthamiana* leaves that are either expressing RNAi::NbTOL9a (NbTOL9a-silenced) or RNAi::GUS (negative control). Consistent with previous findings, overexpression of AVRcap1b suppressed the cell death triggered by NRC3^{D480V} but not by NRC4^{D478V}. However, silencing of NbTOL9a compromised AVRcap1b suppression of NRC3^{D480V} autoimmunity and partially restored the cell death phenotype (Figure 6.7). These results suggest that AVRcap1b co-opts NbTOL9a to down-regulate NRC3 cell death activity.

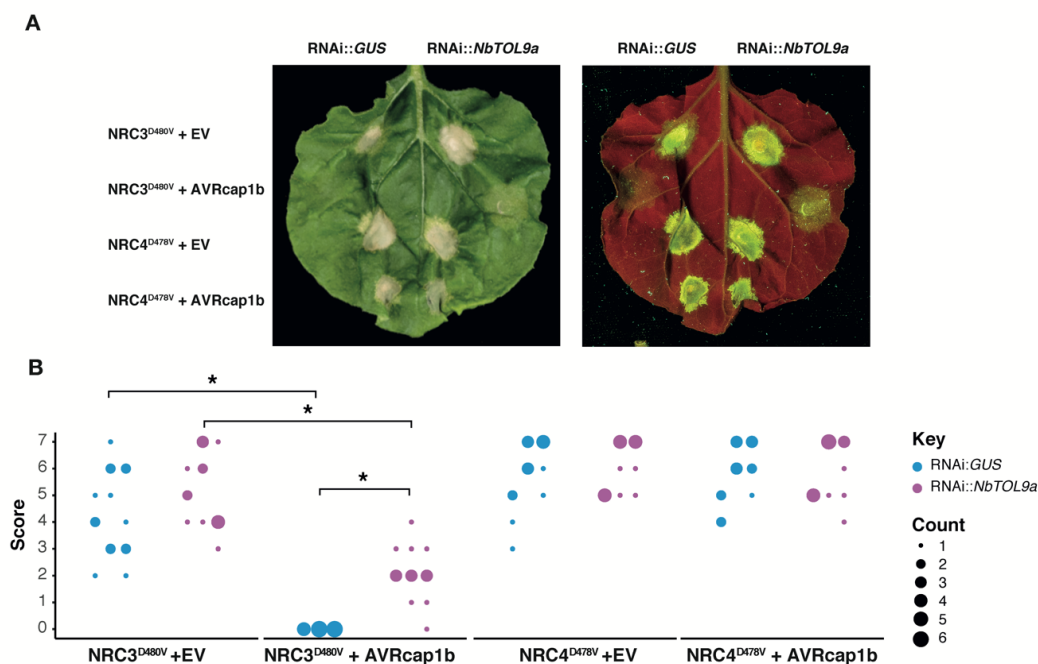


Figure 6.7: Silencing of NbTOL9a compromises AVRcap1b mediated suppression of NRC3.

(A) Photo of representative *N. benthamiana* leaves showing HR after co-expression of RNAi::GUS and RNAi::NbTOL9a with NRC3^{D480V} + EV, NRC3^{D480V} + AVRcap1b, NRC4^{D478V} + EV and NRC4^{D478V} +

AVRcap1b. HR response was scored and photographed 5 days after agroinfiltration (left panel under white light, right panel autofluorescence under UV light). **(B)** HR results are presented as dot plots, where the size of each dot is proportional to the number of samples with the same score (count). Results are based on three biological replicates. Significant differences between the conditions are indicated with an asterisk (*).

6.2.7 ENTH domain truncations of NbTOL9a associate with AVRcap1b *in planta*.

Having determined that NbTOL9a is likely being co-opted by AVRcap1b to execute its suppressor functions, I attempted to narrow down the domains in NbTOL9a responsible for NbTOL9a-AVRcap1b association. To do this, I leveraged other *N. benthamiana* TOLs that do not robustly associate with AVRcap1b in *in planta* CoIP experiments. I settled on NbTOL6 as it did not exhibit association with AVRcap1b in either pulldown and unlike NbTOL3, accumulated well in planta (**Figure 6.2**). I generated a set of 4 chimeras, swapping either the ENTH-GAT domain, ENTH domain, GAT domain or C-terminal region (CTR) after the ENTH-GAT domains of NbTOL9a into NbTOL6 (**Figure 6.8**). I transiently co-expressed GFP-AVRcap1b with C-terminally 6xHA tagged fusions of NbTOL9a, NbTOL6 and the 4 chimeric TOL proteins, NbTOL6^{ENTH-GAT-IX}, NbTOL6^{ENTH-IX}, NbTOL6^{GAT-IX}, and NbTOL6^{CTR-IX} in *N. benthamiana* leaves and performed anti GFP immunoprecipitations. AVRcap1b associated with NbTOL9a as expected. Excitingly, I could also detect association between AVRcap1b and the NbTOL6^{ENTH-GAT-IX} and NbTOL6^{ENTH-IX} chimeric proteins. The negative control NbTOL6 behaved as expected and showed no association (**Figure 6.8**). I conclude that introducing the ENTH of NbTOL9a into NbTOL6 is sufficient for NbTOL6 to gain association to AVRcap1b. While I cannot rule out that other domains are also involved in AVRcap1b-NbTOL9a association, this result indicates that the ENTH domain plays an important role.

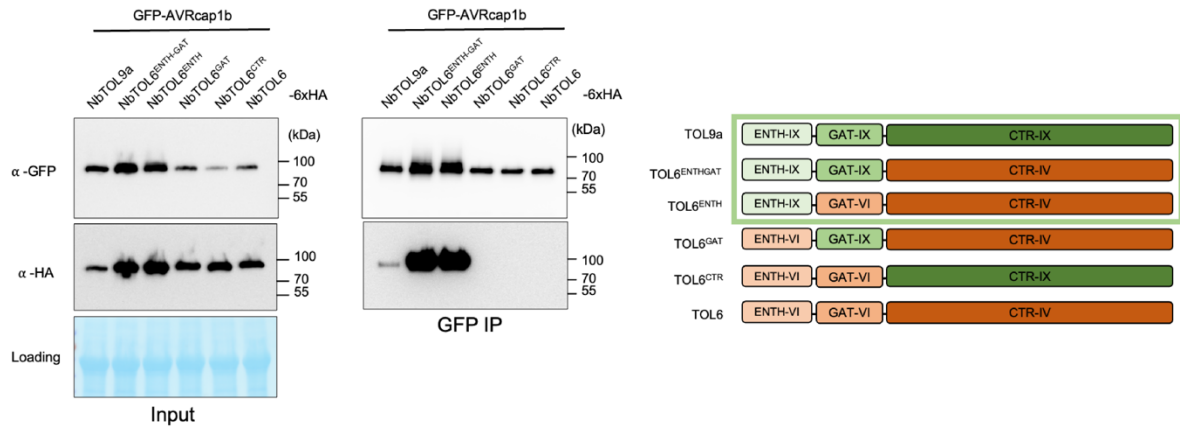


Figure 6.8: NbTOL9a ENTH domain is sufficient for association with AVRcap1b *in planta*.

(A) Co-immunoprecipitation experiment between AVRcap1b and four chimeric NbTOL proteins, NbTOL6^{ENTH+GAT-IX}, NbTOL6^{ENTH-IX}, NbTOL6^{GAT-IX} and NbTOL6^{CTR-IX}. NbTOL9a and NbTOL6 were included as positive and negative controls for AVRcap1b association, respectively. IPs were performed with agarose beads conjugated to GFP (GFP IP) antibodies. Total protein extracts were immunoblotted with appropriate antisera labelled on the left. Approximate molecular weights (kDa) of the proteins are shown on the right. Rubisco loading controls were conducted using Pierce™ staining. (B) Schematic representation of chimeric TOL proteins used in CoIP experiment. Proteins that associated with AVRcap1b in CoIP experiments are highlighted with a green outline. The experiment was repeated two times with similar results.

6.2.8 AVRcap1b homologs from other *Phytophthora* species do not suppress NRCs.

As all members of the *Phytophthora* 1c clade have AVRcap1b homologs, I decided to exploit natural variation present in AVRcap1b homologs of different *Phytophthora* species to narrow down regions that are important for AVRcap1b to mediate suppression of NRC2 and NRC3. I synthesized AVRcap1b homologs from *P. mirabilis*, *P. andina* and *P. ipomoeae* and generated C-terminal 6xHA tagged versions of these effectors and of *P. infestans* AVRcap1b. I then transiently co-expressed these effectors together with autoactive variants of NRC3 in leaves of *N. benthamiana* to assess their capacity to suppress NRC3-mediated hypersensitive cell death. I also included free GFP as a negative control for suppression. Out of all the AVRcap1b homologs tested, only the *P. infestans* AVRcap1b homolog was able to suppress NRC3-mediated cell death (Figure 6.9A). In

parallel, I checked the accumulation of these 6xHA tagged homologs to determine whether the lack of suppression was due to poor accumulation *in planta*. All the homologs tested accumulated to similar levels to the *P. infestans* AVRcap1b (Figure 6.9B).

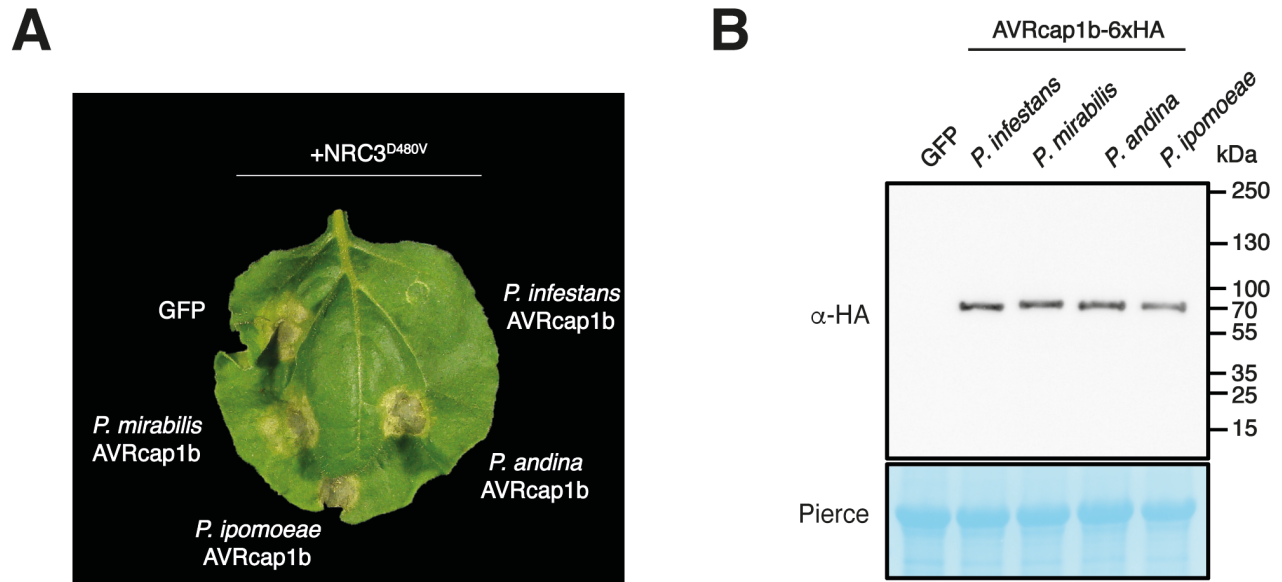


Figure 6.9: AVRcap1b homologs from other *Phytophthora* clade 1c species are unable to suppress NRC3-mediated cell death.

(A) Photo of representative *N. benthamiana* leaves showing HR after co-expression of NRC3^{D480V} and different AVRcap1b homologs from Phytophthora clade 1c species. Free GFP was included as a negative control for suppression. HR response was photographed 5 days after agroinfiltration. (B) Expression of different *Phytophthora* clade 1c AVRcap1b homologs was tested by Western blotting. Blots were probed with appropriate antisera (labeled on the left). Loading control was probed with Pierce Stain. Approximate molecular weights are displayed in kDa on the right. All experiments were repeated 3 times with similar results.

6.2.9 The LWY7 domain of *P. infestans* AVRcap1b is sufficient to confer NRC3 suppression to *P. ipomoeae* AVRcap1b.

AVRcap1b is a modular multi-WY/LWY domain-containing protein. To narrow down which WY/LWY domain encodes the capacity to suppress NRC-mediated cell death, I created a series of chimeric AVRcap1b variants by swapping individual WY/LWY domains between the NRC-suppressing *P. infestans* AVRcap1b homolog and the *P. ipomoeae* AVRcap1b homolog which

is unable to suppress NRCs (**Figure 6.10A**). As described above, we transiently expressed the different chimeric effectors in leaves of *N. benthamiana* together with a constitutively active variant of NRC3. We included the *P. ipomoeae* and *P. infestans* AVRcap1b homologs as negative and positive controls for suppression, respectively. Most of the chimeric variants did not to gain NRC3 suppression activities. The LWY7 chimera, however, can robustly suppress NRC3-mediated cell death to levels comparable to the *P. infestans* AVRcap1b, suggesting that this LWY module plays an important role in mediating suppression (**Figure 6.10B**). In parallel, we also tested the accumulation of these chimeras by Western blotting to determine whether the lack of suppression of some of these variants could be due to poor *in planta* accumulation. All the AVRcap1b chimeric variants tested accumulate to similar levels (**Figure 6.10C**).

6.2.10 NbTOL9a ENTH AND ENTH-GAT domains can form complexes with AVRcap1b in vitro.

To further study the interaction between AVRcap1b and NbTOL9a and to determine whether the association of these two proteins is direct or indirect, I decided to purify these two proteins for in vitro protein-protein interaction assays, using *E. coli* as a heterologous expression system. Constructs to express 6xHis-SUMO-AVRcap1b had been previously generated in the lab. I generated N-terminally cleavable 6xHis or 6xHis-SUMO tagged versions of either full-length NbTOL9a along with the NbTOL9a ENTH-GAT domains (NbTOL9a^{ENTH+GAT}), ENTH domain (NbTOL9a^{ENTH}) and GAT domain (NbTOL9a^{GAT}). I carried out small-scale expression and solubility tests with these constructs to evaluate the accumulation levels of these proteins. I was unable to observe a band matching the expected size for full-length NbTOL9a, both with and without the SUMO solubility tag. Fortunately, I was able to obtain good expression levels of N-terminally 6xHis-SUMO-tagged versions of NbTOL9a^{ENTH-GAT}, NbTOL9a^{ENTH} and NbTOL9a^{GAT} (**Figure AV.4**). Considering the results obtained with the NbTOL9a/TOL6 chimeric proteins, I decided to focus further experiments on NbTOL9a^{ENTH-GAT} and NbTOL9a^{ENTH}.

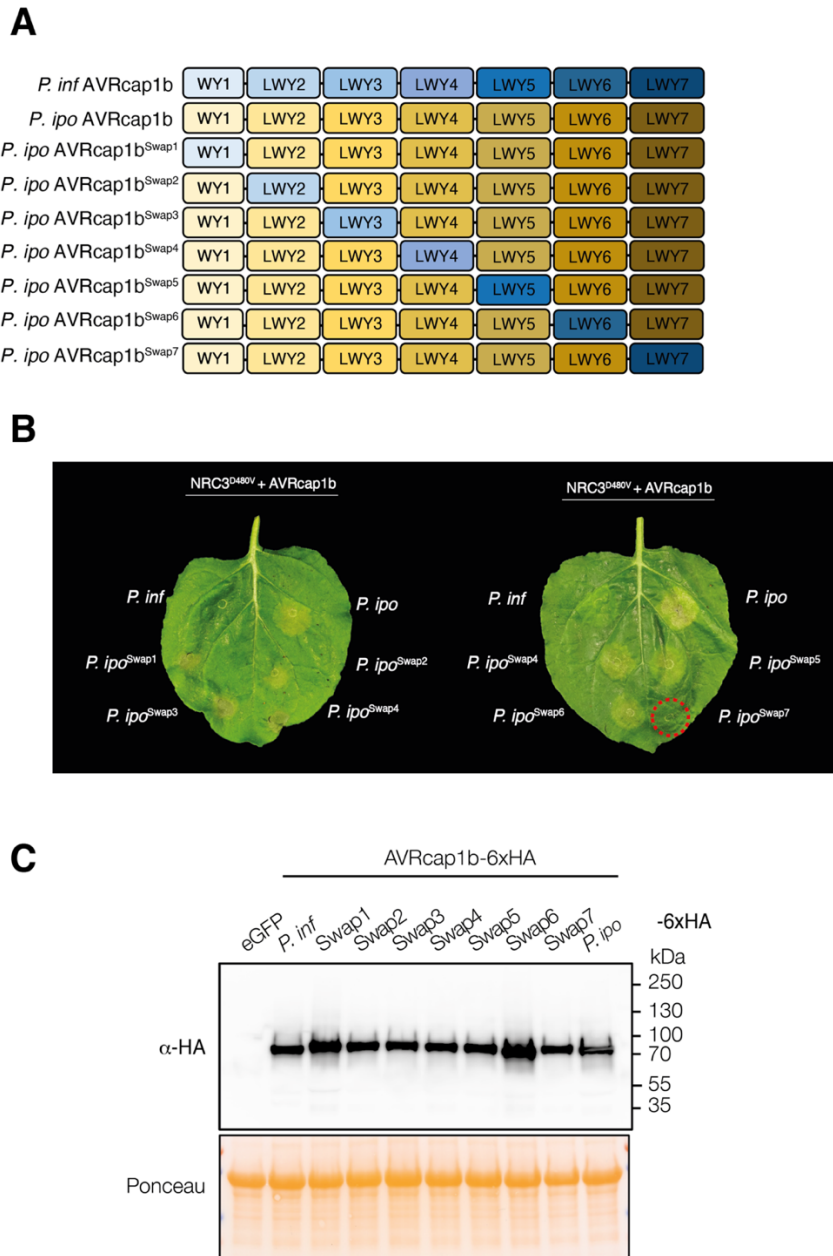


Figure 6.10: *P. ipomoeae* AVRcap1b LWY7 chimera gains the capacity to suppress NRC3.

(A) Schematic representation of all *P. infestans* and *P. ipomoeae* AVRcap1b chimeric effectors generated. (B) Photo of representative *N. benthamiana* leaves showing HR after co-expression of NRC3^{D480V} and different AVRcap1b chimeric variants. *P. infestans* and *P. ipomoeae* AVRcap1b homologs were included as positive and negative controls for suppression respectively. *P. ipomoeae* LWY7 chimera (highlighted with a red dotted line) gained NRC3 suppression capacities. (C) Expression of different AVRcap1b chimeric effectors was tested by Western blotting. Blots were probed with appropriate antisera (labeled on the left). Loading control was probed with Pierce Stain. Approximate molecular weights are displayed in kDa on the right. All experiments were repeated three times with similar results.

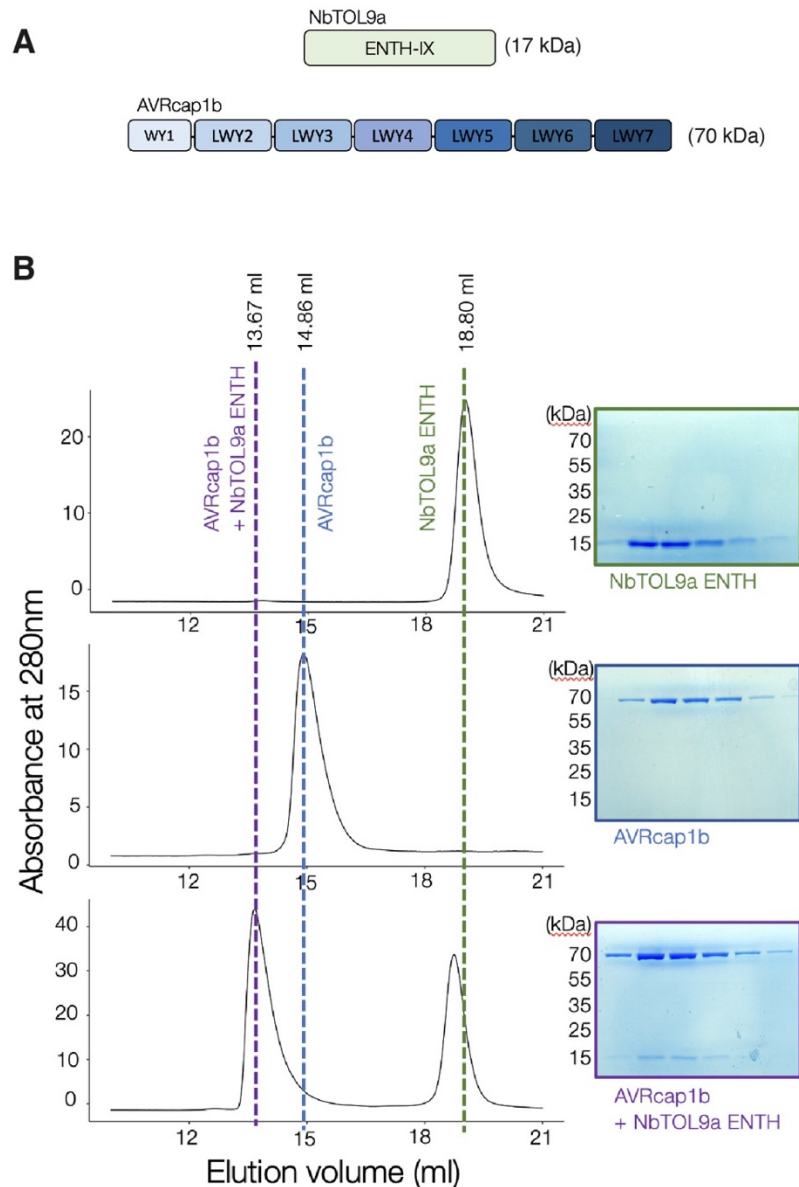


Figure 6.11: AVRcap1b binds the ENTH domain of NbTOL9a in vitro.

(A) Schematic representation of NbTOL9a^{ENTH} and AVRcap1b, indicating the approximate molecular weights of each protein. (B) AVRcap1b binds the ENTH domain of NbTOL9a in vitro. Purified proteins were run on their own or in complex on a S200 10/300 analytical column. Gel filtration traces obtained for AVRcap1b (top), the ENTH domain of NbTOL9a (middle), and a 1:1 mixture of the complex (bottom). Insets show SDS-PAGE gels of the fractions collected across the elution peaks. Approximate molecular weights (kDa) of the proteins are shown on the right.

I first purified NbTOL9a^{ENTH+GAT} and NbTOL9a^{ENTH} domains and AVRcap1b separately and, after removing all N-terminal tags by 3C protease cleavage, added an excess of either NbTOL9a^{ENTH+GAT} or NbTOL9a^{ENTH} to the effector to reconstitute potential complexes in vitro.

These potential complexes were subjected to another round of gel filtration on a Superdex 200 26/200 column. The 280 nm absorbance revealed two peaks for both AVRcap1b incubated with NbTOL9a^{ENTH+GAT} and AVRcap1b incubated with NbTOL9a^{ENTH}. Subjecting all relevant fractions to SDS-PAGE assays revealed that, in both cases, the peak with the lower elution volume (corresponding to higher molecular weight) corresponded to both proteins in complex, whereas the peak with the higher elution volume corresponded to the excess of either NbTOL9a^{ENTH+GAT} or NbTOL9a^{ENTH} (**Figure AV.5**). Although I cannot exclude AVRcap1b interactions with other domains, from these results I conclude that AVRcap1b is able to directly bind NbTOL9a, and that the ENTH domain is sufficient for AVRcap1b to interact with NbTOL9a.

To confirm the interaction between these two proteins with more precision, we performed analytical gel-filtration-based size-exclusion chromatography to determine whether AVRcap1b can form complexes in vitro. To this end, we performed analytical gel filtration on AVRcap1b on its own, NbTOL9a^{ENTH} domain on its own, and AVRcap1b previously incubated with NbTOL9a^{ENTH} domains and, in each case assessed elution volumes of proteins on their own or in complex. We were able to register a shift towards a lower elution volume in the peak obtained for AVRcap1b upon addition of NbTOL9a ENTH domain, suggesting that AVRcap1b and the ENTH domain of NbTOL9a form a complex in vitro. The shift observed was from 14.86 ml to 13.67 ml. (**Figure 6.11**). I conclude that, indeed, AVRcap1b and NbTOL9a^{ENTH} directly interact and form a stable complex in vitro.

6.2.11 AVRcap1b binds NbTOL9a^{ENTH} via its N-terminal WY1 domain.

To obtain more detailed information on the molecular determinants of AVRcap1b-TOL9a interactions, we attempted to solve the structure of AVRcap1b in complex with NbTOL9a domains using X-ray crystallography in collaboration with Prof. Dave Lawson from the John Innes Centre Protein Crystallography Platform. To this end, I purified AVRcap1b in complex with either NbTOL9a^{ENTH-GAT} or NbTOL9a^{ENTH} and attempted to grow crystals suitable for data collection. Crystals grew in multiple different conditions, using commercially available screens. Suitable crystals were selected and sent for further analysis. We obtained electron density maps at 4.4 Å resolution for AVRcap1b in complex with NbTOL9a^{ENTH}. Using AF2 assisted molecular replacement, Prof. Dave Lawson was able to successfully solve the structure of the complex and place ENTH and AVRcap1b relative to each other in the complex. Interestingly, unlike the previously solved structure of another *Phytophthora* RXLR WY/LWY effector PSR2, AVRcap1b

does not exhibit a stick-like structure but an L-shaped conformation (He *et al.*, 2019). Importantly, the structure of the complex revealed that AVRcap1b binds to the ENTH domain of NbTOL9a primarily via its N-terminal WY1 domain and partially via its LWY2 domain. (**Figure 6.12**).

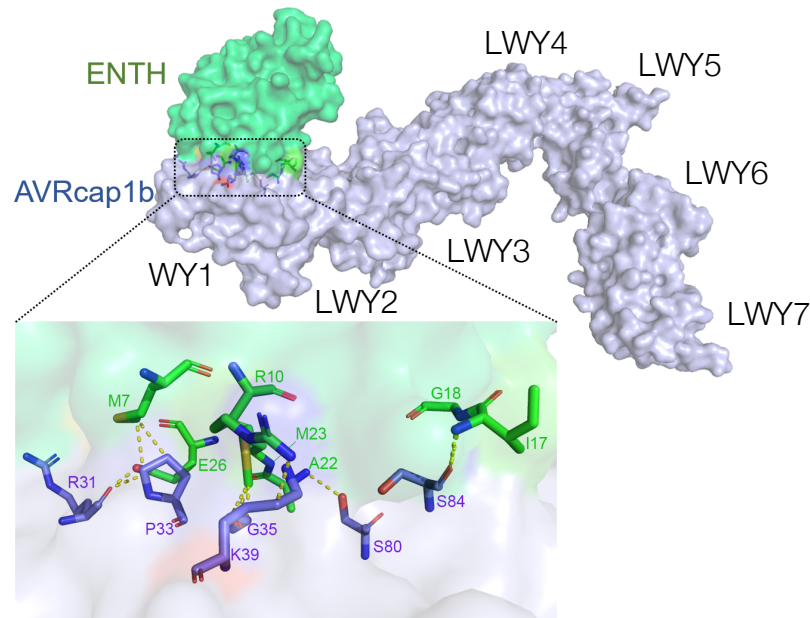


Figure 6.12: Crystal structure of AVRcap1b in complex with NbTOL9a^{ENTH}.

AVRcap1b (in blue) is a WY/LWY domain containing effector composed of 1 N-terminal WY domain and 6 additional LWY domains (LWY2-LWY7). It forms an L-shaped structure and binds the ENTH domain of NbTOL9a (green) via its N-terminal WY1 domain. Zoomed in panel below shows residues within the binding interface predicted to be within 3 angstroms of each other. Green and blue residues correspond to ENTH and AVRcap1b, respectively.

I next attempted to validate our crystal structure by mutagenizing AVRcap1b to generate an AVRcap1b mutant no longer able to interact with NbTOL9a. I was assisted in these experiments by Madhuprakash Jogi, a structural biologist in the lab. First, with Madhu's help I identified a list of candidate residues predicted to be at the AVRcap1b-NbTOL9a^{ENTH} binding interface and within 3 angstroms distance of each other. This yielded a list of 4 residues in WY1 which I mutated to glutamic acid. I tested these mutants for association with NbTOL9a via *in planta* CoIP. I co-expressed C-terminally FLAG-tagged NbTOL9a with C-terminally 6xHA-tagged versions of all AVRcap1b variants generated. I included *WT P. infestans* and *P. ipomoeae* AVRcap1b as controls. Excitingly, out of the four mutants tested, AVRcap1b^{P33E} and AVRcap1b^{G35E} no longer

associated with NbTOL9a. AVRcap1b^{R31E} displayed drastically reduced association to NbTOL9a. In contrast, AVRcap1b^{K39E} associated with NbTOL9a to levels comparable to *WT* AVRcap1b, suggesting that this residue likely does not play an important role in this interaction. This result validates our crystal structure, as mutating residues in the interface we identified has an impact on AVRcap1b-NbTOL9a interactions. Interestingly, while the AVRcap1b homolog from *P. ipomoeae* is unable to suppress NRC3-mediated cell death, it still associates with NbTOL9a (**Figure 6.13**). By generating an amino acid alignment between the WY1 domains of *P. infestans* and *P. ipomoeae* AVRcap1b and looking at the residues in the AVRcap1b-NbTOL9a^{ENTH} binding interface, I noted that all the residues I identified as proximal are conserved between these two effectors (**Figure AV.6**). Previously, I showed that WY7 encodes specificity for NRC-suppression and that swapping the LWY7 from *P. infestans* AVRcap1b into *P. ipomoeae* AVRcap1b allows the latter to gain NRC suppression. This result suggests that while the NbTOL9a binding interface is conserved between *P. ipomoeae* and *P. infestans* AVRcap1b homologs, there is a second binding interface located in the LWY7 module which is distinct in *P. ipomoeae* AVRcap1b, leading to lack of NRC3-suppression.

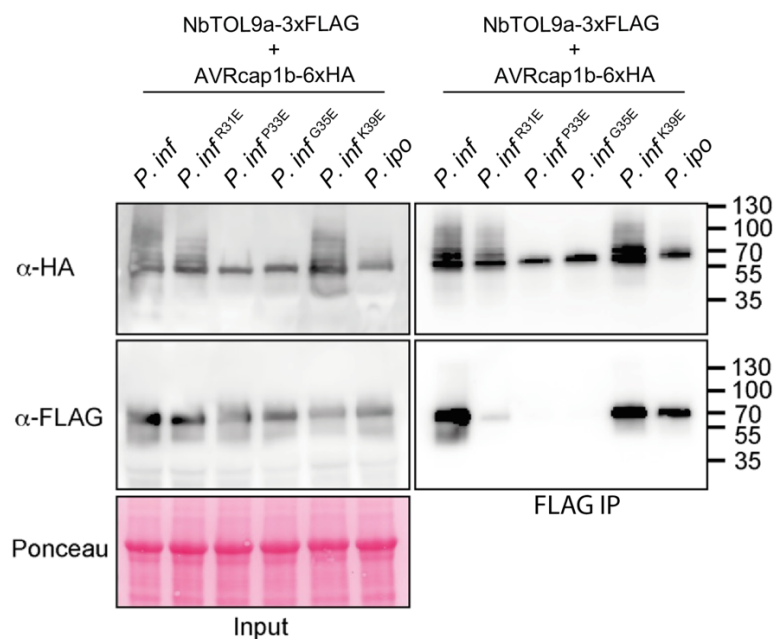


Figure 6.13: AVRcap1b P33E and G35E mutants in NbTOL9a binding interface do not associate with NbTOL9a *in planta*.

Co-immunoprecipitation experiment between different AVRcap1b variants and NbTOL9a. IPs were performed with agarose beads conjugated to FLAG (FLAG IP) antibodies. Total protein extracts were immunoblotted with appropriate antisera labelled on the left. Approximate molecular weights (kDa) of the proteins are shown on the right. Rubisco loading controls were conducted using PierceTM staining. The experiment was repeated two times with similar results.

6.2.12 NbTOL9a binding by AVRcap1b is required for NRC3 suppression.

Having identified AVRcap1b point mutants impaired in NbTOL9a interaction, I tested the 4 mutants for suppression of NRC-mediated cell death by co-expressing them with the autoactive NRC3^{D480V} variant. I included WT *P. infestans* and *P. ipomoeae* AVRcap1b homologs as positive and negative controls for suppression, respectively. Excitingly, AVRcap1b^{P33E} and AVRcap1b^{G35E}, which lost NbTOL9a association, also lost the ability to suppress NRC3-mediated cell death (**Figure 6.14A-C**). Interestingly, the AVRcap1b^{R31E} variant which exhibited drastically reduced NbTOL9a association was still able to suppress NRC3^{D480V}. As before, all effectors accumulated to similar levels, suggesting that the loss of NRC3 suppression of *P. infestans* AVRcap1b^{P33E} and AVRcap1b^{G35E} is not related to effects on protein stability. That complete loss of NbTOL9a association correlates with loss of NRC-suppression suggests that NbTOL9a binding is crucial for AVRcap1b-mediated suppression of NRC3.

6.2.13 AVRcap1b associates with Rx/CP-activated NRC2 in planta.

While I previously saw no association between AVRcap1b and inactive NRCs, following the identification of the activation-and-release model I proposed in Chapter 5, I hypothesized that perhaps AVRcap1b could specifically associate with activated NRC oligomers. To this end, I co-expressed inactive or Rx/CP activated C-terminally 3xFLAG-tagged NRC2^{EEE} with C-terminally 6xHA-tagged *P. infestans* AVRcap1b, *P. ipomoeae* AVRcap1b, *P. ipomoeae* AVRcap1b^{Swap7} or mCherry, and performed in planta CoIP experiments. I used NRC2 as opposed to NRC3 in these experiments because NRC2 is suppressed by AVRcap1b and accumulates to higher levels than NRC3 when transiently expressed *in planta*. As was done in experiments in previous chapters, I leveraged the NRC2^{EEE} mutant to study the activated NRC2 form in the absence of ongoing cell death. These experiments were also done with assistance from Madhuprakash. Excitingly, while *P. infestans* AVRcap1b did not exhibit association with inactive NRC2^{EEE}-3xFLAG, it associated with activated NRC2^{EEE}-3xFLAG. Moreover, while *P. ipomoeae* AVRcap1b did not associate with inactive or activated NRC2^{EEE}-3xFLAG, the *P. ipomoeae* AVRcap1b^{Swap7} gain-of-suppression chimera also gained association with activated NRC2^{EEE}-3xFLAG (**Figure 6.15**). These results suggest that AVRcap1b suppresses NRC2 by specifically targeting the activated form of NRC2 via an interface at the WY7 module which is distinct to the NbTOL9a binding interface encoded in the WY1 module.

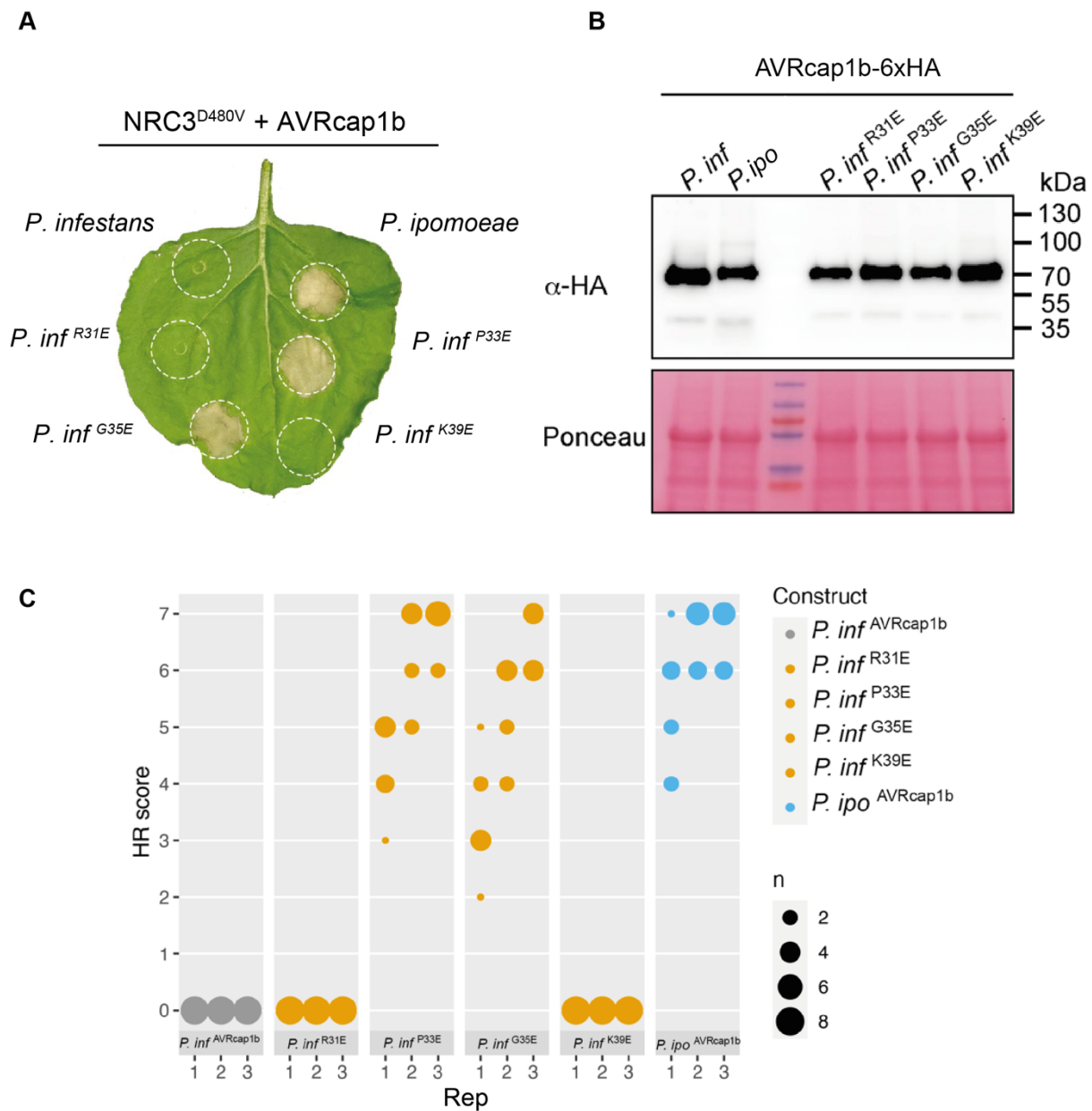


Figure 6.14: Two residues in AVRcap1b-NbTOL9a^{ENTH} binding interface are required for NRC3 suppression.

(A). Photo of representative WT *N. benthamiana* leaves showing HR after co-expression of NRC3^{D480V} and different AVRcap1b variants with mutations in residues predicted to be involved in NbTOL9a^{ENTH} binding. *P. infestans* and *P. ipomoeae* AVRcap1b homologs were included as positive and negative controls for suppression respectively. (B) Expression of all AVRcap1b variants was tested by Western blotting. Blots were probed with appropriate antisera (labeled on the left). Loading control was probed with Ponceau Stain. Approximate molecular weights are displayed in kDa on the right. (C) Quantification of HR assays shown in subpanel A.

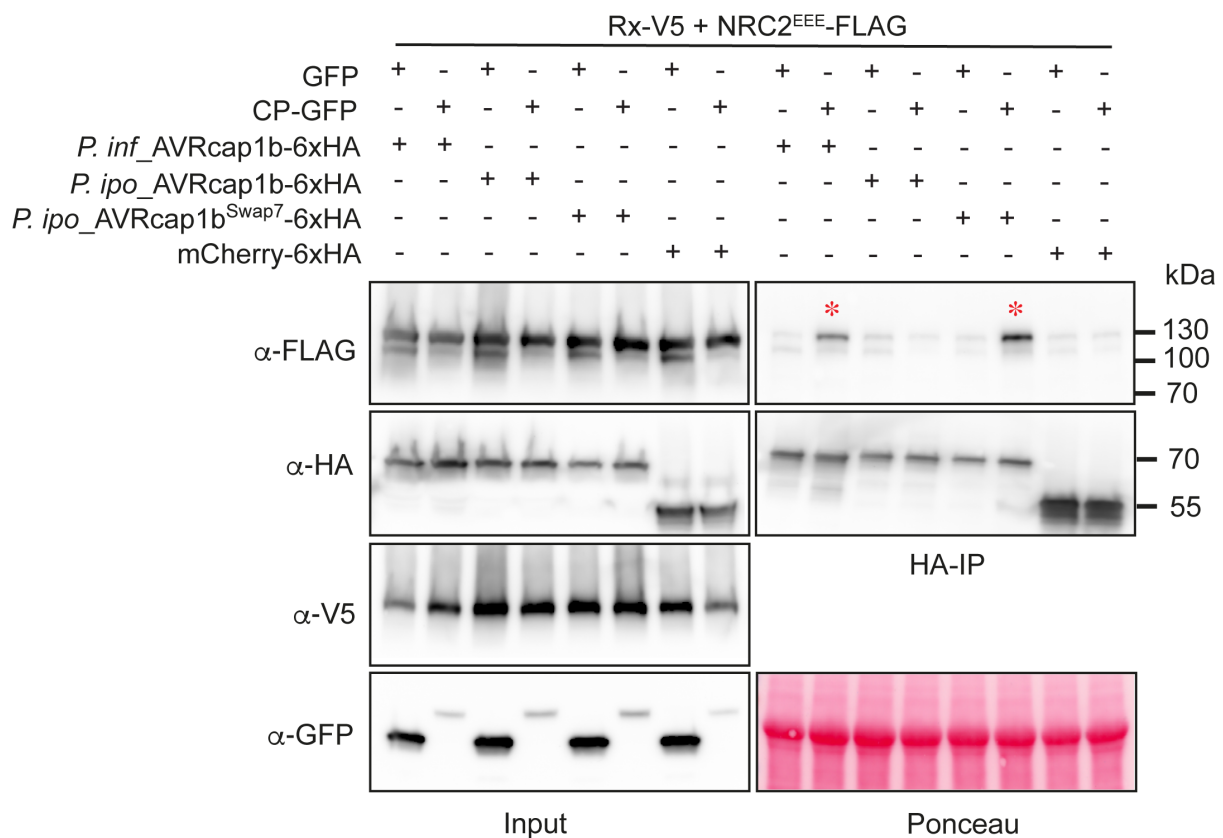


Figure 6.15: AVRcap1b associates with activated NRC2 *in planta* via its C-terminal WY7 module.

Co-immunoprecipitation experiment between AVRcap1b variants and inactive or Rx/CP activated NRC2^{EEE}-mCherry-6xHA was included as a negative control. IPs were performed with agarose beads conjugated to HA (HA IP) antibodies. Total protein extracts were immunoblotted with appropriate antisera labelled on the left. Approximate molecular weights (kDa) of the proteins are shown on the right. Rubisco loading controls were conducted using Pierce™ staining. The experiment was repeated two times with similar results.

6.2.14 AVRcap1b does not prevent NRC2 resistosome formation.

Having observed that AVRcap1b can associate with the activated form of NRC2, I next sought to understand at which step in the NRC2 activation process AVRcap1b was acting. To this end, I leveraged the Blue Native polyacrylamide gel electrophoresis (BN-PAGE) readout I established in Chapter 4 to determine whether AVRcap1b can affect NRC2 oligomerization and to visualize any potential NRC2-AVRcap1b *in planta* complexes. To this end I co-expressed multiple C-terminally 6xHA-tagged AVRcap1b variants with NRC2^{EEE}-4xMyc and Rx-V5.

mCherry-6xHA was included as a negative control. Each of these combinations was either co-expressed with free GFP (inactive control) or CP-GFP (activated state). The AVRcap1b variants tested included *P. infestans* and *P. ipomoeae* AVRcap1b, as well as the previously identified *P. infestans* AVRcap1b^{P33E} mutant which no longer interacts with NbTOL9a or suppresses NRC3. My BN-PAGE assays revealed that activated NRC2^{EEE} was capable of oligomerizing regardless of which AVRcap1b variant is present. Moreover, none of the AVRcap1b variants tested co-migrated with activated NRC2. Intriguingly, while I could see association between AVRcap1b and NRC2 in CoIP experiments (**Figure 6.16**), no clear AVRcap1b-NRC2 complex was recovered. It is possible that only a small fraction of the total pool of AVRcap1b is forming a complex with NRC2 or that the AVRcap1b-NRC2 complex is not stable enough to survive the extraction conditions used for these BN-PAGE assays. Nonetheless, these results suggest that AVRcap1b acts downstream of NRC2 oligomerization to execute its suppression activities.

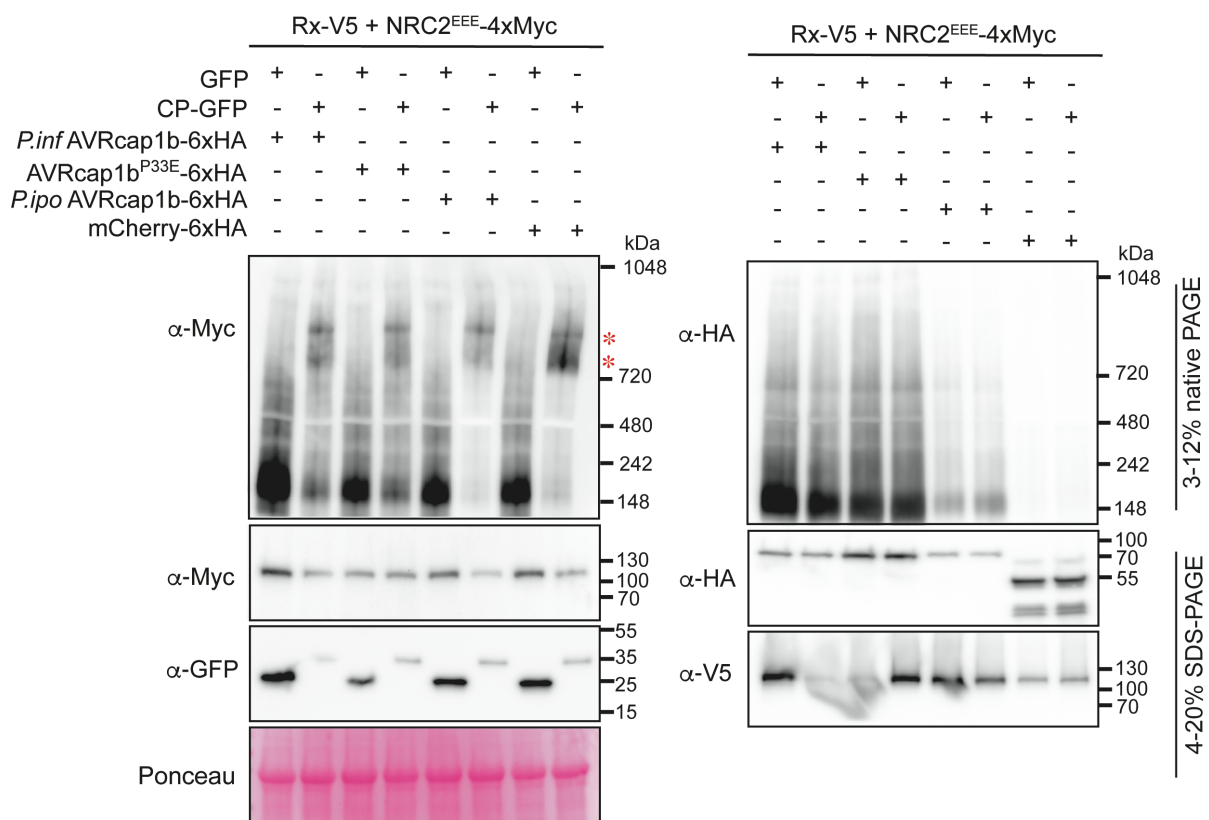


Figure 6.16: AVRcap1b does not inhibit NRC2 oligomerization.

Immunoblots corresponding to BN-PAGE and SDS-PAGE assays with inactive and activated NRC2 co-expressed with AVRcap1b variants indicated. C-terminally 6xHA-tagged AVRcap1b variants, Rx-V5 and NRC2^{EEE}-4xMyc were co-expressed together with either free GFP or PVX CP-GFP. mCherry-6xHA was

used as a control for AVRcap1b. Protein extracts were run on native and denaturing PAGE assays in parallel and immunoblotted with the appropriate antisera labelled on the left. Approximate molecular weights (kDa) of the proteins are shown on the right. Red asterisks indicate bands corresponding to the activated NRC2 complex. Rubisco loading control was carried out using Ponceau stain. The experiment was repeated two times with similar results.

6.3 Conclusion and Discussion.

In this Chapter, I attempted to decipher the molecular mechanism by which the previously identified *P. infestans* RXLR LWY effector AVRcap1b suppresses NRC2 and NRC3-mediated cell death. I determined that AVRcap1b does not interact with inactive NRCs but instead interacts with host TOL proteins, particularly NbTOL9a, involved in the early steps of the ESCRT vesicle trafficking pathway (Moulinier-Anzola *et al.*, 2020) (**Figure 6.1, Figure 6.2**). While NbTOL9a also does not associate with inactive NRCs (**Figure 6.3, Figure 6.4**). Further studies on NbTOL9a revealed that this protein can negatively regulate NRC2 and NRC3-mediated cell death (**Figure 6.5, Figure 6.6**) and that AVRcap1b genetically requires NbTOL9a to fully execute its suppressor functions (**Figure 6.7**). I went on to show that AVRcap1b and NbTOL9a directly interact and form a complex, primarily mediated via the N-terminal WY1 domain of AVRcap1b and the N-terminal ENTH domain of NbTOL9a. I went on to obtain the cocrystal structure of AVRcap1b-NbTOL9a^{ENTH}, which allowed me to generate AVRcap1b mutants which were unable to bind NbTOL9a (**Figure 6.8, Figure 6.11, Figure 6.12**). These mutants were also unable to suppress NRC3-mediated cell death, further supporting the hypothesis that AVRcap1b binding host TOL proteins is required for the effector to execute its suppressor functions (**Figure 6.13, Figure 6.14**). By leveraging natural variation found in AVRcap1b homologs present in various species, I was able to determine that the C-terminal WY7 module of AVRcap1b also contributes to NRC suppression (**Figure 6.9, Figure 6.10**). Finally, I showed that while AVRcap1b does not associate with inactive NRCs, it coimmunoprecipitates with sensor activated NRC2 *in planta*, and that the WY7 module contributes to this association (**Figure 6.15**). Interestingly, while AVRcap1b suppression of activated NRC2 appears to involve association between these two proteins, AVRcap1b does not inhibit NRC2 oligomerization as part of its activation mechanism (**Figure 6.16**). These data have led me to propose a working model for AVRcap1b suppression of NRC2 and NRC3 (**Figure 6.17**).

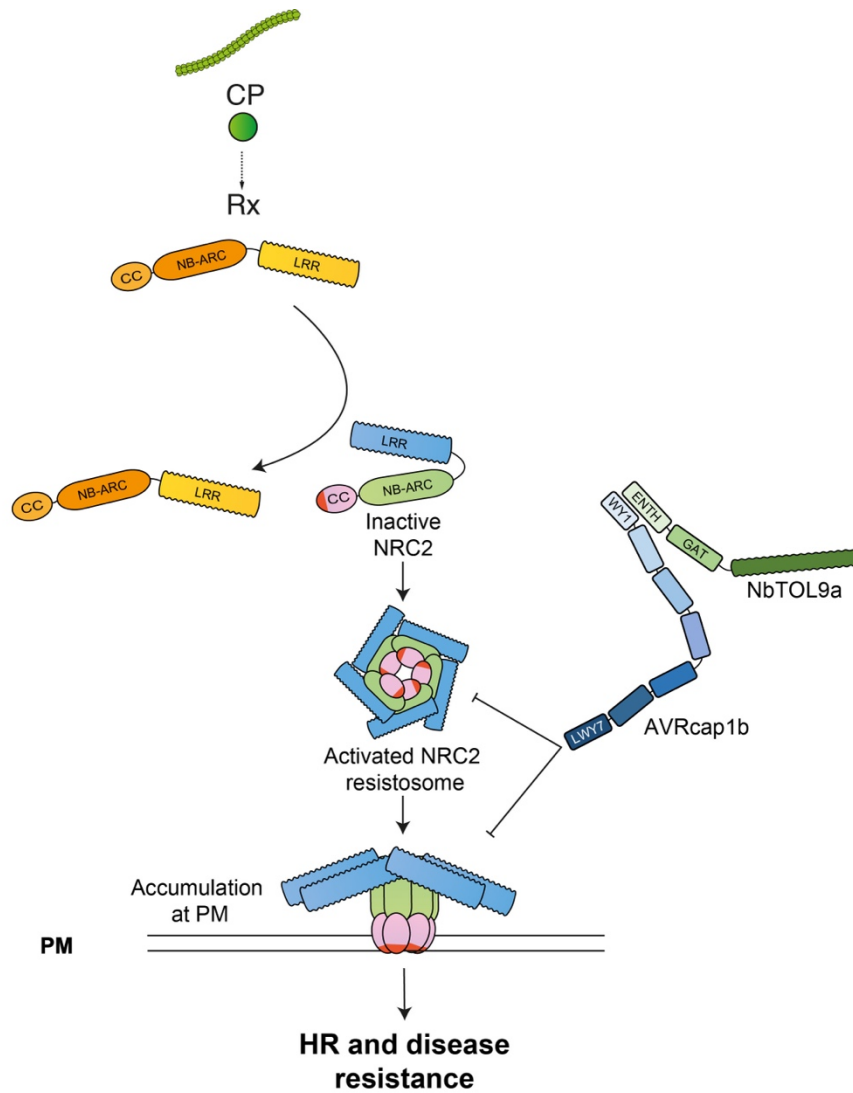


Figure 6.17: Working model for AVRcap1b suppression of NRC2/NRC3-mediated cell death.

To suppress NRC2/NRC3-mediated cell death, AVRcap1b co-opts host TOL proteins such as NbTOL9a. The N-terminal WY1 domain of AVRcap1b interacts with the N-terminal ENTH domain of NbTOL9a, and this interaction is required for suppression. While AVRcap1b does not interact with inactive NRCs, it associates with activated NRC complexes and does not prevent helper NLR oligomerization. Therefore, AVRcap1b could be acting as a bridge, re-directing the ESCRT machinery to activated NRC oligomers to suppress cell death. Whether AVRcap1b directly interacts with NRCs is not known.

In my working model, AVRcap1b acts as a bridge between activated NRC oligomers and NbTOL9a, hijacking the host ESCRT machinery to suppress NRC-mediated cell death (**Figure 6.17**). My experiments revealed that NbTOL9a can act as a negative regulator of NRC2 and NRC3-mediated cell death. This is in line with previous reports that the ESCRT machinery can negatively regulate programmed cell death in non-plant systems by excising damaged sections of membrane and trafficking membrane associated pores or channels away from the host PM (Castro-Gomes *et al.*, 2014; Dai *et al.*, 2020; Gong *et al.*, 2017; Jimenez *et al.*, 2014; Rühl *et al.*, 2018). Notably, it would be the first example in plants of ESCRT components counteracting programmed cell death. That AVRcap1b has helped uncover a previously uncharacterized regulator of cell death in plants highlights how useful effectors can be as probes with which to study various plant processes. Activated NRC oligomers, much like other well characterized CC-NLR resistosomes, have previously shown to accumulate at the PM to execute immune signaling and initiate cell death, presumably by acting as calcium permeable channels. It is possible that AVRcap1b is specifically targeting these PM-associated resistosomes and recruiting the host ESCRT machinery to remove them from the membrane and trafficking them to different sub-cellular compartments, therefore preventing them from acting as channels or pores. The exact dynamics of CC-NLR resistosome assembly, however, are not clear. NRC2^{EEE} was shown to be cytoplasmic prior to activation (Contreras *et al.*, 2023a; Contreras *et al.*, 2023b). It is also possible that NRC oligomers assemble away from the PM and are then trafficked to the membrane. AVRcap1b could also be blocking that pathway, preventing them from arriving at the PM in the first place. Further cell biology-based approaches and/or membrane enrichment assays may help challenge this hypothesis.

Interestingly, NbTOL9a silencing did not completely abolish AVRcap1b-mediated suppression of NRC3. TOL proteins in plants have previously been shown to be highly redundant, so it is possible that in the absence of NbTOL9a, AVRcap1b can still co-opt other endogenous TOLs to execute its suppressor function. My initial CoIP experiments suggested that AVRcap1b could also interact with NbTOL9b and NbTOL9c, which would support this hypothesis. Further studies with higher order TOL silenced or KO plants may help address this question. Moreover, if AVRcap1b interacts with all TOLs via the same interface in WY1, the complete loss of suppression exhibited by AVRcap1b^{P33E} and AVRcap1b^{G35E} mutants in which, presumably, binding of all TOLs would be abolished, supports the notion that TOL-binding is important for suppression.

My chimeric AVRcap1b effectors led me to identify LWY7 as contributing towards NRC-suppression and association. Further mutagenesis studies on AVRcap1b WY7 may help identify individual residues which underpin potential AVRcap1b-NRC interactions. Importantly, whether AVRcap1b interacts directly with NRC complexes or whether this association is indirect is not known. Moreover, the molecular determinants of AVRcap1b-NRC suppression specificity are not clear. AVRcap1b can suppress NRC2 and NRC3 but not NRC4 or other NLRs. Leveraging the resilience of NRC4 to AVRcap1b suppression may prove useful to identify which regions within the helper NLR that encode susceptibility to suppression by AVRcap1b. Chimeric NRC proteins or AlphaFold2 based structural predictions could be useful to this end. In her screen, Lida Derevnina identified an additional NRC2/NRC3 suppressing effector. This is SS15 from *G. rostochiensis*. Unlike AVRcap1b, SS15 shows strong interaction with inactive NRCs (**Figure 6.1**). It will be intriguing to leverage the same set of techniques used in this Chapter to further understand the mechanism by which SS15 suppresses NRCs. Identifying NLR suppressing effectors and determining their mode of action may reveal commonalities and differences that will shed light on strategies used by pathogens to suppress the plant immune system. It is my hope that by understanding the mechanism by which pathogen effectors can interfere with NRC activities I may be able to engineer immune receptors that can no longer be inhibited.

6.4 Research contributions.

I thank Lida Derevnina (The Sainsbury Laboratory, Norwich, UK) for cloning the initial constructs used in the results featured in Derevnina et al., (2021). I thank Max Jordan (The Sainsbury Laboratory, Norwich, UK) for assistance with *in planta* biochemistry of AVRcap1b and *N. benthamiana* TOL homologs. I thank Jessica Upson (The Sainsbury Laboratory, Norwich) for cloning pOPIN-S3C-AVRcap1b. I thank Prof. David Lawson and Clare E. M. Stevenson (John Innes Centre, Norwich, UK) for assistance with crystallography, data collection and solution of AVRcap1b-NbTOL9a^{ENTH} structure. I thank Madhuprakash Jogi (The Sainsbury Laboratory, Norwich, UK) for assistance with interpretation of AVRcap1b-NbTOL9a^{ENTH} structure and for assistance with some of the *in planta* biochemistry experiments.

Chapter 7: Resurrection of disease resistance via helper NLR bioengineering.

Part of the results from this chapter are published as part of a manuscript by [M.P. Contreras et al.](#) (Contreras *et al.*, 2023a).

Doi: <https://doi.org/10.1126/sciadv.adg3861>

My contributions to this manuscript correspond to the results described in this chapter.

7.1 Introduction.

Nucleotide-binding and leucine-rich repeat (NLR)-type receptors are vital for innate immunity of both plants and animals. They mediate intracellular recognition of pathogens and trigger a variety of immune responses to combat infection (Jones & Dangl, 2006; Jones *et al.*, 2016). These NLRs are activated by virulence proteins, also known as effectors, which are secreted by pathogens and translocated inside host cells to modify their physiology (Chou *et al.*, 2023; Duxbury *et al.*, 2021). Upon activation, NLRs often assemble into oligomeric immune complexes, referred to as resistosomes in plants and inflammasomes in animals. These complexes initiate immune signaling that typically culminates in a form of programmed cell death known as the hypersensitive response in plants or pyroptosis in animals (Chou *et al.*, 2023). Recently, proteins with similarity to NLRs have been discovered in prokaryotes which mediate antiviral immunity and programmed cell death, also via oligomerization into inflammasome/resistosome-like complexes (Gao *et al.*, 2022; Kibby *et al.*, 2023). This indicates that oligomerization-based initiation of programmed cell death by NLRs is a conserved defense mechanism across all three domains of life (Chou *et al.*, 2023). Interestingly, pathogen effectors can both activate and suppress NLR-mediated immunity. Adapted pathogens can use effectors to tamper with NLR signaling thus preventing immune activation (Wu & Derevnina, 2023). However, the precise biochemical means by which pathogen effectors subvert NLR-mediated immunity to promote disease are not well understood. Moreover, despite numerous proposed strategies to bioengineer NLRs with novel recognition specificities (Kourelis *et al.*, 2023; Marchal *et al.*, 2022b), approaches to counteract effector-induced immune suppression of NLRs are yet to be developed.

NLRs are part of the STAND (signal adenosine triphosphatases with numerous domains) superfamily (Takken *et al.*, 2006). They generally display a tripartite domain architecture which

includes an N-terminal signaling domain, a central nucleotide-binding and oligomerization domain (NOD), and C-terminal superstructure forming repeats. The central NOD, known as the NB-ARC (nucleotide-binding adaptor shared by APAF-1, plant R proteins, and CED-4) in plant NLRs is a defining characteristic of this protein family (Kourelis *et al.*, 2021). It acts as a molecular switch, contributing to autoinhibition in the inactive state and mediating critical conformational changes for activation upon effector recognition (Takken *et al.*, 2006; Wang *et al.*, 2019b). The NB-ARC module itself is subdivided into three domains, the nucleotide binding (NB) domain, the helical domain 1 (HD1) and the winged-helix domain (WHD). There are various strategies for NLR activation and signaling found in nature. In some cases, an individual NLR protein, referred to as a singleton, can both perceive the elicitor and initiate the subsequent immune signaling (Adachi *et al.*, 2019b). However, in some instances, NLRs function in pairs or higher-order configurations, known as immune receptor networks. In such scenarios, one NLR acts as a pathogen sensor, requiring a second helper NLR for immune signaling (Adachi *et al.*, 2019b; Adachi & Kamoun, 2022; Wu *et al.*, 2018). The NLR required for cell death (NRC) network, for example, is a well-studied model NLR network found in the solanaceous family of plants. It is composed of multiple sensor NLRs that depend on a set of downstream helper NLRs, named NRCs (NLRs required for cell death), to successfully initiate immune signaling (Derevnina *et al.*, 2021; Wu *et al.*, 2017). NLR networks are highly advantageous, both due to the increased robustness provided by the multiple helper nodes and due to the enhanced evolvability provided by the functional specialization into sensor and helper immune receptors (Wu *et al.*, 2018).

In Chapter 4, I found that upon recognizing their cognate effectors, sensor NLRs mediate oligomerization of their downstream NRC helpers, leading to the assembly of a putative NRC resistosome. The sensors are not part of the mature complex themselves, an activation mechanism I coined as the activation and release model (Contreras *et al.*, 2023b). In certain solanaceous plant species, the NRC network can make up as much as half of the NLRome and plays a crucial role in immunity against various plant pathogens, including oomycetes, bacteria, viruses, nematodes, and insects (Derevnina *et al.*, 2021; Wu *et al.*, 2017). As such, interfering with NRC helper resistosome assembly or signaling would appear as an advantageous strategy for solanaceous pathogens to interfere with host immunity, as compromising helper nodes could simultaneously compromise multiple upstream sensors.

Both plant and animal pathogens have evolved effectors that interfere with host NLR signaling to cause disease (Gao *et al.*, 2022; Wu & Derevnina, 2023; Yen *et al.*, 2015). Pathogen

effectors can indirectly suppress NLR-mediated immunity by interfering with host proteins that act downstream of NLR signaling or directly by interacting with NLRs to inhibit their functions (Derevnina *et al.*, 2021; Karki *et al.*, 2021; Yen *et al.*, 2015). An example is SPRYSEC15 (SS15), from the potato cyst nematode (*Globodera rostochiensis*). SS15 can suppress signaling mediated by *Nicotiana benthamiana* helper NLRs NRC2 and NRC3 and tomato (*Solanum lycopersicum*) helper NLR NRC1 by binding to their central NB-ARC domains (**Figure AVI.1**) (Derevnina *et al.*, 2021). As the NB-ARC is known to mediate critical intramolecular rearrangements required for resistosome assembly (Martin *et al.*, 2020; Wang *et al.*, 2019b), it is tempting to speculate that SS15 is interfering with NRC oligomerization. Alternatively, it is also possible that SS15 binds to NRC2 protomers in the assembled helper oligomer and interferes with downstream signaling processes. The precise mechanism by which SS15 prevents NRC2/3-mediated immune signaling and cell death is not understood. Interestingly, another *N. benthamiana* helper NLR NRC4, a paralog of NRC2/3, is immune to suppression by SS15 (Derevnina *et al.*, 2021). The molecular determinants of sensitivity to SS15 suppression are not known. Understanding the molecular basis of NRC4's evasion of SS15 suppression could potentially be leveraged to bioengineer NRC2/3 variants which can no longer be suppressed by SS15 but retain their sensor signaling capacity.

In this chapter, I leveraged the Blue Native polyacrylamide gel electrophoresis (BN-PAGE) based approaches established in Chapter 4 to understand at which step of the activation process SS15 acts to suppress NRC2/3-mediated cell death, once again using Rx and NRC2 as a model sensor-helper pair within the NRC network. I found that SS15 acts as a proteinaceous NLR inhibitor, blocking sensor-mediated oligomerization of NRC2. Using chimeric NRC2-NRC4 proteins, I mapped the binding interface between SS15 and NRCs and found that SS15 binding to the first half of the HD1 domain of the NB-ARC is sufficient for SS15 to inhibit NRC4 oligomerization. Combining the information from these chimeras with the crystal structure of SS15 in complex with the NB-ARC domain of SINRC1 allowed me to identify residues in NRC2 that were leveraged for evasion of SS15-mediated suppression. These bioengineered NLR variants can restore the immune signaling activity of multiple upstream sensors in the NRC network.

7.2 Results.

7.2.1 SS15 inhibits NRC2 but not NRC4 oligomerization and resistosome formation.

In this chapter, I set out to leverage the techniques and approaches used in previous Chapters to understand the mechanism by which the *G. rostochiensis* effector SS15 suppresses NRC-mediated cell death by directly binding to the NB-ARC domain of inactive NRCs (Derevnina *et al.*, 2021). I hypothesized that SS15 binding to NRC2 inhibits immune signaling by preventing NRC oligomerization following sensor NLR Rx and the effector SS15 in leaves of *nrc2/3/4* KO *N. benthamiana* plants, using previously established BN-PAGE-based readouts for NRC resistosome formation. These experiments were done with assistance from Hsuan Pai, a technician in our lab. For biochemical analyses, I employed NRC2 and NRC4 variants with mutations in their N-terminal MADA motifs (NRC2^{EEE} and NRC4^{AAA}, respectively) described in Chapter 3 and Chapter 4. These variants abolish cell death induction without compromising receptor activation, oligomerization, or localization (Adachi *et al.*, 2019a; Contreras *et al.*, 2023b; Duggan *et al.*, 2021).

I activated the sensor-helper Rx-NRC system by co-expressing the *Potato Virus X* Coat Protein (PVX CP) fused to GFP or free GFP as a negative control. In the absence of SS15, both NRC2 and NRC4 oligomerized upon CP-triggered activation of Rx. However, when SS15 is co-expressed, Rx/PVX CP-activated NRC2 is unable to oligomerize and appears as a band of approximately 240 kDa, which co-migrates with SS15. Inactive NRC2 co-expressed with SS15 also migrates as a band of around 240 kDa, which is slower-migrating compared to inactive NRC2 in the absence of SS15, indicating *in vivo* NRC2-SS15 complex formation (**Figure 7.1, Figure AVI.1**). In collaboration with Cian Duggan and Yasin Tumtas from Tolga Bozkurt's lab, I also observed that SS15 co-expression not only blocks NRC2 oligomerization but also prevents the formation of NRC2 PM-associated puncta upon Rx/PVX CP activation and the shift of NRC2 from the cytoplasm to PM and I described in Chapter 4 (**Figure 7.2**). In contrast, NRC4 oligomerization is not affected by the presence of SS15, which aligns with previous findings that NRC4 immune signaling is not suppressed by SS15 (Derevnina *et al.*, 2021). I conclude that SS15 can suppress immune signaling by acting as a direct proteinaceous inhibitor of NRC2, but not NRC4, by directly binding to its NB-ARC domain to block the formation of a signal-competent oligomeric resistosome.

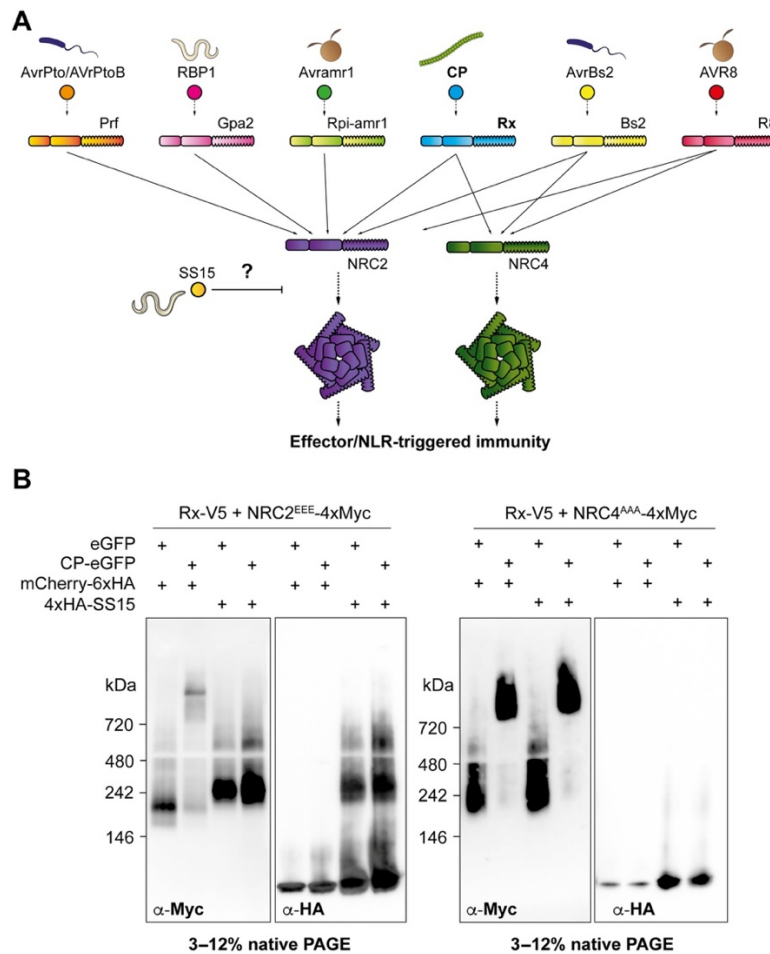


Figure 7.1: SS15 directly inhibits NRC2 but not NRC4 oligomerization.

(A) Schematic representation of the NRC immune receptor network, consisting of multiple sensor NLRs and their downstream helper NLRs, NRC2 and NRC4 (in purple and green, respectively). Potato virus X (PVX) capsid protein (PVX CP) and Rx are in boldface as they are used for most of the experiments in this study. Effector-triggered activation of a sensor leads to downstream helper oligomerization and resistosome formation. The *G. rostochiensis* effector SS15 (in yellow) can directly bind to the NB-ARC domain of NRC2 but not NRC4, thereby inhibiting signaling by directly binding to the NB-ARC domain of this helper NLR. (B) Blue native polyacrylamide gel electrophoresis (BN-PAGE) assays with inactive and PVX CP-activated Rx together with NRC2 or NRC4, in the absence or presence of SS15. C-terminally V5-tagged Rx and C-terminally 4xMyc-tagged NRC2^{EEE} or NRC4^{AAA} were coexpressed with either free green fluorescent protein (GFP) or C-terminally GFP-tagged PVX CP. These effector-sensor-helper combinations were coinfiltrated together with a 6xHA-mCherry fusion protein or with N-terminally 6xHA-tagged SS15. Total protein extracts were run in parallel on native and denaturing PAGE assays and immunoblotted with the appropriate antisera, as labelled below. Approximate molecular weights (in kilodalton) of the proteins are shown on the left. Corresponding SDS-PAGE assays can be found in **Figure AVI.1**. The experiment was repeated three times with similar results.

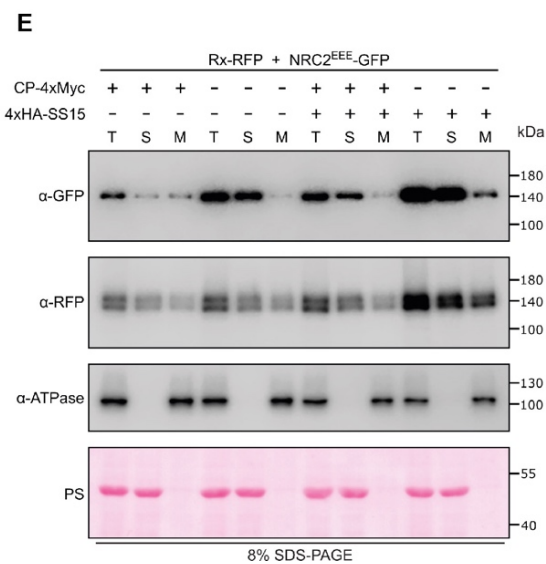
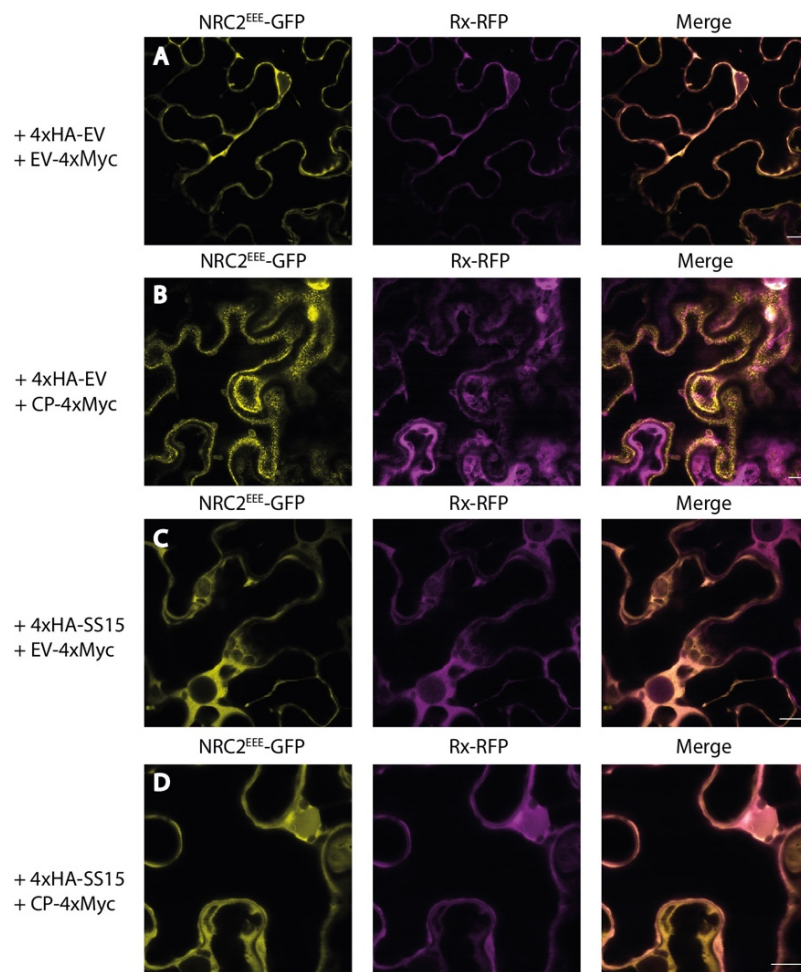


Figure 7.2: SS15 inhibits plasma membrane-association of activated NRC2.

(A-D) C-terminally GFP-tagged NRC2^{EEE} and C-terminally RFP-tagged Rx were co-expressed with an EV-4xMyc construct or a PVX CP-4xMyc construct in leaves of *nrc2/3/4* KO *N. benthamiana*. Representative single-plane confocal micrographs show the localization of both components of the inactive and active Rx-NRC2 system. Scale bars represent 10 μ m. (A) NRC2^{EEE}-GFP and Rx-RFP co-localize in the cytoplasm. (B) As reported previously, Rx/PVX CP activated NRC2^{EEE} forms plasma membrane-associated puncta while Rx remains in the cytoplasm. (C) Co-expression with SS15 does not alter the localization of inactive NRC2^{EEE}-GFP or Rx-RFP. (D) Upon co-expression PVX CP-4xMyc, Rx-RFP and NRC2^{EEE}-GFP with SS15, the punctate localization for NRC2^{EEE}-GFP is no longer observed. (E) Membrane enrichment assays are consistent with microscopy. As reported previously, inactive NRC2^{EEE}-GFP is mostly present in the soluble fraction (S) whereas activated NRC2^{EEE}-GFP exhibits equal distribution across soluble and membrane (M) fractions. Upon co-expression with SS15, NRC2^{EEE}-GFP distribution remains in the soluble fraction regardless of the presence or absence of PVX CP. The experiment was repeated twice with similar results. S and M fractions as well as the Total protein extract (T) were used for SDS-PAGE assays and immunoblotted with the appropriate antisera labelled on the left. Approximate molecular weights (kDa) of the proteins are shown on the right. Rubisco was visualized with Ponceau stain (PS) as a loading control and as a cytoplasmic protein control. ATPase was used as a PM protein control. The experiment was repeated three times with similar results.

7.2.2 SS15 associates with HD1-1 region in the NB-ARC domain of NRC2.

I next aimed to take advantage of the differential SS15 sensitivity exhibited by NRC2 and NRC4 to identify the domain responsible for SS15 association and inhibition. I leveraged a series of previously generated NRC2-NRC4 chimeric proteins which I assessed for SS15 association using in planta co-immunoprecipitation (**Figure 7.3**). NRC2 and NRC4 were included as positive and negative controls for SS15 association, respectively. Multiple NRC2-NRC4 chimeric proteins associated with SS15 in our assays, including NRC⁴²⁴, NRC4^{V3} and NRC4^{V6}. A common feature shared among these chimeras is that they carried the HD1 domain of NRC2. In particular, the NRC4^{V6} chimeras consisted of NRC4 carrying the HD1 of NRC2 (**Figure 7.3A**). This NRC4^{V6} chimera gained association to SS15, suggesting that the HD1 sub-domain within the NB-ARC domain is important for NRC-SS15 interactions.

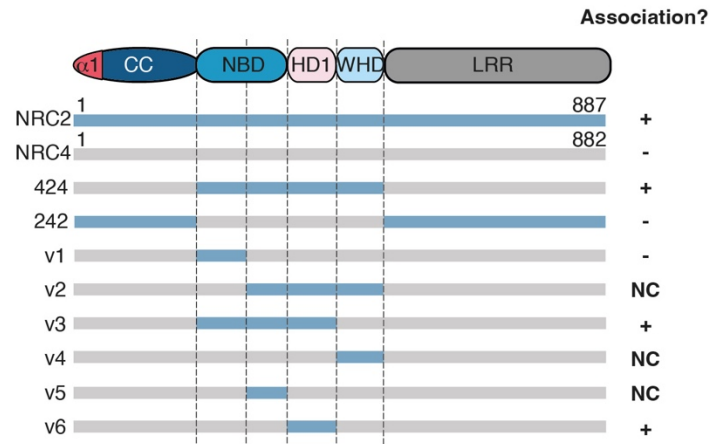
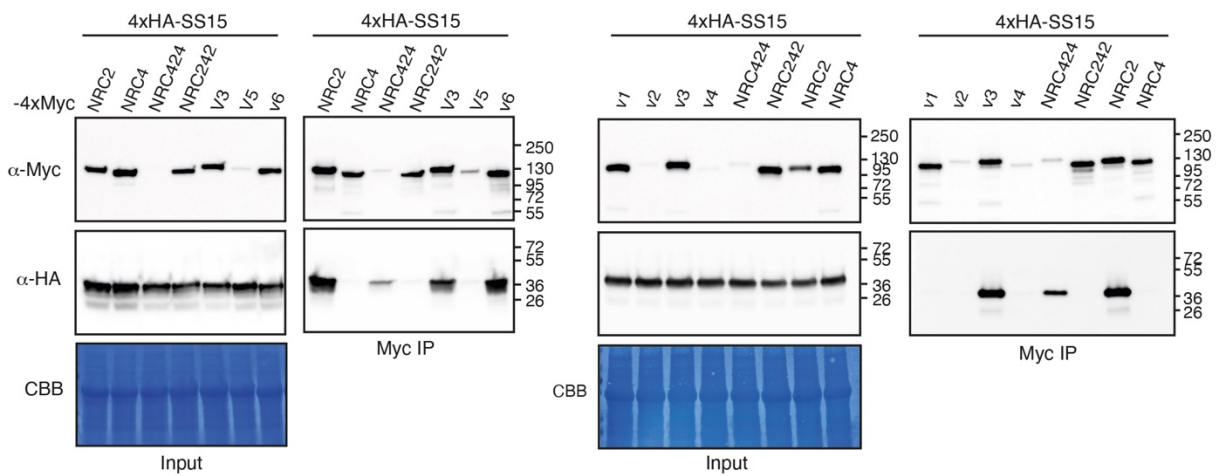
A**B**

Figure 7.3: SS15 inhibits NRC2 by interacting with the HD1-1 region of the NB-ARC domain.

(A) Schematic representation of all NRC2-NRC4 chimeric proteins generated. Association with SS15 (+) or lack thereof (-) is indicated on the right. NC indicates that no conclusion could be drawn for that chimera due to lack of accumulation *in planta*. **(B)** Co-Immunoprecipitation (Co-IP) assays between SS15 and chimeric NRC2-NRC4 variants. C-terminally 4xMyc-tagged NRC proteins were transiently co-expressed with N-terminally 4xHA-tagged SS15. IPs were performed with agarose beads conjugated to Myc antibodies (Myc IP). Total protein extracts were immunoblotted with the appropriate antisera, as labelled on the left. Approximate molecular weights (kDa) of the proteins are shown on the right. Rubisco loading control was carried out using Ponceau stain (PS). The experiment was repeated three times with similar results.

To further narrow down regions in the HD1 contributing to NRC-SS15 interactions, I screened additional NRC2-NRC4 chimeric proteins generated by Lida Derevnina. These chimeras were focused mainly on the HD1 subdomain, which is subdivided into HD1-1 and HD1-2. These chimeras are termed NRC4^{2HD1-1} and NRC4^{2HD1-2} as they consist of NRC4 carrying the HD1-1 or HD1-2 regions of NRC2, respectively (**Figure 7.4A-B**). NRC4^{2HD1-1} gained association to SS15 in my CoIP assays (**Figure 7.4C**). I next tested Rx/PVX CP-activated NRC4^{2HD1-1} and NRC4^{2HD1-2} for susceptibility to inhibition by SS15. NRC2 and NRC4 were included as positive and negative controls for SS15 inhibition respectively. NRC4^{2HD1-1} remained functional, triggering visible HR cell death, but unlike NRC4, this chimera is suppressed by SS15. In contrast, although NRC4^{HD1-2} accumulates *in planta*, it is not functional in HR assays upon Rx/PVX CP activation (**Figure 7.4D**, **Figure AVI.2**). This suggests that gain of association to SS15 mediated by the HD1-1 region swap is sufficient to make NRC4 sensitive to inhibition by this effector. To investigate this correlation between functional HR assays and oligomerisation, I tested the NRC4^{2HD1-1} chimera in BN-PAGE assays. To this end, I generated a variant of this chimera with the triple Alanine mutation in the N-terminal MADA motif to avoid cell death (NRC4^{AAA,2HD1-1}). Unlike NRC4^{AAA}, NRC4^{AAA,2HD1-1} was not able to oligomerize in the presence of SS15. It should be noted that the NRC4^{AAA,2HD1-1} chimera oligomerized less efficiently than NRC4^{AAA}, in the absence of SS15 (**Figure 7.4E**, **Figure AVI.3**). Based on these experiments, I conclude that the HD1-1 region is important for association between SS15 and NRCs and for the effector to directly inhibit NRC oligomerization and programmed cell death. I also conclude that gaining association to SS15 in the HD1-1 region is sufficient for a helper NRC to be inhibited by this effector.

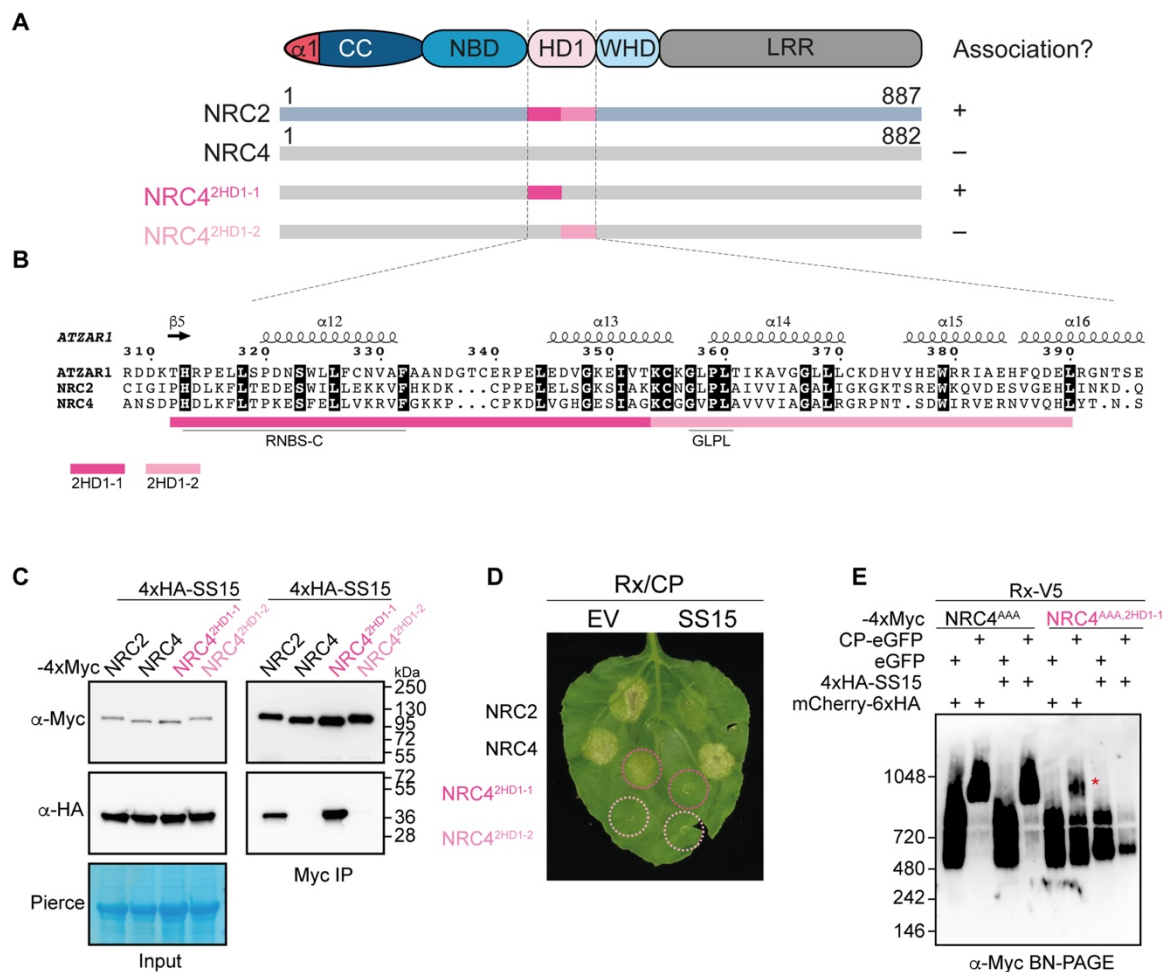


Figure 7.4: The HD1-1 region of NRC NB-ARC domain determines sensitivity to SS15.

(A) Schematic representation of the NRC domain architecture, highlighting regions within the NB-ARC domain swapped between NRC2-NRC4 chimeric proteins. Association (+) or lack thereof (-) between these NLR immune receptors and SS15 determined by in planta co-immunoprecipitation (Co-IP) is detailed on the right. (B) Amino acid sequence alignment of the HD1 region of the NB-ARC domains of AtZAR1, NRC2, and NRC4. Predicted secondary structure is shown above. Well-characterized motifs within this region are underlined below. (C) Co-IP assays between SS15 and chimeric NRC2-NRC4 variants. C-terminally 4xMyc-tagged NRC proteins were co-expressed with N-terminally 4xHA-SS15. IPs were performed with agarose beads conjugated to Myc antibodies (Myc IP). Total protein extracts were immunoblotted with the antisera, as labelled on the left. Approximate molecular weights (in kilodalton) of the proteins are shown on the right. Rubisco loading control was carried out using Ponceau stain (PS). The experiment was repeated three times with similar results. (D) Photo of representative leaves from *N. benthamiana nrc2/3/4* KO plants showing HR after co-expression of Rx/PVX CP with NRC2/NRC4 and the two NRC2-NRC4 chimeras. Combination shown were co-expressed with mCherry-6xHA (EV) or 4xHA-SS15. Three biological replicates with at least six technical replicates each are shown. Quantitative

analyses of the HR phenotypes are found in **Figure AVI.2. (E)** BN-PAGE assay with inactive and activated Rx with NRC4 or an NRC2-NRC4 chimeric protein in the absence or presence of SS15. Effector-sensor-helper combinations shown were co-infiltrated together with mCherry-6xHA or with 4xHA-SS15. Total protein extracts were run in parallel on native and denaturing PAGE and immunoblotted with the antisera, as labelled on the left. SDS-PAGE blots are found in **Figure AVI.3**. Approximate molecular weights (in kilodalton) of the proteins are shown on the left. The experiment was repeated three times with similar results.

7.2.3 SS15 binds and immobilizes a loop in the HD1-1 region to prevent NRC2 oligomerization.

To further define the interface between SS15 and NRC proteins, I attempted to crystallize SS15 in complex with the NB-ARC domain of several NRC proteins. I used previously published constructs to purify SS15 and the NB-ARC of NRC3, which had already been shown to form a complex in vitro (Derevnina *et al.*, 2021). I did not attempt to purify the NB-ARC domain of NRC2 as this was previously shown to be unstable when expressed in *E. coli* (Derevnina *et al.*, 2021). I also attempted purification of the NB-ARC domain of a tomato helper NLR, SINRC1, which is also inhibited by SS15. SINRC1^{NB-ARC} had been previously shown to be easily purified when expressed in *E. coli* and its crystal structure is published (Steele *et al.*, 2019). Fortunately, I was able to obtain crystals of SS15 in complex with the NB-ARC domain of SINRC1. Because crystallization trials of SS15 in complex with NRC3^{NB-ARC} were unsuccessful, I moved forward with the SINRC1^{NB-ARC}-SS15 crystals. In collaboration with Selvaraj Muniyandi, a postdoc in the lab, and Prof. David Lawson from the John Innes Centre Protein Crystallography platform, we solved the structure using X-ray diffraction data collected to 4.5 Å resolution (**Figure 7.5A, Figure AVI.4, Table AVI.1**), which allowed me to determine that SS15 binds to a loop in the HD1-1 region of NRCs which connects the NB domain to the HD1 and WHD domains.

The crystal structure obtained provides orthogonal evidence for the chimera experiments performed (**Figure 7.4**), again pointing to the HD1 region as an interface with biological relevance. The chimera experiments therefore also provide preliminary validation of the structure. In the CC-NLR ZAR1, the region equivalent to the SS15-binding loop was previously shown to act as a “hinge”, allowing the NB domain to rotate relative to the HD1 and WHD domains following activation (**Figure AVI.4, Movie AVI.1**) (Wang *et al.*, 2019b). This led me to hypothesize a mode

of action for SS15 as an NRC inhibitor. SS15 could prevent conformational changes that are critical for NLR activation and resistosome formation by binding and immobilizing the NB-HD1 hinge.

SS15 suppresses cell death induction mediated by SINRC1, NRC2, and NRC3 but not NRC4 or other well-characterized NLRs such as ZAR1 (**Figure AVI.1**) (Derevnina *et al.*, 2021). I therefore took advantage of the high degree of conservation characteristic of plant NB-ARC domains to narrow down residues within the binding interface that underpin this interaction. I shortlisted residues within the HD1-1 region that are similar in SINRC1, NRC2, and NRC3 but different in NRC4 or AtZAR1 in amino acid sequence alignments. Combining information from the co-crystal structure and the alignments allowed me to select 13 candidate residues to test by mutagenesis in NRC2 to further validate the structure (**Figure 7.5A-B**). I also speculated that by mutating these residues, I might be able to bioengineer NRCs to evade inhibition by preventing SS15 binding.

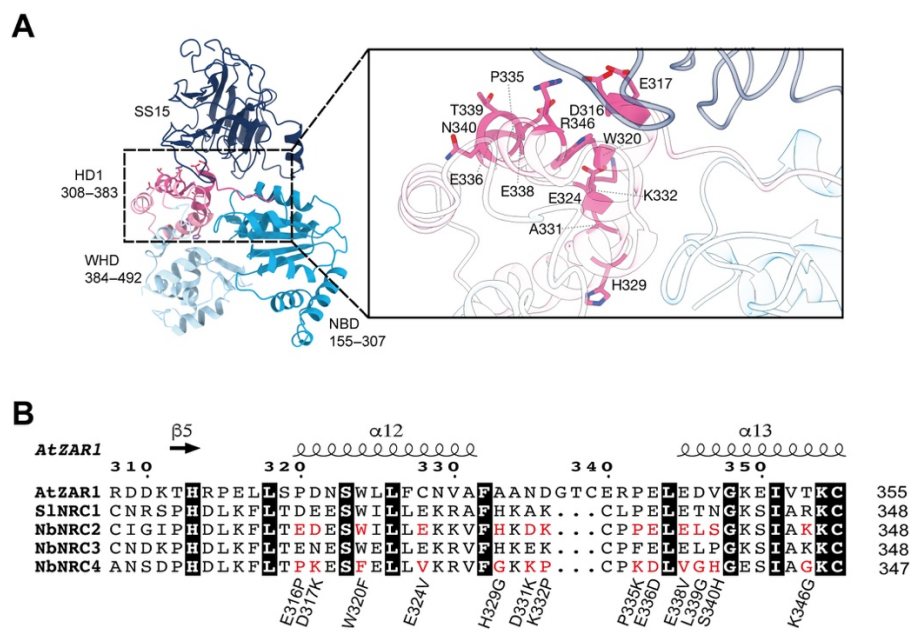


Figure 7.5: Cocystal structure reveals SS15-NRC binding interface and residues contributing to interaction.

(A) Crystal structure of the SS15-SINRC1^{NB-ARC} complex. The NB, HD1, and WHD domains of SINRC1^{NB-ARC} are shown in cyan, pale blue, and magenta, respectively; SS15 is shown in dark blue. The inset displays a close-up image of the SS15-SINRC1^{NB-ARC} HD1 domain interface, with the residues corresponding to those selected for mutagenesis in NRC2 highlighted in stick representation. (B) Alignment of the HD1-1 region of AtZAR1, SINRC1, NRC2, NRC3, and NRC4. Candidate residues (highlighted in red) were shortlisted based on the interface identified in the co-crystal structure of SS15 and SINRC1^{NB-ARC} and

conservation in SINRC1, NRC2, and NRC3 but not NRC4 and AtZAR1. Thirteen NRC2 variants were generated by mutating individual candidate positions to the corresponding amino acid found in NRC4 (detailed underneath the alignment).

7.2.4 Single amino acid variants of NRC2 evade suppression by SS15.

As NRC4 is not inhibited by SS15, I mutated the residues at each of the positions in NRC2 mentioned above to the corresponding amino acid found in NRC4. I screened these NRC2 mutant variants for susceptibility to SS15 inhibition in cell death assays using Rx and PVX CP to activate the system in *nrc2/3/4* KO *N. benthamiana* plants. This revealed that two variants, NRC2^{E316P} and NRC2^{D317K}, which triggered cell death when activated by Rx/PVX CP, could no longer be inhibited by SS15 (**Figure 7.6A, Figure AVI.5**). An additional variant, NRC2^{E324V} was not functional in HR cell death when activated by Rx/PVX CP (**Figure 7.6A**). These results suggested that the E316 and D317 residues in NRC2 play an important role in NRC2-SS15 interactions. Next, I tested all 13 single amino acid mutants for association with SS15 by in planta CoIP and found that NRC2^{E316P} and NRC2^{D317K} exhibited reduced association with SS15 relative to NRC2 (**Figure 7.6B**), which correlates with the observation that SS15 is not able to suppress cell death mediated by these variants. All other NRC2 variants generated retained association to SS15 to similar levels than NRC2, except for NRC2^{E324V}, which did not accumulate in planta (**Figure 7.6B**). The lack of accumulation of NRC2^{E324V} provides an explanation for the absence of cell death when activating this variant with Rx/PVX CP and indicates that this mutation likely compromises NRC2 protein stability. Based on these results, I conclude that the E316 and D317 residues are critical for SS15-mediated inhibition of NRC2, and that mutating these residues to their corresponding amino acid in NRC4 allows Rx/PVX CP-activated NRC2 to evade SS15 association and inhibition.

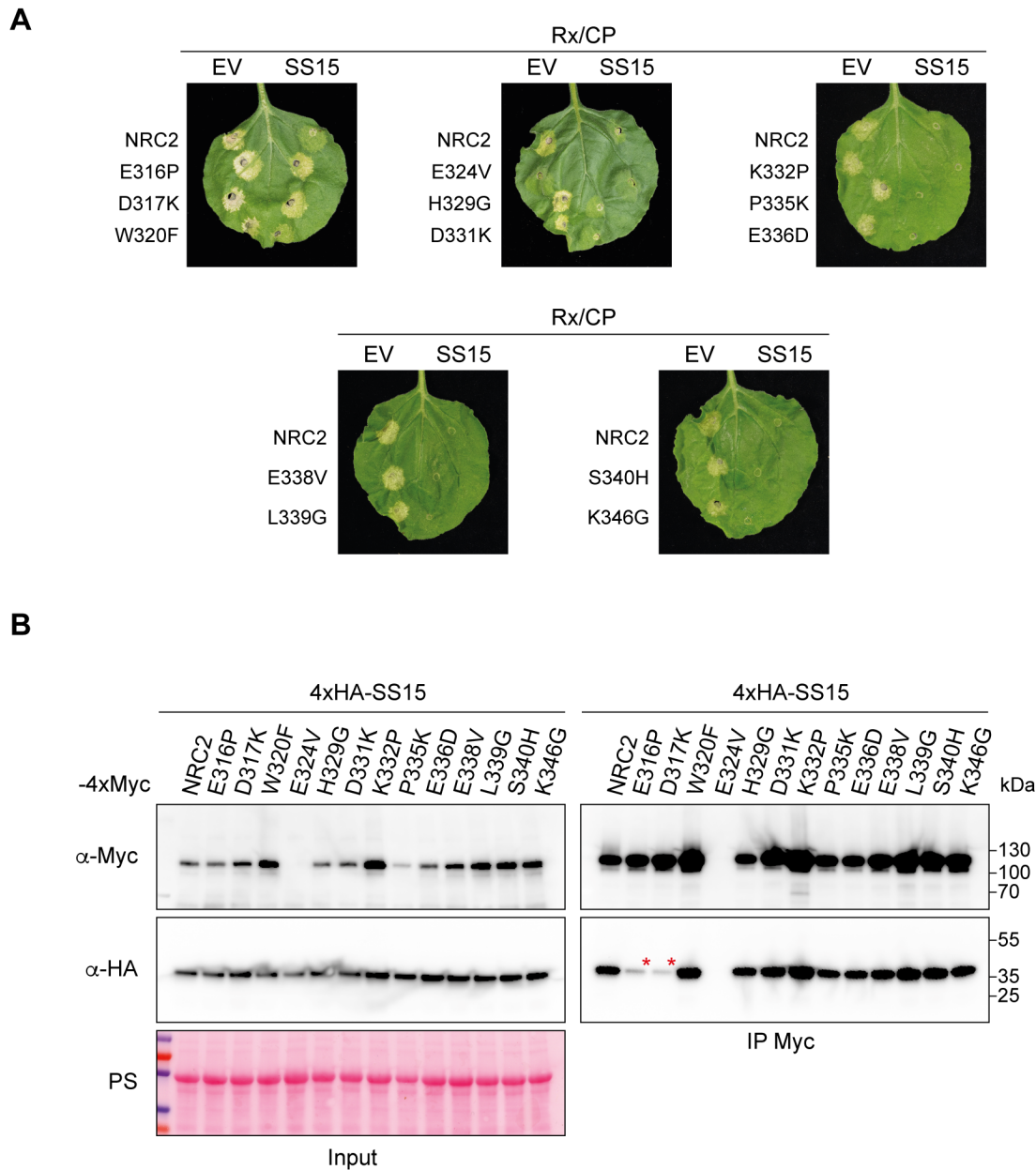


Figure 7.6: Mutagenesis of NRC2-SS15 reveals mutants that evade SS15 association and inhibition.

(A) Photo of representative leaves from *N. benthamiana nrc2/3/4* KO plants showing HR after co-expression of Rx and PVX CP with NRC2, or the different NRC2 variants generated. These effector-sensor-helper combinations were co-expressed with a free mCherry-6xHA fusion protein (EV) or with N-terminally 4xHA-tagged SS15. **(B)** Co-Immunoprecipitation (Co-IP) assays between SS15 and NRC2 variants. C-terminally 4xMyc-tagged NRC2 variants were transiently co-expressed with N-terminally 4xHA-tagged SS15. IPs were performed with agarose beads conjugated to Myc antibodies (Myc IP). Total protein extracts were immunoblotted with appropriate antisera labelled on the left. Approximate molecular weights

(kDa) of the proteins are shown on the right. Rubisco loading control was carried out using Ponceau stain (PS). The experiment was repeated three times with similar results.

7.2.5 A bioengineered NRC2^{D317K} variant resurrects the activity of multiple NRC2-dependent sensors in the presence of SS15.

I next tested whether the SS15-evading variants of NRC2 could restore the functionality of other NRC2-dependent sensor NLRs that are suppressed by the parasite effector. I tested this by performing complementation assays with NRC2^{E316P} and NRC2^{D317K} in *nrc2/3/4* KO *N. benthamiana* plants. I activated the NRC2 variants with a panel of agronomically important sensor NLRs mediating resistance to diverse pathogens, including the potato cyst nematode R protein Gpa2 (an allele of Rx), as well as other well-characterized oomycete and bacterial resistance proteins. NRC2^{D317K} evaded SS15 inhibition with all tested sensor NLRs, restoring their capacity to activate immune signaling in the presence of SS15 (**Figure 7.7A**, **Figure AVI.6**, **Figure AVI.7**). In contrast, NRC2^{E316P} could evade SS15 suppression when activated by Rx, but not when activated by other sensors. I therefore selected NRC2^{D317K} for follow-up biochemical studies, using BN-PAGE–based assays. Unlike NRC2, activated NRC2^{D317K} oligomerized even in the presence of SS15 and did not form an *in vivo* complex with the inhibitor (**Figure 7.7B**). I conclude that NRC2^{D317K} can fully evade SS15-mediated immune suppression, retaining the capacity to oligomerize and mediate cell death when activated by multiple agronomically important sensor NLRs.

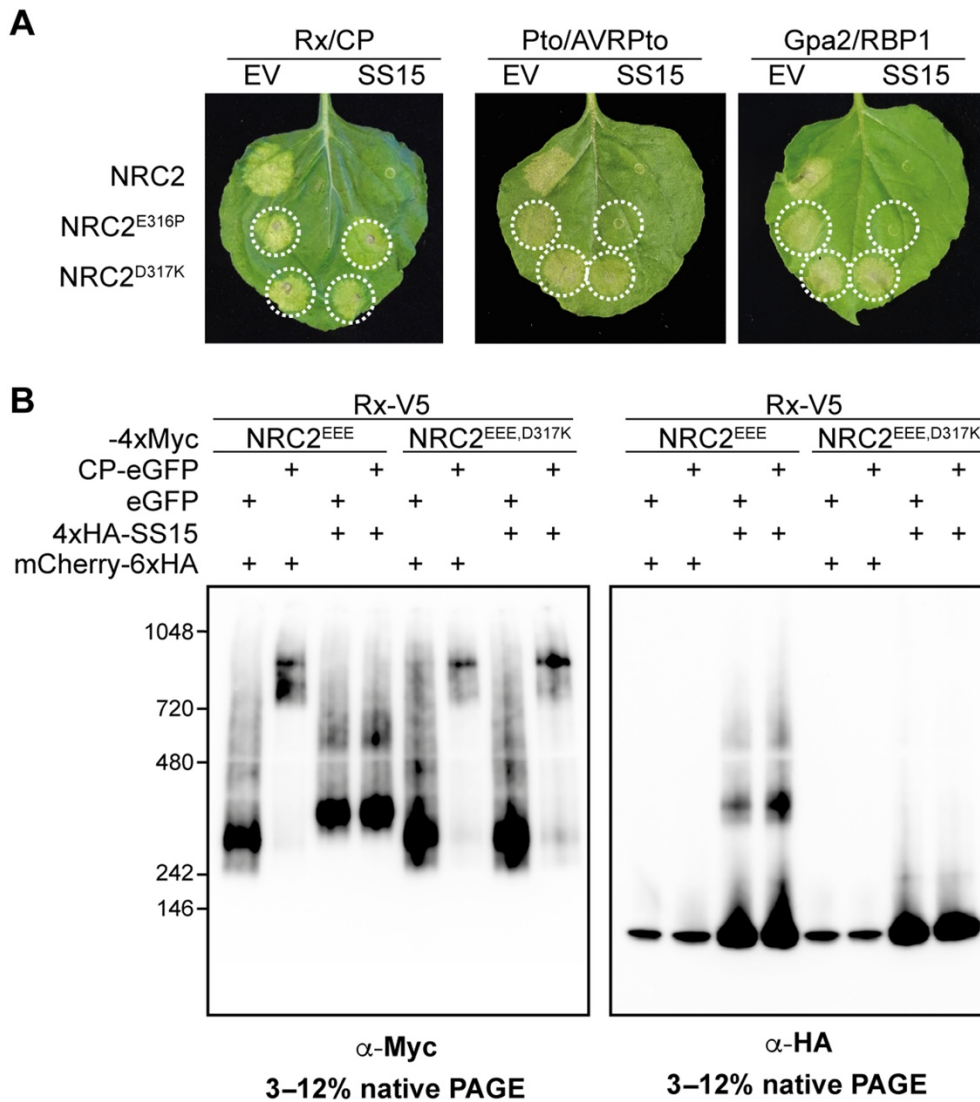


Figure 7.7: NRC2^{D317K} helper restores immune signaling of multiple disease resistance genes in the presence of the effector SS15.

(A) Photo of representative leaves from *N. benthamiana* *nrc2/3/4* KO plants showing HR after co-expression of Rx/PVX CP, Pto/AVR Pto, or Gpa2/RBP1 together with NRC2, NRC2^{E316P}, or NRC2^{D317K} in the absence or presence of SS15. The experiment consisted of three biological replicates. A quantitative analysis of HR phenotypes can be found in **Figure AVI.6**. (B) BN-PAGE assays with inactive and active Rx together with NRC2 or NRC2^{D317K}, in the absence or presence of SS15. C-terminally V5-tagged Rx and C-terminally 4xMyc-tagged NRC2^{EEE} or NRC2^{EEE,D317K} were co-expressed with either free GFP or C-terminally GFP-tagged PVX CP. These effector-sensor-helper combinations were co-expressed together with a 6xHA-mCherry fusion protein or with N-terminally 4xHA-tagged SS15. Total protein extracts were run in parallel on blue native and denaturing PAGE assays and immunoblotted with the appropriate antisera, as labelled below. Approximate molecular weights (in kilodaltons) of the proteins are

shown on the left. Corresponding SDS-PAGE blots can be found in **Figure AVI.7**. The experiment was repeated three times with similar results.

7.3 Conclusions and discussion.

In this chapter, I identified how a parasite effector has evolved as an inhibitor of a helper NLR by directly binding its NB-ARC domain to prevent resistosome formation and immune signaling (**Figure 7.1, Figure 7.2**). By binding and immobilizing a critical hinge loop in the HD1 region of the NB-ARC, SS15 restricts movement of the NB domain relative to the HD1 and WHD domains, preventing immune receptor activation (**Figure 7.3, Figure 7.4, Figure 7.5**). While SS15 can bind and inhibit NRC2, it cannot bind or inhibit the NRC2 paralog NRC4. I exploited NRC4's resilience to SS15 inhibition by making chimeric NRC2-NRC4 variants that, together with structural information to identify the binding interface. Mutational studies of this interface allowed me to generate an amino acid variant of NRC2 (NRC2^{D317K}) that evades SS15 inhibition without compromising receptor signaling capacity. This NRC2^{D317K} variant can now support signaling by any NRC2-dependent sensor even in the presence of SS15 (**Figure 7.6, Figure 7.7, Figure 7.8**).

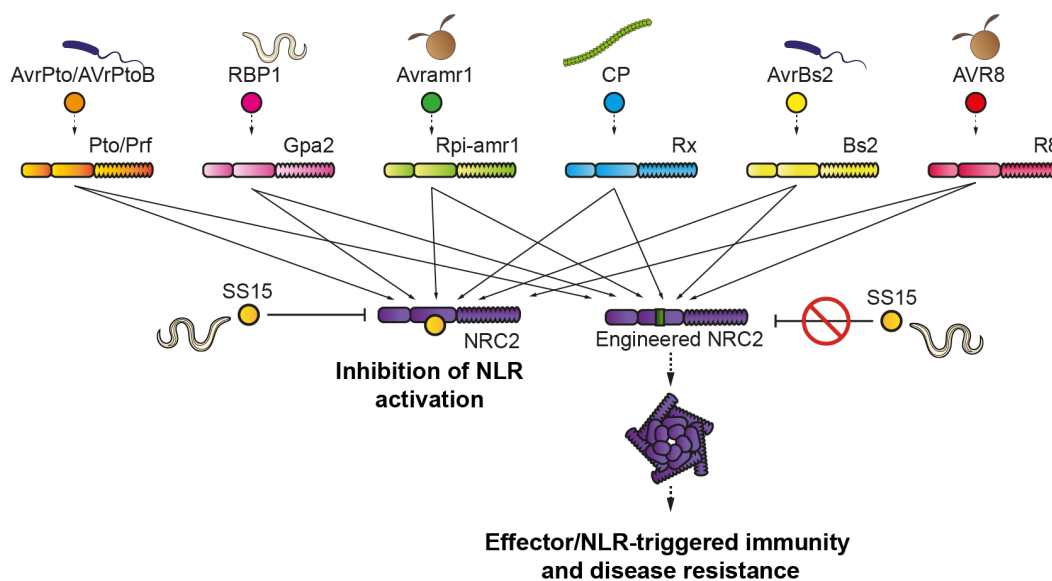


Figure 7.8: Resurrection of sensor NLRs via helper NLR bioengineering.

SS15 blocks binds the NB-ARC domain of NRC2 to inhibit helper NLR oligomerization and resistosome formation. This suppresses signaling by multiple upstream NRC-dependent sensors. By bioengineering NRC2 to prevent inhibitor binding, we can make a helper NLR which simultaneously resurrects signaling by multiple upstream sensor NLRs.

In the future, I will address the conservation of the NRC-SS15 interface across NLR proteins. In particular, understanding the degree of conservation of the NRC-SS15 interface across solanaceous NRCs, notably at position 317, can be of great use. This will allow me to determine whether substitutions analogous to NRC2^{D317K} can be effective at evading SS15 suppression when deployed in NRCs from different solanaceous crop species. Moreover, evolutionary analyses coupled with ancestral sequence reconstruction may enable reconstructing the evolutionary trajectory of the NRC-SS15 interface to gain a deeper understanding of the coevolutionary dynamics between NLRs and their pathogen inhibitors.

The existence of plant parasite secreted NLR inhibitors suggests that suppressed resistance genes may occur in crop genomes. Leveraging the approach detailed in this study, it may be possible to resurrect cryptic or defeated resistance proteins to enhance disease resistance. Moreover, considering that multiple sensors can signal through the same downstream helper, applying this approach to helper NLRs holds potential to simultaneously resurrect multiple upstream sensor NLRs. The single amino acid NRC2 variants I identified could be generated in locus using gene editing technologies in agronomically important crop species, making deployment of this technology viable where transgenic approaches are not feasible. My work describes a potential approach to achieve robust immunity by engineering NLRs that avoid parasite suppression. This could, in theory, be applied to other plant, metazoan, or even prokaryotic NLR immune receptors that are directly targeted by parasite effectors (Derevnina *et al.*, 2021; Gao *et al.*, 2022; Karki *et al.*, 2021; Yen *et al.*, 2015). Combined with recent advances in NLR engineering to bioengineer pathogen recognition specificities (Kourelis *et al.*, 2023; Marchal *et al.*, 2022b), this technology holds the potential to facilitate synthetic disease resistance breeding.

7.4 Research contributions.

I thank Cian Duggan and Yasin Tumtas (Imperial College, London, UK) for assistance with cell biology and membrane fractionation assays. I thank Lida Derevnina (The Sainsbury Laboratory, Norwich, UK) for cloning NRC2-NRC4 chimeric constructs. I thank Selvaraj Muniyandi (The Sainsbury Laboratory, Norwich, UK), Clare E. M. Stevenson and Prof. David Lawson (John Innes Centre, Norwich, UK) for assistance with crystallography, x-ray data collection and solving the structure of SS15 in complex with SINRC1^{NB-ARC}. I thank Hsuan Pai (The Sainsbury Laboratory, Norwich, UK) for general assistance in the lab.

Chapter 8: General discussion

Despite significant advances in our understanding of NLR biology, the mechanisms by which NLR immune receptors activate and translate effector recognition into immune signaling and disease resistance remain poorly understood. The recent cryo-EM structures of the ZAR1, Sr35, Roq1 and RPP1 resistosomes have shed light on our understanding of these mechanisms (Förderer *et al.*, 2022; Ma *et al.*, 2020; Wang *et al.*, 2019a; Wang *et al.*, 2019b; Zhao *et al.*, 2022). It is now becoming clear that conditional oligomerization upon direct or indirect effector recognition appears to be a common mechanism among NLRs from all kingdoms of life, including plants, metazoans and prokaryotes (Chou *et al.*, 2023; Gao *et al.*, 2022). Nonetheless, the cryo-EM structures of activated plant CC-NLR complexes resolved to date correspond to NLRs which fall in the functional singleton category; that is, NLRs that can mediate both pathogen perception and downstream signaling (Adachi *et al.*, 2019b). However, in some cases, these two functions are uncoupled in two functionally specialized immune receptors with a sensor-helper dynamic. Sensor NLRs specialize in effector recognition and rely on helper NLRs to execute immune signaling (Gong *et al.*, 2023). Sensors and helpers exist in one-to-one paired arrangements or in higher order immune receptor networks with “many-to-one” and “one-to-many” sensor-helper connections (Adachi *et al.*, 2019b; Kourelis & Adachi, 2022; Wu *et al.*, 2018). How paired and networked sensor-helper CC-NLRs activate is poorly understood, in large part, due to the lack of tools and genetic backgrounds with which to study activated CC-NLRs in the absence of cell death.

In this thesis, I studied the solanaceous NRC CC-NLR immune receptor network and attempted to understand how sensor-helper pairs in the NRC network activate upon pathogen perception. In Chapter 3, I collaborated with Hiroaki Adachi to study a cell death inducing truncation of the CC-NLR helper NRC4, NRC4₁₋₂₉. This led to the identification of a conserved N-terminal motif found in about 20% of angiosperm CC-NLRs, termed the “MADA” motif, which defines the α 1 helix of the CC domain. Importantly, NRC4-mediated cell death and disease resistance require an intact MADA motif, as mutants in conserved residues within this motif were compromised in these two immune functions (Adachi *et al.*, 2019a). In Chapter 4, I leveraged NRC MADA mutants to carry out biochemical analyses of activated sensor-helper pairs in the NRC network. My experiments led me to propose an activation-and-release model for sensor-helper pairs in the NRC network, where effector perception by sensors leads to oligomerization of downstream helpers into resistosome-like homo-complexes which accumulate at the host plasma membrane, separate from the sensors that activated them (Contreras *et al.*, 2023b). In Chapter 5, I

leveraged previous discoveries by Peter Moffett and colleagues related to Rx autoinhibition and signaling to understand how NRC-dependent sensors communicate with NRC helpers (Moffett *et al.*, 2002; Rairdan *et al.*, 2008; Rairdan & Moffett, 2006). This revealed that the NB domain of multiple sensor NLRs can act as the minimal activation signal for NRC helpers. Based on my data, I propose that previously reported conformational changes of sensor NLRs undergo upon effector perception serve to conditionally expose regions of the NB domain to trigger NRC helpers to oligomerize and initiate immune signaling. These first three chapters expand our mechanistic understanding of sensor-helper activation and communication in the NRC network.

In the two final chapters of this thesis, I leveraged my findings on NRC network activation to determine the mechanism by which two previously identified NRC immunosuppressing effectors, AVRcap1b and SS15, compromise NRC-mediated cell death (Derevnina *et al.*, 2021). In Chapter 6, I studied the NRC2/3-suppressing *P. infestans* effector AVRcap1b and its link to putative host targets, the endosomal sorting complex required for transport (ESCRT)-related Target of Myb 1-like (TOL) proteins. I found that NbTOL9a can negatively regulate NRC2/3-mediated cell death and that AVRcap1b directly interacts with NbTOL9a, likely suppressing cell death by acting as a bridge between TOL proteins and the activated NRC complexes. Finally, In Chapter 7 I leveraged the techniques established in previous chapters to study how the potato cyst nematode effector SS15 suppresses NRC2/3-mediated cell death. My data revealed that SS15 acts as a proteinaceous inhibitor of NRC2 and NRC3, suppressing cell death by binding and likely immobilizing a critical “hinge” loop in the NB-ARC domain which mediates conformational changes upon helper NLR activation. Identification of the SS15-NRC binding interface allowed me to bioengineer NRC2 variants which evade inhibition, thereby resurrecting signaling by multiple upstream NRC2-dependent sensor NLRs in the presence of SS15 (Contreras *et al.*, 2023a).

8.1 The MADA motif: serendipity strikes.

8.2 α 1: the business end of CC domains.

In Chapter 3, I characterized a small 29 amino acid truncated NRC4 variant (NRC4₁₋₂₉) which, when fused to YFP, recapitulates the cell death mediated by full length NRC4^{D478V}. Computational analyses revealed that this region of NRC4, which corresponds to the α 1-helix of the CC domain, is defined by a consensus sequence termed the MADA motif. This motif is present in around 20% of angiosperm CC-NLRs including the NRCs, ZAR1 and Sr35. Importantly, this motif is functionally conserved between ZAR1 and NRC4, as chimeric NRC4 proteins carrying

the MADA motif-containing α 1-helix of ZAR1 retained the capacity to trigger cell death and mediated disease resistance (Adachi *et al.*, 2019a). This led us to first hypothesize that ZAR1 and NRC4 may be operating via analogous oligomerization-based activation mechanisms. Indeed, in Chapter 4 I was able to show that NRCs form oligomers upon activation, further supporting the hypothesis that the resistosome “death switch” model proposed for singleton CC-NLRs likely applies to cell death executing CC-NLR helpers in networked configurations (Contreras *et al.*, 2023b). Recent works have shown that MADA CC-NLRs ZAR1 can act as calcium channels, an activity that has also been assigned to helper NLRs NRG1 and ADR1. Whether NRC oligomers also exhibit calcium channel activity remains to be tested.

How does NRC4₁₋₂₉-YFP trigger cell death? My data suggest that NRC4₁₋₂₉-YFP may require YFP’s capacity to oligomerize, potentially forming a complex analogous to a resistosome in which the α 1-helices of NRC4 are forming a funnel like structure. Indeed, like full-length NRC4, NRC4₁₋₂₉-YFP is visualized as plasma membrane-associated punctate structures which are no longer observed when NRC4₁₋₂₉ when fused to the monomeric YFP^{A206K} variant that cannot form oligomers (Adachi *et al.*, 2019a). Does NRC4₁₋₂₉-YFP fully recapitulate all activities assigned to CC-NLR resistosomes? Whether NRC4₁₋₂₉-YFP functions as a calcium channel and confers disease resistance remains to be tested. It is possible that NRC4₁₋₂₉-YFP is acting as a membrane pore which compromises membrane stability, triggering cell death in a similar manner to pore forming toxins or gasdermins instead of acting as a bonafide calcium channel (Xia *et al.*, 2020). Interestingly, the cell death triggered by NRC4₁₋₂₉-YFP required an intact MADA motif, as NRC4₁₋₂₉^{L9E}-YFP was compromised in cell death induction (Adachi *et al.*, 2019a). This favours the hypothesis that NRC4₁₋₂₉-YFP shares at least some mechanistic commonalities with its full-length counterpart and outlines the importance of the identified MADA motif for some aspects of helper CC-NLR functionality.

Taken together, my data suggests that the N-terminal α 1-helices within the CC domains can encode the minimal regions required for execution of cell death in CC-NLRs. Interestingly, no other truncations in the library generated by Adachi and colleagues were autoactive (Adachi *et al.*, 2019a). Although this could be due to impaired protein stability for many of the truncations generated, it could also suggest that there are intradomain autoinhibitory interactions acting on the CC domain four-helical bundle of NRC4 which prevent spontaneous rearrangement of the α 1-helices into funnel-like structures. This would imply that NLR-NLR interactions and conformational rearrangements that take place upon immune receptor activation can relieve this

intra-CC domain autoinhibition, leading to conditional exposure of the α 1-helix. Some CC domains have been shown to be autoactive when fused to fluorescent proteins, or even when expressed on their own (Bai *et al.*, 2012; Baudin *et al.*, 2017; Casey *et al.*, 2016; Cesari *et al.*, 2016; Wang *et al.*, 2015b). Why some CC domains are autoactive while others aren't is not clear. Moreover, whether the isolated α 1-helices of other CC domains can also trigger cell death when fused to fluorescent proteins remains to be tested. In this sense, NRC4₁₋₂₉-YFP may serve as a reduced experimental system with which to understand the basis for CC-NLR triggered cell death.

8.2.1 MADA mutants: unlocking new possibilities in CC-NLR research.

Importantly, our study of NRC4₁₋₂₉ and the identification of the MADA motif led to an unexpected tool which proved to be invaluable throughout this thesis: MADA motif mutants. In Chapter 3, I showed that mutations in conserved residues within the MADA motif of various CC-NLRs abolishes their cell death inducing activity. Importantly, work in this thesis and in multiple publications revealed that while cell death is abolished, these mutants appear to retain the capacity to oligomerize and relocalize to the plasma membrane upon effector perception (Duggan *et al.*, 2021; Förderer *et al.*, 2022; Hu *et al.*, 2020; Wang *et al.*, 2019a). In Chapter 4, I showed that NRC2^{EEE} and NRC4^{AAA} retain the capacity to oligomerize upon activation by upstream sensors. I also showed that NRC2^{EEE} is capable of dynamically relocalizing upon activation, shifting from cytosolic to PM associated (Contreras *et al.*, 2023b). Two studies on NRC4 and ZAR1, respectively, showed that mutations in the N-terminal MADA-motif containing α 1-helices abolished cell death triggered by these NLRs but had no apparent effect on PM localization (Duggan *et al.*, 2021; Hu *et al.*, 2020). Similar to NRC2^{EEE} and NRC4^{AAA}, ZAR1 and Sr35 with mutated N-termini were still able to form resistosomes (Förderer *et al.*, 2022; Hu *et al.*, 2020). ZAR1 was shown to retain PM association and resistosome formation even when the α 1-helix was completely truncated, although cell death was also abolished (Hu *et al.*, 2020). Resistosome assembly and PM localization are therefore required but not sufficient to mediate cell death. In the case of Sr35, expression in insect cells also triggers cell death in a MADA motif-dependent manner (Förderer *et al.*, 2022), suggesting that no further downstream components are required or that the signaling initiated by these resistosomes can engage with highly conserved pathways present across the plant and animal kingdoms.

How do MADA motif mutations interfere with cell death? Assuming a pentameric NRC resistosome, the MADA motif amino acids mutated in NRC4^{AAA} and NRC2^{EEE} (residues L9, L13, V14 and L17) are predicted to fall on the outer surface of the funnel formed by the five α 1-helices (**Figure 3.2, Figure 4.1, Figure AII.2**). One possibility is that the MADA mutations interfere with the calcium channel activity that was recently assigned to activated CC and CC_R-NLR proteins (Bi *et al.*, 2021; Förderer *et al.*, 2022; Jacob *et al.*, 2021). Alternatively, CC-NLRs with mutated MADA motifs may result in resistosomes that associate with the plasma membrane but are unable to fully penetrate the lipid bilayer to form a functional pore or channel, perhaps due to destabilization of the N-terminal funnel formed by the α 1-helices. Interestingly, mutations in this region unexpectedly rendered the Mla13 allele autoactive (Crean *et al.*, 2023), suggesting that some residues in this motif can be involved in intramolecular autoinhibitory interactions that likely are required to keep the α 1-helix buried in the CC domain four-helix bundle. Similarly, not every MADA mutation in our NRC4 glutamic acid scan led to loss of cell death induction. Each residue or combination of residues likely contributes in a different manner to CC-NLR activities. Further research will dissect the precise role of this N-terminal motif in NRC and CC-NLR-mediated cell death. Nonetheless, MADA mutants are a highly useful tool to study of activated CC-NLRs which will hopefully accelerate CC-NLR research and lead to many more future discoveries in NLR biology.

8.2.2 The MADA motif and CC-NLR N-terminal diversity: the alpha but certainly not the omega.

It should be noted that the MADA motif may be just the tip of the iceberg. This motif is present in about 20% of angiosperm CC-NLRs. What about the other 80%? Or non-angiosperm NLRs? Recent work by Chia and colleagues identified the MAEPL motif, found in the α 1-helices of cell death executing CC-NLRs from non-flowering plant species including algae and gymnosperms. Interestingly, the MAEPL motif exhibits several similarities with the MADA motif, including similarly positioned conserved leucine residues. Much like the MADA motif, the MAEPL motif is required for cell death execution and is functionally interchangeable with the MADA motif of NRC4, suggesting deep evolutionary conservation of NLR immune receptor executioner domains (Chia *et al.*, 2022). Many other such motifs may exist across the green lineage that currently remain undiscovered. Further research may identify additional conserved motifs in plant CC-NLRs. Moreover, a better understanding of CC-NLR N-terminal diversity may help understand the precise contributions of the MADA motif and of the N-termini of CC-NLRs to

cell death induction and immune signaling. Moreover, the 80% of non-MADA containing NLRs includes many CC-NLRs which feature degenerated MADA motifs. This is the case for NRC-dependent sensors which rely on their helpers for cell death induction, as will be discussed below. A broader and more complete picture of CC-NLR N-terminal diversity across the plant lineage will help identify new motifs associated with cell death induction and shed light on how these N-terminal motifs evolved, potentially allowing us to reconstruct how their cell death activity arose.

8.3 Activation and release: a new activation mechanism for NLR networks.

The recent elucidation of multiple plant NLR structures has demonstrated that plant, prokaryotic and metazoan NLRs exhibit functional differences despite several commonalities (Chou *et al.*, 2023; Duxbury *et al.*, 2021). Oligomerization is certainly a shared feature, as evidenced by the metazoan and prokaryotic inflammasomes and the plant resistosome. In this thesis, I propose an activation-and-release working model for sensor-helper pairs in the NRC network (Contreras *et al.*, 2023b). In this working model, effector-triggered activation of a sensor NLR leads to intramolecular conformational changes. These conformational changes are sensed, either directly or indirectly, by downstream helpers which subsequently activate, oligomerize and form resistosomes. The activated helper complexes then part ways with their sensors and re-localize to the plasma membrane where they initiate immune signaling and cell death induction. It is possible that transient intermediates exist in which sensors interact with their helpers to trigger their activation. This might be analogous to the first steps of NAIP/NLRC4 activation in which the sensor nucleates polymerization of the NLRC4 inflammasome (Zhang *et al.*, 2015). However, BN-PAGE assays with differently sized versions of Rx with NRC2 and confocal microscopy suggest that a stable hetero-complex scenario is unlikely for the mature activated Rx-NRC2 system. This points to a biochemical model for plant paired NLR activation that differs from activation processes previously characterized for metazoan NLR pairs. I conclude that plant and metazoan paired and networked NLRs exhibit distinct activation mechanisms and biochemical processes. Whether this activation-and-release model applies to other paired plant CC-NLRs or even other paired metazoan or prokaryotic NLRs remains to be tested.

8.3.1 Sensor-helper activation in the NRC network: immune receptor specialization at its finest.

The activation and release model for the NRC network nicely complements previous evolutionary models proposed for this NLR network based on phylogenetic structure. Studies by the Kamoun lab proposed that this solanaceous network expanded from an ancestral sensor-helper pair which itself evolved from an ancestral functional singleton CC-NLR by duplication and sub-functionalization events (Adachi *et al.*, 2019a; Adachi *et al.*, 2019b; Wu *et al.*, 2017; Wu *et al.*, 2018). Singleton CC-NLRs, such as ZAR1 and Sr35, feature an intact MADA motif and form pentameric resistosomes upon activation. In CC-NLR pairs and networks, sensors specialize in effector perception and have lost the capacity to oligomerize and form resistosomes. Some sensors also acquired novel effector perception domains, such as the SD domain found in the N-termini of many NRC-dependent sensors. While NRC-dependent sensors have lost the capacity to form resistosomes, they conditionally undergo conformational changes upon effector perception which lead to activation and resistosome formation of helper CC-NLRs. The evolution of a system in which the sensors do not need to participate in the mature resistosome likely facilitated the acquisition of novel domains, as N-terminal domain integrations would likely complicate the assembly of a sensor-helper heterocomplex if the sensors participated as a “spoke” in the resistosome wheel.

Helper NLRs oligomerizing separately from their upstream sensors is an emerging theme in immune receptor networks. In some ways, the activation and release model for the NRC network is analogous to the activation mechanism found in the NRG1/ADR1 network, in which TIR-NLR sensors trigger activation of downstream helper oligomers which form resistosomes independently of their upstream sensors (Feehan *et al.*, 2023; Gong *et al.*, 2023; Jacob *et al.*, 2021; Jia *et al.*, 2022; Sun *et al.*, 2021). These activation mechanisms likely contribute to the evolvability and robustness that is characteristic of NLR networks and serve as a means to amplify immune signals (Wu *et al.*, 2018). However, unlike sensor CC-NLRs in the NRC network, TIR-NLRs in the NRG1/ADR1 network form tetrameric resistosomes in which the N-terminal TIR domains exhibit enzymatic activity. This enzymatic activity is what indirectly activates downstream helpers via the EDS1 signaling hub (Huang *et al.*, 2022; Jia *et al.*, 2022; Ma *et al.*, 2020; Martin *et al.*, 2020). In the case of the NRC network, no enzymatic activity has been assigned to CC-NLRs to date and how NRC-dependent sensors activate helpers is not known. It should be noted that Rx constitutively forms a complex of a higher molecular weight than what would be expected for an Rx monomer (Contreras *et al.*, 2023b). This, however, appears to be an Rx specific phenomenon as no such complexes were observed for Rpi-amr1 and Rpi-amr3 (Ahn *et al.*, 2023). This difference may simply reflect differences in effector recognition mechanisms, as Rpi-amr1 and Rpi-amr3 are

proposed to directly recognize their cognate effectors and therefore do not need to form complexes with other host proteins (Ahn *et al.*, 2023; Lin *et al.*, 2022b), whereas Rx recognition of PVX CP is proposed to be indirect and mediated by co-factors such as RanGAP2. Rx is therefore likely that Rx is constitutively in complex with host proteins, similar to how ZAR1 constitutively associates with its partner receptor-like cytoplasmic kinases (Baudin *et al.*, 2017; Hu *et al.*, 2020; Lewis *et al.*, 2013; Seto *et al.*, 2017; Tameling & Baulcombe, 2007).

Sensor NLRs rely on helpers for cell death induction and as a result typically have degenerated N-terminal MADA motifs or contain N-terminally fused domains such as the SD. In contrast, cell death executing helpers retain a functional, N-terminal MADA motif. This has been termed the “use it or lose it” model, in which immune receptor specialization has led to regressive evolution in the form of MADA motif degeneration (Adachi *et al.*, 2019a; Adachi *et al.*, 2019b). While both sensors and helpers have lost certain activities present in their singleton ancestors, different domains within sensors and helpers have likely acquired new sets of functions because of this sub-functionalization. While an intact CC domain is required for NRC-mediated cell death, the observation that the NB domain of Rx and Gpa2 is sufficient to activate helpers suggests that their CC-domain is not required for communication with helper NLRs for downstream signaling. Interestingly, in the case of these two sensors, their N-terminal CC domains have been shown to interact with RanGAP2 and this interaction has been shown to be required for disease resistance (Tameling & Baulcombe, 2007; Tameling *et al.*, 2010). Perhaps in some NRC-dependent sensors the CC domain has foregone signaling functions and became a platform to mediate NLR-host protein interactions or to facilitate effector perception.

8.3.2 A swift response: re-localization of helpers upon pathogen infection.

In this thesis, the PVX pathosystem allowed me to study paired NLR activation during pathogen infection, taking the state-of-the-art of NLR biochemistry beyond activation with effector proteins. This work complements previous studies on NLR oligomerization upon heterologous expression of cognate effectors (Duxbury *et al.*, 2020; Hu *et al.*, 2020; Li *et al.*, 2020; Ma *et al.*, 2020; Martin *et al.*, 2020; Williams *et al.*, 2014), showing that the same mechanism likely applies during infection by pathogenic organisms. Investigating the oligomeric state and subcellular localization of paired/networked NLRs upon infection will provide further insights into the mechanisms and dynamics that underpin NLR-mediated immunity. The NRC4 helper can focally accumulate at the interface between *P. infestans* and the host plant at the site where effectors are

delivered before re-localizing and forming discrete puncta at the PM following activation (Duggan *et al.*, 2021). Interestingly, the puncta observed for activated NRC2 and NRC4 are distributed throughout the PM of the cell. What is the exact nature of these puncta, how many resistosomes accumulate in the observed PM micro-domains and whether they form macro-complexes remain open questions.

8.4 Rx as a model NLR: building on solid ground.

8.4.1 Rx intramolecular rearrangements: no resistosome but still complex

The study of the CC-NLR Rx has led to many important discoveries in NLR biology and helped to establish many fundamental concepts of NLR biology (Bendahmane *et al.*, 2002; Moffett *et al.*, 2002; Rairdan *et al.*, 2008; Rairdan & Moffett, 2006). Previous work by Moffett and colleagues showed that Rx domains could complement each other when expressed in trans and trigger cell death upon co-expression with PVX CP (Moffett *et al.*, 2002). This highlights the high degree of modularity exhibited by these proteins. Indeed, recent studies have found that in prokaryotes, NOD-TPR proteins work together with Bell signaling domains encoded in separate genes. The signaling domains assemble with the NOD-TPR protein via the N-terminus of the NOD, assembling into a protein analogous to a tripartite canonical NLR (Dyrka *et al.*, 2020). Based on the observation that Rx N-terminal and C-terminal halves associate when expressed in trans, a similar mechanism might apply for Rx. This suggests that the intramolecular interactions found in full-length Rx are sufficient to bring separately expressed domains together and reconstitute a functional NLR.

Although in our assays Rx does not exhibit significant changes in oligomerization upon PVX CP perception (Contreras *et al.*, 2023b), the previously reported association and PVX CP-triggered dissociation of the Rx halves suggest that it undergoes significant intramolecular rearrangements upon activation (Moffett *et al.*, 2002). The Rx halves associate with each other independently of the presence of their helpers. Evidently, NRCs are not needed as a scaffold for these two halves to interact. However, NRC2 with an intact MADA motif was required for the dissociation of the Rx^{CCNBARC} and Rx^{LRR} halves. Co-expression of the Rx halves with PVX CP in the absence of NRC helpers did not lead to dissociation of the separate Rx domains. Complementing the system with NRC0, a helper that Rx cannot activate, was not enough to restore the Rx halves dissociation. This implies that there may be trans-activation taking place

between NRC2 and the Rx halves that leads to conformational changes in Rx and dissociation of its domains upon PVX CP perception. This hypothetical trans-activation would require an intact MADA motif, as the NRC2^{EEE} mutant did not complement the dissociation of the Rx halves upon co-expression with their cognate effector. Importantly, the ongoing cell death in the treatment with PVX CP, Rx halves and NRC2 led to decreased protein accumulation which complicates interpretation of these results. Moffett and colleagues used SGT1 silencing to abolish cell death triggered by Rx rather than *nrc2/3/4* KO *N. benthamiana* lines, so our experimental setups differ (Moffett *et al.*, 2002). Further experimentation is needed to clarify what intra and intermolecular interactions take place upon sensor NLR activation.

Although my experiments with the Rx halves suggest that Rx^{LRR} engages in non-specific interactions, at least part of the Rx^{LRR} population retains the capacity to co-operate with Rx^{CCNBARC} to translate PVX CP perception into activation. BN-PAGE assays with the Rx halves revealed that unlike the Rx^{LRR}, which is visualized as high molecular weight smears, the Rx^{CCNBARC} is visualized as more discrete bands of molecular weight that resembles full-length Rx, albeit migrating slightly faster. This could imply that the Rx^{CCNBARC} is forming more ordered complexes that resemble full-length Rx, perhaps even interacting with endogenous host proteins required for PVX CP perception. Rx^{LRR} is visualized in a range of molecular weights, suggesting that it may be interacting non-specifically with various proteins or perhaps even forming LRR-LRR aggregates or complexes when it is expressed separately from Rx^{CCNBARC}. The precise contributions of each Rx domain to NRC activation require further investigation.

8.4.2 Sensor NLR NB domains: A Rosetta stone to decoding the sensor-helper language.

Importantly, by leveraging *nrc2/3/4* KO *N. benthamiana* lines I was able to show that the NB domain of Rx and other NRC-dependent sensor NLRs can trigger cell death via canonical NRC-dependent pathways, leading to helper oligomerization and MADA-motif dependent cell death. The NB domain can encode the minimal helper activation unit, suggesting that other domains of the sensor could mainly contribute towards autoinhibitory interactions and pathogen perception, not helper activation. In turn, NRCs can perceive the NB domain of various sensor NLRs as an activation signal. I propose that helper CC-NLRs may have evolved to detect conserved features of sensor CC-NLR activation, encoded in the NB domain. This would be analogous to how helper CC_R-NLRs NRG1 and ADR1 can “sense” the TIR-NLR resistosome-

mediated assembly of the EDS1-PAD4 and EDS1-SAG101 dimers. EDS1 heterodimer assembly is a signature TIR-NLR activation and CC_R-NLR helpers translate it into resistosome formation (Gong *et al.*, 2023). In contrast to the NRG1/ADR1 network, CC-NLR sensors have not been assigned any enzymatic activity to date. Moreover, the sensor's NB domain can recapitulate the outcome of full-length sensors for helper activation even when nucleotide binding is presumably abolished by mutations in the conserved p-loop. These observations make an indirect small molecule or ATP hydrolysis-based mechanism unlikely. Based on the available data, it is tempting to speculate that the NB domain is being physically perceived by helpers. Perhaps NRCs can physically “sense” the exposure of the NB domain of their upstream sensors and in turn activate, analogous to effectors acting on NLR sensors. Considering that the NB-ARC is the most conserved feature of the NLR family and that NB-ARC/NACHT conformational changes are a hallmark of NLR activation across all kingdoms of life (Chou *et al.*, 2023; Gao *et al.*, 2022; Kourelis *et al.*, 2021; Wang *et al.*, 2019b), sensing specific conformational changes or states in sensor CC-NLR NB-ARC domains that are indicative of immune receptor activation would seem like an effective strategy for helper CC-NLRs. NRC helpers may be constantly monitoring the activation state of sensors, becoming activated upon detection of conformational changes in sensor NLRs. Combined with an activation and release model in which sensors activate and release their helpers, one activated sensor can in turn activate multiple helper NLRs.

Although the NB domain of Rx alone is sufficient to activate NRCs, expression of Rx^{CCNBARC} and Rx^{NBARCLRR} does not lead to NRC activation. Evidently, there is autoinhibition exerted by both the CC and LRR domains on the NB-ARC domain, or perhaps intra-NB-ARC domain inhibition keeping the NB domain in a conformation not suitable for activating NRCs. Moreover, each Rx half on its own cannot perceive PVX CP and convert perception into activation in the absence of the other Rx half. Although the CC domain of Rx has been implicated in pathogen perception and has been shown to play a role in interaction with co-factors, the LRR of Rx has major contributions to effector perception. Moffett and colleagues showed that full-length Gpa2, which cannot recognize PVX CP, can complement Rx^{NBARCLRR} in trans and mediate CP-triggered cell death (Moffett *et al.*, 2002). This suggests that while the CC domain is required for signaling, it is possible that the LRR is determining the effector recognition specificity. Indeed, random mutagenesis studies by Farnham and Baulcombe revealed that mutations in the LRR, but not the CC domain, can expand the recognition specificity of Rx, allowing it to recognize additional strains of PVX as well as the distantly related poplar mosaic virus (Farnham & Baulcombe, 2006). One could envision the CC domain being involved in interaction with co-factors and having

autoinhibitory effects on the NB, and the LRR determining effector recognition specificity. It is possible that there are inter-domain trans-activation events taking place that are required for signaling. For example, following CP perception, the Rx^{LRR} may be triggering changes in the $Rx^{CCNBARC}$ and vice-versa, leading to exposure of the NB domain and full activation. This would also explain why the $Rx^{CCNBARC}$ with a mutated MHD motif still requires the Rx^{LRR} to trigger cell death (Moffett *et al.*, 2002). Given that the NB domain of Rx has been shown to be sufficient for signaling, one could predict the $Rx^{CCNBARC}$ with a mutated MHD motif ($Rx^{CCNBARC-D460V}$) to be able to release its autoinhibition and activate. The fact that $Rx^{CCNBARC}$ with a mutated MHD requires Rx^{LRR} to trigger cell death suggests that there are autoinhibitory interactions within $Rx^{CCNBARC}$ that require Rx^{LRR} to be relieved.

The precise contributions of the eGFP tag in Rx^{NB} -eGFP-mediated activation of NRCs are not well understood. While eGFP could just be helping stabilize an otherwise unstable protein, it is also possible that eGFP is contributing to steric clashes that are required for helper activation assuming sensor-helper physical interactions. It is also possible that, as in the case of $NRC4_{1-29}$ -YFP, eGFP is acting as an oligomerization scaffold for Rx^{NB} , with Rx^{NB} oligomers leading to helper activation. Indeed, my BN-PAGE studies revealed that Rx^{NB} -eGFP is visualized as two bands, with one of them corresponding to a putative Rx^{NB} -eGFP complex. Whether this complex has any biological relevance or whether it is an artifact of the tag is unclear. Further studies using monomeric GFP variants and testing additional tags may help address these hypotheses.

8.4.3 NB domain-mediated helper activation: how did we get here?

How has an NB-based activation mechanism evolved? In the case of singleton NLRs such as ZAR1, individual protomers are proposed to assemble into oligomers following ADP release triggered NLR priming (Wang *et al.*, 2019a; Wang *et al.*, 2019b). However, we do not know whether two primed ZAR1 intermediates can trans-activate to drive oligomerization, or whether a single primed ZAR1 monomer can act as a polymerization scaffold for other ZAR1 protomers, as is the case for the metazoan NAIP/NLRC4 system (Zhang *et al.*, 2015). The precise dynamics of singleton NLR resistosome assembly are not fully understood. In the hypothetical singleton NLR ancestor that gave rise to the NRC network, NLR protomers could oligomerize via such trans-activation-based mechanisms in which the NB-ARC or NB domain of a single activated immune receptor can drive conformational changes in other protomers, amplifying immune activation in a prion like fashion. Over evolutionary time, as singletons give rise to pairs and networks, the sub

functionalization of immune receptors into sensors and helpers may have resulted in sensors losing the capacity to oligomerize, but retaining a prion-like function, conditionally activating a helper oligomerization cascade. One important question that I have not addressed in this thesis is whether NB domains from sensors are the only NB domains capable of driving helper oligomerization in the NRC network. Perhaps isolated helper NB domains can also activate a helper oligomerization cascade in a prion like fashion. Moreover, can NB domains of NRC-independent sensors activate their corresponding helpers or is this mechanism unique to the NRC network? Does this NB domain-mediated activation of helpers require other host co-factors? Further experiments and evolutionary analyses will allow us to understand how widespread this activation mechanism is and how it evolved.

Interestingly, most of the Rx-like clade sensors tested retained the capacity to activate NRCs as NB domain only constructs, while none of the SD-clade containing sensors tested triggered NRC activation. Even within the NRC network this NB domain-based activation mechanism does not always apply. It is possible that the NB-ARC domains of SD-type sensors have mutated to accommodate the N-terminal SD fusion, leading to different activation dynamics or mechanisms compared to Rx-type sensors. Interestingly, the SD containing sensor Sw5-b can trigger cell death as an Sw5-b^{NB-ARC}-GFP fusion (De Oliveira *et al.*, 2016). It is possible that for SD-containing sensors, the whole NB-ARC or residues of the ARC region in addition to the NB domain are required as a minimal unit to activate helpers. How the NB-ARC domains of SD-containing sensors have evolved to accommodate SD-fusion and how this has impacted sensor-helper communication and helper activation remains an open question.

8.4.4 Understanding sensor-helper specificity.

Interestingly, the NB domains of Rx, Gpa2 and Rpi-amr1e retained the helper specificity profiles of their full-length counterparts. While we cannot rule out that other domains in the sensor are contributing to sensor-helper specificity, it appears that this specificity is at least partly encoded in the NB domain. The NB domain of sensors are not a one-size-fits-all NRC activator, but selectively activate a subset of NRCs. Interestingly, by studying differences in Rx and Gpa2 strength of NRC4 activation, I identified residues that when mutated, can increase the efficacy by which Gpa2 activates NRC4. These residues are predicted to be surface-exposed and do not impact protein stability. It is tempting to speculate that NB domains interact physically with NRCs leading to their activation, and that these surface exposed residues are involved in mediating sensor

NLR-NRC interactions. Polymorphisms in these residues lead to differences in sensor-helper communication efficiency or may determine sensor-helper compatibility. Understanding which regions within sensor or helper NLRs contribute to sensor-helper communication and specificity may help engineer broader sensor-helper compatibilities. Why do some sensors signal through NRC2, NRC3 and NRC4 and some can only signal through a subset of available helpers? Is this due to sensors hyperspecializing to more efficiently activating some helpers, leading to more efficient signaling? Is it an undesired consequence of co-evolution with effectors? Further studies on the molecular basis and evolution of sensor-helper specificity may help answer these questions.

8.4.5 Disease resistance without death?

Whether the immune activation mediated by Rx^{NB} can recapitulate all immune signaling mediated by full-length Rx remains to be shown. For example, can Rx^{NB} mediate disease resistance against PVX? Previous reports have suggested that Rx is capable of mediating disease resistance against PVX without triggering cell death (Bendahmane *et al.*, 1999). Are there any NRC-independent immune responses mediated by activated full-length Rx that are not mediated by Rx^{NB}? It is possible that the NB domain of Rx is important for NRC activation and cell death, but other domains of Rx are engaged in immune signaling activities that are important for PVX resistance and that are independent of cell death. Interestingly, in Chapter 4 I showed that *nrc2/3/4* KO *N. benthamiana* plants complemented with Rx and NRC2^{EEE} were unable to mediate resistance to PVX, as the virus was capable of accumulating in this treatment to the same level of plants not expressing Rx (Contreras *et al.*, 2023b). This suggests that NRC helpers with an intact MADA motif are required for Rx to mediate disease resistance against PVX. Although the MADA motif has been shown to be required for cell death, perhaps it is mediating other cell-death independent responses. Moreover, Kourelis and colleagues recently showed that the Pikobody system, a synthetic NLR system derived from rice resistance genes against the fungus *Magnaporthe oryzae*, could be engineered to confer resistance to PVX strains expressing GFP. The levels of resistance provided by the Pikobodies were comparable to Rx (Kourelis *et al.*, 2023). Although whether the Pikobodies are triggering cell death-independent responses that are also contributing to viral resistance is not known, these results suggest that cell death could be sufficient for viral resistance. The precise contributions of sensors, helpers, and their individual domains to disease resistance are not fully understood. Moreover, whether disease resistance against PVX is truly cell death independent requires further experimentation.

8.5 Effectors as both activators and suppressors of NLRs.

8.5.1 NRC suppression by AVRcap1b and SS15: different approaches with common themes.

By studying SS15 and AVRcap1b, two NRC-suppressing effectors from the potato cyst nematode *Globodera rostochiensis* and the potato late blight oomycete *Phytophthora infestans*, I attempted to gain insights into the molecular mechanisms by which pathogen effectors can suppress NLR activation. In particular, the study of AVRcap1b presented the unique opportunity to help characterize the role of a novel player in regulation of programmed cell death in plants, TOL proteins. While both effectors suppress NRC2 and NRC3-mediated cell death, my data revealed different suppression mechanisms. AVRcap1b doesn't block resistosome formation and functions downstream of helper activation. Remarkably, it associates specifically with the activated form of NRC2. Moreover, AVRcap1b doesn't suppress NRC2 on its own, as it requires host TOL proteins to execute its virulence activities. NbTOL9a is a negative regulator of NRC2/3-mediated cell death which AVRcap1b co-opts to suppress immunity (Derevnina *et al.*, 2021). Interestingly, TOL proteins were shown to be proximal to the bacterial effector AvrPto, suggesting that other pathogens may be hijacking TOL-related pathways in order to promote virulence (Conlan *et al.*, 2018). SS15 on the other hand, can interact directly with inactive or activated NRCs, functioning as a direct inhibitor that blocks resistosome assembly (Contreras *et al.*, 2023a; Derevnina *et al.*, 2021). Unlike AVRcap1b, SS15 does not appear to require any co-factors to inhibit NRC activation. SS15 binding to NRCs is sufficient to trigger immune suppression. Blocking NLR oligomerization via direct binding is not a mechanism unique to plant pathogens. Metazoan pathogens have been shown to deploy effectors that block inflammasome assembly as well. Enteropathogenic *E. coli* deploys the NleA effector that directly binds to NLRP3 to block inflammasome assembly (Yen *et al.*, 2015). The Kaposi's sarcoma-associated herpesvirus (KSHV) encodes a truncated NLR with homology to NLRP1 which blocks host NLRP1 oligomerization (Gregory *et al.*, 2011). Directly targeting NLRs therefore is a mechanism conserved across distantly related pathogens that infect diverse hosts.

Despite these differences in their mechanisms of suppression, there are some commonalities. The mode of action of both effectors involves association with NRCs, albeit in different stages of their activation. AVRcap1b associates with activated NRCs and does not block resistosome formation. SS15 interacts with a loop in the NB-ARC of NRCs that connects the NB

domain to the HD1 and which mediates critical conformational changes required for immune receptor activation, and can interact with inactive NRCs (Contreras *et al.*, 2023a). Importantly, by breaking the interaction between NRCs and SS15 binding, we can bioengineer helper variants that evade inhibition by this effector. Identifying the interaction interface between AVRcap1b and NRCs remains an important unanswered question, and the current hypothesis is that AVRcap1b interacts directly with NRCs via its C-terminal LWY7 domain. If we identify residues in NRCs that encode susceptibility to suppression by AVRcap1b, we may be able to employ a similar strategy to create immune receptor variants that evade suppression by this *P. infestans* effector as with SS15.

It is quite striking that both NRC-suppressing effectors are targeting NRC2 and NRC3 but that no effectors acting on NRC4 were found as part of our screen (Derevnina *et al.*, 2021). Importantly, recent findings by Kourelis and colleagues revealed that NRC3 is downstream of cell-surface receptors such as Cf-4, and that SS15 and AVRcap1b can suppress Cf-4 mediated cell death by targeting NRC3 (Kourelis *et al.*, 2022). NRC2 was also shown to be capable of contributing to Cf-4 signaling. It is possible that multiple cell-surface receptors require NRC2 or NRC3 and that targeting these helpers is particularly advantageous for pathogens, as it can lead to simultaneous suppression of cell-surface and intracellular immunity. Moreover, SS15 can suppress Cf-4 mediated cell death suggesting that cell-surface receptors require NRC resistosome formation for cell death induction. Whether cell-surface receptors are communicating directly with NRC helpers or whether helper activation is mediated by NRC-dependent sensors that guard components of cell-surface immunity is not known. Regardless, it appears that NRC3 and NRC2 are particularly good targets for pathogen effectors, presumably as they are central nodes in PRR/NLR networks.

8.5.2 NLR suppression: a double-edged sword for pathogens.

Although directly interfering with NLR activities can lead to robust suppression of immunity, particularly when effectors target helper NLRs that are required downstream of multiple sensors, this is not without potential drawbacks. Effector-NLR interactions that have evolved as a means for the effector to suppress NLR-mediated signaling could conceivably evolve into an interaction that leads to NLR activation, turning the suppressor into an AVR. Moreover, because key immune nodes are often guarded by NLRs, interfering with NLR activities may lead to immune detection. The bacterial effector AvrPtoB has recently been shown to interfere with host immunity

in *Arabidopsis* by targeting ADR1-L1 and ADR1-L2 for degradation. However, the TIR-NLR SNC1 guards ADR1-L1 and ADR1-L2 in and can sense perturbation of these two helpers to activate immunity via ADR1, which is not targeted by AvrPtoB (Wang *et al.*, 2023a). Like AvrPtoB, AVRcap1b and SS15 are AVRs in some plant species. AVRcap1b and SS15 are recognized by unknown NLRs in *Solanum capsicibaccatum* and *Nicotiana tabacum*, respectively (Ali *et al.*, 2015; Rietman, 2011). How they are recognized remains unknown, but considering the important role the NRC network plays in solanaceous immunity it is tempting to speculate that there are NLRs guarding NRCs in *S. capsicibaccatum* and in *N. tabacum* which can recognize immune suppression exerted by these two effectors. The NRCs are important for both cell-surface and intracellular immunity in solanaceous plants and are targeted by pathogens and as such, would be an ideal immune node for NLRs to guard. Further work will hopefully clarify whether NRC helpers are guarded by other NLRs, in a similar fashion to the ADR1 helpers.

8.5.3 Gene-for-gene 2.0.

The existence of pathogen effector-NLR interactions in the context of suppression suggests that there is additional complexity to the intricate NLR evolutionary landscape. Harold Flor's gene-for-gene model paired each avirulence gene from a pathogen with a resistance gene from the host plant (Flor, 1971). We previously considered NLR evolution to be driven by the necessity of NLRs to detect and keep up with rapidly evolving pathogen effectors that are constantly attempting to avoid recognition, while avoiding mis-activation or incompatibility with other downstream genetic components required for NLR signaling (Barragan & Weigel, 2021). This paradigm becomes more complex, as coevolution between NLRs and their suppressors needs to be considered. While NLRs are likely under positive selection to evade suppression by effectors, effectors are evolving to maintain said suppression. The fact that effectors can act as both a suppressor and a trigger of immunity highlights the complexity of NLR-effector coevolutionary dynamics, as effectors can be co-evolving with two NLRs simultaneously, trying to suppress one of them while attempting to evade recognition from the other. Studying these effectors holds the potential to uncover new components of the plant immune system, to shed light on NLR-effector coevolution and to unlock a new wave of strategies for R-gene discovery, bioengineering and deployment.

8.5.4 Pathogen suppression of NLRs: the dark matter of R-gene discovery.

One question raised by the existence of effectors that suppress NLRs is: How many R genes are currently present in crop genomes that have remained cryptic due to pathogen suppression? The presence of hitherto unknown NLR suppressors may have masked many potential R-genes. This R-gene masking becomes even more severe if pathogens suppress helper NLRs, which could be inhibiting multiple different sensor NLRs simultaneously (Contreras *et al.*, 2023a; Derevnina *et al.*, 2021; Wang *et al.*, 2023a). Pathogen NLR suppressors may even explain some cases in which NLR genes cannot be successfully transferred between plant families, also known as restricted taxonomic functionality (RTF) (Tai *et al.*, 1999). While in most cases RTF is due to missing genetic components in the heterologous plant, it is possible that pathogen suppressors could underpin the lack of functionality of some NLR transgenes. It is imperative that we integrate NLR-suppressing effectors into R-gene discovery and disease resistance breeding pipelines in the coming years, to avoid missing a potentially vast and yet untapped reservoir of immune receptors.

8.5.5 ESCRTing the resistosome: a new player in NLR regulation.

By studying AVRcap1b and TOLs, I have identified a novel player in the regulation of NLR signaling regulation. TOL proteins are the gatekeepers of the ESCRT trafficking pathway, targeting ubiquitinated plasma membrane-associated proteins for ESCRT-mediated trafficking (Moulinier-Anzola *et al.*, 2020; Winter & Hauser, 2006). In plants, this pathway has previously been implicated in regulating cell-surface receptor signal intensity by shuttling FLS2 to and from the membrane (Spallek *et al.*, 2013). In metazoans, the ESCRT trafficking pathway has been shown to negatively regulate programmed cell death by removing pore-forming proteins such as gasdermins from the plasma membrane as well as by excising damaged sections of the plasma membrane (Castro-Gomes *et al.*, 2014; Dai *et al.*, 2020; Gong *et al.*, 2017; Jimenez *et al.*, 2014; Pedrera *et al.*, 2021; Rühl *et al.*, 2018). Considering the discovery of the CC-NLR resistosome, which inserts itself into the plasma membrane to act as a calcium channel and potentially to act as a plasma membrane pore, it is tempting to speculate that TOL proteins in plants may be negatively regulating NLR activities via similar mechanisms in plants. Based on my findings, NRCs are likely forming oligomeric resistosome-like complexes upon activation (Contreras *et al.*, 2023b). Perhaps NbTOL9a-mediated negative regulation of NRC2 and NRC3-mediated cell death involves ESCRT-dependent removal of membrane-associated helper resistosomes from the plasma membrane to prevent or regulate signaling. Further cell biology and membrane fractionation assays may help test this hypothesis.

Why does NbTOL9a negatively regulate NRC2 and NRC3-mediated cell death but not NRC4-mediated cell death? Where is the specificity for NRC2/3-negative regulation encoded? Previous reports have determined that the N-terminal ENTH and GAT domains of TOLs bind ubiquitinated cargo proteins (Korbei *et al.*, 2013; Moulinier-Anzola *et al.*, 2020; Winter & Hauser, 2006). The fact that AVRcap1b has evolved to directly bind the N-terminal ENTH domain of NbTOL9a and that this interaction is important for NRC suppression suggests that this domain is likely important for cargo binding in NbTOL9a. It is tempting to speculate that the capacity to negatively regulate NRC2 and NRC3 is specifically encoded in the ENTH domain. Nonetheless, the C-terminal region of TOL proteins display far more diversity, and it is also possible that this region contributes to cargo specificity. However, whether TOL proteins can interact with activated NRC resistosomes at all remains to be conclusively shown. Understanding the interplay between NLRs and ESCRT-pathway components may help fine-tune NLR regulation to improve disease resistance or to attenuate autoimmunity.

8.5.6 More complexity means more regulation?

It is possible that NbTOL9a-mediated regulation of NRCs has arisen as a result of the evolutionary transitions from singleton to genetically linked pairs and networks. In genetically dispersed NLR networks, novel regulatory mechanisms likely evolve to compensate for the lack of transcriptional co-regulation that is found in genetically linked pairs. This might also apply to atypical modulator NLRs such as NRCX and NRG1c, which appear to specialize in negatively regulating helper NLRs within NLR networks (Adachi *et al.*, 2023; Wu *et al.*, 2022). Strikingly, both NbTOL9a and NRCX negatively regulate NRC2 and NRC3 (Adachi *et al.*, 2023; Derevnina *et al.*, 2021). Why have these two helpers evolved these additional layers of regulation not found for other NLRs? As mentioned above, NRC3 acts downstream of cell-surface receptors (Kourelis *et al.*, 2022). Its dual role in cell-surface and intracellular immunity potentially requires additional layers of regulation. Alternatively, differences in subcellular localization of helpers or sensors may lead to different regulation mechanisms for NRC2/3 and NRC4. One could speculate that NRC2 and NRC3 are somehow more prone to spurious activation or that there are more sensors that rely on these two helpers as compared to NRC4, necessitating the emergence of additional NRC2/3 regulatory mechanisms. The precise interplay between TOL proteins and NRCs and how these regulatory mechanisms emerged remain open questions.

It should be noted that I have not ruled out that other TOL proteins can negatively regulate NRC-dependent cell death. NbTOL9a was tested for involvement in NRC-dependent cell death based on its interaction with the NRC-suppressor AVRcap1b, but other TOLs that do not interact with AVRcap1b may also negatively regulate NRCs. Moreover, while NbTOL9a can specifically negatively regulate NRC2 and NRC3, it is possible that other TOL proteins have evolved to negatively regulate other NRCs or other NLRs in general as TOL proteins are found in all plants and are present in plant species which do not encode NRCs. It will be interesting to carry out evolutionary analyses of NbTOL9a and assess whether it co-occurs with species that encode NRCs to investigate if NbTOL9a has co-evolved with the NRC network. Further work on TOL protein evolution and functional specialization will help clarify this.

8.5.7 NLR networks: making plant immunity more robust.

That unrelated pathogens have evolved effectors to interfere with NLR networks suggest this is an evolutionarily favourable virulence strategy. Importantly, AVRcap1b and SS15 can suppress NRC2 and NRC3 but not NRC4. This highlights how advantageous the redundancy provided by networked signaling architectures is, as even in the presence of robust NRC2/3 suppressors, many sensors would still be able to signal through NRC4. Moreover, functional specialization likely enhances evolvability for both sensors and helpers. Sensors are less evolutionarily constrained and can keep up with rapidly evolving effectors. In parallel, helpers can more easily evolve escape immunosuppression by effectors.

It is of course possible that pathogens exist that feature effector repertoires capable of suppressing all helpers simultaneously, therefore compromising the entire network. As discussed above, many of the NLR network suppressing effectors are AVRs in some plant species, such as the NRC-suppressing SS15 and AVRcap1b as well as the ADR1 suppressing AvrPtoB (Ali *et al.*, 2015; Rietman, 2011; Wang *et al.*, 2023a). It is therefore likely that there are NLRs guarding NRCs to prevent a pathogen from completely suppressing the NLR network, in the same way that the ADR1-like helpers are guarded by SNC1. Much like SNC1, which signals through an ADR1 helper which is not suppressed by AvrPtoB, one could envision that NRC-independent CC-NLRs or TIR-NLRs may guard NRCs, therefore providing a failsafe in the case that a pathogen can shut down all helper nodes in the NRC network. By combining enhanced evolvability, redundancy, and potentially mechanisms by which sensors with non-immunosuppressed downstream pathways

guard helper NLRs, NLR networks can provide extremely robust immunity against multiple pathogens while avoiding interference from effectors.

8.6 A bright future for synthetic disease resistance.

As the NLR biology field gains a better understanding of how singleton, paired and networked NLRs perceive their cognate effectors and activate immunity, we are on the verge of a new era of synthetic disease resistance. Multiple strategies have been developed to bioengineer novel recognition specificities, and we now possess novel strategies to potentially bioengineer NLRs that evade immune suppression (Contreras *et al.*, 2023a; Kourelis *et al.*, 2023; Marchal *et al.*, 2022b). As we gain more mechanistic insight into how paired and networked NLRs function, more opportunities for bioengineering emerge. For example, making modifications in sensors and helpers may help expand sensor-helper communication or make it more efficient, increasing signaling intensity or altering its dynamics to achieve more robust immunity. Moreover, as we understand more about how NLR modulators such as NRCX, NRG1c or NbTOL9a function, we can potentially alter this modulation to make the immune system more efficient. In many cases, NLR engineering efforts to achieve novel effector recognition specificities leads to autoimmunity (Marchal *et al.*, 2022b). Perhaps endogenous negative regulatory pathways can be bioengineered and harnessed to mitigate autoimmunity of synthetic immune receptors.

My findings with the previously identified Rx^{NB}-eGFP system are a source of potential inspiration for NLR bioengineering. I showed that the NB domain can act as the minimal helper activation domain. One could perhaps leverage this NRC activator and engineer novel ways in which to repress and conditionally de-repress it to generate a synthetic NRC-dependent sensor NLR. These synthetic sensors would ideally be programmable and allow us to harness the NRC-network to provide disease resistance against effectors of choice, for example by leveraging nanobodies as done previously by Kourelis and Marchal with the Pikobody technology (Kourelis *et al.*, 2023). One could also conceive of engineering a protease trap. By inserting protease cleavage sites recognized by pathogen effectors with protease activity, the Rx^{NB} could be conditionally released in the presence of these effectors. This would be analogous to previous approaches with the singleton RPS5 system (Helm *et al.*, 2019; Kim *et al.*, 2016a; Pottinger & Innes, 2020). The Rx^{NB}-eGFP could also be coupled to a degron to prevent NRC activation. This degron could be conditionally repressed in response to pathogen infection. Alternatively, Rx^{NB}-eGFP could be put under the control of a pathogen-inducible promoter which is constitutively off and conditionally

gets turned on during infection, leading to NRC activation. Rx^{NB}-eGFP could be turned into an executor type gene by putting TAL effector targeted DNA sequences upstream of Rx^{NB}-eGFP. Further experimentation will reveal how Rx^{NB}-eGFP may be leveraged to engineer synthetic disease resistance strategies.

Similarly, the Rx halves system could be leveraged. One could envision a “mix-and-match” system in which a single N-terminal sensor NLR CC-NBARC half is co-expressed with multiple different LRR domains, each recognising a different effector but all of them compatible with the same CC-NBARC half. Upon recognition of a specific effector, the LRRs would then co-operate with the CC-NBARC half to activate NRCs. One could use this to engineer an immune receptor network of sorts, with multiple separate LRRs acting as sensors and co-operating with a reduced number of CC-NBARC halves to activate NRCs.

8.7 Concluding remarks and future questions.

In this thesis, I aimed to understand the molecular mechanisms that underpin sensor-helper activation and cell death execution in networked NLR immune receptors. Moreover, I attempted to use these insights to understand how pathogen effectors can interfere with NLR activation. The work in this thesis also highlights how integrating evolutionary biology and phylogenomics into NLR research can lead to a more profound understanding of core principles that underpin NLR signaling, as evidenced by the identification of the MADA motif through large-scale comparative analyses. The identification of the MADA motif and MADA motif mutants allowed us to test several hypotheses, leading to a deeper understanding of how CC-NLR sensors and helpers in the NRC network communicate and activate (Adachi *et al.*, 2019a). This led me to propose the activation and release model, in which sensor NLRs mediate oligomerization of their helpers into resistosome-like complexes that do not include the helpers (Contreras *et al.*, 2023b). Moreover, our findings related to activation in the NRC helper allowed us to better understand how pathogen effectors can interfere with NRC-mediated immunity. I was able to shed light on the mechanisms by which two effectors, AVRcap1b and SS15, suppress NRC2/3-mediated signaling (Derevnina *et al.*, 2021). In the case of SS15, understanding its suppression mechanism allowed me to devise a strategy to bioengineer helper NLRs which evade inhibition (Contreras *et al.*, 2023a). This exemplifies how a fundamental understanding of NLR and effector biology can have an impact on applied disease resistance research.

While significant progress has been made in understanding how NLR immune receptors translate effector recognition into immune signaling and disease resistance, many important questions remain unanswered. How has the MADA motif evolved and what other important motifs remain undiscovered? What are the precise dynamics of resistosome assembly for singletons, pairs, and networks? What is the mechanism by which resistosomes trigger cell death and contribute to disease resistance? What is the precise nature of the signal between sensors and helpers? Considering that plant and metazoan NLRs exhibit distinct activation mechanisms, it appears that NLRs may exhibit more mechanistic diversity than previously anticipated. Does the activation and release mechanism apply to other CC-NLR pairs? Does this mechanism even apply to all NRC-dependent CC-NLRs or are there diverse strategies to activate NRC helpers within the NRC network? The fact that the NB domain of multiple Rx-type sensors, but not those of SD-type sensors, activate NRCs suggests that the SD-type sensors may exhibit different activation mechanisms, potentially as a result of the N-terminal fusion of SDs. How sensor NLRs evolve to accommodate SD fusions and whether different sensor NLR clades within the NRC network exhibit different activation mechanisms remain important unanswered questions.

We have also made significant advances with regards to how effectors can suppress NLRs and NLR networks, but there is much that we have yet to understand about NLR suppressing effectors. Further evolutionary and phylogenetic analyses will hopefully clarify the precise co-evolutionary dynamics between NLRs and their suppressors. With regards to AVRcap1b, while I have constructed a possible working model based on the available data, the exact mechanism of suppression remains elusive. Further work including cell biology, membrane fractionation assays, and potentially structural biology may help clarify the interplay between TOL proteins, NRCs and AVRcap1b. Moreover, further work on plant TOL proteins and ESCRT-mediated trafficking will help us understand TOL protein functional diversity and evolution and the precise contributions of TOL proteins to immune regulation in plants with mechanistic detail. Moreover, given that AVRcap1b and SS15 are both AVRs, understanding the mechanism by which they are recognized may lead to the identification of NLRs that are guarding sensors. Beyond the robustness provided by helper NLR redundancy, NLRs guarding other NLRs, particularly helpers, could be a failsafe to achieve robust immunity even in the face of inhibition by effectors.

In this thesis, I proposed a novel strategy to bioengineer NLRs that evade suppression by pathogen effectors (Contreras *et al.*, 2023a). We refer to this approach as disease resistance resurrection and a spinout company – Resurrect Bio Ltd. – has been incorporated to further

develop this approach. While AVRcap1b and SS15, from *P. infestans* and *G. rostochiensis* respectively, can robustly suppress NRC2 and NRC3 in transient expression assays, the precise contributions of AVRcap1b and SS15 to virulence during pathogen infection are not known. Further experiments with pathogen infection assays will determine how much effector mediated NLR immunosuppression contributes to disease and what contributions helper NLR bioengineering can make to durable disease resistance. Moreover, more research is required to determine whether and how this strategy can be deployed in the field. Perhaps single amino acid mutants may not be durable to deploy and instead multiple mutations that abolish NLR-inhibition must be deployed into a helper as a “stack” to prevent effectors from evolving to regain immunosuppression. Finally, further studies will determine how we can leverage our newfound understanding of NLR and NLR network biology to optimize the plant immune system in a rational manner. Hopefully multiple engineering strategies can be combined to make the plant system more robust, versatile, and resilient to manipulation by pathogens.

NLR biology remains an area of intense research. Breakthroughs are made faster than ever before, taking the community a long way from the early days when NLR genes were first cloned in the mid 90s. However, much work remains to be done. Many exciting avenues of exploration remain. Answering the fundamental questions mentioned above will help advance our understanding of plant immunity and plant pathogen co-evolution, contributing to bridging the gap between mechanistic, evolutionary, and applied research. Achieving a more integral view of plant and microbial systems, will hopefully usher a new era of synthetic, durable disease resistance, sustainable agriculture, and food security.

Appendix I

Supplementary information for Chapter 2: Materials & Methods

Table AI.1: Constructs used in this thesis.

Construct name	Made by*	Parts used	Antibiotic resistance	Reference
Chapter 3				
NRC4^{WT}-YFP	H.A.	pICH47742 acceptor, pICH85281 MAS promoter, pCR8-NRC4 ^{WT} syn, pICSL50005 C-terminal YFP tag, pICS6008 AtHSP18 terminator	Carb/Rif	(Adachi <i>et al.</i> , 2019a)
NRC4^{DV}-YFP	H.A.	pICH47742 acceptor, pICH85281 MAS promoter, pCR8-NRC4 ^{DV} syn, pICSL50005 C-terminal YFP tag, pICS6008 AtHSP18 terminator	Carb/Rif	(Adachi <i>et al.</i> , 2019a)
YFP	H.A.	pICH47742 acceptor, pICH85281 MAS promoter, pUC57K-YFP, pICSL50005 C-terminal YFP tag, pICS6008 AtHSP18 terminator	Carb/Rif	(Adachi <i>et al.</i> , 2019a)
NRC4₁₋₂₉-YFP	H.A.	pICH47742 acceptor, pICH85281 MAS promoter, pCR8-NRC4 ₁₋₂₉ , pICSL50005 C-terminal YFP tag, pICS6008 AtHSP18 terminator	Carb/Rif	(Adachi <i>et al.</i> , 2019a)
NRC4^{WT}-6xHA	H.A.	pICH47742 acceptor, pICH85281 MAS promoter, pCR8-NRC4, pICSL50009 C-terminal 6xHA tag, pICS6008 AtHSP18 terminator	Carb/Rif	(Adachi <i>et al.</i> , 2019a)
NRC4^{DV}-6xHA	H.A.	pICH47742 acceptor, pICH85281 MAS promoter, pCR8-NRC4 ^{DV} , pICSL50009 C-terminal 6xHA tag, pICS6008 AtHSP18 terminator	Carb/Rif	(Adachi <i>et al.</i> , 2019a)
NRC4^{AAA}-6xHA	H.A.	pICH47742 acceptor, pICH85281 MAS promoter, pCR8-NRC4 ^{L9A/V10A/L14A} ,	Carb/Rif	(Adachi <i>et al.</i> , 2019a)

		pICSL50009 C-terminal 6xHA tag, pICS6008 AtHSP18 terminator		
NRC4^{EEE}-6xHA	H.A.	pICH47742 acceptor, pICH85281 MAS promoter, pCR8-NRC4 ^{L9E/V10E/L14E} , pICSL50009 C-terminal 6xHA tag, pICS6008 AtHSP18 terminator	Carb/Rif	(Adachi <i>et al.</i> , 2019a)
NRC4^{A2E}-6xHA	H.A.	pICH47742 acceptor, pICH85281 MAS promoter, pCR8-NRC4 ^{A2E} , pICSL50009 C-terminal 6xHA tag, pICS6008 AtHSP18 terminator	Carb/Rif	(Adachi <i>et al.</i> , 2019a)
NRC4^{D3E}-6xHA	H.A.	pICH47742 acceptor, pICH85281 MAS promoter, pCR8-NRC4 ^{D3E} , pICSL50009 C-terminal 6xHA tag, pICS6008 AtHSP18 terminator	Carb/Rif	(Adachi <i>et al.</i> , 2019a)
NRC4^{A4E}-6xHA	H.A.	pICH47742 acceptor, pICH85281 MAS promoter, pCR8-NRC4 ^{A4E} , pICSL50009 C-terminal 6xHA tag, pICS6008 AtHSP18 terminator	Carb/Rif	(Adachi <i>et al.</i> , 2019a)
NRC4^{V5E}-6xHA	H.A.	pICH47742 acceptor, pICH85281 MAS promoter, pCR8-NRC4 ^{V5E} , pICSL50009 C-terminal 6xHA tag, pICS6008 AtHSP18 terminator	Carb/Rif	(Adachi <i>et al.</i> , 2019a)
NRC4^{V6E}-6xHA	H.A.	pICH47742 acceptor, pICH85281 MAS promoter, pCR8-NRC4 ^{V6E} , pICSL50009 C-terminal 6xHA tag, pICS6008 AtHSP18 terminator	Carb/Rif	(Adachi <i>et al.</i> , 2019a)
NRC4^{N7E}-6xHA	H.A.	pICH47742 acceptor, pICH85281 MAS promoter, pCR8-NRC4 ^{N7E} , pICSL50009 C-terminal 6xHA tag, pICS6008 AtHSP18 terminator	Carb/Rif	(Adachi <i>et al.</i> , 2019a)
NRC4^{F8E}-6xHA	H.A.	pICH47742 acceptor, pICH85281 MAS promoter, pCR8-NRC4 ^{F8E} , pICSL50009 C-terminal 6xHA tag, pICS6008 AtHSP18 terminator	Carb/Rif	(Adachi <i>et al.</i> , 2019a)
NRC4^{L9E}-6xHA	H.A.	pICH47742 acceptor, pICH85281 MAS promoter, pCR8-NRC4 ^{L9E} , pICSL50009 C-	Carb/Rif	(Adachi <i>et al.</i> , 2019a)

		terminal 6xHA tag, pICS6008 AtHSP18 terminator		
NRC4^{V10E}-6xHA	H.A.	pICH47742 acceptor, pICH85281 MAS promoter, pCR8-NRC4 ^{V10E} , pICSL50009 C-terminal 6xHA tag, pICS6008 AtHSP18 terminator	Carb/Rif	(Adachi <i>et al.</i> , 2019a)
NRC4^{N12E}-6xHA	H.A.	pICH47742 acceptor, pICH85281 MAS promoter, pCR8-NRC4 ^{N12E} , pICSL50009 C-terminal 6xHA tag, pICS6008 AtHSP18 terminator	Carb/Rif	(Adachi <i>et al.</i> , 2019a)
NRC4^{L13E}-6xHA	H.A.	pICH47742 acceptor, pICH85281 MAS promoter, pCR8-NRC4 ^{L13E} , pICSL50009 C-terminal 6xHA tag, pICS6008 AtHSP18 terminator	Carb/Rif	(Adachi <i>et al.</i> , 2019a)
NRC4^{L14E}-6xHA	H.A.	pICH47742 acceptor, pICH85281 MAS promoter, pCR8-NRC4 ^{L14E} , pICSL50009 C-terminal 6xHA tag, pICS6008 AtHSP18 terminator	Carb/Rif	(Adachi <i>et al.</i> , 2019a)
NRC4^{Q15E}-6xHA	H.A.	pICH47742 acceptor, pICH85281 MAS promoter, pCR8-NRC4 ^{Q15E} , pICSL50009 C-terminal 6xHA tag, pICS6008 AtHSP18 terminator	Carb/Rif	(Adachi <i>et al.</i> , 2019a)
NRC4^{L16E}-6xHA	H.A.	pICH47742 acceptor, pICH85281 MAS promoter, pCR8-NRC4 ^{L16E} , pICSL50009 C-terminal 6xHA tag, pICS6008 AtHSP18 terminator	Carb/Rif	(Adachi <i>et al.</i> , 2019a)
NRC4^{L17E}-6xHA	H.A.	pICH47742 acceptor, pICH85281 MAS promoter, pCR8-NRC4 ^{L17E} , pICSL50009 C-terminal 6xHA tag, pICS6008 AtHSP18 terminator	Carb/Rif	(Adachi <i>et al.</i> , 2019a)
NRC4^{T18E}-6xHA	H.A.	pICH47742 acceptor, pICH85281 MAS promoter, pCR8-NRC4 ^{T18E} , pICSL50009 C-terminal 6xHA tag, pICS6008 AtHSP18 terminator	Carb/Rif	(Adachi <i>et al.</i> , 2019a)
NRC4^{D19E}-6xHA	H.A.	pICH47742 acceptor, pICH85281 MAS promoter, pCR8-NRC4 ^{D19E} , pICSL50009 C-	Carb/Rif	(Adachi <i>et al.</i> , 2019a)

		terminal 6xHA tag, pICS6008 AtHSP18 terminator		
NRC4^{N20E}-6xHA	H.A.	pICH47742 acceptor, pICH85281 MAS promoter, pCR8-NRC4 ^{N20E} , pICSL50009 C-terminal 6xHA tag, pICS6008 AtHSP18 terminator	Carb/Rif	(Adachi <i>et al.</i> , 2019a)
NRC4^{V21E}-6xHA	H.A.	pICH47742 acceptor, pICH85281 MAS promoter, pCR8-NRC4 ^{V21E} , pICSL50009 C-terminal 6xHA tag, pICS6008 AtHSP18 terminator	Carb/Rif	(Adachi <i>et al.</i> , 2019a)
ZAR1₁₋₁₇-NRC4^{WT}-6xHA	H.A.	pICH47742 acceptor, pICH85281 MAS promoter, pCR8-NRC4 ^{V21E} , pICSL50009 C-terminal 6xHA tag, pICS6008 AtHSP18 terminator	Carb/Rif	(Adachi <i>et al.</i> , 2019a)
RFP-Rpi-blb2	C.H.W.	See reference for details.	Spec/Rif	(Wu <i>et al.</i> , 2017)
Chapter 4				
Construct info can be found in Supplementary information for Contreras et al., 2023, The EMBO Journal				
Chapter 5				
eGFP	J.K.	pJK268c acceptor, pICH51288 2x35S terminator, pCR8-eGFP, pICH41414 35S terminator	Kan/Rif	(Kourelis <i>et al.</i> , 2022)
CP-eGFP	M.P.C	pJK268c acceptor, pICH51288 2x35S terminator, pCR8-CP, pICSL50034 C-term eGFP tag, pICH41414 35S terminator	Kan/Rif	(Contreras <i>et al.</i> , 2023b)
Rx-6xHA	J.K.	pJK268c acceptor, pICH51288 2x35S terminator, pCR8-Rx, pICH41414 35S terminator	Kan/Rif	(Contreras <i>et al.</i> , 2023b)
ZAR1^{D481V}-6xHA	H.A.	pICH86988 acceptor with integrated 35S promoter and OCS terminator, pZA14 ZAR1 ^{D481V}	Kan/Rif	(Adachi <i>et al.</i> , 2019a)
Rx^{CCNBARC}-4xMyc	M.P.C.	pICH86988 acceptor with integrated 35S promoter and OCS terminator, pCR8-Rx ^{CCNBARC}	Kan/Rif	This thesis.
Rx^{CC}-4xMyc	M.P.C.	pICH86988 acceptor with integrated 35S promoter and OCS terminator, pCR8-Rx ^{CCNBARC}	Kan/Rif	This thesis.

R_x^{NBARCLRR}-6xHA	M.P.C.	pICH86988 acceptor with integrated 35S promoter and OCS terminator, pCR8-R _x ^{NBARCLRR}	Kan/Rif	This thesis.
R_x^{LRR}-6xHA	M.P.C.	pICH86988 acceptor with integrated 35S promoter and OCS terminator, pCR8-R _x ^{LRR}	Kan/Rif	This thesis.
SINRC0	C.H.W.	pICH86988 acceptor with integrated 35S promoter and OCS terminator, pCR8-SINRC0	Kan/Rif	This thesis.
NRC2	C.H.W.	pICH86988 acceptor with integrated 35S promoter and OCS terminator, pCR8-NRC2	Kan/Rif	(Wu <i>et al.</i> , 2017)
NRC3	C.H.W.	pICH86988 acceptor with integrated 35S promoter and OCS terminator, pCR8-NRC3	Kan/Rif	(Wu <i>et al.</i> , 2017)
NRC4	C.H.W.	pICH86988 acceptor with integrated 35S promoter and OCS terminator, pCR8-NRC4	Kan/Rif	(Wu <i>et al.</i> , 2017)
NRC2-3xFLAG	J.K.	pICH86988 acceptor with integrated 35S promoter and OCS terminator, pCR8-NRC2, pICSL50007 C-term 3xFLAG tag	Kan/Rif	(Contreras <i>et al.</i> , 2023b)
NRC2^{EEE}-3xFLAG	J.K.	pICH86988 acceptor with integrated 35S promoter and OCS terminator, pCR8-NRC2 ^{EEE} , pICSL50007 C-term 3xFLAG tag	Kan/Rif	(Contreras <i>et al.</i> , 2023b)
SINRC0-3xFLAG	M.P.C.	pICH86988 acceptor with integrated 35S promoter and OCS terminator, pCR8-SINRC0, pICSL50007 C-term 3xFLAG tag	Kan/Rif	This thesis.
R_x^{CCNBARC}-V5	M.P.C.	pICH86988 acceptor with integrated 35S promoter and OCS terminator, pCR8-R _x ^{CCNBARC} , pICSL50012 C-term V5 tag	Kan/Rif	This thesis.
R_x^{NB}-eGFP	M.P.C.	pJK268c acceptor, pICH51288 2x35S terminator, R _x ^{NB} synthetic fragmentGENE (Genewiz), pICSL50034 C-term eGFP tag, pICH41414 35S terminator	Kan/Rif	This thesis.
R_x^{NB-KR}-eGFP	M.P.C.	pJK268c acceptor, pICH51288 2x35S terminator, R _x ^{NB-KR} synthetic fragmentGENE (Genewiz), pICSL50034 C-term eGFP tag, pICH41414 35S terminator	Kan/Rif	This thesis.
NRC2^{EEE}-4xMyc	J.K.	pJK268c acceptor, pICH51288 2x35S terminator, pCR8-NRC2 ^{EEE} , pICSL50010 C-term 4xMyc tag, pICH41414 35S terminator	Kan/Rif	(Contreras <i>et al.</i> , 2023b)

Rx^{D460V}-6xHA	JK	pJK268c acceptor, pICH51288 2x35S terminator, pCR8-Rx ^{DV} , pICSL50009 C-term 6xHA tag, pICH41414 35S terminator	Kan/Rif	This thesis.
Gpa2^{NB}-eGFP	M.P.C.	pJK268c acceptor, pICH51288 2x35S terminator, Gpa2 ^{NB} synthetic fragmentGENE (Genewiz), pICSL50034 C-term eGFP tag, pICH41414 35S terminator	Kan/Rif	This thesis.
Rpiamr1e^{NB}-eGFP	M.P.C.	pJK268c acceptor, pICH51288 2x35S terminator, Rpiamr1e ^{NB} synthetic fragmentGENE (Genewiz), pICSL50034 C-term eGFP tag, pICH41414 35S terminator	Kan/Rif	This thesis.
Rpiamr3^{NB}-eGFP	M.P.C.	pJK268c acceptor, pICH51288 2x35S terminator, Rpiamr3 ^{NB} synthetic fragmentGENE (Genewiz), pICSL50034 C-term eGFP tag, pICH41414 35S terminator	Kan/Rif	This thesis.
Bs2^{NB}-eGFP	M.P.C.	pJK268c acceptor, pICH51288 2x35S terminator, Bs2 ^{NB} synthetic fragmentGENE (Genewiz), pICSL50034 C-term eGFP tag, pICH41414 35S terminator	Kan/Rif	This thesis.
Mi^{NB}-eGFP	M.P.C.	pJK268c acceptor, pICH51288 2x35S terminator, Mi ^{NB} synthetic fragmentGENE (Genewiz), pICSL50034 C-term eGFP tag, pICH41414 35S terminator	Kan/Rif	This thesis.
Rpi-blb2^{NB}-eGFP	M.P.C.	pJK268c acceptor, pICH51288 2x35S terminator, Rpi-blb2 ^{NB} synthetic fragmentGENE (Genewiz), pICSL50034 C-term eGFP tag, pICH41414 35S terminator	Kan/Rif	This thesis.
Gpa2^{NB-A181T}-eGFP	M.P.C.	pJK268c acceptor, pICH51288 2x35S terminator, Gpa2 ^{NB-A181T} synthetic fragmentGENE (Genewiz), pICSL50034 C-term eGFP tag, pICH41414 35S terminator	Kan/Rif	This thesis.
Gpa2^{NB-Y188C}-eGFP	M.P.C.	pJK268c acceptor, pICH51288 2x35S terminator, Gpa2 ^{NB-Y188C} synthetic fragmentGENE (Genewiz), pICSL50034 C-term eGFP tag, pICH41414 35S terminator	Kan/Rif	This thesis.
Gpa2^{NB-Y224D}-eGFP	M.P.C.	pJK268c acceptor, pICH51288 2x35S terminator, Gpa2 ^{NB-Y224D} synthetic	Kan/Rif	This thesis.

		fragmentGENE (Genewiz), pICSL50034 C-term eGFP tag, pICH41414 35S terminator		
Gpa2^{NB-Q229R}-eGFP	M.P.C.	pJK268c acceptor, pICH51288 2x35S terminator, Gpa2 ^{NB-Q229R} synthetic fragmentGENE (Genewiz), pICSL50034 C-term eGFP tag, pICH41414 35S terminator	Kan/Rif	This thesis.
Gpa2^{NB-D263Y}-eGFP	M.P.C.	pJK268c acceptor, pICH51288 2x35S terminator, Gpa2 ^{NB-D263Y} synthetic fragmentGENE (Genewiz), pICSL50034 C-term eGFP tag, pICH41414 35S terminator	Kan/Rif	This thesis.
Chapter 6				
AVRcap1b-6xHA	L.D.	pICH47742 acceptor, pICH85281 MAS promoter, pCR8-AVRcap1b, pICSL50009 C-terminal 6xHA tag, pICS6008 AtHSP18 terminator	Carb/Rif	(Derevnina <i>et al.</i> , 2021)
4xHA-SS15	L.D.	N/A	Kan/Rif	(Derevnina <i>et al.</i> , 2021)
NRC2-4xMyc	C.H.W.	pICH86988 acceptor with integrated 35S promoter and OCS terminator, pCR8-NRC2, pICSL50010 C-term 4xMyc tag	Kan/Rif	(Derevnina <i>et al.</i> , 2021)
NRC3-4xMyc	C.H.W.	pICH86988 acceptor with integrated 35S promoter and OCS terminator, pCR8-NRC3, pICSL50010 C-term 4xMyc tag	Kan/Rif	(Derevnina <i>et al.</i> , 2021)
NRC4-4xMyc	C.H.W.	pICH86988 acceptor with integrated 35S promoter and OCS terminator, pCR8-NRC4, pICSL50010 C-term 4xMyc tag	Kan/Rif	(Derevnina <i>et al.</i> , 2021)
GFP-PexRD54	L.D.	pICH86988 acceptor with integrated 35S promoter and OCS terminator, pCR8-PexRD54, pICSL50010 C-term 4xMyc tag	Kan/Rif	(Derevnina <i>et al.</i> , 2021)
GFP-AVRcap1b	L.D.	pICH86988 acceptor with integrated 35S promoter and OCS terminator, pCR8-AVRcap1b, pICSL50010 C-term 4xMyc tag	Kan/Rif	(Derevnina <i>et al.</i> , 2021)
NbTOL9a-6xHA	L.D.	pICH47732 acceptor, pICH51288 2x35S terminator, pCR8-E1, pICSL50009 C-terminal 6xHA tag, pICH41432 OCS terminator	Carb/Rif	(Derevnina <i>et al.</i> , 2021)

NbTOL9b-6xHA	L.D.	pICH47732 acceptor, pICH51288 2x35S terminator, pCR8-E2, pICSL50009 C-terminal 6xHA tag, pICH41432 OCS terminator	Carb/Rif	(Derevnina <i>et al.</i> , 2021)
NbTOL9c-6xHA	L.D.	pICH47732 acceptor, pICH51288 2x35S terminator, pCR8-E5, pICSL50009 C-terminal 6xHA tag, pICH41432 OCS terminator	Carb/Rif	(Derevnina <i>et al.</i> , 2021)
NbTOL3-6xHA	L.D.	pICH47732 acceptor, pICH51288 2x35S terminator, pCR8-E3, pICSL50009 C-terminal 6xHA tag, pICH41432 OCS terminator	Carb/Rif	(Derevnina <i>et al.</i> , 2021)
NbTOL6-6xHA	L.D.	pICH47732 acceptor, pICH51288 2x35S terminator, pCR8-E3, pICSL50009 C-terminal 6xHA tag, pICH41432 OCS terminator	Carb/Rif	(Derevnina <i>et al.</i> , 2021)
AVRcap1b-4xMyc	L.D.	pICH47742 acceptor, pICH85281 MAS promoter, pCR8-AVRcap1b, pICSL50010 C-terminal 4xMyc tag, pICS6008 AtHSP18 terminator	Carb/Rif	(Derevnina <i>et al.</i> , 2021)
NRCx-4xMyc	H.A.	pICH86988 acceptor with integrated 35S promoter and OCS terminator, pCR8-NRCx, pICSL50010 C-term 4xMyc tag	Kan/Rif	(Adachi <i>et al.</i> , 2023)
MEK2^{DD}	C.H.W.	N/A	Spec/Rif	(Derevnina <i>et al.</i> , 2021)
NRC3^{D480V}	C.H.W.	pICH86988 acceptor with integrated 35S promoter and OCS terminator, pCR8-NRC3 ^{DV}	Kan/Rif	(Derevnina <i>et al.</i> , 2021)
NRC4^{D478V}	C.H.W.	pICH86988 acceptor with integrated 35S promoter and OCS terminator, pCR8-NRC3 ^{DV}	Kan/Rif	(Derevnina <i>et al.</i> , 2021)
pRNAi::GUS	L.D.	pRNAi-GG acceptor, synthetic GUS silencing fragment GENE (Genewiz)	Kan/Rif	(Derevnina <i>et al.</i> , 2021)
pRNAi::NbTOL9a	L.D.	pRNAi-GG acceptor, synthetic GUS silencing fragment GENE (Genewiz)	Kan/Rif	(Derevnina <i>et al.</i> , 2021)
NbTOL6^{ENTH-GAT}-6xHA	M.P.C.	pICH47742 acceptor, pICH51288 2x35S terminator, PCR products X*, pICSL50009	Carb/Rif	This thesis.

		C-terminal 6xHA tag, pICH41432 OCS terminator		
NbTOL6^{ENTH}-6xHA	M.P.C.	pICH47742 acceptor, pICH51288 2x35S terminator, pCR8-T6 ^{ENTH} , pICSL50009 C-terminal 6xHA tag, pICH41432 OCS terminator	Carb/Rif	This thesis.
NbTOL6^{GAT}-6xHA	M.P.C.	pICH47742 acceptor, pICH51288 2x35S terminator, pCR8-T6 ^{GAT} , pICSL50009 C-terminal 6xHA tag, pICH41432 OCS terminator	Carb/Rif	This thesis.
NbTOL6^{CTR}-6xHA	M.P.C.	pICH47742 acceptor, pICH51288 2x35S terminator, pCR8-T6 ^{CTR} , pICSL50009 C-terminal 6xHA tag, pICH41432 OCS terminator	Carb/Rif	This thesis.
<i>P. mirabilis</i> AVRcap1b-6xHA	M.P.C.	pICH47742 acceptor, pICH51288 2x35S terminator, pCR8-PmirACAP, pICSL50009 C-terminal 6xHA tag, pICH41432 OCS terminator	Carb/Rif	This thesis.
<i>P. andina</i> AVRcap1b-6xHA	M.P.C.	pICH47742 acceptor, pICH51288 2x35S terminator, pCR8-PandACAP, pICSL50009 C-terminal 6xHA tag, pICH41432 OCS terminator	Carb/Rif	This thesis.
<i>P. ipomoeae</i> AVRcap1b-6xHA	M.P.C.	pICH47742 acceptor, pICH51288 2x35S terminator, pCR8-PipoACAP, pICSL50009 C-terminal 6xHA tag, pICH41432 OCS terminator	Carb/Rif	This thesis.
<i>P. ipomoeae</i> AVRcap1b^{Swap1}-6xHA	M.P.C.	pICH47742 acceptor, pICH51288 2x35S terminator, pCR8-PipoACAP-S1, pICSL50009 C-terminal 6xHA tag, pICH41432 OCS terminator	Carb/Rif	This thesis.
<i>P. ipomoeae</i> AVRcap1b^{Swap2}-6xHA	M.P.C.	pICH47742 acceptor, pICH51288 2x35S terminator, pCR8-PipoACAP-S2, pICSL50009 C-terminal 6xHA tag, pICH41432 OCS terminator	Carb/Rif	This thesis.
<i>P. ipomoeae</i> AVRcap1b^{Swap3}-6xHA	M.P.C.	pICH47742 acceptor, pICH51288 2x35S terminator, pCR8-PipoACAP-S3,	Carb/Rif	This thesis.

		pICSL50009 C-terminal 6xHA tag, pICH41432 OCS terminator		
<i>P. ipomoeae</i> AVRcap1b^{Swap4-} 6xHA	M.P.C.	pICH47742 acceptor, pICH51288 2x35S terminator, pCR8-PipoACAP-S4, pICSL50009 C-terminal 6xHA tag, pICH41432 OCS terminator	Carb/Rif	This thesis.
<i>P. ipomoeae</i> AVRcap1b^{Swap5-} 6xHA	M.P.C.	pICH47742 acceptor, pICH51288 2x35S terminator, pCR8-PipoACAP-S5, pICSL50009 C-terminal 6xHA tag, pICH41432 OCS terminator	Carb/Rif	This thesis.
<i>P. ipomoeae</i> AVRcap1b^{Swap6-} 6xHA	M.P.C.	pICH47742 acceptor, pICH51288 2x35S terminator, pCR8-PipoACAP-S6, pICSL50009 C-terminal 6xHA tag, pICH41432 OCS terminator	Carb/Rif	This thesis.
<i>P. ipomoeae</i> AVRcap1b^{Swap7-} 6xHA	M.P.C.	pICH47742 acceptor, pICH51288 2x35S terminator, pCR8-PipoACAP-S7, pICSL50009 C-terminal 6xHA tag, pICH41432 OCS terminator	Carb/Rif	This thesis.
<i>P. ipomoeae</i> AVRcap1b-6xHA	M.P.C.	pICH47742 acceptor, pICH51288 2x35S terminator, pCR8-PipoACAP, pICSL50009 C-terminal 6xHA tag, pICH41432 OCS terminator	Carb/Rif	This thesis.
<i>P. ipomoeae</i> AVRcap1b-6xHA	M.P.C.	pICH47742 acceptor, pICH51288 2x35S terminator, pCR8-PipoACAP, pICSL50009 C-terminal 6xHA tag, pICH41432 OCS terminator	Carb/Rif	This thesis.
<i>P. ipomoeae</i> AVRcap1b-6xHA	M.P.C.	pICH47742 acceptor, pICH51288 2x35S terminator, pCR8-PipoACAP, pICSL50009 C-terminal 6xHA tag, pICH41432 OCS terminator	Carb/Rif	This thesis.
<i>P. ipomoeae</i> AVRcap1b-6xHA	M.P.C.	pICH47742 acceptor, pICH51288 2x35S terminator, pCR8-PipoACAP, pICSL50009 C-terminal 6xHA tag, pICH41432 OCS terminator	Carb/Rif	This thesis.
pOPIN-S3C- AVRcap1b	L.D.	pOPIN-F-GG, pCR8-AVRcap1b, pICSL30018 N-term 6xHis-SUMO-3C tag	Carb	This thesis.

pOPIN-S3C-NbTOL9a	M.P.C.	pOPIN-F-GG, pCR8-NbTOL9a, pICSL30018 N-term 6xHis-SUMO-3C tag	Carb	This thesis.
pOPIN-F-NbTOL9a	M.P.C.	pOPIN-F-GG, pCR8-NbTOL9a, pICSL30017 N-term 6xHis-3C tag	Carb	This thesis.
pOPIN-S3C-NbTOL9a^{ENTH-GAT}	M.P.C.	pOPIN-F-GG, pCR8-NbTOL9a ^{ENTH-GAT} , pICSL30018 N-term 6xHis-SUMO-3C tag	Carb	This thesis.
pOPIN-F-NbTOL9a^{ENTH-GAT}	M.P.C.	pOPIN-F-GG, pCR8-NbTOL9a ^{ENTH-GAT} , pICSL30017 N-term 6xHis-3C tag	Carb	This thesis.
pOPIN-S3C-NbTOL9a^{ENTH}	M.P.C.	pOPIN-F-GG, pCR8-NbTOL9a ^{ENTH} , pICSL30018 N-term 6xHis-SUMO-3C tag	Carb	This thesis.
pOPIN-F-NbTOL9a^{ENTH}	M.P.C.	pOPIN-F-GG, pCR8-NbTOL9a ^{ENTH} , pICSL30017 N-term 6xHis-3C tag	Carb	This thesis.
pOPIN-S3C-NbTOL9a^{GAT}	M.P.C.	pOPIN-F-GG, pCR8-NbTOL9a ^{GAT} , pICSL30018 N-term 6xHis-SUMO-3C tag	Carb	This thesis.
pOPIN-F-NbTOL9a^{GAT}	M.P.C.	pOPIN-F-GG, pCR8-NbTOL9a ^{GAT} , pICSL30017 N-term 6xHis-3C tag	Carb	This thesis.
<i>P. ipomoeae</i> AVRcap1b-6xHA	M.P.C.	pICH47742 acceptor, pICH51288 2x35S terminator, pCR8-PipoACAP, pICSL50009 C-terminal 6xHA tag, pICH41432 OCS terminator	Carb/Rif	This thesis.
<i>P. infestans</i> AVRcap1b^{R31E}-6xHA	M.P.C.	pICH47742 acceptor, pICH51288 2x35S terminator, pCR8-PinfACAP ^{R31E} , pICSL50009 C-terminal 6xHA tag, pICH41432 OCS terminator	Carb/Rif	This thesis.
<i>P. infestans</i> AVRcap1b^{P33E}-6xHA	M.P.C.	pICH47742 acceptor, pICH51288 2x35S terminator, pCR8-PinfACAP ^{P33E} , pICSL50009 C-terminal 6xHA tag, pICH41432 OCS terminator	Carb/Rif	This thesis.
<i>P. infestans</i> AVRcap1b^{G35E}-6xHA	M.P.C.	pICH47742 acceptor, pICH51288 2x35S terminator, pCR8-PinfACAP ^{G35E} , pICSL50009 C-terminal 6xHA tag, pICH41432 OCS terminator	Carb/Rif	This thesis.
<i>P. infestans</i> AVRcap1b^{K39E}-6xHA	M.P.C.	pICH47742 acceptor, pICH51288 2x35S terminator, pCR8-PinfACAP ^{K39E} , pICSL50009 C-terminal 6xHA tag, pICH41432 OCS terminator	Carb/Rif	This thesis.

mCherry-6xHA	L.D.	pICH86988 acceptor with integrated 35S promoter and OCS terminator, pCR8-mCherry-6xHA	Kan/Rif	(Contreras <i>et al.</i> , 2023b)
Chapter 7				
Construct info can be found in Supplementary information for Contreras et al. (2023) Science Advances .				

*: H.A. – Hiroaki Adachi, L.D. Lida Derevnina, C-H.W. – Chih-Hang Wu, M.P.C. – Mauricio Pablo Contreras, J.K. – Jiorgos Kourelis

Table AI.2: OD₆₀₀ used for each experiment.

Chapter 3	
See Materials & Methods and Supplementary Information of Adachi et al. (2019) eLife .	
Chapter 4	
See Materials & Methods and Supplementary Information of Contreras et al. (2023) The EMBO Journal .	
Chapter 5	
Figure 5.1	
Construct	OD ₆₀₀ used
eGFP	0.1
CP-eGFP	0.1
Rx ^{CCNBARC} -4xMyc	0.3
Rx ^{LRR} -6xHA	0.3
Rx-6xHA	0.3
ZAR1 ^{D481V} -6xHA	0.3
SINRC0	0.3
NRC2	0.3

NRC3	0.3
NRC4	0.3
Figure 5.3 and Figure 5.4	
Construct	OD ₆₀₀ used
Rx ^{CCNBARC} -4xMyc	0.3
Rx ^{LRR} -6xHA	0.3
Figure 5.3	
Construct	OD ₆₀₀ used
eGFP	0.1
CP-eGFP	0.1
Rx ^{CCNBARC} -4xMyc	0.3
Rx ^{LRR} -6xHA	0.3
SINRC0-3xFLAG	0.3
NRC2-3xFLAG	0.3
NRC2 ^{EEE} -3xFLAG	0.3
Figure 5.5	
Construct	OD ₆₀₀ used
NRC2 ^{EEE} -4xMyc	0.3
Rx ^{CCNBARC} -V5	0.3
Rx ^{LRR} -6xHA	0.3
Rx-6xHA	0.3
eGFP	0.1

CP-eGFP	0.1
Figure 5.6	
Construct	OD ₆₀₀ used
NbZAR1 ^{D481V}	0.3
eGFP	0.3
Rx ^{NB} -eGFP	0.3
Rx ^{NB-p-loop} -eGFP	0.3
Figure 5.7	
Construct	OD ₆₀₀ used
eGFP	0.1
CP-eGFP	0.1
Rx-6xHA	0.3
Rx ^{NB} -eGFP	0.3
NRC2 ^{EEE} -4xMyc	0.3
Figure 5.8	
Construct	OD ₆₀₀ used
eGFP	0.3
NbZAR1 ^{D481V}	0.3
Rx ^{D460V}	0.3
Rx ^{NB} -eGFP	0.3
Gpa2 ^{NB} -eGFP	0.3
Rpiamr1e ^{NB} -eGFP	0.3

Rpiamr3 ^{NB} -eGFP	0.3
Bs2 ^{NB} -eGFP	0.3
Mi ^{NB} -eGFP	0.3
Rpi-blb2 ^{NB} -eGFP	0.3

Figure 5.9

Construct	OD ₆₀₀ used
NbZAR1 ^{D481V}	0.3
Rx ^{D460V}	0.3
Rx ^{NB} -eGFP	0.3
SINRC0	0.3
NRC2	0.3
NRC3	0.3
NRC4	0.3
Gpa2 ^{NB} -eGFP	0.3
Rpiamr1e ^{NB} -eGFP	0.3

Figure 5.10

Construct	OD ₆₀₀ used
NbZAR1 ^{D481V}	0.2
Rx ^{D460V}	0.2
NRC2	0.3
NRC4	0.3
eGFP	0.1

Gpa2 ^{NB} -eGFP	0.1
Gpa2 ^{NB-A181T} -eGFP	0.1
Gpa2 ^{NB-A188C} -eGFP	0.1
Gpa2 ^{NB-Y224D} -eGFP	0.1
Gpa2 ^{NB-Q229R} -eGFP	0.1
Gpa2 ^{NB-D263Y} -eGFP	0.1

Chapter 6

Figure 6.1

Construct	OD ₆₀₀ used
AVRcap1b-6xHA	0.2
4xHA-SS15	0.2
NRC2	0.2
NRC3	0.2
NRC4	0.2

Figure 6.2

Construct	OD ₆₀₀ used
GFP-PexRD54	0.2
GFP-AVRcap1b	0.2
NbTOL9a-6xHA	0.2
NbTOL9b-6xHA	0.2
NbTOL9c-6xHA	0.2
NbTOL3-6xHA	0.2

NbTOL6-6xHA	0.2
Figure 6.3	
Construct	OD ₆₀₀ used
NbTOL9a-6xHA	0.2
AVRcap1b-4xMyc	0.2
NRC2-4xMyc	0.2
NRC3-4xMyc	0.2
NRC4-4xMyc	0.2
NRCx-4xMyc	0.2
Figure 6.4	
Construct	OD ₆₀₀ used
NbTOL9a-6xHA	0.2
GFP	0.2
GFP-AVRcap1b	0.2
AVRcap1b-4xMyc	0.2
NRC2-4xMyc	0.2
NRC3-4xMyc	0.2
NRC4-4xMyc	0.2
Figure 6.5	
Construct	OD ₆₀₀ used
MEK2 ^{DD}	0.2
NRC3 ^{D480V}	0.2

NRC4 ^{D478V}	0.2
EV	0.2
NbTOL9a-6xHA	0.2

Figure 6.6

Construct	OD ₆₀₀ used
NRC3 ^{D480V}	0.1 – 0.25 – 0.5
NRC4 ^{478V}	0.1 – 0.25 – 0.5
EV	0.4 – 0.5 - 0
RNAi:: <i>GUS</i>	0.5
RNAi:: <i>NbTOL9a</i>	0.5

Figure 6.7

Construct	OD ₆₀₀ used
RNAi:: <i>GUS</i>	0.5
RNAi:: <i>NbTOL9a</i>	0.5
NRC3 ^{D480V}	0.3
NRC4 ^{478V}	0.3
EV	0.1
AVRcap1b	0.1

Figure 6.8

Construct	OD ₆₀₀ used
GFP-AVRcap1b	0.2
NbTOL9a-6xHA	0.2

NbTOL6-6xHA	0.2
NbTOL6 ^{ENTH-GAT} -6xHA	0.2
NbTOL6 ^{ENTH} -6xHA	0.2
NbTOL6 ^{GAT} -6xHA	0.2
NbTOL6 ^{CTR} -6xHA	0.2

Figure 6.9

Construct	OD ₆₀₀ used
NRC3 ^{D480V}	0.3
GFP	0.3
<i>P.inf</i> AVRcap1b-6xHA	0.3
<i>P.mir</i> AVRcap1b-6xHA	0.3
<i>P.ipo</i> AVRcap1b-6xHA	0.3
<i>P.and</i> AVRcap1b-6xHA	0.3

Figure 6.10

Construct	OD ₆₀₀ used
NRC3 ^{D480V}	0.3
<i>P.inf</i> AVRcap1b-6xHA	0.3
<i>P.ipo</i> AVRcap1b-6xHA	0.3
<i>P.ipo</i> AVRcap1b ^{Swap1} -6xHA	0.3
<i>P.ipo</i> AVRcap1b ^{Swap2} -6xHA	0.3
<i>P.ipo</i> AVRcap1b ^{Swap3} -6xHA	0.3
<i>P.ipo</i> AVRcap1b ^{Swap4} -6xHA	0.3

<i>P. ipso</i> AVRcap1b ^{Swap5} -6xHA	0.3
<i>P. ipso</i> AVRcap1b ^{Swap6} -6xHA	0.3
<i>P. ipso</i> AVRcap1b ^{Swap7} -6xHA	0.3

Figure 6.13

Construct	OD ₆₀₀ used
NbTOL9a-3xFLAG	0.2
<i>P. inf</i> AVRcap1b-6xHA	0.2
<i>P. inf</i> AVRcap1b ^{R31E} -6xHA	0.2
<i>P. inf</i> AVRcap1b ^{R33E} -6xHA	0.2
<i>P. inf</i> AVRcap1b ^{G35E} -6xHA	0.2
<i>P. inf</i> AVRcap1b ^{K39E} -6xHA	0.2
<i>P. ipso</i> AVRcap1b-6xHA	0.2

Figure 6.14

Construct	OD ₆₀₀ used
NRC3 ^{D480V}	0.3
<i>P. inf</i> AVRcap1b-6xHA	0.2
<i>P. inf</i> AVRcap1b ^{R31E} -6xHA	0.2
<i>P. inf</i> AVRcap1b ^{R33E} -6xHA	0.2
<i>P. inf</i> AVRcap1b ^{G35E} -6xHA	0.2
<i>P. inf</i> AVRcap1b ^{K39E} -6xHA	0.2
<i>P. ipso</i> AVRcap1b-6xHA	0.2

Figure 6.15

Construct	OD ₆₀₀ used
Rx-V5	0.2
NRC2 ^{EEE} -3xFLAG	0.2
eGFP	0.1
CP-eGFP	0.1
<i>P. inf</i> AVRcap1b-6xHA	0.2
<i>P. ipa</i> AVRcap1b-6xHA	0.2
<i>P. ipa</i> AVRcap1b ^{Swap7} -6xHA	0.2
mCherry-6xHA	0.2

Figure 6.16

Construct	OD ₆₀₀ used
Rx-V5	0.2
NRC2 ^{EEE} -3xFLAG	0.2
eGFP	0.1
CP-eGFP	0.1
<i>P. inf</i> AVRcap1b-6xHA	0.2
<i>P. inf</i> AVRcap1b ^{P33E} -6xHA	0.2
<i>P. ipa</i> AVRcap1b-6xHA	0.2
mCherry-6xHA	0.2

Chapter 7

See Materials & Methods and Supplementary Information of [Contreras et al., \(2023\)](#) [Science Advances](#).

Appendix II:

Supplementary information for Chapter 3:

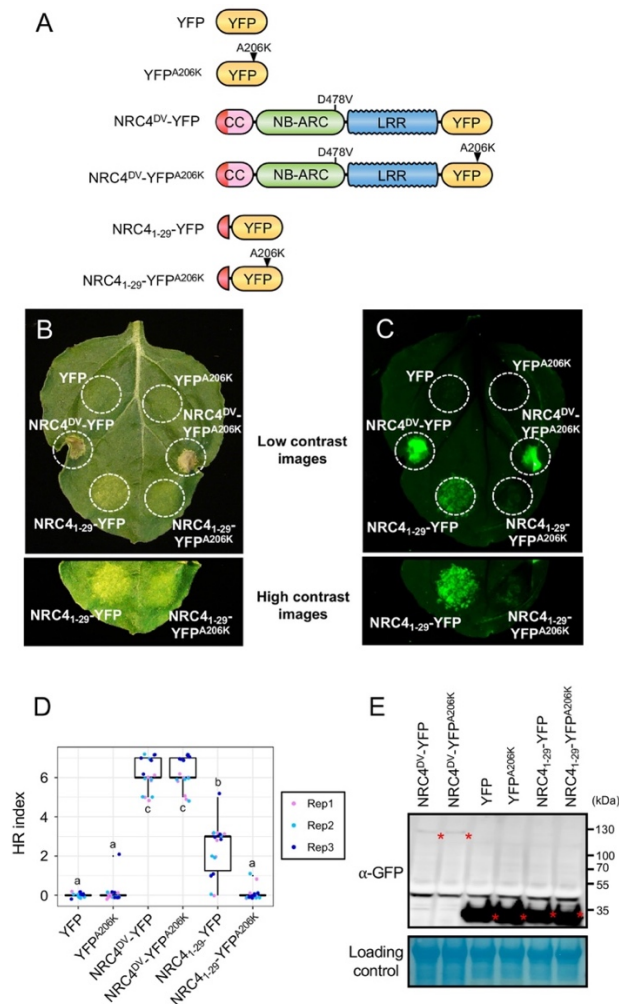


Figure AII.1: NRC4₁₋₂₉-YFP cell death is compromised by YFP A206K mutation.

(A) Schematic representation of NRC4^{DV}-YFP, NRC4₁₋₂₉-YFP and the variants used for the *in planta* expression assays. Arrowheads show A206K mutation site in YFP. The red colour represents NRC4 1 to 29 amino acid region. (B, C) YFP A206K mutation reduces NRC4₁₋₂₉-YFP cell death in wild-type *N. benthamiana* leaves. NRC4^{DV}-YFP, NRC4₁₋₂₉-YFP, YFP and the A206K variants were co-expressed with p19 and photographed at 7 days after agroinfiltration. Cell death-related autofluorescence was detected with Odyssey Infrared Imager (800 nm channel, LI-COR) (D) Box plots showing cell death intensity scored as an HR index based on three independent experiments. (E) In planta accumulation of NRC proteins. For anti-GFP immunoblots of NRC4^{DV}-YFP, NRC4₁₋₂₉-YFP, YFP and the mutant proteins, total proteins were

prepared from wild-type *N. benthamiana* leaves at 36 hr after agroinfiltration. Red asterisks indicate expected band sizes.

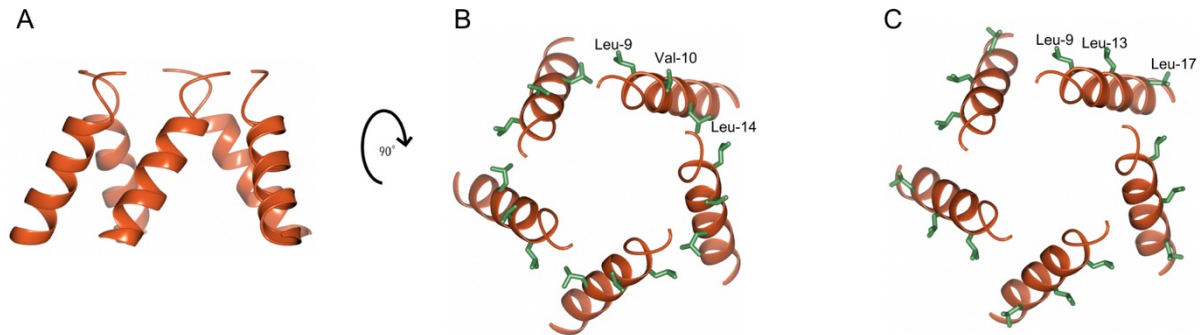


Figure AII.2: Mapping loss of function mutations on N-terminal α helices of NRC4.

(A) Cartoon representation of N-terminal α helices of NRC4 resistosome. (B, C) N-terminal α helices are rotated 90 degrees and amino acids mutated in NRC4^{AAA} and NRC2^{EEE} are shown as stick representation and labelled.

Appendix III

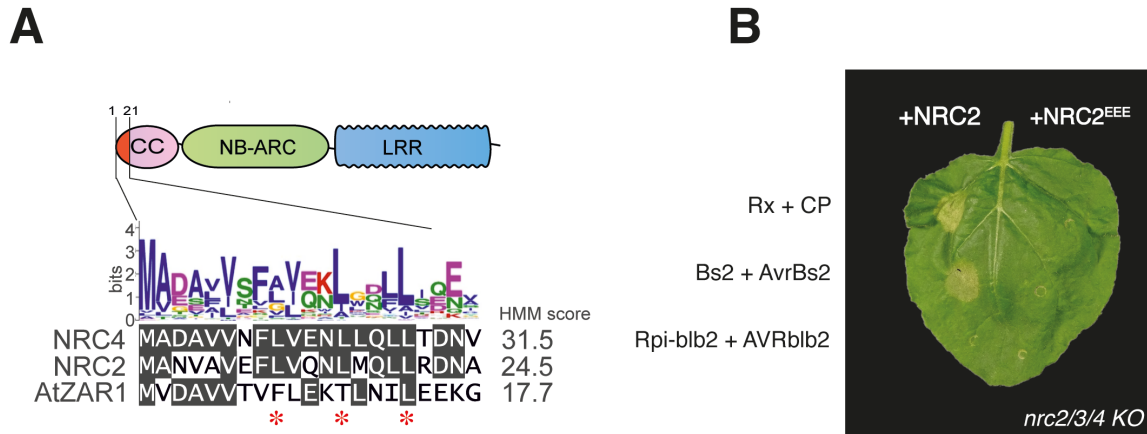


Figure AIII.1: MADA motif mutants of NRC2 are unable to trigger cell death.

(A) Much like AtZAR1 and NRC4, NRC2 has an N-terminal MADA motif. Alignment of NRC2, NRC4 and AtZAR1 N-terminal MADA motifs along with the consensus sequence pattern for the motif and the HMM score for MADA prediction of each sequence. Residues mutated in NRC2^{EEE} mutant are highlighted with red asterisks (positions 9, 13 and 17 respectively). (B) Unlike NRC2, NRC2^{EEE} does not complement Rx/PVX CP and Bs2/AvrBs2-triggered hypersensitive cell death in leaves of *nrc2/3/4* KO *N. benthamiana* mutant lines. Representative leaves infiltrated with the appropriate constructs were photographed 5-7 days after infiltration. NRC2 and NRC2^{EEE} constructs are C-terminally 4xMyc-tagged. All effectors used are C-terminally GFP-tagged. All sensors used are C-terminally 6xHA tagged. One representative leaf is shown.

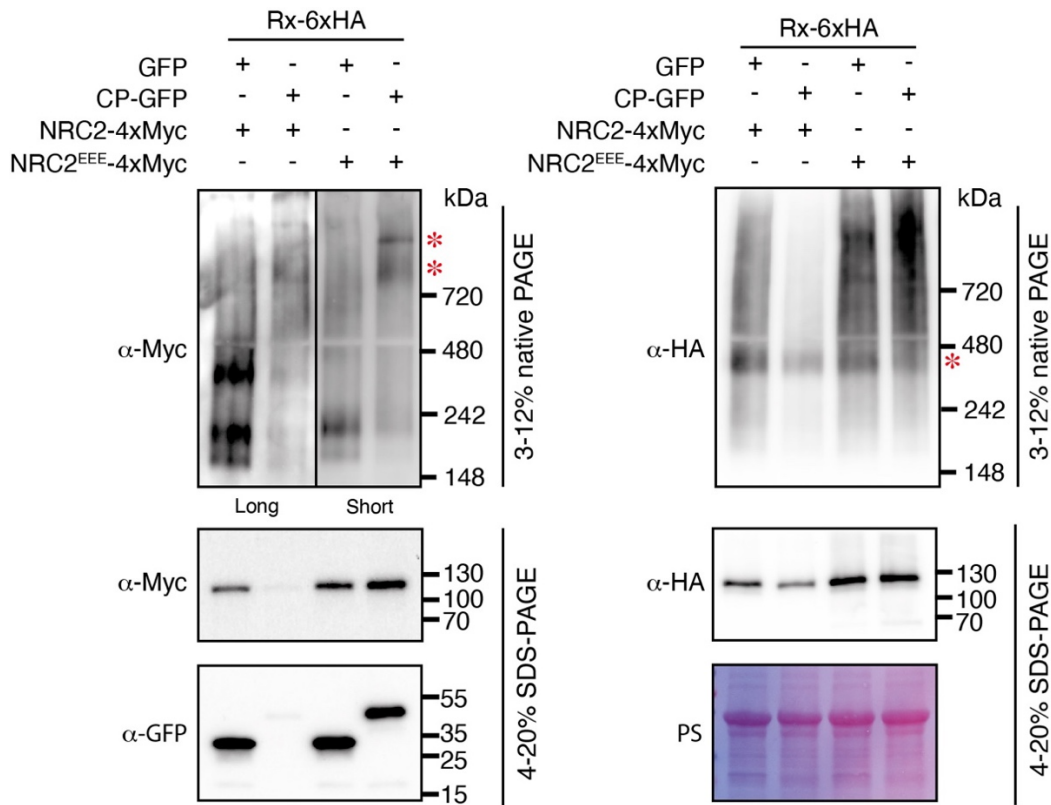


Figure AIII.2: NRC2 with an intact N-terminal MADA motif also oligomerizes upon Rx-mediated activation.

BN-PAGE and SDS-PAGE assays with inactive and activated Rx-NRC2. C-terminally 6xHA tagged Rx and C-terminally 4xMyc-tagged NRC2 or NRC2^{EEE} were co-expressed with either free GFP or C-terminally GFP-tagged PVX CP. Total protein was extracted with a Tris-HCl-based buffer, as described in materials and methods. Extracts were run on native and denaturing PAGE assays in parallel and immunoblotted with the appropriate antisera labelled on the left. Approximate molecular weights (kDa) of the proteins are shown on the right. Red asterisks indicate bands corresponding to the activated NRC2 complex (α -Myc blot) and Rx (α -HA blot). Given that the ongoing cell death triggered by NRC2 activation resulted in lower protein accumulation, we showed different exposures (long and short) as indicated by the black line. Rubisco loading control was carried out using Ponceau stain (PS). The experiment was repeated 2 times.

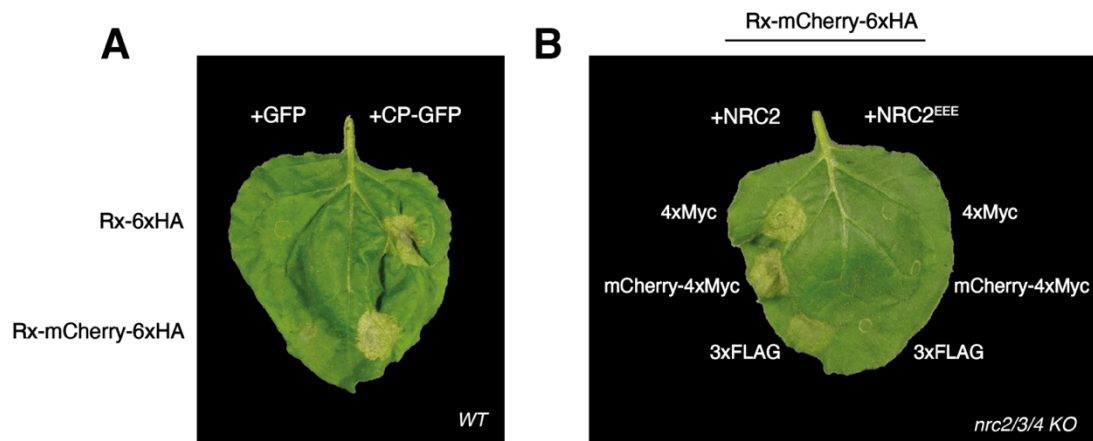


Figure AIII.3: All C-terminally tagged sensors and helpers used retain the capacity to trigger hypersensitive cell death.

(A) Much like C-terminally 6xHA tagged Rx, C-terminally mCherry-6xHA tagged Rx can mediate hypersensitive cell death when activated by PVX CP. Representative leaves of *WT N. benthamiana* were infiltrated with the appropriate constructs and photographed 5-7 days after infiltration. C-terminal tags are indicated. Free GFP (+GFP) was used as a negative control for C-terminally GFP-tagged PVX CP (PVX CP-GFP). One representative leaf is shown. (B) Rx-mCherry-6xHA is compatible with all C-terminally tagged versions of NRC2 tested. Rx/PVX CP-triggered hypersensitive cell death was complemented by C-terminally 4xMyc, mCherry-4xMyc and 3xFLAG variants of NRC2 respectively in leaves of *nrc2/3/4* KO *N. benthamiana* mutant lines when Rx was C-terminally tagged with mCherry-6xHA. The corresponding NRC2^{EEE} variants with the same C-terminal tag were no longer able to complement hypersensitive cell death. Representative leaves were infiltrated with the appropriate constructs and photographed 5-7 days after infiltration. One representative leaf is shown.

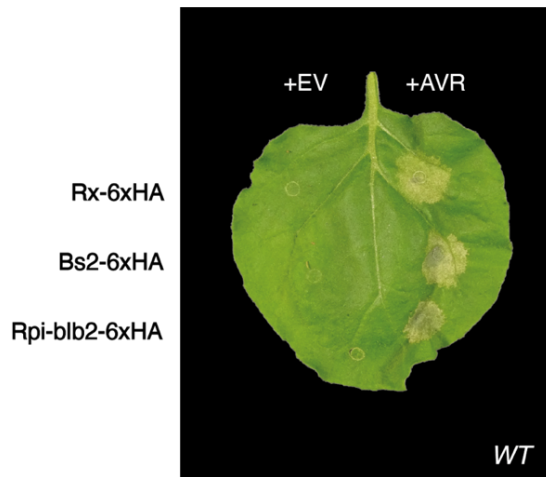


Figure AIII.4: C-terminally 6xHA tagged sensors retain the capacity to mediate cell death.

C-terminally 6xHA tagged Rx, Bs2 and Rpi-blb2 can mediate hypersensitive cell death in leaves of *nrc2/3/4* KO *N. benthamiana* mutant lines when activated by PVX CP, AvrBs2 and AVRblb2, respectively. Representative leaves of *WT N. benthamiana* were infiltrated with the appropriate constructs and photographed 5-7 days after infiltration. Free GFP was used as a negative control (EV) for C-terminally GFP-tagged effectors (AVR). One representative leaf is shown.

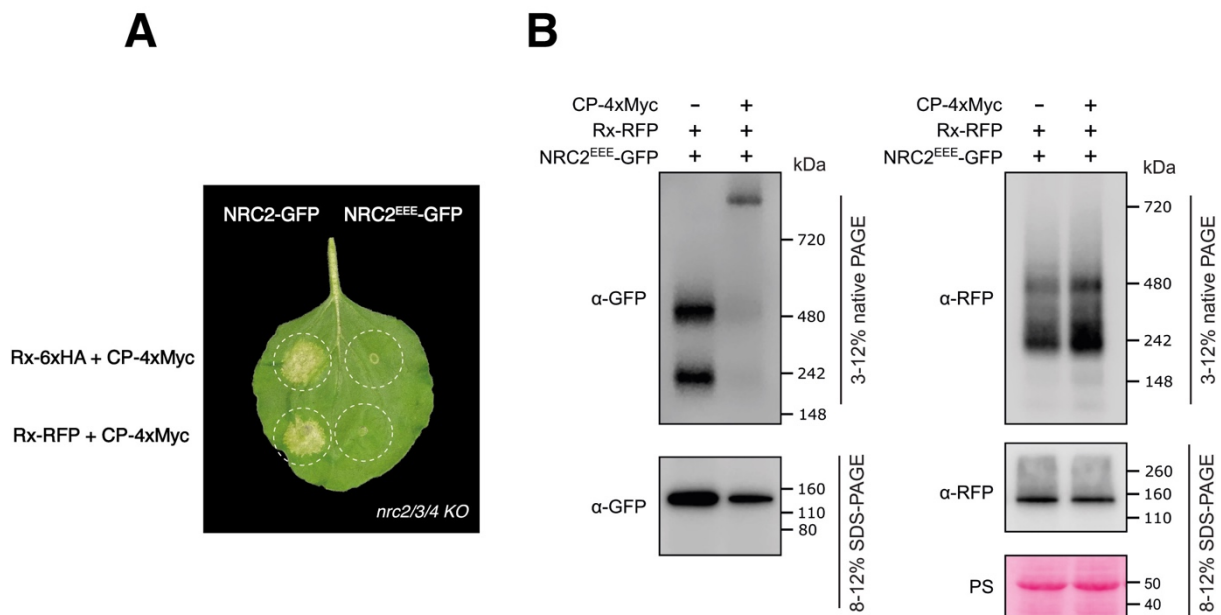


Figure AIII.5: Fluorescent protein-tagged Rx and NRC2 retain cell death-mediating capacity and can oligomerize upon activation.

(A) C-terminally GFP-tagged NRC2 complements Rx/PVX CP cell death in leaves of *nrc2/3/4 N. benthamiana* KO mutant lines when Rx is C-terminally tagged with 6xHA or RFP. This cell death is not

complemented with C-terminally GFP-tagged NRC2^{EEE}. Representative leaves were infiltrated with the appropriate constructs and photographed 5-7 days after infiltration. One representative leaf is shown. **(B)** BN-PAGE and SDS-PAGE assays performed in parallel on protein extracts used for membrane enrichment assays with inactive and activated C-terminally RFP-tagged Rx and C-terminally GFP-tagged NRC2^{EEE}. Total protein was extracted with a Tris-HCl-based buffer, as described in materials and methods. Extracts were run on native and denaturing PAGE assays in parallel and immunoblotted with the appropriate antisera labelled on the left. Approximate molecular weights (kDa) of the proteins are shown on the right. Rubisco loading control was carried out using Ponceau stain (PS). The experiment was repeated 2 times.

Appendix IV

Supplementary information for Chapter 5

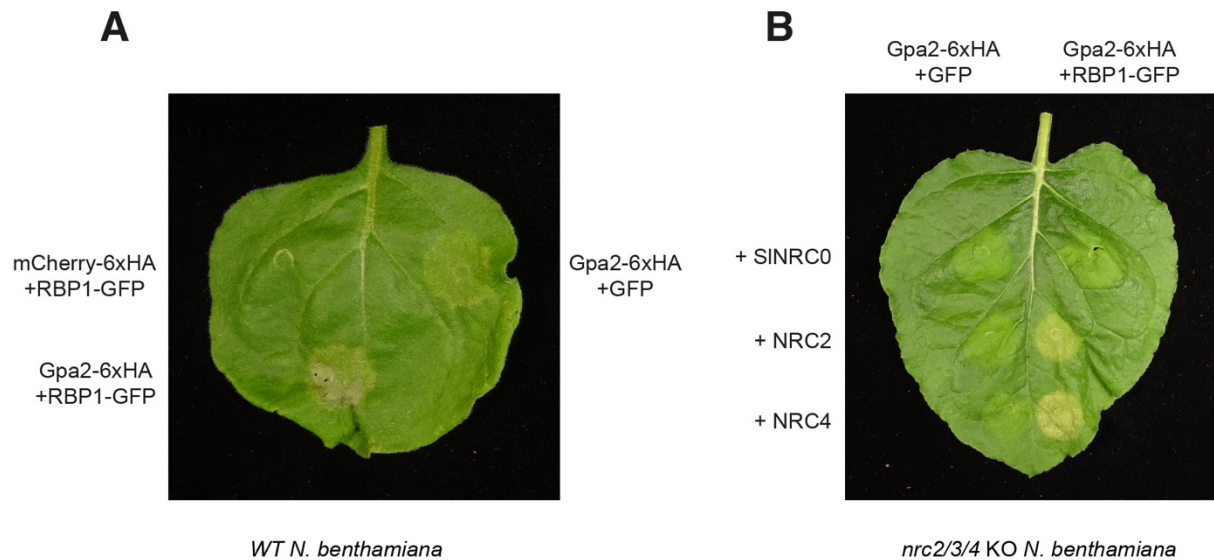


Figure AIV.1: Gpa2 signals through NRC2 and NRC4.

(A) Representative photos of HR assays with Gpa2 in leaves of WT *N. benthamiana*. Gpa2-6xHA was expressed on its own or co-expressed with free GFP or RBP1-GFP. RBP1-GFP was co-expressed with mCherry-6xHA as a control. Leaves were infiltrated with the constructs indicated and photographed 5-7 days after infiltration. One representative leaf is shown. (B) Representative photos of HR assays with Gpa2 in leaves of *nrc2/3/4* KO *N. benthamiana* with NRC complementation. Gpa2-6xHA was co-expressed with NRC2 or NRC4. GFP was included as a negative control for RBP1-eGFP. SINRC0 was included as a negative control for NRC2 and NRC4. Leaves were infiltrated with the constructs indicated and photographed 5-7 days after infiltration. One representative leaf is shown.

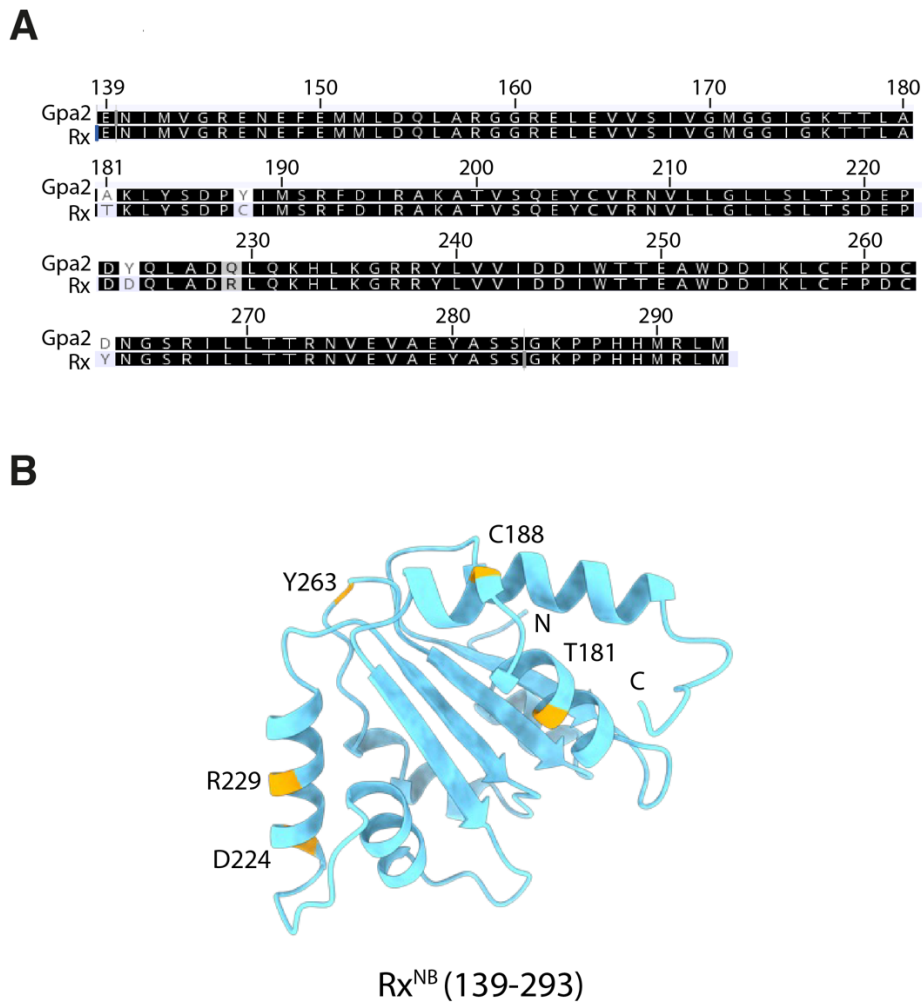


Figure AIV.2: Polymorphic surface-exposed residues in the NB domains of Gpa2 and Rx explain differences in NRC4 activation strength.

(A) Amino acid alignment between NB domains of Gpa2 and Rx. Polymorphic residues are marked in white/grey. **(B)** AF2 prediction of Rx^{NB} domain. Residues that are polymorphic between Rx and Gpa2 are highlighted in orange and numbered.

Appendix V

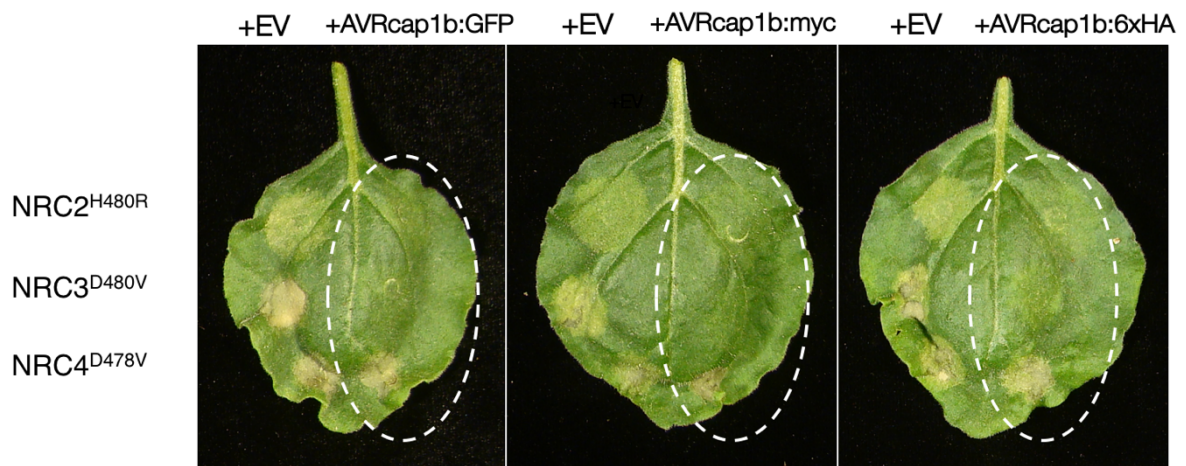


Figure AV.1: C-terminally tagged versions of AVRcap1b are still able to suppress NRC2 and NRC3 mediated cell-death.

Photos are representative images of *N. benthamiana* leaves imaged at 5 days post-agroinfiltration. Autoactive MHD mutants of NRC2, NRC3 and NRC4 were co-infiltrated with empty vector (left hand side of the leaves) or with AVRcap1b (right hand side, circled in white).

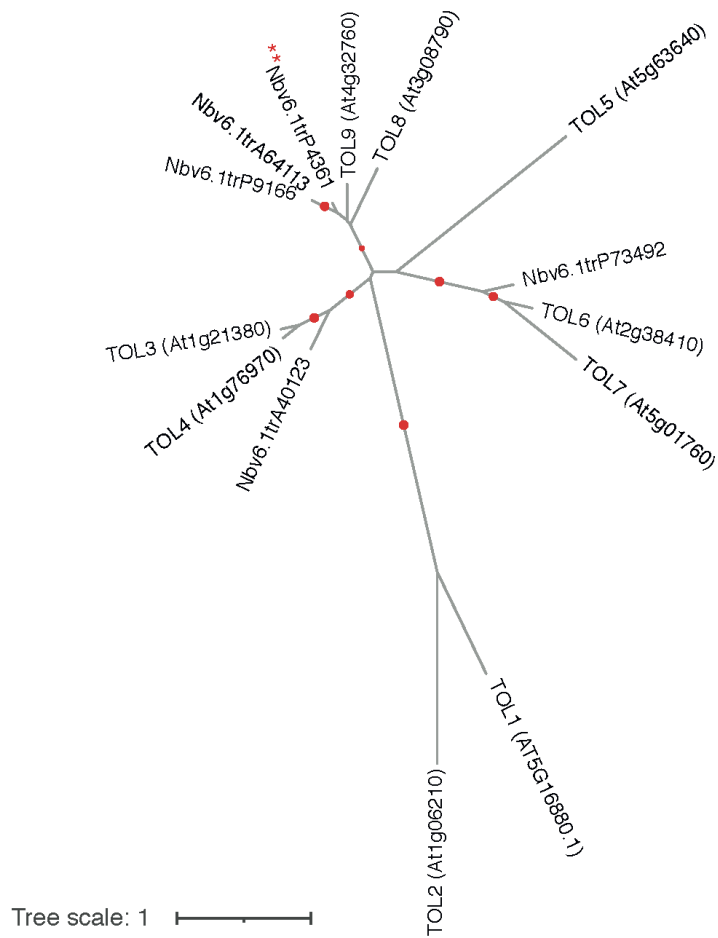


Figure AV.2: Maximum-likelihood phylogenetic tree of TOL proteins from *N. benthamiana* and *A. thaliana*.

Protein sequences were aligned using Clustal Omega. The ENTH and GAT domains were used for further analysis. The phylogenetic tree was constructed in MEGAX using the Jones-Taylor-Thornton (JTT) substitution model and 1000 bootstrap iterations. Branches with bootstrap support higher than 80 are indicated with red dots. NbTOL9a is indicated by two red asterisks. The scale bar indicates the evolutionary distance in amino acid substitutions per site.

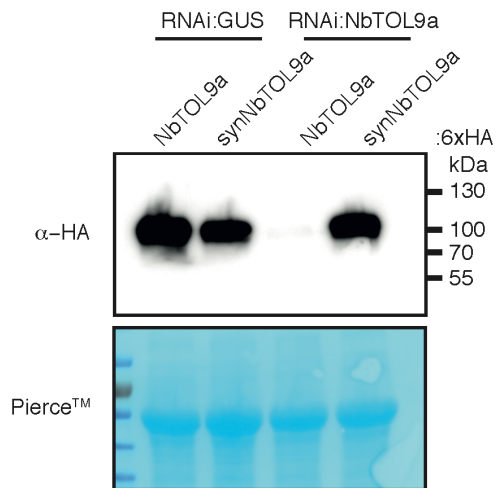


Figure AV.3: RNAi:*NbTOL9a* silencing construct reduces protein accumulation levels of *NbTOL9a*.

Wild-type *NbTOL9a* (*NbTOL9a*:6xHA) and the synthetic version (*synNbTOL9a*:6xHA) were transiently co-expressed with RNAi:*GUS* or RNAi:*NbTOL9a*. *synNbTOL9a*:6xHA was used as a control that is not targeted for knockdown by the RNAi:*NbTOL9a*. Total protein extracts were immunoblotted with HA antiserum. Approximate molecular weights (kDa) of the proteins are shown on the right. Rubisco loading controls were conducted using Pierce™ staining.

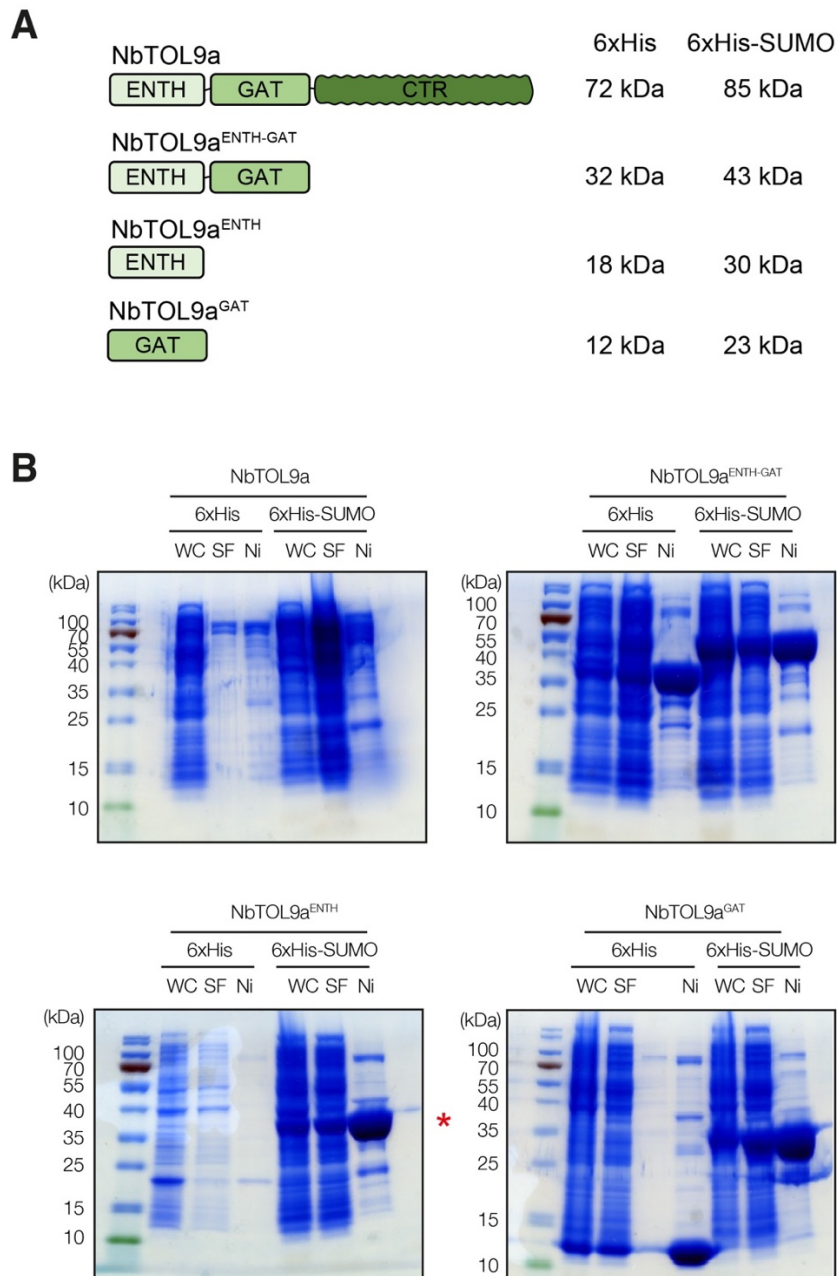


Figure AV.4: Expression tests of NbTOL9a and different NbTOL9a domains in *E. coli*.

(A) Schematic representation of NbTOL9a variants tested in *E. coli* expression. Approximate molecular weights of each variant with either N-terminal 6xHis or N-terminal 6xHis-SUMO tags are indicated on the right. (B) SDS-PAGE gels of protein extracts from *E. coli* strains expressing NbTOL9a and different NbTOL9a variants. For each construct, samples from the total cell lysate (insoluble + soluble), soluble, and post-Nickel affinity purification (Ni) fractions were loaded. Gels were stained with Coomassie brilliant blue. Approximate molecular weights in kDa are indicated on the left. Red asterisks indicate overexpression bands matching the expected size.

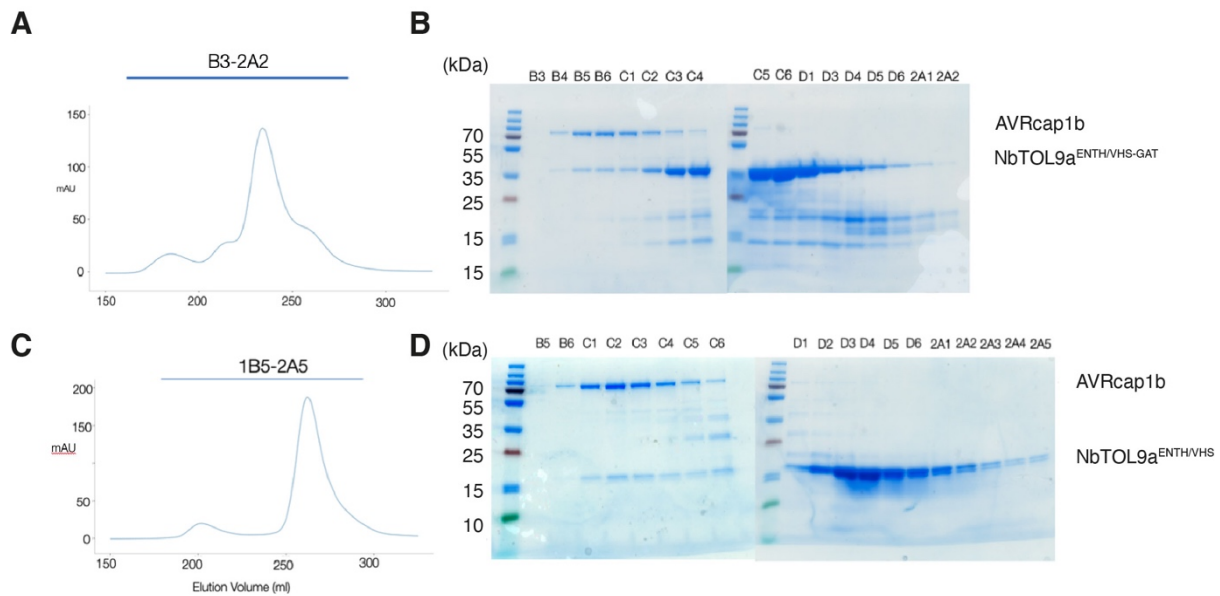


Figure AV.5: NbTOL9a^{ENTH+GAT} and NbTOL9a^{ENTH} domains form a complex with AVRcap1b in vitro.

(A) Gel filtration trace of AVRcap1b incubated overnight with NbTOL9a^{ENTH+GAT}. Absorbance at 280 nm is plotted against elution volume. (B) SDS-PAGE gels of fractions indicated in panel A, stained with Coomassie Brilliant Blue. Fractions B4 to C2 correspond to AVRcap1b in complex with NbTOL9a^{ENTH}. Fractions C3 to D5 correspond to excess NbTOL9a^{ENTH+GAT} not bound to AVRcap1b. Approximate molecular weights are indicated of the left in kDa. (C) Gel filtration trace of AVRcap1b incubated overnight with NbTOL9a^{ENTH}. Absorbance at 280 nm is plotted against elution volume. (D) SDS-PAGE gels of fractions indicated in panel C, stained with Coomassie Brilliant Blue. Fractions B6 to C6 correspond to AVRcap1b in complex with NbTOL9a^{ENTH}. Fractions D1 to 2A5 correspond to excess NbTOL9a^{ENTH} not bound to AVRcap1b. Approximate molecular weights are indicated of the left in kDa. Approximate molecular weights of each of the purified proteins are 70 kDa for AVRcap1b, 30 kDa for NbTOL9a^{ENTH+GAT} and 17 kDa for NbTOL9a^{ENTH} (without N-terminal cleavable tags).



Figure AV.6: Residues predicted to be involved in NbTOL9a binding are conserved between *P. infestans* and *P. ipomoeae* AVRcap1b.

Amino acid sequence alignment of residues within the WY1 domain of AVRcap1b homologs from *P. infestans* and *P. ipomoeae*. Red asterisks indicate residues found to be proximal to NbTOL9a^{ENTH} in the cocrystal structure.

Table AV.1: Summary of X-ray data and model parameters for AVRcap1b – NbTOL9a^{ENTH}.

Data collection	
Diamond Light Source beamline	I04
Wavelength (Å)	0.9795
Detector	Eiger2 XE 16M
Resolution range (Å)	79.57 – 4.10 (4.49 – 4.10)
Space Group	<i>P</i> 2 ₁ 2 ₁ 2 ₁
Cell parameters (Å)	<i>a</i> = 85.9, <i>b</i> = 136.9, <i>c</i> = 195.6
Total no. of measured intensities	242580 (59716)
Unique reflections	18772 (4401)
Multiplicity	12.9 (13.6)
Mean <i>I</i> / σ (<i>I</i>)	9.6 (1.0)
Completeness (%)	100.0 (100.0)
$R_{\text{merge}}^{\text{a}}$	0.106 (2.126)
$R_{\text{meas}}^{\text{b}}$	0.110 (2.208)
$CC_{1/2}^{\text{c}}$	1.000 (0.518)
Refinement	
Resolution range (Å)	79.70 – 4.10 (4.21 – 4.10)
Reflections: working/free ^d	17766/938
$R_{\text{work}}/R_{\text{free}}^{\text{e}}$	0.225/0.305
MolProbity score/Clashscore ^f	3.15/31.08
Ramachandran plot: favoured/allowed/disallowed ^f (%)	95.9/3.1/1.0
R.m.s. bond distance deviation (Å)	0.008
R.m.s. bond angle deviation (°)	1.68
AVRcap1b – chains/no. protein residues/ranges	A,B/598/19-616
NbTOL9a ^{ENTH} – chains/no. protein residues/ranges	C,D/138/1-140

Values in parentheses are for the outer resolution shell.

^a $R_{\text{merge}} = \frac{\sum_{hkl} \sum_i |I_i(hkl) - \langle I(hkl) \rangle|}{\sum_{hkl} \sum_i I_i(hkl)}$.

^b $R_{\text{meas}} = \frac{\sum_{hkl} [N/(N-1)]^{1/2} \times \sum_i |I_i(hkl) - \langle I(hkl) \rangle|}{\sum_{hkl} \sum_i I_i(hkl)}$, where $I_i(hkl)$ is the *i*th observation of reflection *hkl*, $\langle I(hkl) \rangle$ is the weighted average intensity for all observations *i* of reflection *hkl* and *N* is the number of observations of reflection *hkl*.

^c $CC_{1/2}$ is the correlation coefficient between symmetry equivalent intensities from random halves of the dataset.

^d The data set was split into "working" and "free" sets consisting of 90 and 10% of the data respectively. The free set was not used for refinement.

^e The R-factors R_{work} and R_{free} are calculated as follows: $R = \frac{\sum (|F_{\text{obs}} - F_{\text{calc}}|)}{\sum |F_{\text{obs}}|}$, where F_{obs} and F_{calc} are the observed and calculated structure factor amplitudes, respectively.

^f As calculated using MolProbity (Davis *et al.*, 2007).

Appendix VI

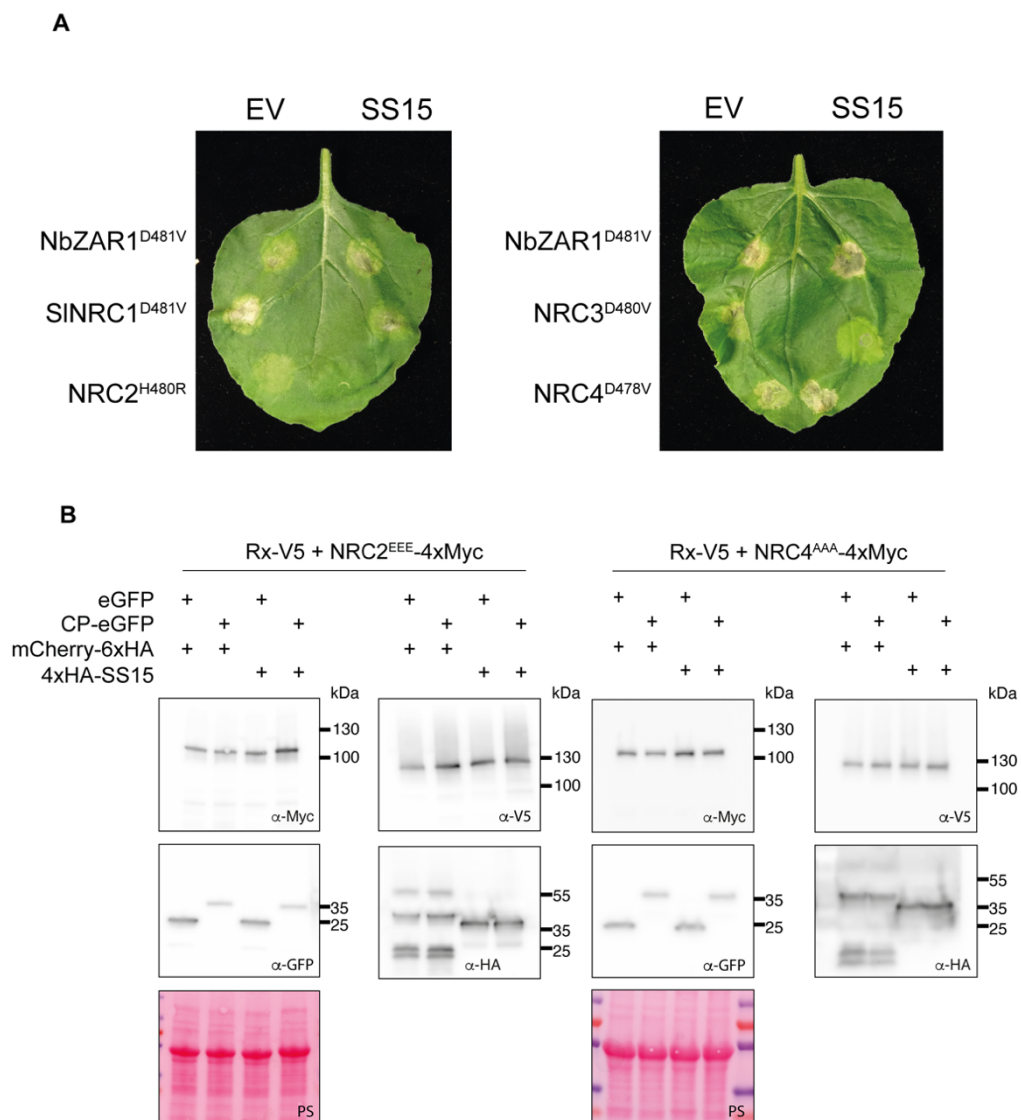


Figure AVI.1: SS15 suppresses cell death mediated by SINRC1, NRC2 and NRC3 but not NRC4 or NbZAR1.

(A) Photo of representative leaves from *N. benthamiana nrc2/3/4* KO plants showing HR after co-expression of various autoactive NLR variants with a free mCherry-6xHA fusion protein (EV) or with N-terminally 4xHA-tagged SS15. (B) SDS-PAGE accompanying BN-PAGE shown in **Figure 7.1B**. Total protein extracts were immunoblotted with the appropriate antisera labelled on the left. Approximate molecular weights (kDa) of the proteins are shown on the right. Rubisco loading control was carried out using Ponceau stain (PS). The experiment was repeated three times with similar results.

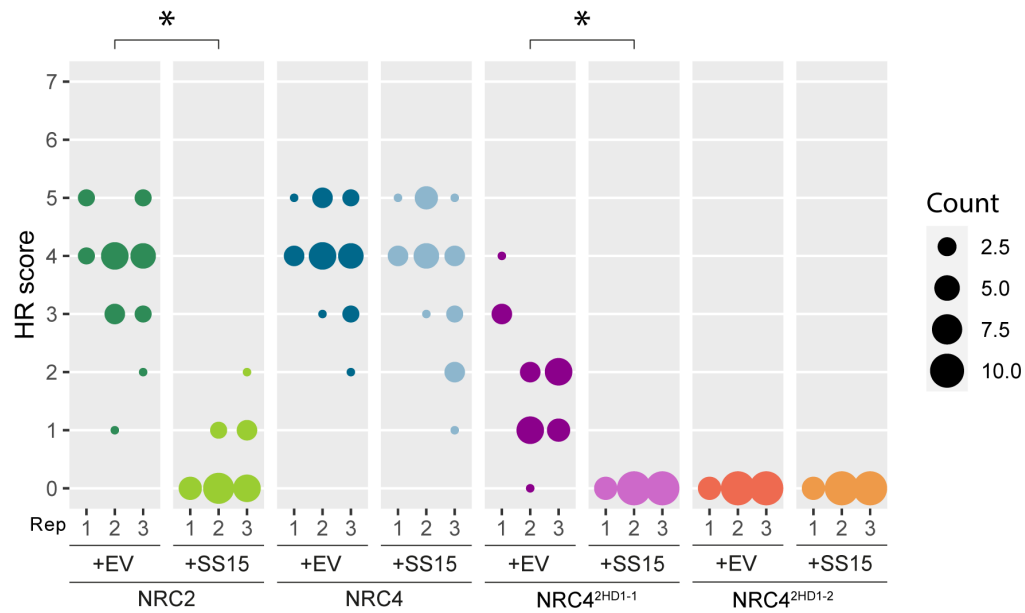


Figure AVI.2: NRC4^{HD1-1} chimera is susceptible to inhibition by SS15.

HR scores accompanying **Figure 7.4D**. In all cases, Rx/PVX CP was used to activate the system. HR was scored based on a modified 0–7 scale between 5–7 days post-infiltration (Segretin *et al.*, 2014). HR scores are presented as dot plots, where the size of each dot is proportional to the number of samples with the same score (Count). Results are based on 3 biological replicates. Statistical tests were implemented using the besthr R library. We performed bootstrap resampling tests using a lower significance cut-off of 0.025 and an upper cut-off of 0.975. Mean ranks of test samples falling outside of these cut-offs in the control samples bootstrap population were considered significant. Significant differences between the conditions are indicated with an asterisk (*).

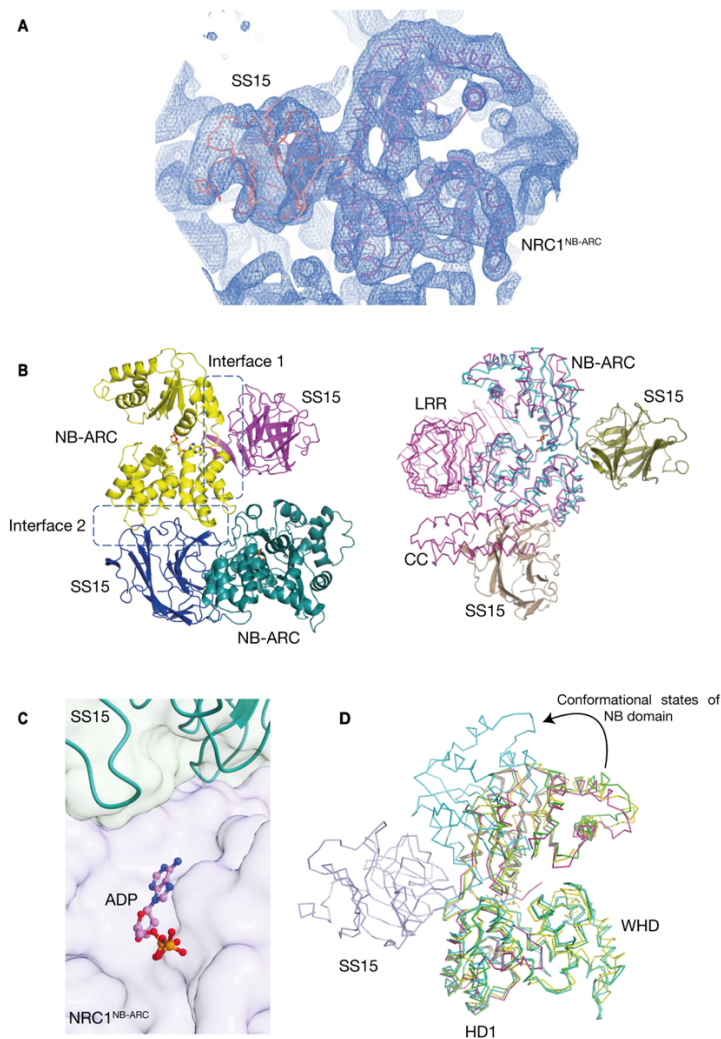


Figure AVI.4: Crystal structure of SS15 in complex with SINRC1^{NB-ARC}.

Electron density map showing the relative orientation and arrangement of SS15 (orange) and SINRC1^{NB-ARC} (violet) within an asymmetric unit. 2Fo-Fc map countered at 1σ **(B)** Two possible interfaces between SS15 and SINRC1^{NB-ARC} revealed from the crystal packing. Both interfaces (Interface 1 and Interface 2) are outlined (Left). Modelling of both potential binding interfaces for SS15 complex with full length SINRC1 (magenta) reveals a steric clash between the CC-domain of SINRC1 and SS15, making interface 2 unlikely to be biologically relevant in the full-length context (Right). **(C)** Close up view of interaction between SS15-SINRC1^{NB-ARC} interaction interface relative to the ATP-binding site within the NB-ARC domain of SINRC1. The pyrophosphate moiety of ADP is oriented facing opposite the SS15 binding interface (shown as ball and sticks), suggesting that SS15 is unlikely to displace bound nucleotide or prevent ATP hydrolysis. **(D)** Structure of SS15-SINRC1^{NB-ARC} (yellow, PDB 8BV0) is superimposed over the NB-ARC domain of AtZAR1 in its inactive (green, PDB 6J5W), intermediate (cyan, PDB 6J5V), and active resistosome (magenta, 6J5T) conformations. Visualizing these three states reveals the trajectory of the NB domain as it

moves relative to the HD1 and WHD domains while changing from inactive to activated states. The binding of SS15 at the critical hinge region between the NB and HD1-WHD domains likely immobilizes this loop, preventing these critical intramolecular rearrangements and therefore preventing NLR activation.

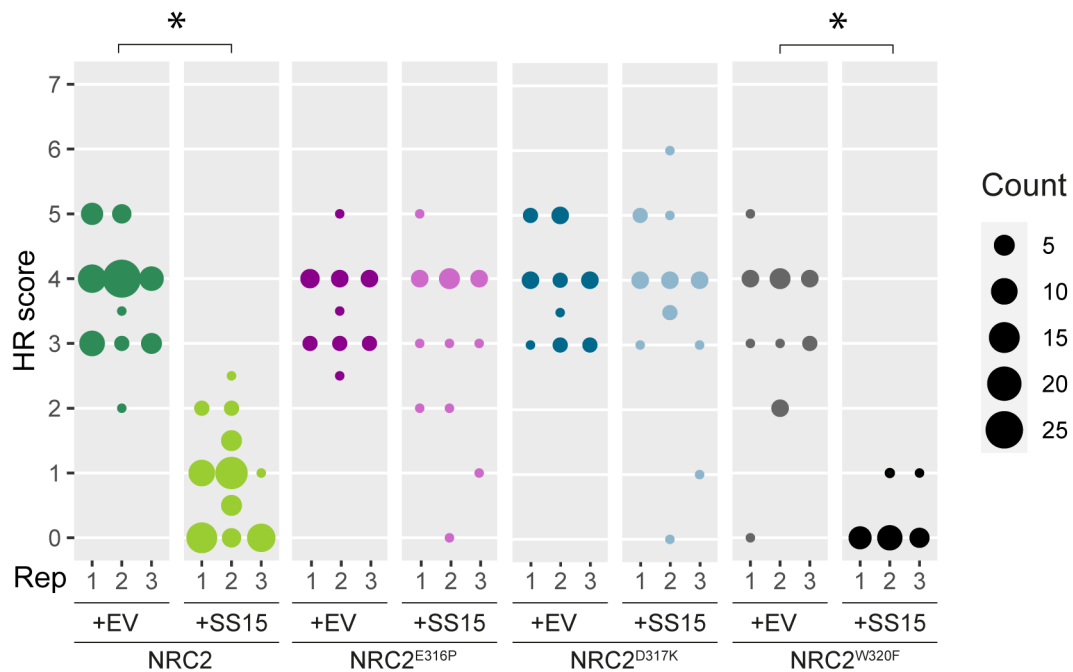


Figure AVI.5: NRC2^{E316P} and NRC2^{D317K} abolish SS15-mediated suppression of Rx.

HR scores accompanying **Figure 7.6**. In all cases, Rx/PVX CP was used to activate the system. HR was scored based on a modified 0–7 scale (49) between 5–7 days post-infiltration. HR scores are presented as dot plots, where the size of each dot is proportional to the number of samples with the same score (Count). Results are based on 3 biological replicates. Statistical tests were implemented using the besthr R library (MacLean, 2019). We performed bootstrap resampling tests using a lower significance cut-off of 0.025 and an upper cut-off of 0.975. Mean ranks of test samples falling outside of these cut-offs in the control samples bootstrap population were considered significant. Significant differences between the conditions are indicated with an asterisk (*).

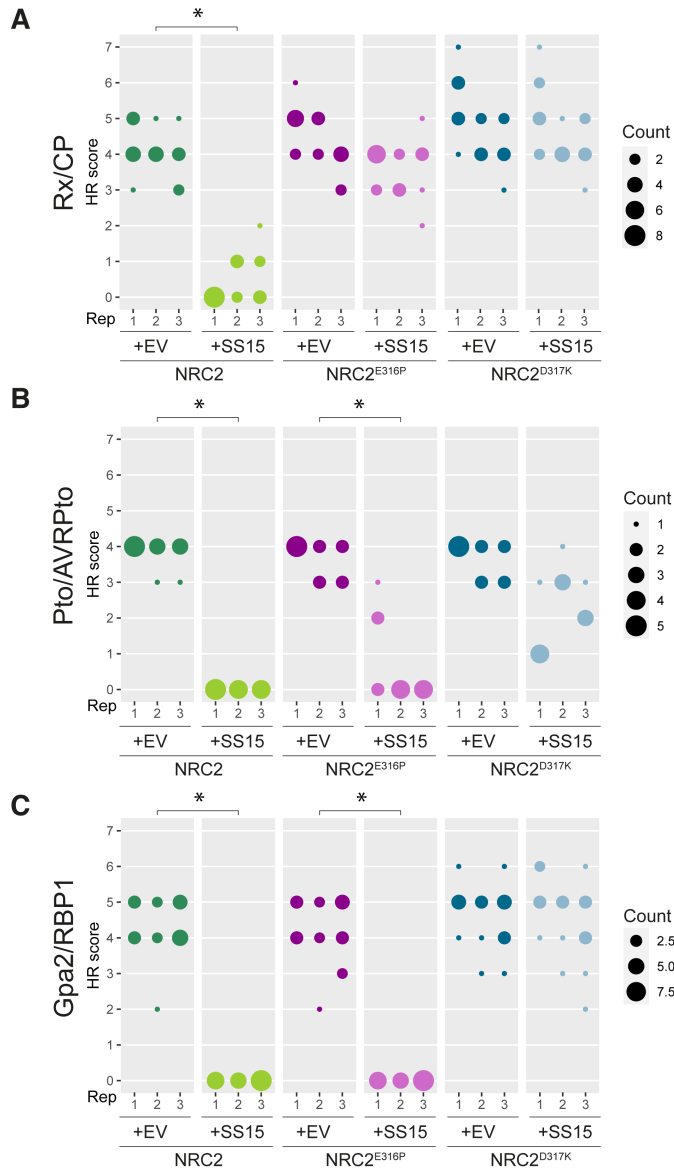


Figure AVI.6: NRC2^{D317K} abolishes SS15-mediated suppression of Rx, Gpa2 and Prf.

HR scores accompanying **Figure 7.7**. NRCs were activated using Rx/PVX CP (**A**), Pto/AVRPto (**B**) or Gpa2/RBP1 (**C**). HR was scored based on a modified 0–7 scale between 5–7 days post-infiltration (Segretin *et al.*, 2014). HR scores are presented as dot plots, where the size of each dot is proportional to the number of samples with the same score (count). Results are based on 3 biological replicates. Statistical tests were implemented using the *besthr* R library. We performed bootstrap resampling tests using a lower significance cut-off of 0.025 and an upper cut-off of 0.975. Mean ranks of test samples falling outside of these cut-offs in the control samples bootstrap population were considered significant. Significant differences between the conditions are indicated with an asterisk (*).

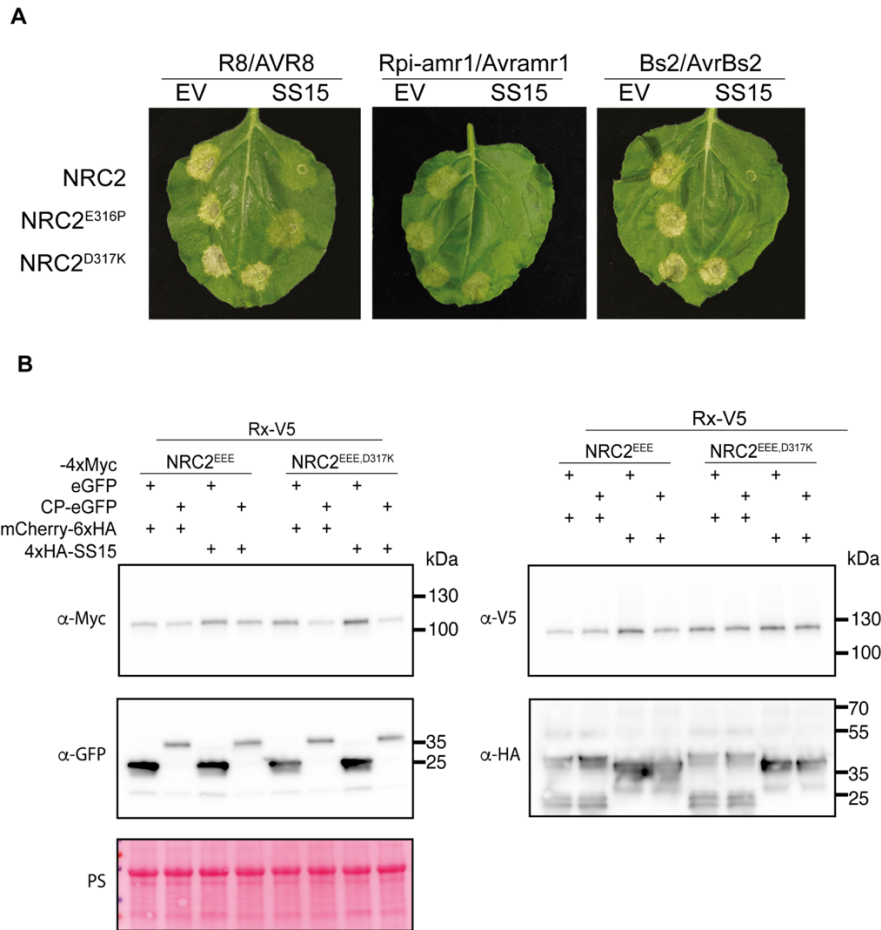


Figure AVI.7: NRC2^{D317K} abolishes SS15-mediated suppression of all NRC2-dependent sensors tested and restores NRC2 resistosome formation.

Photo of representative leaves from *N. benthamiana* *nrc2/3/4* KO plants showing HR after co-expression of NRC2, or different NRC2 variants generated with various sensor/effector pairs. These effector-sensor-helper combinations were co-expressed with a free mCherry-6xHA fusion protein (EV) or with N-terminally 4xHA-tagged SS15. **(B)** SDS-PAGE accompanying BN-PAGE shown in **Figure 7.7B**. Total protein extracts were immunoblotted with the appropriate antisera labelled on the left. Approximate molecular weights (kDa) of the proteins are shown on the right. Rubisco loading control was carried out using Ponceau stain (PS). The experiment was repeated three times with similar results.

Table AVI.1: Summary of X-ray data and model parameters for NRC1^{NB-ARC}-SS15.

Data collection	
Diamond Light Source beamline	I03
Wavelength (Å)	0.9763
Detector	Eiger2 XE 16M
Resolution range (Å)	51.34 – 4.50 (5.03 – 4.50)
Space Group	<i>P</i> 6 ₁
Cell parameters (Å)	<i>a</i> = <i>b</i> = 128.6, <i>c</i> = 170.7
Total no. of measured intensities	77102 (13865)
Unique reflections	8981 (2263)
Multiplicity	8.6 (6.1)
Mean <i>I</i> / σ (<i>I</i>)	7.2 (1.5)
Completeness (%)	94.0 (84.0)
<i>R</i> _{merge} ^a	0.084 (1.513)
<i>R</i> _{meas} ^b	0.033 (0.612)
<i>CC</i> _{1/2} ^c	0.998 (0.588)
Refinement	
Resolution range (Å)	51.34 – 4.50 (4.62 – 4.50)
Reflections: working/free ^d	8075/883
<i>R</i> _{work} / <i>R</i> _{free} ^e	0.237/0.275
MolProbity score/Clashscore ^f	1.58/5.41
Ramachandran plot: favoured/allowed/disallowed ^f (%)	95.9/4.1/0.0
R.m.s. bond distance deviation (Å)	0.003
R.m.s. bond angle deviation (°)	0.79
NRC1 – chains/no. protein residues/ranges	A,C/343/153-494
SS15 – chains/no. protein residues/ranges	B,D/206/18-223
No. ADP molecules/RSCC ^g	2/0.72,0.84
PDB accession code	8BV0

Values in parentheses are for the outer resolution shell.

^a $R_{\text{merge}} = \frac{\sum_{hkl} \sum_i |I_i(hkl) - \langle I(hkl) \rangle|}{\sum_{hkl} \sum_i I_i(hkl)}$.

^b $R_{\text{meas}} = \frac{\sum_{hkl} [N/(N-1)]^{1/2} \times \sum_i |I_i(hkl) - \langle I(hkl) \rangle|}{\sum_{hkl} \sum_i I_i(hkl)}$, where *I*_{*i*}(*hkl*) is the *i*th observation of reflection *hkl*, $\langle I(hkl) \rangle$ is the weighted average intensity for all observations *I* of reflection *hkl* and *N* is the number of observations of reflection *hkl*.

^c *CC*_{1/2} is the correlation coefficient between symmetry equivalent intensities from random halves of the dataset.

^d The data set was split into “working” and “free” sets consisting of 90 and 10% of the data respectively. The free set was not used for refinement.

^e The R-factors *R*_{work} and *R*_{free} are calculated as follows: $R = \frac{\sum (|F_{\text{obs}} - F_{\text{calc}}|)}{\sum |F_{\text{obs}}|}$, where *F*_{obs} and *F*_{calc} are the observed and calculated structure factor amplitudes, respectively.

^f As calculated using MolProbity.

^g Real Space Correlation Coefficient as calculated by the PDB validation server.

References

- Abas L, Luschnig C (2010) Maximum yields of microsomal-type membranes from small amounts of plant material without requiring ultracentrifugation. *Analytical biochemistry* 401: 217-227
- Adachi H, Contreras MP, Harant A, Wu C-h, Derevnina L, Sakai T, Duggan C, Moratto E, Bozkurt TO, Maqbool A *et al* (2019a) An N-terminal motif in NLR immune receptors is functionally conserved across distantly related plant species. *Elife* 8: e49956
- Adachi H, Derevnina L, Kamoun S (2019b) NLR singletons, pairs, and networks: evolution, assembly, and regulation of the intracellular immunoreceptor circuitry of plants. *Current opinion in plant biology* 50: 121-131
- Adachi H, Kamoun S (2022) NLR receptor networks in plants. *Essays in Biochemistry* 66: 541-549
- Adachi H, Kamoun S, Maqbool A (2019c) A resistosome-activated ‘death switch’. *Nature plants* 5: 457-458
- Adachi H, Sakai T, Harant A, Pai H, Honda K, Toghiani A, Claeys J, Duggan C, Bozkurt TO, Wu C-h *et al* (2023) An atypical NLR protein modulates the NRC immune receptor network in *Nicotiana benthamiana*. *PLoS genetics* 19: e1010500
- Adachi H, Sakai T, Kourelis J, Pai H, Gonzalez Hernandez JL, Maqbool A, Kamoun S (2020) Jurassic NLR: conserved and dynamic evolutionary features of the atypically ancient immune receptor ZAR1. *bioRxiv*: 2020.2010.2012.333484
- Ade J, DeYoung BJ, Golstein C, Innes RW (2007) Indirect activation of a plant nucleotide binding site–leucine-rich repeat protein by a bacterial protease. *Proceedings of the National Academy of Sciences* 104: 2531-2536
- Ahn HK, Lin X, Olave-Achury AC, Derevnina L, Contreras MP, Kourelis J, Wu CH, Kamoun S, Jones JD (2023) Effector-dependent activation and oligomerization of plant NRC class helper NLRs by sensor NLR immune receptors Rpi-amr3 and Rpi-amr1. *The EMBO Journal*: e111484
- Ali S, Magne M, Chen S, Obradovic N, Jamshaid L, Wang X, Bélair G, Moffett P (2015) Analysis of *Globodera rostochiensis* effectors reveals conserved functions of SPRYSEC proteins in suppressing and eliciting plant immune responses. *Frontiers in plant science* 6: 623
- Andolfo G, Di Donato A, Chiaiese P, De Natale A, Pollio A, Jones JD, Frusciante L, Ercolano MR (2019) Alien domains shaped the modular structure of plant NLR proteins. *Genome Biology and Evolution* 11: 3466-3477
- Andreeva L, David L, Rawson S, Shen C, Pasricha T, Pelegrin P, Wu H (2021) NLRP3 cages revealed by full-length mouse NLRP3 structure control pathway activation. *Cell* 184: 6299-6312. e6222
- Asai S, Shirasu K (2015) Plant cells under siege: plant immune system versus pathogen effectors. *Current opinion in plant biology* 28: 1-8

- Axtell MJ, Staskawicz BJ (2003) Initiation of RPS2-specified disease resistance in Arabidopsis is coupled to the AvrRpt2-directed elimination of RIN4. *Cell* 112: 369-377
- Azevedo C, Betsuyaku S, Peart J, Takahashi A, Noel L, Sadanandom A, Casais C, Parker J, Shirasu K (2006) Role of SGT1 in resistance protein accumulation in plant immunity. *The EMBO journal* 25: 2007-2016
- Baggs E, Dagdas G, Krasileva KV (2017) NLR diversity, helpers and integrated domains: making sense of the NLR IDentity. *Current Opinion in Plant Biology* 38: 59-67
- Bai S, Liu J, Chang C, Zhang L, Maekawa T, Wang Q, Xiao W, Liu Y, Chai J, Takken FL (2012) Structure-function analysis of barley NLR immune receptor MLA10 reveals its cell compartment specific activity in cell death and disease resistance. *PLoS Pathogens* 8: e1002752
- Barragan AC, Weigel D (2021) Plant NLR diversity: the known unknowns of pan-NLRomes. *The Plant Cell* 33: 814-831
- Baudin M, Hassan JA, Schreiber KJ, Lewis JD (2017) Analysis of the ZAR1 immune complex reveals determinants for immunity and molecular interactions. *Plant physiology* 174: 2038-2053
- Bauer S, Yu D, Lawson AW, Saur IM, Frantzeskakis L, Kracher B, Logemann E, Chai J, Maekawa T, Schulze-Lefert P (2021) The leucine-rich repeats in allelic barley MLA immune receptors define specificity towards sequence-unrelated powdery mildew avirulence effectors with a predicted common RNase-like fold. *PLoS pathogens* 17: e1009223
- Bendahmane A, Farnham G, Moffett P, Baulcombe DC (2002) Constitutive gain-of-function mutants in a nucleotide binding site–leucine rich repeat protein encoded at the Rx locus of potato. *The Plant Journal* 32: 195-204
- Bendahmane A, Kanyuka K, Baulcombe DC (1999) The Rx gene from potato controls separate virus resistance and cell death responses. *The Plant Cell* 11: 781-791
- Bendahmane A, Köhm BA, Dedi C, Baulcombe DC (1995) The coat protein of potato virus X is a strain-specific elicitor of Rx1-mediated virus resistance in potato. *The Plant Journal* 8: 933-941
- Bentham AR, De la Concepcion JC, Benjumea JV, Jones S, Mendel M, Stubbs J, Stevenson CE, Maidment JH, Kourelis J, Zdrzalek R *et al* (2022) Allelic compatibility in plant immune receptors facilitates engineering of new effector recognition specificities. *bioRxiv*: 2022.2010. 2010.511592
- Bentham AR, Petit-Houdenot Y, Win J, Chuma I, Terauchi R, Banfield MJ, Kamoun S, Langner T (2021) A single amino acid polymorphism in a conserved effector of the multihost blast fungus pathogen expands host-target binding spectrum. *PLoS Pathogens* 17: e1009957
- Bentham AR, Zdrzalek R, De la Concepcion JC, Banfield MJ (2018) Uncoiling CNLs: structure/function approaches to understanding CC domain function in plant NLRs. *Plant and Cell Physiology* 59: 2398-2408
- Bi G, Su M, Li N, Liang Y, Dang S, Xu J, Hu M, Wang J, Zou M, Deng Y (2021) The ZAR1 resistosome is a calcium-permeable channel triggering plant immune signaling. *Cell* 184: 3528-3541. e3512

- Bialas A, Langner T, Harant A, Contreras MP, Stevenson CE, Lawson DM, Sklenar J, Kellner R, Moscou MJ, Terauchi R *et al* (2021) Two NLR immune receptors acquired high-affinity binding to a fungal effector through convergent evolution of their integrated domain. *Elife* 10: e66961
- Bialas A, Zess EK, De la Concepcion JC, Franceschetti M, Pennington HG, Yoshida K, Upson JL, Chanclud E, Wu C-H, Langner T *et al* (2018) Lessons in effector and NLR biology of plant-microbe systems. *Molecular Plant-Microbe Interactions* 31: 34-45
- Birker D, Heidrich K, Takahara H, Narusaka M, Deslandes L, Narusaka Y, Reymond M, Parker JE, O'Connell R (2009) A locus conferring resistance to *Colletotrichum higginsianum* is shared by four geographically distinct *Arabidopsis* accessions. *The Plant Journal* 60: 602-613
- Boevink PC, Birch PR, Turnbull D, Whisson SC (2020) Devastating intimacy: the cell biology of plant-Phytophthora interactions. *New Phytologist* 228: 445-458
- Bogdanove AJ, Schornack S, Lahaye T (2010) TAL effectors: finding plant genes for disease and defense. *Current opinion in plant biology* 13: 394-401
- Bonardi V, Cherkis K, Nishimura MT, Dangl JL (2012) A new eye on NLR proteins: focused on clarity or diffused by complexity? *Current opinion in immunology* 24: 41-50
- Bonardi V, Tang S, Stallmann A, Roberts M, Cherkis K, Dangl JL (2011) Expanded functions for a family of plant intracellular immune receptors beyond specific recognition of pathogen effectors. *Proceedings of the National Academy of Sciences* 108: 16463-16468
- Bos JL, Kanneganti TD, Young C, Cakir C, Huitema E, Win J, Armstrong MR, Birch PR, Kamoun S (2006) The C-terminal half of *Phytophthora infestans* RXLR effector AVR3a is sufficient to trigger R3a-mediated hypersensitivity and suppress INF1-induced cell death in *Nicotiana benthamiana*. *The Plant Journal* 48: 165-176
- Boyle TA, Hatoum-Aslan A (2023) Recurring and emerging themes in prokaryotic innate immunity. *Current Opinion in Microbiology* 73: 102324
- Bozkurt TO, Belhaj K, Dagdas YF, Chaparro-Garcia A, Wu CH, Cano LM, Kamoun S (2015) Rerouting of plant late endocytic trafficking toward a pathogen interface. *Traffic* 16: 204-226
- Bozkurt TO, Schornack S, Banfield MJ, Kamoun S (2012) Oomycetes, effectors, and all that jazz. *Current opinion in plant biology* 15: 483-492
- Bozkurt TO, Schornack S, Win J, Shindo T, Ilyas M, Oliva R, Cano LM, Jones AM, Huitema E, van der Hoorn RA *et al* (2011) *Phytophthora infestans* effector AVRblb2 prevents secretion of a plant immune protease at the haustorial interface. *Proceedings of the National Academy of Sciences* 108: 20832-20837
- Brommonschenkel SH, Frary A, Frary A, Tanksley SD (2000) The broad-spectrum tospovirus resistance gene Sw-5 of tomato is a homolog of the root-knot nematode resistance gene Mi. *Molecular Plant-Microbe Interactions* 13: 1130-1138
- Burdett H, Kobe B, Anderson PA (2019) Animal NLRs continue to inform plant NLR structure and function. *Archives of biochemistry and biophysics* 670: 58-68
- Buscaill P, van der Hoorn RA (2021) Defeated by the nines: nine extracellular strategies to avoid microbe-associated molecular patterns recognition in plants. *The Plant Cell* 33: 2116-2130

- Carpentier J, Esquibet M, Fouville D, Manzanares-Dauleux MJ, Kerlan M-C, Grenier E (2012) The evolution of the Gp-Rbp-1 gene in *Globodera pallida* includes multiple selective replacements. *Molecular Plant Pathology* 13: 546-555
- Casey LW, Lavrencic P, Bentham AR, Cesari S, Ericsson DJ, Croll T, Turk D, Anderson PA, Mark AE, Dodds PN *et al* (2016) The CC domain structure from the wheat stem rust resistance protein Sr33 challenges paradigms for dimerization in plant NLR proteins. *Proceedings of the National Academy of Sciences* 113: 12856-12861
- Castel B, Ngou P-M, Cevik V, Redkar A, Kim D-S, Yang Y, Ding P, Jones JDG (2019) Diverse NLR immune receptors activate defence via the RPW8-NLR NRG1. *New Phytologist* 222: 966-980
- Castro-Gomes T, Koushik A, Andrews N (2014) ESCRT: Nipping the wound in the bud? *Trends in biochemical sciences* 39: 307-309
- Catanzariti A-M, Dodds PN, Ve T, Kobe B, Ellis JG, Staskawicz BJ (2010) The AvrM effector from flax rust has a structured C-terminal domain and interacts directly with the M resistance protein. *Molecular Plant-Microbe Interactions* 23: 49-57
- Cesari S, Bernoux M, Moncuquet P, Kroj T, Dodds PN (2014) A novel conserved mechanism for plant NLR protein pairs: the “integrated decoy” hypothesis. *Frontiers in plant science* 5: 606
- Césari S, Kanzaki H, Fujiwara T, Bernoux M, Chalvon V, Kawano Y, Shimamoto K, Dodds P, Terauchi R, Kroj T (2014) The NB-LRR proteins RGA 4 and RGA 5 interact functionally and physically to confer disease resistance. *The EMBO journal* 33: 1941-1959
- Cesari S, Moore J, Chen C, Webb D, Periyannan S, Mago R, Bernoux M, Lagudah ES, Dodds PN (2016) Cytosolic activation of cell death and stem rust resistance by cereal MLA-family CC–NLR proteins. *Proceedings of the National Academy of Sciences* 113: 10204-10209
- Cesari S, Thilliez G, Ribot C, Chalvon V, Michel C, Jauneau A, Rivas S, Alaux L, Kanzaki H, Okuyama Y *et al* (2013) The rice resistance protein pair RGA4/RGA5 recognizes the Magnaporthe oryzae effectors AVR-Pia and AVR1-CO39 by direct binding. *The Plant Cell* 25: 1463-1481
- Cesari S, Xi Y, Declerck N, Chalvon V, Mammri L, Pugnière M, Henriquet C, De Guillen K, Chochois V, Padilla A *et al* (2022) New recognition specificity in a plant immune receptor by molecular engineering of its integrated domain. *Nature Communications* 13: 1524
- Chai Q, Yu S, Zhong Y, Lu Z, Qiu C, Yu Y, Zhang X, Zhang Y, Lei Z, Qiang L (2022) A bacterial phospholipid phosphatase inhibits host pyroptosis by hijacking ubiquitin. *Science* 378: eabq0132
- Chen J, Upadhyaya NM, Ortiz D, Sperschneider J, Li F, Bouton C, Breen S, Dong C, Xu B, Zhang X (2017) Loss of AvrSr50 by somatic exchange in stem rust leads to virulence for Sr50 resistance in wheat. *Science* 358: 1607-1610
- Chen Y, Liu Z, Halterman DA (2012) Molecular determinants of resistance activation and suppression by *Phytophthora infestans* effector IPI-O. *PLoS Pathog* 8: e1002595
- Chia K-S, Kourelis J, Vickers M, Sakai T, Kamoun S, Carella P (2022) The N-terminal executioner domains of NLR immune receptors are functionally conserved across major plant lineages. *bioRxiv*: 2022.2010.2019.512840

- Chou W-C, Jha S, Linhoff MW, Ting JP-Y (2023) The NLR gene family: from discovery to present day. *Nature Reviews Immunology*: 1-20
- Clark RM, Schweikert G, Toomajian C, Ossowski S, Zeller G, Shinn P, Warthmann N, Hu TT, Fu G, Hinds DA (2007) Common sequence polymorphisms shaping genetic diversity in *Arabidopsis thaliana*. *science* 317: 338-342
- Conlan B, Stoll T, Gorman JJ, Saur I, Rathjen JP (2018) Development of a rapid in planta BioID system as a probe for plasma membrane-associated immunity proteins. *Frontiers in plant science* 9: 1882
- Contreras MP, Pai H, Selvaraj M, Toghiani A, Lawson DM, Tumtas Y, Duggan C, Yuen ELH, Stevenson CEM, Harant A *et al* (2023a) Resurrection of plant disease resistance proteins via helper NLR bioengineering. *Science Advances* 9: eadg3861
- Contreras MP, Pai H, Tumtas Y, Duggan C, Yuen ELH, Cruces AV, Kourelis J, Ahn HK, Lee KT, Wu CH *et al* (2023b) Sensor NLR immune proteins activate oligomerization of their NRC helpers in response to plant pathogens. *The EMBO Journal* 42: e111519
- Couto D, Zipfel C (2016) Regulation of pattern recognition receptor signalling in plants. *Nature Reviews Immunology* 16: 537-552
- Crean EE, Bilstein-Schloemer M, Maekawa T, Schulze-Lefert P, Saur IM-L (2023) A dominant-negative avirulence effector of the barley powdery mildew fungus provides mechanistic insight to barley MLA immune receptor activation. *bioRxiv*: 2023.2001. 2011.523539
- Cui H, Tsuda K, Parker JE (2015) Effector-triggered immunity: from pathogen perception to robust defense. *Annual review of plant biology* 66: 487-511
- Dagdas YF, Belhaj K, Maqbool A, Chaparro-Garcia A, Pandey P, Petre B, Tabassum N, Cruz-Mireles N, Hughes RK, Sklenar J *et al* (2016) An effector of the Irish potato famine pathogen antagonizes a host autophagy cargo receptor. *Elife* 5: e10856
- Dagdas YF, Pandey P, Tumtas Y, Sanguankiatichai N, Belhaj K, Duggan C, Leary AY, Segretin ME, Contreras MP, Savage Z *et al* (2018) Host autophagy machinery is diverted to the pathogen interface to mediate focal defense responses against the Irish potato famine pathogen. *Elife* 7: e37476
- Dai E, Meng L, Kang R, Wang X, Tang D (2020) ESCRT-III-dependent membrane repair blocks ferroptosis. *Biochemical and biophysical research communications* 522: 415-421
- De Craene J-O, Ripp R, Lecompte O, Thompson JD, Poch O, Friant S (2012) Evolutionary analysis of the ENTH/ANTH/VHS protein superfamily reveals a coevolution between membrane trafficking and metabolism. *BMC genomics* 13: 1-12
- de Guillen K, Ortiz-Vallejo D, Gracy J, Fournier E, Kroj T, Padilla A (2015) Structure analysis uncovers a highly diverse but structurally conserved effector family in phytopathogenic fungi. *PLoS pathogens* 11: e1005228
- De Jonge R, Peter van Esse H, Maruthachalam K, Bolton MD, Santhanam P, Saber MK, Zhang Z, Usami T, Lievens B, Subbarao KV (2012) Tomato immune receptor Ve1 recognizes effector of multiple fungal pathogens uncovered by genome and RNA sequencing. *Proceedings of the National Academy of Sciences* 109: 5110-5115

De la Concepcion JC, Benjumea JV, Bialas A, Terauchi R, Kamoun S, Banfield MJ (2021) Functional diversification gave rise to allelic specialization in a rice NLR immune receptor pair. *Elife* 10: e71662

De la Concepcion JC, Franceschetti M, MacLean D, Terauchi R, Kamoun S, Banfield MJ (2019) Protein engineering expands the effector recognition profile of a rice NLR immune receptor. *elife* 8: e47713

De la Concepcion JC, Franceschetti M, Maqbool A, Saitoh H, Terauchi R, Kamoun S, Banfield MJ (2018) Polymorphic residues in rice NLRs expand binding and response to effectors of the blast pathogen. *Nature plants* 4: 576-585

De Oliveira AS, Koolhaas I, Boiteux LS, Caldararu OF, Petrescu AJ, Oliveira Resende R, Kormelink R (2016) Cell death triggering and effector recognition by Sw-5 SD-CNL proteins from resistant and susceptible tomato isolines to Tomato spotted wilt virus. *Molecular Plant Pathology* 17: 1442-1454

DeFalco TA, Zipfel C (2021) Molecular mechanisms of early plant pattern-triggered immune signaling. *Molecular Cell* 81: 3449-3467

Derevnina L, Contreras MP, Adachi H, Upson J, Vergara Cruces A, Xie R, Sklenar J, Menke FL, Mugford ST, MacLean D *et al* (2021) Plant pathogens convergently evolved to counteract redundant nodes of an NLR immune receptor network. *PLoS biology* 19: e3001136

Derevnina L, Kamoun S, Wu C-h (2019) Dude, where is my mutant? *Nicotiana benthamiana* meets forward genetics. *The New Phytologist* 221: 607-610

Deslandes L, Olivier J, Theulières F, Hirsch J, Feng DX, Bittner-Eddy P, Beynon J, Marco Y (2002) Resistance to *Ralstonia solanacearum* in *Arabidopsis thaliana* is conferred by the recessive RRS1-R gene, a member of a novel family of resistance genes. *Proceedings of the National Academy of Sciences* 99: 2404-2409

Deslandes L, Rivas S (2012) Catch me if you can: bacterial effectors and plant targets. *Trends in plant science* 17: 644-655

Diaz-Granados A, Petrescu A-J, Goverse A, Smant G (2016) SPRYSEC effectors: a versatile protein-binding platform to disrupt plant innate immunity. *Frontiers in plant science* 7: 1575

Dodds PN, Lawrence GJ, Catanzariti A-M, Teh T, Wang C-I, Ayliffe MA, Kobe B, Ellis JG (2006) Direct protein interaction underlies gene-for-gene specificity and coevolution of the flax resistance genes and flax rust avirulence genes. *Proceedings of the National Academy of Sciences* 103: 8888-8893

Duggan C, Moratto E, Savage Z, Hamilton E, Adachi H, Wu C-H, Leary AY, Tumtas Y, Rothery SM, Maqbool A *et al* (2021) Dynamic localization of a helper NLR at the plant–pathogen interface underpins pathogen recognition. *Proceedings of the National Academy of Sciences* 118: e2104997118

Duxbury Z, Wang S, MacKenzie CI, Tenthorey JL, Zhang X, Huh SU, Hu L, Hill L, Ngou PM, Ding P *et al* (2020) Induced proximity of a TIR signaling domain on a plant-mammalian NLR chimera activates defense in plants. *Proceedings of the National Academy of Sciences* 117: 18832-18839

Duxbury Z, Wu C-h, Ding P (2021) A comparative overview of the intracellular guardians of plants and animals: NLRs in innate immunity and beyond. *Annual review of plant biology* 72: 155-184

- Dyrka W, Coustou V, Daskalov A, Lends A, Bardin T, Berbon M, Kauffmann B, Blancard C, Salin B, Loquet A (2020) Identification of NLR-associated amyloid signaling motifs in bacterial genomes. *Journal of molecular biology* 432: 6005-6027
- El Kasmi F, Chung E-H, Anderson RG, Li J, Wan L, Eitas TK, Gao Z, Dangl JL (2017) Signaling from the plasma-membrane localized plant immune receptor RPM1 requires self-association of the full-length protein. *Proceedings of the National Academy of Sciences* 114: E7385-E7394
- Emsley P, Lohkamp B, Scott WG, Cowtan K (2010) Features and development of Coot. *Acta Crystallographica Section D: Biological Crystallography* 66: 486-501
- Engler C, Youles M, Gruetzner R, Ehnert T-M, Werner S, Jones JD, Patron NJ, Marillonnet S (2014) A golden gate modular cloning toolbox for plants. *ACS synthetic biology* 3: 839-843
- Evans PR, Murshudov GN (2013) How good are my data and what is the resolution? *Acta Crystallographica Section D: Biological Crystallography* 69: 1204-1214
- Evans R, O'Neill M, Pritzel A, Antropova N, Senior A, Green T, Žídek A, Bates R, Blackwell S, Yim J (2021) Protein complex prediction with AlphaFold-Multimer. *BioRxiv*: 2021.2010.2004.463034
- Eves-van den Akker S (2021) Plant–nematode interactions. *Current Opinion in Plant Biology* 62: 102035
- Farnham G, Baulcombe DC (2006) Artificial evolution extends the spectrum of viruses that are targeted by a disease-resistance gene from potato. *Proceedings of the National Academy of Sciences* 103: 18828-18833
- Feehan JM, Castel B, Bentham AR, Jones JD (2020) Plant NLRs get by with a little help from their friends. *Current opinion in plant biology* 56: 99-108
- Feehan JM, Wang J, Sun X, Choi J, Ahn H-K, Ngou BPM, Parker JE, Jones JD (2023) Oligomerization of a plant helper NLR requires cell-surface and intracellular immune receptor activation. *Proceedings of the National Academy of Sciences* 120: e2210406120
- Flor HH (1971) Current status of the gene-for-gene concept. *Annual review of phytopathology* 9: 275-296
- Förderer A, Li E, Lawson AW, Deng Y-n, Sun Y, Logemann E, Zhang X, Wen J, Han Z, Chang J *et al* (2022) A wheat resistosome defines common principles of immune receptor channels. *Nature* 610: 532-539
- Fradin EF, Zhang Z, Juarez Ayala JC, Castroverde CD, Nazar RN, Robb J, Liu C-M, Thomma BP (2009) Genetic dissection of Verticillium wilt resistance mediated by tomato Ve1. *Plant physiology* 150: 320-332
- Fujisaki K, Abe Y, Ito A, Saitoh H, Yoshida K, Kanzaki H, Kanzaki E, Utsushi H, Yamashita T, Kamoun S (2015) Rice Exo70 interacts with a fungal effector, AVR-Pii, and is required for AVR-Pii-triggered immunity. *The Plant Journal* 83: 875-887
- Gabriëls SH, Takken FL, Vossen JH, de Jong CF, Liu Q, Turk SC, Wachowski LK, Peters J, Witsenboer HM, de Wit PJ (2006) cDNA-AFLP combined with functional analysis reveals novel genes involved in the hypersensitive response. *Molecular Plant-Microbe Interactions* 19: 567-576

- Gabriëls SH, Vossen JH, Ekengren SK, Ooijen Gv, Abd-El-Halim AM, Berg GCvd, Rainey DY, Martin GB, Takken FL, Wit Pjd (2007) An NB-LRR protein required for HR signalling mediated by both extra-and intracellular resistance proteins. *The Plant Journal* 50: 14-28
- Gantner J, Ordon J, Kretschmer C, Guerois R, Stuttmann J (2019) An EDS1-SAG101 complex functions in TNL-mediated immunity in Solanaceae. *bioRxiv*: 511956
- Gao LA, Wilkinson ME, Strecker J, Makarova KS, Macrae RK, Koonin EV, Zhang F (2022) Prokaryotic innate immunity through pattern recognition of conserved viral proteins. *Science* 377: eabm4096
- Giannakopoulou A, Steele JF, Segretin ME, Bozkurt TO, Zhou J, Robatzek S, Banfield MJ, Pais M, Kamoun S (2015) Tomato I2 immune receptor can be engineered to confer partial resistance to the oomycete *Phytophthora infestans* in addition to the fungus *Fusarium oxysporum*. *Molecular Plant-Microbe Interactions* 28: 1316-1329
- Gong Y, Tian L, Kontos I, Li J, Li X (2023) Plant immune signaling network mediated by helper NLRs. *Current Opinion in Plant Biology* 73: 102354
- Gong Y-N, Guy C, Olauson H, Becker JU, Yang M, Fitzgerald P, Linkermann A, Green DR (2017) ESCRT-III acts downstream of MLKL to regulate necroptotic cell death and its consequences. *Cell* 169: 286-300. e216
- Gregory SM, Davis BK, West JA, Taxman DJ, Matsuzawa S-i, Reed JC, Ting JP, Damania B (2011) Discovery of a viral NLR homolog that inhibits the inflammasome. *Science* 331: 330-334
- Guo L, Cesari S, de Guillen K, Chalvon V, Mammri L, Ma M, Meusnier I, Bonnot F, Padilla A, Peng Y-L (2018) Specific recognition of two MAX effectors by integrated HMA domains in plant immune receptors involves distinct binding surfaces. *Proceedings of the National Academy of Sciences* 115: 11637-11642
- Gutierrez JR, Balmuth AL, Ntoukakis V, Mucyn TS, Gimenez-Ibanez S, Jones AM, Rathjen JP (2010) Prf immune complexes of tomato are oligomeric and contain multiple Pto-like kinases that diversify effector recognition. *The Plant Journal* 61: 507-518
- Hallwass M, De Oliveira AS, de Campos Dianese E, Lohuis D, Boiteux LS, Inoue-Nagata AK, Resende RO, Kormelink R (2014) The Tomato spotted wilt virus cell-to-cell movement protein (NSM) triggers a hypersensitive response in Sw-5-containing resistant tomato lines and in *Nicotiana benthamiana* transformed with the functional Sw-5b resistance gene copy. *Molecular plant pathology* 15: 871-880
- He J, Ye W, Choi DS, Wu B, Zhai Y, Guo B, Duan S, Wang Y, Gan J, Ma W (2019) Structural analysis of *Phytophthora* suppressor of RNA silencing 2 (PSR2) reveals a conserved modular fold contributing to virulence. *Proceedings of the National Academy of Sciences* 116: 8054-8059
- Helm M, Qi M, Sarkar S, Yu H, Whitham SA, Innes RW (2019) Engineering a decoy substrate in soybean to enable recognition of the soybean mosaic virus NIa protease. *Molecular Plant-Microbe Interactions* 32: 760-769
- Hochheiser IV, Pils M, Hagelueken G, Moecking J, Marleaux M, Brinkschulte R, Latz E, Engel C, Geyer M (2022) Structure of the NLRP3 decamer bound to the cytokine release inhibitor CRID3. *Nature* 604: 184-189

- Houterman PM, Cornelissen BJ, Rep M (2008) Suppression of plant resistance gene-based immunity by a fungal effector. *PLoS Pathog* 4: e1000061
- Hu G, DeHart AK, Li Y, Ustach C, Handley V, Navarre R, Hwang CF, Aegerter BJ, Williamson VM, Baker B (2005) EDS1 in tomato is required for resistance mediated by TIR-class R genes and the receptor-like R gene Ve. *The Plant Journal* 42: 376-391
- Hu M, Qi J, Bi G, Zhou J-M (2020) Bacterial effectors induce oligomerization of immune receptor ZAR1 in vivo. *Molecular Plant* 13: 793-801
- Hu Z, Zhou Q, Zhang C, Fan S, Cheng W, Zhao Y, Shao F, Wang H-W, Sui S-F, Chai J (2015) Structural and biochemical basis for induced self-propagation of NLRC4. *Science* 350: 399-404
- Huang H, Huang S, Li J, Wang H, Zhao Y, Feng M, Dai J, Wang T, Zhu M, Tao X (2021a) Stepwise artificial evolution of an Sw-5b immune receptor extends its resistance spectrum against resistance-breaking isolates of Tomato spotted wilt virus. *Plant Biotechnology Journal* 19: 2164-2176
- Huang S, Jia A, Song W, Hessler G, Meng Y, Sun Y, Xu L, Laessle H, Jirschitzka J, Ma S (2022) Identification and receptor mechanism of TIR-catalyzed small molecules in plant immunity. *Science* 377: eabq3297
- Huang W, MacLean AM, Sugio A, Maqbool A, Busscher M, Cho S-T, Kamoun S, Kuo C-H, Immink RG, Hogenhout SA (2021b) Parasitic modulation of host development by ubiquitin-independent protein degradation. *Cell* 184: 5201-5214. e5212
- Huh SU, Cevik V, Ding P, Duxbury Z, Ma Y, Tomlinson L, Sarris PF, Jones JD (2017) Protein-protein interactions in the RPS4/RRS1 immune receptor complex. *PLoS pathogens* 13: e1006376
- Hulin MT, Hill L, Jones JD, Ma W (2023) Pangenomic analysis reveals plant NAD⁺ manipulation as an important virulence activity of bacterial pathogen effectors. *Proceedings of the National Academy of Sciences* 120: e2217114120
- Jacob P, Kim NH, Wu F, El-Kasmi F, Chi Y, Walton WG, Furzer OJ, Lietzan AD, Sunil S, Kempthorn K (2021) Plant “helper” immune receptors are Ca²⁺-permeable nonselective cation channels. *Science* 373: 420-425
- Jia A, Huang S, Song W, Wang J, Meng Y, Sun Y, Xu L, Laessle H, Jirschitzka J, Hou J *et al* (2022) TIR-catalyzed ADP-ribosylation reactions produce signaling molecules for plant immunity. *Science* 377: eabq8180
- Jia Y, McAdams SA, Bryan GT, Hershey HP, Valent B (2000) Direct interaction of resistance gene and avirulence gene products confers rice blast resistance. *The EMBO journal* 19: 4004-4014
- Jia Y, Yuan Y, Zhang Y, Yang S, Zhang X (2015) Extreme expansion of NBS-encoding genes in Rosaceae. *BMC genetics* 16: 1-12
- Jiang L, Erickson AH, Rogers JC (2002) Multivesicular bodies: a mechanism to package lytic and storage functions in one organelle? *Trends in cell biology* 12: 362-367
- Jimenez AJ, Maiuri P, Lafaurie-Janvove J, Divoux S, Piel M, Perez F (2014) ESCRT machinery is required for plasma membrane repair. *Science* 343: 1247136
- Jones JD, Dangl JL (2006) The plant immune system. *nature* 444: 323-329

- Jones JD, Vance RE, Dangl JL (2016) Intracellular innate immune surveillance devices in plants and animals. *Science* 354: aaf6395
- Kabsch W (2010) xds. *Acta Crystallographica Section D: Biological Crystallography* 66: 125-132
- Kamoun S, Furzer O, Jones JD, Judelson HS, Ali GS, Dalio RJ, Roy SG, Schena L, Zambounis A, Panabières F *et al* (2015) The Top 10 oomycete pathogens in molecular plant pathology. *Molecular plant pathology* 16: 413-434
- Karki H, Abdullah S, Chen Y, Halterman D (2020) Natural genetic diversity in the potato resistance gene RB confers suppression avoidance from Phytophthora effector IPI-O4. *bioRxiv*
- Karki HS, Abdullah S, Chen Y, Halterman DA (2021) Natural genetic diversity in the potato resistance gene RB confers suppression avoidance from Phytophthora effector IPI-O4. *Molecular Plant-Microbe Interactions* 34: 1048-1056
- Kayagaki N, Stowe IB, Lee BL, O'Rourke K, Anderson K, Warming S, Cuellar T, Haley B, Roose-Girma M, Phung QT (2015) Caspase-11 cleaves gasdermin D for non-canonical inflammasome signalling. *Nature* 526: 666-671
- Kibby EM, Conte AN, Burroughs AM, Nagy TA, Vargas JA, Whalen LA, Aravind L, Whiteley AT (2023) Bacterial NLR-related proteins protect against phage. *Cell*
- Kim SH, Qi D, Ashfield T, Helm M, Innes RW (2016a) Using decoys to expand the recognition specificity of a plant disease resistance protein. *Science* 351: 684-687
- Kim YE, Kim Y-n, Kim JA, Kim HM, Jung Y (2015) Green fluorescent protein nanopolygons as monodisperse supramolecular assemblies of functional proteins with defined valency. *Nature communications* 6: 7134
- Kim YJ, Lin N-C, Martin GB (2002) Two distinct Pseudomonas effector proteins interact with the Pto kinase and activate plant immunity. *Cell* 109: 589-598
- Kim YK, Shin J-S, Nahm MH (2016b) NOD-like receptors in infection, immunity, and diseases. *Yonsei medical journal* 57: 5-14
- Kofoed EM, Vance RE (2011) Innate immune recognition of bacterial ligands by NAIPs determines inflammasome specificity. *Nature* 477: 592-595
- Korbei B, Moulinier-Anzola J, De-Araujo L, Lucyshyn D, Retzer K, Khan MA, Luschnig C (2013) Arabidopsis TOL proteins act as gatekeepers for vacuolar sorting of PIN2 plasma membrane protein. *Current Biology* 23: 2500-2505
- Kourelis J, Adachi H (2022) Activation and regulation of NLR immune receptor networks. *Plant and Cell Physiology* 63: 1366-1377
- Kourelis J, Contreras MP, Harant A, Pai H, Lüdke D, Adachi H, Derevnina L, Wu C-H, Kamoun S (2022) The helper NLR immune protein NRC3 mediates the hypersensitive cell death caused by the cell-surface receptor Cf-4. *PLoS Genetics* 18: e1010414
- Kourelis J, Marchal C, Posbeyikian A, Harant A, Kamoun S (2023) NLR immune receptor–nanobody fusions confer plant disease resistance. *Science* 379: 934-939

- Kourelis J, Sakai T, Adachi H, Kamoun S (2021) RefPlantNLR is a comprehensive collection of experimentally validated plant disease resistance proteins from the NLR family. *PLoS Biology* 19: e3001124
- Kourelis J, Van Der Hoorn RA (2018) Defended to the nines: 25 years of resistance gene cloning identifies nine mechanisms for R protein function. *The Plant Cell* 30: 285-299
- Kroon L, Bakker F, Van Den Bosch G, Bonants P, Flier W (2004) Phylogenetic analysis of *Phytophthora* species based on mitochondrial and nuclear DNA sequences. *Fungal Genetics and Biology* 41: 766-782
- Kud J, Wang W, Gross R, Fan Y, Huang L, Yuan Y, Gray A, Duarte A, Kuhl JC, Caplan A (2019) The potato cyst nematode effector RHA1B is a ubiquitin ligase and uses two distinct mechanisms to suppress plant immune signaling. *PLoS Pathogens* 15: e1007720
- Laflamme B, Dillon MM, Martel A, Almeida RN, Desveaux D, Guttman DS (2020) The pan-genome effector-triggered immunity landscape of a host-pathogen interaction. *Science* 367: 763-768
- Lapin D, Kovacova V, Sun X, Dongus JA, Bhandari D, von Born P, Bautor J, Guarneri N, Rzemieniewski J, Stuttmann J *et al* (2019) A coevolved EDS1-SAG101-NRG1 module mediates cell death signaling by TIR-domain immune receptors. *The Plant Cell* 31: 2430-2455
- Larkin MA, Blackshields G, Brown NP, Chenna R, McGettigan PA, McWilliam H, Valentin F, Wallace IM, Wilm A, Lopez R (2007) Clustal W and Clustal X version 2.0. *bioinformatics* 23: 2947-2948
- Le Roux C, Huet G, Jauneau A, Camborde L, Trémousaygue D, Kraut A, Zhou B, Levaillant M, Adachi H, Yoshioka H *et al* (2015) A receptor pair with an integrated decoy converts pathogen disabling of transcription factors to immunity. *Cell* 161: 1074-1088
- Lechtenberg BC, Mace PD, Riedl SJ (2014) Structural mechanisms in NLR inflammasome signaling. *Current opinion in structural biology* 29: 17-25
- Lee J, Manning AJ, Wolfgeher D, Jelenska J, Cavanaugh KA, Xu H, Fernandez SM, Michelmore RW, Kron SJ, Greenberg JT (2015) Acetylation of an NB-LRR plant immune-effector complex suppresses immunity. *Cell reports* 13: 1670-1682
- Letunic I, Bork P (2021) Interactive Tree Of Life (iTOL) v5: an online tool for phylogenetic tree display and annotation. *Nucleic acids research* 49: W293-W296
- Levy JG, Gross R, Mendoza Herrera MA, Tang X, Babilonia K, Shan L, Kuhl J, Dibble M, Xiao F, Tamborindeguy C (2019) Lso-HPE1, an effector of 'Candidatus Liberibacter solanacearum' can repress plant immune response. *Phytopathology*
- Lewis JD, Lee AH-Y, Hassan JA, Wan J, Hurley B, Jhingree JR, Wang PW, Lo T, Youn J-Y, Guttman DS *et al* (2013) The Arabidopsis ZED1 pseudokinase is required for ZAR1-mediated immunity induced by the *Pseudomonas syringae* type III effector HopZ1a. *Proceedings of the National Academy of Sciences* 110: 18722-18727
- Li H, Wang J, Kuan T, Tang B, Feng L, Wang J, Cheng Z, Sklenar J, Derbyshire P, Hulin M *et al* (2023) Pathogen protein modularity enables elaborate mimicry of a host phosphatase. *bioRxiv*: 2023.2005.2005.539533

- Li J, Huang H, Zhu M, Huang S, Zhang W, Dinesh-Kumar SP, Tao X (2019) A Plant Immune Receptor Adopts a Two-Step Recognition Mechanism to Enhance Viral Effector Perception. *Molecular plant* 12: 248-262
- Li L, Habring A, Wang K, Weigel D (2020) Atypical Resistance Protein RPW8/HR Triggers Oligomerization of the NLR Immune Receptor RPP7 and Autoimmunity. *Cell Host & Microbe* 27: 405-417.e406
- Lin X, Jia Y, Heal R, Prokchorchik M, Sindalovskaya M, Olave-Achury A, Makechemu M, Fairhead S, Noureen A, Heo J *et al* (2022a) The *Solanum americanum* pangenome and effectoromics reveal new resistance genes against potato late blight. *bioRxiv*: 2022.2008.2011.503608
- Lin X, Olave-Achury A, Heal R, Pais M, Witek K, Ahn H-K, Zhao H, Bhanvadia S, Karki HS, Song T *et al* (2022b) A potato late blight resistance gene protects against multiple *Phytophthora* species by recognizing a broadly conserved RXLR-WY effector. *Molecular Plant* 15: 1457-1469
- Lin X, Song T, Fairhead S, Witek K, Jouet A, Jupe F, Witek AI, Karki HS, Vleeshouwers VG, Hein I (2020) Identification of Avramr1 from *Phytophthora infestans* using long read and cDNA pathogen-enrichment sequencing (PenSeq). *Molecular Plant Pathology* 21: 1502-1512
- Liu Y, Zhang X, Yuan G, Wang D, Zheng Y, Ma M, Guo L, Bhadauria V, Peng Y-L, Liu J (2021) A designer rice NLR immune receptor confers resistance to the rice blast fungus carrying noncorresponding avirulence effectors. *Proceedings of the National Academy of Sciences* 118: e2110751118
- Locci F, Wang J, Parker JE (2023) TIR-domain enzymatic activities at the heart of plant immunity. *Current Opinion in Plant Biology* 74: 102373
- Lopez VA, Park BC, Nowak D, Sreelatha A, Zembek P, Fernandez J, Servage KA, Gradowski M, Hennig J, Tomchick DR (2019) A bacterial effector mimics a host HSP90 client to undermine immunity. *Cell* 179: 205-218. e221
- Lovelace AH, Dorhmi S, Hulin MT, Li Y, Mansfield JW, Ma W (2023) Effector identification in plant pathogens. *Phytopathology*®: PHYTO-09-22-0337-KD
- Luderer R, Takken FL, Wit Pjd, Joosten MH (2002) *Cladosporium fulvum* overcomes Cf-2-mediated resistance by producing truncated AVR2 elicitor proteins. *Molecular microbiology* 45: 875-884
- Lüdke D, Yan Q, Rohmann PF, Wiermer M (2022) NLR we there yet? Nucleocytoplasmic coordination of NLR-mediated immunity. *New Phytologist* 236: 24-42
- Lukasik-Shreepaathy E, Slootweg E, Richter H, Goverse A, Cornelissen BJ, Takken FL (2012) Dual regulatory roles of the extended N terminus for activation of the tomato MI-1.2 resistance protein. *Molecular Plant-Microbe Interactions* 25: 1045-1057
- Ma S, Lapin D, Liu L, Sun Y, Song W, Zhang X, Logemann E, Yu D, Wang J, Jirschitzka J *et al* (2020) Direct pathogen-induced assembly of an NLR immune receptor complex to form a holoenzyme. *Science* 370: eabe3069

- Ma Y, Guo H, Hu L, Martinez PP, Moschou PN, Cevik V, Ding P, Duxbury Z, Sarris PF, Jones JD (2018) Distinct modes of derepression of an Arabidopsis immune receptor complex by two different bacterial effectors. *Proceedings of the National Academy of Sciences* 115: 10218-10227
- Macho AP, Zipfel C (2014) Plant PRRs and the activation of innate immune signaling. *Molecular cell* 54: 263-272
- Macho AP, Zipfel C (2015) Targeting of plant pattern recognition receptor-triggered immunity by bacterial type-III secretion system effectors. *Current Opinion in Microbiology* 23: 14-22
- Mackey D, Belkhadir Y, Alonso JM, Ecker JR, Dangl JL (2003) Arabidopsis RIN4 is a target of the type III virulence effector AvrRpt2 and modulates RPS2-mediated resistance. *Cell* 112: 379-389
- MacLean D (2019) Besthr. *Zenodo*
- MacQueen A, Tian D, Chang W, Holub E, Kreitman M, Bergelson J (2019) Population genetics of the highly polymorphic RPP8 gene family. *Genes* 10: 691
- Maekawa T, Kashkar H, Coll NS (2023) Dying in self-defence: a comparative overview of immunogenic cell death signalling in animals and plants. *Cell Death & Differentiation* 30: 258-268
- Maekawa T, Kracher B, Saur IM, Yoshikawa-Maekawa M, Kellner R, Pankin A, von Korff M, Schulze-Lefert P (2019) Subfamily-specific specialization of RGH1/MLA immune receptors in wild barley. *Molecular Plant-Microbe Interactions* 32: 107-119
- Maidment JH, Franceschetti M, Maqbool A, Saitoh H, Jantasuriyarat C, Kamoun S, Terauchi R, Banfield MJ (2021) Multiple variants of the fungal effector AVR-Pik bind the HMA domain of the rice protein OsHIPP19, providing a foundation to engineer plant defense. *Journal of Biological Chemistry* 296
- Maidment JH, Shimizu M, Vera S, Franceschetti M, Longya A, Stevenson CE, De la Concepcion JC, Bialas A, Kamoun S, Terauchi R *et al* (2022) Effector target-guided engineering of an integrated domain expands the disease resistance profile of a rice NLR immune receptor. *bioRxiv*: 2022.2006.2014.496076
- Maqbool A, Hughes RK, Dagdas YF, Tregidgo N, Zess E, Belhaj K, Round A, Bozkurt TO, Kamoun S, Banfield MJ (2016) Structural Basis of Host Autophagy-related Protein 8 (ATG8) Binding by the Irish Potato Famine Pathogen Effector Protein PexRD54. *Journal of Biological Chemistry* 291: 20270-20282
- Maqbool A, Saitoh H, Franceschetti M, Stevenson C, Uemura A, Kanzaki H, Kamoun S, Terauchi R, Banfield M (2015) Structural basis of pathogen recognition by an integrated HMA domain in a plant NLR immune receptor. *Elife* 4: e08709
- Marchal C, Michalopoulou VA, Zou Z, Cevik V, Sarris PF (2022a) Show me your ID: NLR immune receptors with integrated domains in plants. *Essays in biochemistry* 66: 527-539
- Marchal C, Pai H, Kamoun S, Kourelis J (2022b) Emerging principles in the design of bioengineered made-to-order plant immune receptors. *Current Opinion in Plant Biology*: 102311

- Martin R, Qi T, Zhang H, Liu F, King M, Toth C, Nogales E, Staskawicz BJ (2020) Structure of the activated ROQ1 resistosome directly recognizing the pathogen effector XopQ. *Science* 370: eabd9993
- McCoy AJ, Grosse-Kunstleve RW, Adams PD, Winn MD, Storoni LC, Read RJ (2007) Phaser crystallographic software. *Journal of applied crystallography* 40: 658-674
- Milligan SB, Bodeau J, Yaghoobi J, Kaloshian I, Zabel P, Williamson VM (1998) The root knot nematode resistance gene Mi from tomato is a member of the leucine zipper, nucleotide binding, leucine-rich repeat family of plant genes. *The Plant Cell* 10: 1307-1319
- Mirdita M, Schütze K, Moriwaki Y, Heo L, Ovchinnikov S, Steinegger M (2022) ColabFold: making protein folding accessible to all. *Nature methods* 19: 679-682
- Moffett P, Farnham G, Peart J, Baulcombe DC (2002) Interaction between domains of a plant NBS-LRR protein in disease resistance-related cell death. *The EMBO journal* 21: 4511-4519
- Mosesso N, Nagel M-K, Isono E (2019) Ubiquitin recognition in endocytic trafficking—with or without ESCRT-0. *Journal of cell science* 132: jcs232868
- Moulinier-Anzola J, Schwihla M, De-Araújo L, Artner C, Jörg L, Konstantinova N, Luschnig C, Korbei B (2020) TOLs function as ubiquitin receptors in the early steps of the ESCRT pathway in higher plants. *Molecular plant* 13: 717-731
- Mucyn TS, Clemente A, Andriotis VM, Balmuth AL, Oldroyd GE, Staskawicz BJ, Rathjen JP (2006) The tomato NBARC-LRR protein Prf interacts with Pto kinase in vivo to regulate specific plant immunity. *The Plant Cell* 18: 2792-2806
- Mukhi N, Brown H, Gorenkin D, Ding P, Bentham AR, Stevenson CE, Jones JD, Banfield MJ (2021) Perception of structurally distinct effectors by the integrated WRKY domain of a plant immune receptor. *Proceedings of the National Academy of Sciences* 118: e2113996118
- Mukhtar MS, Carvunis A-R, Dreze M, Epple P, Steinbrenner J, Moore J, Tasan M, Galli M, Hao T, Nishimura MT (2011) Independently evolved virulence effectors converge onto hubs in a plant immune system network. *science* 333: 596-601
- Murshudov GN, Skubák P, Lebedev AA, Pannu NS, Steiner RA, Nicholls RA, Winn MD, Long F, Vagin AA (2011) REFMAC5 for the refinement of macromolecular crystal structures. *Acta Crystallographica Section D: Biological Crystallography* 67: 355-367
- Nakano M, Ichinose Y, Mukaihara T (2020) *Ralstonia solanacearum* type III effector RipAC targets SGT1 to suppress effector-triggered immunity. *Plant and Cell Physiology* 61: 2067-2076
- Narusaka M, Shirasu K, Noutoshi Y, Kubo Y, Shiraishi T, Iwabuchi M, Narusaka Y (2009) RRS1 and RPS4 provide a dual Resistance-gene system against fungal and bacterial pathogens. *The Plant Journal* 60: 218-226
- Ng A, Xavier RJ (2011) Leucine-rich repeat (LRR) proteins: integrators of pattern recognition and signaling in immunity. *Autophagy* 7: 1082-1084
- Ngou BPM, Ahn H-K, Ding P, Jones JD (2021) Mutual potentiation of plant immunity by cell-surface and intracellular receptors. *Nature* 592: 110-115

- Ngou BPM, Ding P, Jones JDG (2022a) Thirty years of resistance: Zig-zag through the plant immune system. *The Plant Cell*
- Ngou BPM, Heal R, Wyler M, Schmid MW, Jones JD (2022b) Concerted expansion and contraction of immune receptor gene repertoires in plant genomes. *Nature Plants* 8: 1146-1152
- Nicholls RA, Fischer M, McNicholas S, Murshudov GN (2014) Conformation-independent structural comparison of macromolecules with ProSMART. *Acta Crystallographica Section D: Biological Crystallography* 70: 2487-2499
- Nombela G, Williamson VM, Muñoz M (2003) The root-knot nematode resistance gene Mi-1.2 of tomato is responsible for resistance against the whitefly *Bemisia tabaci*. *Molecular Plant-Microbe Interactions* 16: 645-649
- Oh S, Kim S, Park HJ, Kim MS, Seo MK, Wu CH, Lee HA, Kim HS, Kamoun S, Choi D (2023) Nucleotide-binding leucine-rich repeat network underlies nonhost resistance of pepper against the Irish potato famine pathogen *Phytophthora infestans*. *Plant Biotechnology Journal*
- Oh S-K, Young C, Lee M, Oliva R, Bozkurt TO, Cano LM, Win J, Bos JI, Liu H-Y, van Damme M (2009) In planta expression screens of *Phytophthora infestans* RXLR effectors reveal diverse phenotypes, including activation of the *Solanum bulbocastanum* disease resistance protein Rpi-*blb2*. *The Plant Cell* 21: 2928-2947
- Ohto U, Kamitsukasa Y, Ishida H, Zhang Z, Murakami K, Hirama C, Maekawa S, Shimizu T (2022) Structural basis for the oligomerization-mediated regulation of NLRP3 inflammasome activation. *Proceedings of the National Academy of Sciences* 119: e2121353119
- Oikawa K, Fujisaki K, Shimizu M, Takeda T, Saitoh H, Hirabuchi A, Hiraka Y, Bialas A, Langner T, Kellner R (2020) The blast pathogen effector AVR-Pik binds and stabilizes rice heavy metal-associated (HMA) proteins to co-opt their function in immunity. *BioRxiv*: 2020.2012. 2001.406389
- Pandey P, Leary AY, Tumtas Y, Savage Z, Dagvadorj B, Duggan C, Yuen EL, Sanguankiatichai N, Tan E, Khandare V *et al* (2021) An oomycete effector subverts host vesicle trafficking to channel starvation-induced autophagy to the pathogen interface. *Elife* 10: e65285
- Pandey SP, Somssich IE (2009) The role of WRKY transcription factors in plant immunity. *Plant physiology* 150: 1648-1655
- Pedreira L, Espiritu RA, Ros U, Weber J, Schmitt A, Stroh J, Hailfinger S, von Karstedt S, García-Sáez AJ (2021) Ferroptotic pores induce Ca²⁺ fluxes and ESCRT-III activation to modulate cell death kinetics. *Cell Death & Differentiation* 28: 1644-1657
- Peiró A, Cañizares MC, Rubio L, López C, Moriones E, Aramburu J, Sánchez-Navarro J (2014) The movement protein (NSm) of Tomato spotted wilt virus is the avirulence determinant in the tomato Sw-5 gene-based resistance. *Molecular Plant Pathology* 15: 802-813
- Petre B, Contreras MP, Bozkurt TO, Schattat MH, Sklenar J, Schornack S, Abd-El-Halim A, Castells-Graells R, Lozano-Durán R, Dagdas YF *et al* (2021) Host-interactor screens of *Phytophthora infestans* RXLR proteins reveal vesicle trafficking as a major effector-targeted process. *The Plant Cell* 33: 1447-1471

- Pettersen EF, Goddard TD, Huang CC, Meng EC, Couch GS, Croll TI, Morris JH, Ferrin TE (2021) UCSF ChimeraX: Structure visualization for researchers, educators, and developers. *Protein Science* 30: 70-82
- Postma WJ, Slootweg EJ, Rehman S, Finkers-Tomczak A, Tytgat TO, van Gelderen K, Lozano-Torres JL, Roosien J, Pomp R, van Schaik C (2012) The effector SPRYSEC-19 of *Globodera rostochiensis* suppresses CC-NB-LRR-mediated disease resistance in plants. *Plant physiology* 160: 944-954
- Pottinger SE, Innes RW (2020) RPS5-mediated disease resistance: fundamental insights and translational applications. *Annual Review of Phytopathology* 58: 139-160
- Poyet J-L, Srinivasula SM, Tnani M, Razmara M, Fernandes-Alnemri T, Alnemri ES (2001) Identification of Ipaf, a human caspase-1-activating protein related to Apaf-1. *Journal of Biological Chemistry* 276: 28309-28313
- Prigozhin DM, Krasileva KV (2021) Analysis of intraspecies diversity reveals a subset of highly variable plant immune receptors and predicts their binding sites. *The Plant Cell* 33: 998-1015
- Pruitt RN, Locci F, Wanke F, Zhang L, Saile SC, Joe A, Karelina D, Hua C, Fröhlich K, Wan W-L (2021) The EDS1–PAD4–ADR1 node mediates Arabidopsis pattern-triggered immunity. *Nature* 598: 495-499
- Qi D, DeYoung BJ, Innes RW (2012) Structure–function analysis of the coiled-coil and leucine-rich repeat domains of the RPS5 disease resistance protein. *Plant physiology* 158: 1819-1832
- Qi T, Seong K, Thomazella DP, Kim JR, Pham J, Seo E, Cho M-J, Schultink A, Staskawicz BJ (2018) NRG1 functions downstream of EDS1 to regulate TIR-NLR-mediated plant immunity in *Nicotiana benthamiana*. *Proceedings of the National Academy of Sciences* 115: E10979-E10987
- Qu Y, Misaghi S, Izrael-Tomasevic A, Newton K, Gilmour LL, Lamkanfi M, Louie S, Kayagaki N, Liu J, Kömüves L (2012) Phosphorylation of NLRC4 is critical for inflammasome activation. *Nature* 490: 539-542
- Raab M, Gentili M, de Belly H, Thiam H-R, Vargas P, Jimenez AJ, Lautenschlaeger F, Voituriez R, Lennon-Duménil A-M, Manel N (2016) ESCRT III repairs nuclear envelope ruptures during cell migration to limit DNA damage and cell death. *Science* 352: 359-362
- Raffaele S, Kamoun S (2012) Genome evolution in filamentous plant pathogens: why bigger can be better. *Nature Reviews Microbiology* 10: 417-430
- Rairdan GJ, Collier SM, Sacco MA, Baldwin IT, Boetrich T, Moffett P (2008) The coiled-coil and nucleotide binding domains of the potato Rx disease resistance protein function in pathogen recognition and signaling. *The Plant Cell* 20: 739-751
- Rairdan GJ, Moffett P (2006) Distinct domains in the ARC region of the potato resistance protein Rx mediate LRR binding and inhibition of activation. *The Plant Cell* 18: 2082-2093
- Ravensdale M, Bernoux M, Ve T, Kobe B, Thrall PH, Ellis JG, Dodds PN (2012) Intramolecular interaction influences binding of the Flax L5 and L6 resistance proteins to their AvrL567 ligands. *PLoS pathogens* 8: e1003004

- Rietman H (2011) *Putting the Phytophthora infestans genome sequence at work: multiple novel avirulence and potato resistance gene candidates revealed*. Wageningen University and Research
- Rivas S, Thomas CM (2005) Molecular interactions between tomato and the leaf mold pathogen *Cladosporium fulvum*. *Annu Rev Phytopathol* 43: 395-436
- Robinson DG, Ding Y, Jiang L (2016) Unconventional protein secretion in plants: a critical assessment. *Protoplasts* 253: 31-43
- Robinson DG, Neuhaus J-M (2016) Receptor-mediated sorting of soluble vacuolar proteins: myths, facts, and a new model. *Journal of experimental botany* 67: 4435-4449
- Rocafort M, Fudal I, Mesarich CH (2020) Apoplastic effector proteins of plant-associated fungi and oomycetes. *Current opinion in plant biology* 56: 9-19
- Rossi M, Goggin FL, Milligan SB, Kaloshian I, Ullman DE, Williamson VM (1998) The nematode resistance gene Mi of tomato confers resistance against the potato aphid. *Proceedings of the National Academy of Sciences* 95: 9750-9754
- Rühl S, Shkarina K, Demarco B, Heilig R, Santos JC, Broz P (2018) ESCRT-dependent membrane repair negatively regulates pyroptosis downstream of GSDMD activation. *Science* 362: 956-960
- Sacco MA, Koropacka K, Grenier E, Jaubert MJ, Blanchard A, Goverse A, Smant G, Moffett P (2009) The cyst nematode SPRYSEC protein RBP-1 elicits Gpa2- and RanGAP2-dependent plant cell death. *PLoS pathogens* 5: e1000564
- Sacco MA, Mansoor S, Moffett P (2007) A RanGAP protein physically interacts with the NB-LRR protein Rx, and is required for Rx-mediated viral resistance. *The Plant Journal* 52: 82-93
- Saile SC, Ackermann FM, Sunil S, Keicher J, Bayless A, Bonardi V, Wan L, Doumane M, Stöbbe E, Jaillais Y (2021) Arabidopsis ADR1 helper NLR immune receptors localize and function at the plasma membrane in a phospholipid dependent manner. *New Phytologist* 232: 2440-2456
- Saile SC, Jacob P, Castel B, Jubic LM, Salas-González I, Bäcker M, Jones JD, Dangl JL, El Kasmi F (2020) Two unequally redundant "helper" immune receptor families mediate Arabidopsis thaliana intracellular "sensor" immune receptor functions. *PLoS biology* 18: e3000783
- Saraste M, Sibbald PR, Wittinghofer A (1990) The P-loop—a common motif in ATP- and GTP-binding proteins. *Trends in biochemical sciences* 15: 430-434
- Sarris PF, Cevik V, Dagdas G, Jones JD, Krasileva KV (2016) Comparative analysis of plant immune receptor architectures uncovers host proteins likely targeted by pathogens. *BMC biology* 14: 1-19
- Sarris PF, Duxbury Z, Huh SU, Ma Y, Segonzac C, Sklenar J, Derbyshire P, Cevik V, Rallapalli G, Saucet SB *et al* (2015) A plant immune receptor detects pathogen effectors that target WRKY transcription factors. *Cell* 161: 1089-1100
- Saunders DG, Breen S, Win J, Schornack S, Hein I, Bozkurt TO, Champouret N, Vleeshouwers VG, Birch PR, Gilroy EM *et al* (2012) Host protein BSL1 associates with *Phytophthora infestans* RXLR effector AVR2 and the *Solanum demissum* immune receptor R2 to mediate disease resistance. *The Plant Cell* 24: 3420-3434

- Saur IM, Bauer S, Kracher B, Lu X, Franzeskakis L, Müller MC, Sabelleck B, Kümme F, Panstruga R, Maekawa T *et al* (2019) Multiple pairs of allelic MLA immune receptor-powdery mildew AVRAs effectors argue for a direct recognition mechanism. *Elife* 8: e44471
- Schornack S, Moscou MJ, Ward ER, Horvath DM (2013) Engineering plant disease resistance based on TAL effectors. *Annual review of phytopathology* 51: 383-406
- Schultink A, Qi T, Bally J, Staskawicz B (2019) Using forward genetics in *Nicotiana benthamiana* to uncover the immune signaling pathway mediating recognition of the *Xanthomonas perforans* effector XopJ4. *The New Phytologist* 221: 1001-1009
- Schulze S, Yu L, Hua C, Zhang L, Kolb D, Weber H, Ehinger A, Saile SC, Stahl M, Franz-Wachtel M (2022) The Arabidopsis TIR-NBS-LRR protein CSA1 guards BAK1-BIR3 homeostasis and mediates convergence of pattern-and effector-induced immune responses. *Cell Host & Microbe* 30: 1717-1731. e1716
- Seear PJ, Dixon MS (2003) Variable leucine-rich repeats of tomato disease resistance genes Cf-2 and Cf-5 determine specificity. *Molecular Plant Pathology* 4: 199-202
- Seeholzer S, Tsuchimatsu T, Jordan T, Bieri S, Pajonk S, Yang W, Jahoor A, Shimizu KK, Keller B, Schulze-Lefert P (2010) Diversity at the *Mla* powdery mildew resistance locus from cultivated barley reveals sites of positive selection. *Molecular plant-microbe interactions* 23: 497-509
- Segretin ME, Pais M, Franceschetti M, Chaparro-Garcia A, Bos JI, Banfield MJ, Kamoun S (2014) Single amino acid mutations in the potato immune receptor R3a expand response to *Phytophthora* effectors. *Molecular Plant-Microbe Interactions* 27: 624-637
- Seo E, Kim S, Yeom S-I, Choi D (2016) Genome-wide comparative analyses reveal the dynamic evolution of nucleotide-binding leucine-rich repeat gene family among Solanaceae plants. *Frontiers in plant science* 7: 1205
- Seong K, Seo E, Witek K, Li M, Staskawicz B (2020) Evolution of NLR resistance genes with noncanonical N-terminal domains in wild tomato species. *New Phytologist* 227: 1530-1543
- Seto D, Koulena N, Lo T, Menna A, Guttman D, Desveaux D, 2017. Expanded type III effector recognition by the ZAR1 NLR protein using ZED1-related kinases. *Nat Plants* 3: 17027.
- Shao Z-Q, Xue J-Y, Wang Q, Wang B, Chen J-Q (2019) Revisiting the origin of plant NBS-LRR genes. *Trends in plant science* 24: 9-12
- Sharif H, Wang L, Wang WL, Magupalli VG, Andreeva L, Qiao Q, Hauenstein AV, Wu Z, Núñez G, Mao Y (2019) Structural mechanism for NEK7-licensed activation of NLRP3 inflammasome. *Nature* 570: 338-343
- Shepherd S, Yuen ELH, Carella P, Bozkurt TO (2023) The wheels of destruction: Plant NLR immune receptors are mobile and structurally dynamic disease resistance proteins. *Current Opinion in Plant Biology* 74: 102372
- Shi J, Zhao Y, Wang K, Shi X, Wang Y, Huang H, Zhuang Y, Cai T, Wang F, Shao F (2015) Cleavage of GSDMD by inflammatory caspases determines pyroptotic cell death. *Nature* 526: 660-665

- Shimizu M, Hirabuchi A, Sugihara Y, Abe A, Takeda T, Kobayashi M, Hiraka Y, Kanzaki E, Oikawa K, Saitoh H *et al* (2022) A genetically linked pair of NLR immune receptors shows contrasting patterns of evolution. *Proceedings of the National Academy of Sciences* 119: e2116896119
- Slootweg E, Roosien J, Spiridon LN, Petrescu A-J, Tameling W, Joosten M, Pomp R, van Schaik C, Dees R, Borst JW (2010) Nucleocytoplasmic distribution is required for activation of resistance by the potato NB-LRR receptor Rx1 and is balanced by its functional domains. *The Plant Cell* 22: 4195-4215
- Song J, Win J, Tian M, Schornack S, Kaschani F, Ilyas M, van der Hoorn RA, Kamoun S (2009) Apoplastic effectors secreted by two unrelated eukaryotic plant pathogens target the tomato defense protease Rcr3. *Proceedings of the National Academy of Sciences* 106: 1654-1659
- Spallek T, Beck M, Ben Khaled S, Salomon S, Bourdais G, Schellmann S, Robatzek S (2013) ESCRT-I mediates FLS2 endosomal sorting and plant immunity. *PLoS genetics* 9: e1004035
- Stecher G, Tamura K, Kumar S (2020) Molecular evolutionary genetics analysis (MEGA) for macOS. *Molecular biology and evolution* 37: 1237-1239
- Steele JF, Hughes RK, Banfield MJ (2019) Structural and biochemical studies of an NB-ARC domain from a plant NLR immune receptor. *PLoS one* 14: e0221226
- Steuernagel B, Witek K, Krattinger SG, Ramirez-Gonzalez RH, Schoonbeek H-j, Yu G, Baggs E, Witek AI, Yadav I, Krasileva KV *et al* (2020) The NLR-annotator tool enables annotation of the intracellular immune receptor repertoire. *Plant Physiology* 183: 468-482
- Sugihara Y, Abe Y, Takagi H, Abe A, Shimizu M, Ito K, Kanzaki E, Oikawa K, Kourelis J, Langner T *et al* (2023) Disentangling the complex gene interaction networks between rice and the blast fungus identifies a new pathogen effector. *PLoS biology* 21: e3001945
- Sun X, Lapin D, Feehan JM, Stolze SC, Kramer K, Dongus JA, Rzemieniewski J, Blanvillain-Baufumé S, Harzen A, Bautor J *et al* (2021) Pathogen effector recognition-dependent association of NRG1 with EDS1 and SAG101 in TNL receptor immunity. *Nature communications* 12: 1-15
- Sun Y, Wang Y, Zhang X, Chen Z, Xia Y, Wang L, Sun Y, Zhang M, Xiao Y, Han Z (2022) Plant receptor-like protein activation by a microbial glycoside hydrolase. *Nature* 610: 335-342
- Swords K, Dahlbeck D, Kearney B, Roy M, Staskawicz BJ (1996) Spontaneous and induced mutations in a single open reading frame alter both virulence and avirulence in *Xanthomonas campestris* pv. *vesicatoria* avrBs2. *Journal of Bacteriology* 178: 4661-4669
- Tai TH, Dahlbeck D, Clark ET, Gajiwala P, Pasion R, Whalen MC, Stall RE, Staskawicz BJ (1999) Expression of the Bs2 pepper gene confers resistance to bacterial spot disease in tomato. *Proceedings of the National Academy of Sciences* 96: 14153-14158
- Takken FL, Albrecht M, Tameling WI (2006) Resistance proteins: molecular switches of plant defence. *Current opinion in plant biology* 9: 383-390
- Takken FL, Govere A (2012) How to build a pathogen detector: structural basis of NB-LRR function. *Current opinion in plant biology* 15: 375-384

- Tamborski J, Seong K, Liu F, Staskawicz B, Krasileva K (2023) Altering specificity and auto-activity of plant immune receptors Sr33 and Sr50 via a rational engineering approach. *Molecular Plant-Microbe Interactions*
- Tameling WI, Baulcombe DC (2007) Physical association of the NB-LRR resistance protein Rx with a Ran GTPase-activating protein is required for extreme resistance to Potato virus X. *The Plant Cell* 19: 1682-1694
- Tameling WI, Elzinga SD, Darmin PS, Vossen JH, Takken FL, Haring MA, Cornelissen BJ (2002) The tomato R gene products I-2 and MI-1 are functional ATP binding proteins with ATPase activity. *The Plant Cell* 14: 2929-2939
- Tameling WI, Nooijen C, Ludwig N, Boter M, Slootweg E, Goverse A, Shirasu K, Joosten MH (2010) RanGAP2 mediates nucleocytoplasmic partitioning of the NB-LRR immune receptor Rx in the Solanaceae, thereby dictating Rx function. *The Plant Cell* 22: 4176-4194
- Tenthorey JL, Haloupek N, López-Blanco JR, Grob P, Adamson E, Hartenian E, Lind NA, Bourgeois NM, Chacón P, Nogales E (2017) The structural basis of flagellin detection by NAIP5: A strategy to limit pathogen immune evasion. *Science* 358: 888-893
- Teper D, Salomon D, Sunitha S, Kim JG, Mudgett MB, Sessa G (2014) Xanthomonas euvesicatoria type III effector XopQ interacts with tomato and pepper 14-3-3 isoforms to suppress effector-triggered immunity. *The Plant Journal* 77: 297-309
- Tian H, Wu Z, Chen S, Ao K, Huang W, Yaghmaiean H, Sun T, Xu F, Zhang Y, Wang S (2021) Activation of TIR signalling boosts pattern-triggered immunity. *Nature* 598: 500-503
- Tornero P, Chao RA, Luthin WN, Goff SA, Dangl JL (2002) Large-scale structure-function analysis of the Arabidopsis RPM1 disease resistance protein. *The Plant Cell* 14: 435-450
- Toruño TY, Stergiopoulos I, Coaker G (2016) Plant-pathogen effectors: cellular probes interfering with plant defenses in spatial and temporal manners. *Annual review of phytopathology* 54: 419-441
- Uehling J, Deveau A, Paoletti M (2017) Do fungi have an innate immune response? An NLR-based comparison to plant and animal immune systems. *PLoS pathogens* 13: e1006578
- Van de Weyer A-L, Monteiro F, Furzer OJ, Nishimura MT, Cevik V, Witek K, Jones JD, Dangl JL, Weigel D, Bemm F (2019) A species-wide inventory of NLR genes and alleles in Arabidopsis thaliana. *Cell* 178: 1260-1272. e1214
- van der Hoorn RA, Kamoun S (2008) From guard to decoy: a new model for perception of plant pathogen effectors. *The Plant Cell* 20: 2009-2017
- Van Der Vossen E, Sikkema A, Hekkert BtL, Gros J, Stevens P, Muskens M, Wouters D, Pereira A, Stiekema W, Allefs S (2003) An ancient R gene from the wild potato species Solanum bulbocastanum confers broad-spectrum resistance to Phytophthora infestans in cultivated potato and tomato. *The plant journal* 36: 867-882
- van der Vossen EA, Gros J, Sikkema A, Muskens M, Wouters D, Wolters P, Pereira A, Allefs S (2005) The Rpi-blb2 gene from Solanum bulbocastanum is an Mi-1 gene homolog conferring broad-spectrum late blight resistance in potato. *The Plant Journal* 44: 208-222

- Van Ooijen G, Mayr G, Kasiem MM, Albrecht M, Cornelissen BJ, Takken FL (2008) Structure–function analysis of the NB-ARC domain of plant disease resistance proteins. *Journal of experimental botany* 59: 1383-1397
- Vance RE (2015) The naip/nlrc4 inflammasomes. *Current opinion in immunology* 32: 84-89
- Vieira P, Gleason C (2019) Plant-parasitic nematode effectors—insights into their diversity and new tools for their identification. *Current opinion in plant biology* 50: 37-43
- Vossen JH, van Arkel G, Bergervoet M, Jo K-R, Jacobsen E, Visser RG (2016) The *Solanum demissum* R8 late blight resistance gene is an Sw-5 homologue that has been deployed worldwide in late blight resistant varieties. *Theoretical and Applied Genetics* 129: 1785-1796
- Wang G, Roux B, Feng F, Guy E, Li L, Li N, Zhang X, Lautier M, Jardinaud M-F, Chabannes M (2015a) The decoy substrate of a pathogen effector and a pseudokinase specify pathogen-induced modified-self recognition and immunity in plants. *Cell host & microbe* 18: 285-295
- Wang G-F, Ji J, Ei-Kasmi F, Dangl JL, Johal G, Balint-Kurti PJ (2015b) Molecular and functional analyses of a maize autoactive NB-LRR protein identify precise structural requirements for activity. *PLoS pathogens* 11: e1004674
- Wang J, Hu M, Wang J, Qi J, Han Z, Wang G, Qi Y, Wang H-W, Zhou J-M, Chai J (2019a) Reconstitution and structure of a plant NLR resistosome conferring immunity. *Science* 364: eaav5870
- Wang J, Wang J, Hu M, Wu S, Qi J, Wang G, Han Z, Qi Y, Gao N, Wang H-W *et al* (2019b) Ligand-triggered allosteric ADP release primes a plant NLR complex. *Science* 364: eaav5868
- Wang M, Chen J, Wu R, Guo H, Chen Y, Li Z, Wei L, Liu C, He S, Du M (2023a) The immune receptor SNC1 monitors helper NLRs targeted by a bacterial effector. *bioRxiv*: 2023.2003.2023.533910
- Wang S, Huang W, Duxbury Z, Hogenhout SA, Jones JD (2021) Novel effector recognition capacity engineered into a paired NLR complex. *bioRxiv*: 2021.2009.2006.459143
- Wang S, McLellan H, Bukharova T, He Q, Murphy F, Shi J, Sun S, van Weymers P, Ren Y, Thilliez G *et al* (2018) *Phytophthora infestans* RXLR effectors act in concert at diverse subcellular locations to enhance host colonization. *Journal of Experimental Botany* 70: 343-356
- Wang Z, Liu X, Yu J, Yin S, Cai W-J, Kim NH, Kasmi FE, Dangl JL, Wan L (2023b) Plasma membrane association and resistosome formation of plant helper immune receptors. *bioRxiv*: 2023.2001.2023.525201
- Weber E, Engler C, Gruetzner R, Werner S, Marillonnet S (2011) A modular cloning system for standardized assembly of multigene constructs. *PLoS one* 6: e16765
- Wei T, Gong J, Jamitzky F, Heckl WM, Stark RW, Rössle SC (2008) LRRML: a conformational database and an XML description of leucine-rich repeats (LRRs). *BMC Structural Biology* 8: 1-9
- Williams SJ, Sohn KH, Wan L, Bernoux M, Sarris PF, Segonzac C, Ve T, Ma Y, Saucet SB, Ericsson DJ (2014) Structural basis for assembly and function of a heterodimeric plant immune receptor. *Science* 344: 299-303

- Williams SJ, Sornaraj P, deCourcy-Ireland E, Menz RI, Kobe B, Ellis JG, Dodds PN, Anderson PA (2011) An autoactive mutant of the M flax rust resistance protein has a preference for binding ATP, whereas wild-type M protein binds ADP. *Molecular plant-microbe interactions* 24: 897-906
- Win J, Chaparro-Garcia A, Belhaj K, Saunders D, Yoshida K, Dong S, Schornack S, Zipfel C, Robatzek S, Hogenhout S, 2012a. Effector biology of plant-associated organisms: concepts and perspectives, Cold Spring Harbor symposia on quantitative biology. Cold spring harbor laboratory press, pp. 235-247.
- Win J, Krasileva KV, Kamoun S, Shirasu K, Staskawicz BJ, Banfield MJ (2012b) Sequence divergent RXLR effectors share a structural fold conserved across plant pathogenic oomycete species. *PLoS pathogens* 8: e1002400
- Winn M (2003) An overview of the CCP4 project in protein crystallography: an example of a collaborative project. *Journal of synchrotron radiation* 10: 23-25
- Winter G (2010) xia2: an expert system for macromolecular crystallography data reduction. *Journal of applied crystallography* 43: 186-190
- Winter V, Hauser M-T (2006) Exploring the ESCRTing machinery in eukaryotes. *Trends in plant science* 11: 115-123
- Witek K, Jupe F, Witek AI, Baker D, Clark MD, Jones JD (2016) Accelerated cloning of a potato late blight-resistance gene using RenSeq and SMRT sequencing. *Nature biotechnology* 34: 656-660
- Witek K, Lin X, Karki HS, Jupe F, Witek AI, Steuernagel B, Stam R, Van Oosterhout C, Fairhead S, Heal R (2021) A complex resistance locus in *Solanum americanum* recognizes a conserved *Phytophthora* effector. *Nature Plants* 7: 198-208
- Wu C-H, Abd-El-Haliem A, Bozkurt TO, Belhaj K, Terauchi R, Vossen JH, Kamoun S (2017) NLR network mediates immunity to diverse plant pathogens. *Proceedings of the National Academy of Sciences* 114: 8113-8118
- Wu C-H, Derevnina L (2023) The battle within: How pathogen effectors suppress NLR-mediated immunity. *Current opinion in plant biology*
- Wu C-H, Derevnina L, Kamoun S (2018) Receptor networks underpin plant immunity. *Science* 360: 1300-1301
- Wu CH, Belhaj K, Bozkurt TO, Birk MS, Kamoun S (2016) Helper NLR proteins NRC2a/b and NRC3 but not NRC1 are required for Pto-mediated cell death and resistance in *Nicotiana benthamiana*. *New Phytol* 209: 1344-1352
- Wu Z, Li M, Dong OX, Xia S, Liang W, Bao Y, Wasteneys G, Li X (2019) Differential regulation of TNL-mediated immune signaling by redundant helper CNLs. *New Phytologist* 222: 938-953
- Wu Z, Tian L, Liu X, Huang W, Zhang Y, Li X (2022) The N-terminally truncated helper NLR NRG1C antagonizes immunity mediated by its full-length neighbors NRG1A and NRG1B. *The Plant Cell* 34: 1621-1640
- Xi Y, Cesari S, Kroj T (2022) Insight into the structure and molecular mode of action of plant paired NLR immune receptors. *Essays in Biochemistry* 66: 513-526

- Xia S, Hollingsworth LR, Wu H (2020) Mechanism and regulation of gasdermin-mediated cell death. *Cold Spring Harbor Perspectives in Biology* 12: a036400
- Xiao L, Magupalli VG, Wu H (2023) Cryo-EM structures of the active NLRP3 inflammasome disc. *Nature* 613: 595-600
- Xiong Q, Ye W, Choi D, Wong J, Qiao Y, Tao K, Wang Y, Ma W (2014) Phytophthora suppressor of RNA silencing 2 is a conserved RxLR effector that promotes infection in soybean and Arabidopsis thaliana. *Molecular Plant-Microbe Interactions* 27: 1379-1389
- Yen H, Sugimoto N, Tobe T (2015) Enteropathogenic Escherichia coli uses NleA to inhibit NLRP3 inflammasome activation. *PLoS pathogens* 11: e1005121
- Yu G, Xian L, Xue H, Yu W, Rufian J, Sang Y, Morcillo R, Wang Y, Macho A (2019) A bacterial effector protein prevents MAPK-mediated phosphorylation of SGT1 to suppress plant immunity. bioRxiv, 641241. *Preprint at* 10: 641241
- Yu G, Xian L, Xue H, Yu W, Rufian JS, Sang Y, Morcillo RJ, Wang Y, Macho AP (2020) A bacterial effector protein prevents MAPK-mediated phosphorylation of SGT1 to suppress plant immunity. *PLoS pathogens* 16: e1008933
- Yuan M, Jiang Z, Bi G, Nomura K, Liu M, Wang Y, Cai B, Zhou J-M, He SY, Xin X-F (2021) Pattern-recognition receptors are required for NLR-mediated plant immunity. *Nature* 592: 105-109
- Yuen ELH, Shepherd S, Bozkurt TO (2023) Traffic Control: Subversion of Plant Membrane Trafficking by Pathogens. *Annual Review of Phytopathology* 61
- Zacharias DA, Violin JD, Newton AC, Tsien RY (2002) Partitioning of lipid-modified monomeric GFPs into membrane microdomains of live cells. *Science* 296: 913-916
- Zdrzalek R, Kamoun S, Terauchi R, Saitoh H, Banfield MJ (2020) The rice NLR pair Pikp-1/Pikp-2 initiates cell death through receptor cooperation rather than negative regulation. *PloS one* 15: e0238616
- Zess EK, Dagdas YF, Peers E, Maqbool A, Banfield MJ, Bozkurt TO, Kamoun S (2022) Regressive evolution of an effector following a host jump in the Irish potato famine pathogen lineage. *PLoS Pathogens* 18: e1010918
- Zhang L, Chen S, Ruan J, Wu J, Tong AB, Yin Q, Li Y, David L, Lu A, Wang WL (2015) Cryo-EM structure of the activated NAIP2-NLRC4 inflammasome reveals nucleated polymerization. *Science* 350: 404-409
- Zhao Y, Yang J, Shi J, Gong Y-N, Lu Q, Xu H, Liu L, Shao F (2011) The NLRC4 inflammasome receptors for bacterial flagellin and type III secretion apparatus. *Nature* 477: 596-600
- Zhao Y-B, Liu M-X, Chen T-T, Ma X, Li Z-K, Zheng Z, Zheng S-R, Chen L, Li Y-Z, Tang L-R (2022) Pathogen effector AvrSr35 triggers Sr35 resistosome assembly via a direct recognition mechanism. *Science Advances* 8: eabq5108
- Zhu M, Jiang L, Bai B, Zhao W, Chen X, Li J, Liu Y, Chen Z, Wang B, Wang C (2017) The intracellular immune receptor Sw-5b confers broad-spectrum resistance to tospoviruses through recognition of a conserved 21-amino acid viral effector epitope. *The Plant Cell* 29: 2214-2232